RLO/2438-78/1
UC-60

SITES FOR WIND-POWER INSTALLATIONS:
Wind Characteristics Over Ridges

PART I

R. J. B. Bouwmeester
R. N. Meroney
V. A. Sandborn

Fluid Mechanics and Wind Engineering Program
Civil Engineering Department
Colorado State University
Fort Collins, Colorado 80523

June 1978

Prepared for the United States
Department of Energy
Division of Distributed Solar Technology
Federal Wind Energy Program

DOE Contract No. EY-76-S-06-2438, A001

CER77-78RJBB-RNM-VAS51

ACKNOWLEDGMENT

The authors wish to express their appreciation to Drs. William Pennell and Ronald Drake of Battelle, Pacific Northwest Laboratories, for their technical review and advice, to Ms. Pamela Partch for her careful editorial review and criticism, and to Mrs. Louise Warren for her patience during typing many revisions of this report. Special thanks is given to George Tennyson and Louis Divone of the Department of Energy Wind Systems Branch for their support and advice.

EXECUTIVE SUMMARY

The purpose of this research was to increase knowledge of the physical processes that govern wind characteristics over ridges and, subsequently, to improve empirical and numerical techniques for wind velocities over ridges. These objectives were achieved by conducting a wind-tunnel study of the flow field over triangular-shaped and sinusoidal-shaped ridge models with varying upwind and downwind slopes under various thermal stratification conditions.

A simple technique was developed to predict the velocity-amplification profile above a ridge crest for an arbitrary ridge slope. Largest speedups were measured for the steepest symmetrical ridge which did not cause flow separation. Criteria for flow separation over ridges are provided in this report. Effects of turbulence, surface roughness, and thermal stratification on speedup are generally of secondary importance. However, these effects and the slopes of the ridge are significant in determining whether or not separation occurs. Applicability of the results for ridges with finite width is discussed.

The separation phenomenon downwind of a ridge was investigated by analyzing the effects of upwind and downwind ridge slopes on the longitudinal extent of the separation region. It appeared that the downwind slope particularly affected the length of this region.

The turbulence structure over ridges was investigated by analyzing the longitudinal velocity fluctuations. It was found that the directional energy distribution of the turbulence above the crest is significantly different from that of the upwind turbulence. Changes in power spectra and probability density functions are relatively small.

Physical and numerical techniques to simulate flow over ridges were critically reviewed. It was shown that similarity requirements for wind-tunnel modeling techniques were generally met. In some cases similarity could not be achieved in a thin surface layer ($\tilde{\sim}$ 3 percent of the hill length). The overall flow, however, was not affected.

TABLE OF CONTENTS

LIST OF TABLES

LIST OF FIGURES

LIST OF SYMBOLS

Symbol	Description	Dimension
A	Hot-wire anemometer calibration constant	
A	Amplification factor $\bar{u}_c(z)/\bar{u}_o(z)$	
a	Constant $a = z_{ref}/h$	
a_1, a_2	Stress coefficients	
B	Hot-wire anemometer calibration constant	
b	Half width of ridge	L
C_{disk}	Disk calibration constant	
C_p	Static pressure coefficient $C_p = p/[1/2\ \bar{u}_o^2(10h)]$	
ΔC_p	Contour interval static pressures	
d	Displacement height	L
D_d	Distance from crest to downwind boundary	L
D_u	Distance from crest to upwind boundary	L
$\bar{e}$	Mean anemometer bridge voltage	
e'	Root-mean-square anemometer bridge voltage	
G	Clauser parameter (Equation (2.33))	
g	Gravity constant	LT^{-2}
H	Distance from surface to top boundary	L
h	Ridge height	L
k	von Karman constant	
L	Hill half length: distance from crest to half height	L
L	Characteristic hill length = 2L (symmetric hill)	L
L_b	Hill length: distance from crest to base (symmetric hill)	L
L_d	Downwind characteristic hill length	L
L_u	Upwind characteristic hill length	L

Symbol	Description	Dimension
L_x	Turbulence integral length scale	L
l	Mixing length	L
ℓ	Inner layer thickness	L
m	Hot-wire anemometer calibration constant	
P	Total head (kinematic)	L^2T^{-2}
ΔP	Change in total head (kinematic)	L^2T^{-2}
$\Delta P'$	Additional change in total head (kinematic)	L^2T^{-2}
p	Static pressure (kinematic)	L^2T^{-2}
p_o	Static pressure at "infinity" (kinematic)	L^2T^{-2}
p_s	Surface static pressure (kinematic)	L^2T^{-2}
$\overline{q^2}$	Twice turbulence kinetic energy	L^2T^{-2}
R	Characteristic change in Reynolds stress along streamlines	L^2T^{-2}
Re	Reynolds number	
R_p	Nondimensional pressure gradient (Equation (5.1))	
Ri	Richardson number	
R_m	Maximum Reynolds stress	L^2T^{-2}
Ro	Rossby number	
r	Radius of streamline curvature	L
ΔS	Fractional speedup ratio	
T	Temperature	θ
ΔT	Characteristic change in temperature over h	θ
t	Time	T
t_f	Traveling time of a fluid particle	T
ΔU_x	Characteristic change in velocity over L	LT^{-1}
ΔU_z	Characteristic change in velocity over h	LT^{-1}

Symbol	Description	Dimension
$\bar{u}$	Mean longitudinal velocity	LT^{-1}
$\bar{u}'$	Root-mean-square of longitudinal velocity fluctuation	LT^{-1}
$\bar{u}_c$	Mean longitudinal velocity at the crest	LT^{-1}
$\bar{u}_{ref}$	$\bar{u}_{ref} = \bar{u}_o(10h)$	LT^{-1}
$\overline{uw}$	Reynolds shear stress (kinematic)	L^2T^{-2}
$\bar{u}_o$	Mean longitudinal velocity upwind	LT^{-1}
$\bar{u}_\infty$	$\bar{u}_\infty = \bar{u}_o(\delta)$	LT^{-1}
u_*	Shear velocity	LT^{-1}
Δu	Contour interval longitudinal velocities [non-dimensionalized with $\bar{u}_o$ (10h)]	
$\Delta u'$	Contour interval rms of velocity fluctuations [non-dimensionalized with $\bar{u}_o$ (10h)]	
$\bar{w}$	Mean vertical velocity	LT^{-1}
w'	Root-mean-square of vertical velocity fluctuations	LT^{-1}
x	Longitudinal coordinate	L
z	Vertical coordinate	L
z_s	Surface elevation	L
z_o	Equivalent roughness length	L
Greek		
α_o	Exponent of upwind-powerlaw velocity profile	
α_c	Exponent of crest-powerlaw velocity profile	
β	Tangent of mean flow direction	
γ	Extra rate of strain ratio	
δ	Boundary layer thickness	L
δ_v	Thickness of viscous sublayer	L
ε	Turbulence dissipation rate	L^2T^3

1.0 INTRODUCTION

This report is the first in a series produced as part of the Wind-Tunnel Wind Energy Conversion System (WECS) Siting Program. The program was designed to study the characteristics of the wind in complex terrain, especially hilly terrain, so that installation sites for WECS can be identified. This report identifies the topographical features of hills most favorable for siting WECS. Specifically it considers the role of hill slope, hill shape, surface roughness, and stratification. Wind-tunnel measurements of the mean wind flow over model hills provide data to substantiate an empirical hill crest and speed up algorithm. Analysis of turbulence characteristics suggest what simplifications are permissible in analytic or numerical model procedures.

1.1 THE OBJECTIVES OF THIS WIND-TUNNEL WECS SITING PROGRAM

The objectives of this portion of the physical modeling program have been

1. To study the wind characteristics over hills as influenced by
   a. hill shape,
   b. surface roughness and upwind turbulence, and
   c. thermal stratification;
2. To correlate hillcrest wind conditions with upwind conditions for a wide range of hill shapes; and
3. To identify the dominant physical mechanisms that govern flow characteristics over hills and, hence, provide guidance for the development or selection of analytic or numerical models for WECS siting.

The information contained in this report deals primarily with two-dimensional flow (to be interpreted as flow over ridges of infinite width and with a flow direction perpendicular to the crest). However many of the findings should hold, at least qualitatively, for three-dimensional flow over hills. Relations between the upwind velocity profiles and velocity profiles at the crest have been established by varying hill and flow features.

Measurements have been made of wind speed, turbulence intensity static pressure, probability density function, and spectra over a number of triangular and sinusoidal two-dimensional hill shapes. Measurement techniques are described in Meroney et al. (1976a,b), Rider and Sandborn (1977a), and in this report. Data are tabulated in detail in Meroney et al. (1976b), and Rider and Sandborn (1977b) for neutral stratification measurements. A set of measurements investigating the flow field when the downslope hill varies to incipient

separation are discussed and tabulated in this report. A set of measurements associated with stratified flow over two-dimensional hills has been compiled into Appendix C, Meroney et al. (1978b). Additional measurements over a set of six different hill shapes are described in Rider and Sandborn (1977b).

Three-dimensional flow field data are provided in tabulation form by Chien et al. (1978). Their interpretation is discussed in Merony et al. (1978b).

A review of physical-modeling similarity requirements has been placed in reports by Meroney et al. (1976a, 1978a,b). This report emphasizes particularly the similarity requirements for flow over a surface obstacle in a deep shear layer.

A validation study was performed through a joint effort between Colorado State University and the University of Canterbury, New Zealand. The results of this program have been gathered into Meroney et al., 1978a.

1.2 ORGANIZATION OF THIS REPORT

The remaining chapters of this report are organized in the following manner. In Chapter 2 the physical processes that govern flow over ridges are discussed. If the reader is familiar with the literature concerning flow over obstacles in shear flows, he may prefer to proceed directly to the result sections in Chapters 3, 4, and 5. Chapter 3.0 discusses the experimental results of the wind tunnel measurements of mean flow over ridges. The hill shape and flow condition are parameterized to describe the dependency of speedup over the crest on such variables. Experimental results and additional information are presented to extend the conclusions of the two-dimensional analysis to flow over ridges with finite width. An empirical prediction technique for the velocity profile at hill crest is proposed in Chapter 4.0. Turbulence characteristics are considered in Chapter 5.0. In Chapter 6.0 there is a recapitulation of the major conclusions of this study including suggestions about worthwhile areas for further investigation.

Details of experimental methodology, data analysis techniques, a review of the constraints of and characteristics over ridges on mathematical prediction procedures, and tabulated data are summarized in a series of appendices at the end of the report. The tabulated data should be particularly helpful to those interested in the construction or validation of analytic or numerical WECS siting models.

2.0 PHYSICS OF FLOW OVER RIDGES

The accuracy of analytical or numerical prediction techniques that approximate wind flow over hills depends a great deal upon

1. An understanding of the turbulence structure over the hill and its interaction with the mean flow,
2. An understanding of the mechanism that causes flow separation and the development of a wake, and
3. The sophistication and validity of current mathematical models for flow over hills.

This chapter considers these aspects of flow over a hill.

The literature on the physics of boundary layer flow over obstacles is not generally familiar to most meteorologists or engineers, nor has it been consolidated into any single reference. Pertinent material is reviewed in this section and is used to support the results of a perturbation analysis of changes in total head as wind flows over a hill crest at various lengths from the surface. The analysis and review provide a context for evaluation of the experimental results discussed in Chapters 3.0, 4.0, and 5.0. The analysis also provides a context for review of mathematical prediction procedures for hill flows. Appendix E considers the constraints of wind characteristics over ridges on various analytic and numerical methodologies.

The turbulent action on the mean flow is analyzed by considering flow over hills as a departure from the flow of an inviscid fluid. Regions are distinguished where the effect of turbulence on the mean flow is different. The most important flow and hill features affecting flow separation are considered, and the large, separated flow region which results from the interaction between wake and main flow is investigated.

The analysis is carried out by considering two-dimensional flow over ridges. However, the general approach of the analysis justifies application to three-dimensional flow over ridges. Section 4 of Chapter 3 is devoted to discussing quantitatively the applicability of the insights gained to ridges with finite width and to other three-dimensional effects such as Coriolis accelerations and ridges at an angle to the flow.

2.1 IDENTIFICATION OF FLOW REGIONS

Flow regions are identified to indicate portions of the flow field where the turbulence structure affects the mean flow differently. In flat plate boundary layers two regions are usually distinguished, the inner and the outer

regions. In the inner region the flow is directly affected by the surface shear stress; in the outer region the flow closely resembles free turbulence, with properties of the turbulence being strongly dependent on conditions far upstream.

Jackson and Hunt (1975) conducted an analytical study on flow over low hills and also divided the flow field into an inner and outer region. By definition, the inertia, pressure, and Reynolds stress gradients in the inner region were of the same order of magnitude; whereas in the outer region the fluid had effectively inviscid properties. Although the changes in Reynolds stresses in the region outside the inner region may be orders of magnitudes smaller than the inertia stresses, after extended periods of transport over long hills they may cause significant additional total head losses.

In order to include the long-range effects of the turbulence on the mean flow over the hill, three regions rather than two need to be distinguished.

a) An Inner Region. The inertia, pressure, and Reynolds stress gradients in this region are of the same order of magnitude. It may be assumed that the turbulence energy production and dissipation rates are so large that they are the only dominant terms in the turbulence kinetic energy equation; thus

$$\overline{uw}\,\frac{\partial \bar{u}}{\partial z} = \varepsilon \qquad (2.1)$$

Under such conditions structural similarity exists between the Reynolds stresses (Townsend, 1962).

b) A Middle Region. In this region inertia stress gradients are much larger than Reynolds stress gradients. But changes in Reynolds stresses are sufficiently large to cause substantial additional change in total head.

The advective terms in the Reynolds transport equations may reach the same orders of magnitude or become even larger than the production and dissipation terms. If longitudinal velocity accelerations are sufficiently large, boundary-layer approximations may not be applied. As a result, the prediction of the turbulence stresses may become very difficult. Moreover, Bradshaw (1973a) pointed out that the effect of extra strain rates (additional velocity gradients to the simple shear $\partial \bar{u}/\partial z$) is often an order of magnitude larger than expected from the explicit extra terms they introduce into the Reynolds-stress transport equations. He indicated that the unexpected effects

of extra strain rates could be identified by classifying the flow according to the ratio of the extra strain rate to main shear, γ. A flow is

strongly distorted if $|\gamma| \tilde{\approx} 0.1 - 10$

a fairly thin shear layer if $|\gamma| \tilde{\approx} .01 - .1$

a simple shear layer if $|\gamma| < .01$

The significance of each of the classes is that in a strongly distorted flow, the Reynolds stresses are locally insignificant since pressure gradients greatly exceed Reynolds stress gradients; in a fairly thin shear layer Reynolds stress gradients may become unexpectedly large; and in a simple shear layer the turbulence is not affected by the extra strain rates.

The rates of extra strain in flow over hills are related to the curvature of the streamlines. A convenient way of defining γ is by writing the strain rates in s-n coordinates (Castro, 1976). Different extra rate of strain ratios can be defined. First the following ratio will be considered:

$$\gamma = \frac{-\frac{\bar{u}}{r}}{\frac{\partial \bar{u}}{\partial n}} . \tag{2.2}$$

Close to the surface the streamlines approximately follow the curvature of the surface. In this region the radius of curvature may be estimated by the hill parameters h and L. A typical value of r over the crest is

$$r_{crest} = 0 \left[\frac{L^2}{h}\right] \tag{2.3a}$$

and at the foot of the hill

$$r_{foot} = 0 \left[-\frac{L^2}{2h}\right]. \tag{2.3b}$$

Velocities are approximately of the same order, and the length scale of the normal velocity gradient is typically equal to δ. The extra rate of strain ratio is then

$$\gamma_{foot} = 0 \left[\frac{h\delta}{2L^2}\right] \tag{2.4a}$$

$$\gamma_{crest} = 0\ [\frac{-h\delta}{L^2}] \tag{2.4b}$$

Thus these extra strain rates are large for steep, short hills and small for long low hills. The highest values for γ exist when flow separation does not occur ($h/L \lesssim 0.3$), and when the hill is deeply embedded in the boundary layer. Therefore values of $|\gamma|$ of interest are less than 1. Streamline curvature decreases with increasing height. Thus flow close to the surface may be strongly distorted, further away from the surface, the flow may be characterized as a fairly thin shear layer.

The change in streamline curvature with height is directly related to the longitudinal acceleration. The ratio of this extra strain rate to main shear is

$$\gamma' = \frac{\frac{\partial \bar{u}}{\partial s}}{\frac{\partial \bar{u}}{\partial n}} \quad . \tag{2.5}$$

The order of magnitude of the longitudinal acceleration will be expressed in terms of the fractional speedup ratio, defined by

$$\Delta S = \frac{\bar{u}_c(z) - \bar{u}_o(z)}{\bar{u}_o(z)}$$

where $\bar{u}_o$ is the upwind velocity, and $\bar{u}_c$ is the velocity at the crest. Thus

$$\gamma' = 0\ [\frac{\Delta S \delta}{L}] \ , \tag{2.6}$$

The fractional speedup factor ΔS in the surface region of steep hills is large with respect to h/L. Therefore γ' dominates the extra strains for steep hills in the surface region; γ [Equation (2.4)] may dominate in the upper part of the middle region. The flow field over a hill should be classified according to the largest occurring extra rate of strain ratio. Thus the middle region contains usually two flow regimes: a fairly thin shear layer and a strongly distorted flow. This concept makes the mean flow prediction particularly difficult.

In some cases the prediction may be less complex as a result of the varying curvature of the streamlines; γ is negative at the foot of the hill and positive over the crest. The turbulence structure does not immediately adjust to the extra strain rate. Therefore γ is effectively less. Bradshaw (1973b) proposes the following lag equation to calculate the effective value of γ

$$\frac{D\gamma_{eff}}{Dt} = \frac{-1}{T} (\gamma_{eff} - \gamma) , \tag{2.7}$$

where T is a time scale of the stress-bearing eddies: $T \tilde{\approx} \frac{1}{\partial \bar{u}_o / \partial z}$.

In the flow field over a hill, a region exists where γ falls in the range that defines a fairly thin shear layer. Suppose that in this region $T \tilde{\approx} \delta/\bar{u}_o$. The time it takes a fluid particle to travel from $x = -1/2\ L$ to $x = 1/2\ L$ is the order of $L/\bar{u}_o$. Suppose further that γ is constant for $-1/2\ L < x < 1/2\ L$ and $\gamma = 0$ for $x < -1/2\ L$. Then, at the crest:

$$\gamma_{eff} = \gamma(1 - \exp(-\frac{L}{2\delta})). \tag{2.8}$$

Now for $L/\delta = 1$, $\gamma_{eff} = 0.4\ \gamma$. Thus, although curvature is significant over this hill, this result shows that extra strain rates do not always affect the Reynolds stress significantly.

It seems reasonable, based on the foregoing arguments to state that for short hills ($L<\delta$) in the region where $0.01 < \gamma < 0.1$, the stress-bearing eddies do not change considerably due to streamline curvature. Consequently, Reynolds shear stresses stay approximately constant along streamlines. This result will be used in the next section to show that under these conditions the flow may be essentially inviscid.

c) An Outer Region. In this region the flow is essentially a simple shear layer. Extra strain rates do not affect the turbulence structure nor the mean flow. The region is defined by,

$$\gamma = \frac{\bar{u}/r}{\partial u/\partial n} < 0.01 \quad \text{and} \quad \frac{\partial \bar{u}/\partial s}{\partial \bar{u}/\partial n} < 0.01.$$

Because the curvature changes continuously along a streamline, a better definition of the region would be obtained if the effective value of the extra strain rate were applied.

The three flow regions are illustrated in Figure 2.1. It is noted that if

$$\frac{h\delta}{L^2} < 0.01 \quad \text{and} \quad \frac{\Delta S\delta}{L} < 0.01$$

the middle region vanishes. In case $L < \delta$ the middle region does not necessarily vanish, but its size is reduced, since the effective strain rate is much less than γ.

Classification of the different regions in the flow will be particularly valuable to a discussion of closure models frequently used in numerical models (see Appendix E, Section E.1) and to discuss the inviscid character of the flow in the middle region.

2.2 THE INVISCID CHARACTER OF FLOW OVER RIDGES

Turbulent flow fields may be approximated as flow with an effectively inviscid fluid if work done by friction is small compared to the kinetic energy of the flow. In stationary boundary-layer flow which is driven by a pressure gradient, the work done by the pressure gradient equals the work done by the friction; therefore, total head loss in the streamwise direction is equal to the pressure drop of the driving-pressure system. Thus, if the pressure drop over a hill is small (short hill), the fluid can be considered as effectively inviscid. Over large distances the pressure drop becomes significant, and total head losses have to be taken into account.

One of the characteristics of inviscid flow is that vorticity stays constant along streamlines. This characteristic is not restricted to inviscid flows alone. Along streamlines in boundary layer flow over a flat plate, for example vorticity (mean velocity gradient) stays practically constant over a distance in which the boundary layer thickness does not change significantly. In terms of total head, this may be interpreted to mean that total head along a streamline decreases at the same rate as the pressure that drives the flow. Since the synoptic-pressure system of flow over hills is often known, it is convenient to analyze a specific case by considering the departure from flow with constant vorticity along streamlines or, alternatively, to analyze the flow by considering the departure from the total head loss as given by the driving-pressure gradient. The latter case will be referred to as additional

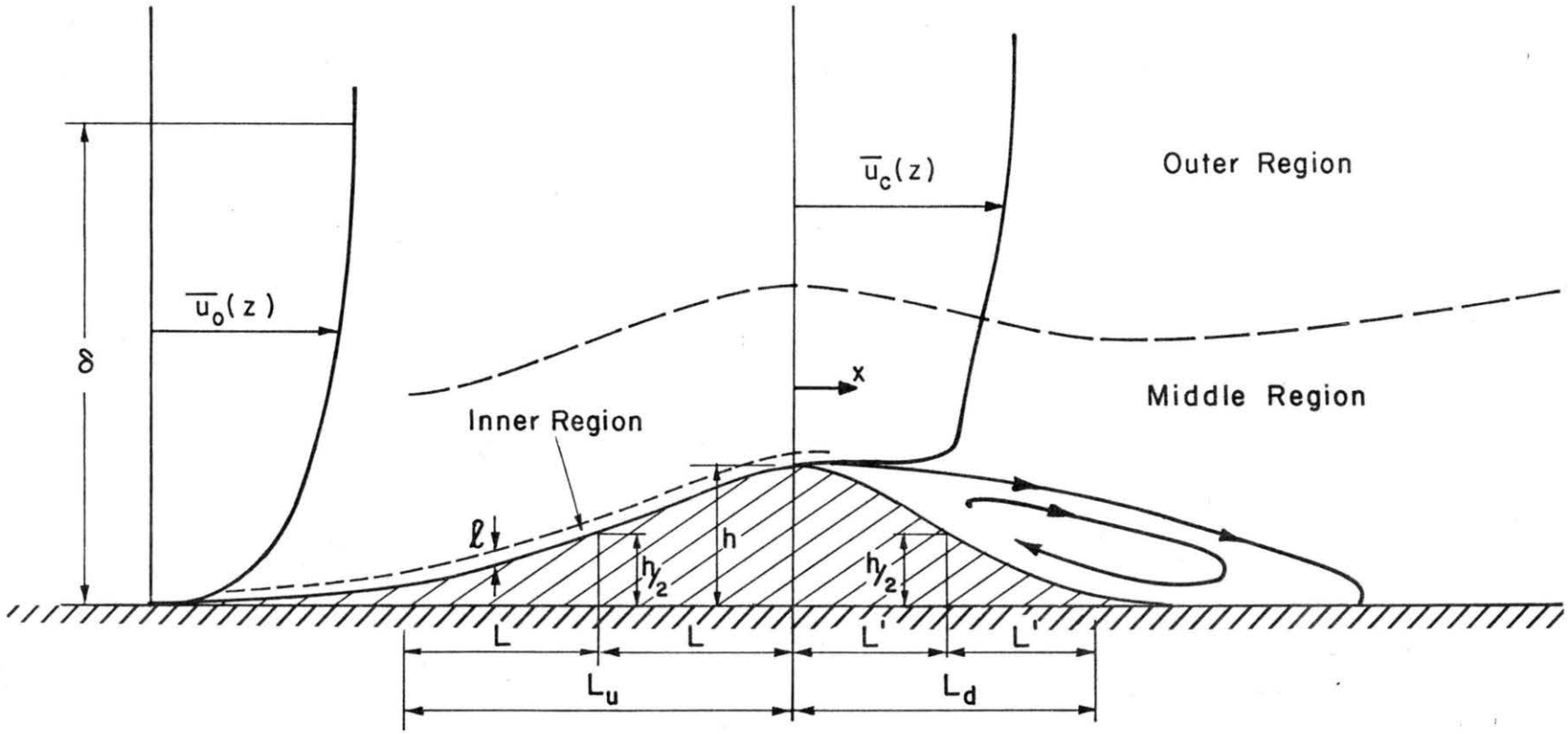

FIGURE 2.1. Schematic of Flow Regions

total head loss. An initial analysis of flow over hills is most easily carried out by considering the additional total head loss, because the working equations contain expressions for the Reynolds stress gradients which are relatively easy to measure. Analysis of the change of vorticity requires the use of the full vorticity equations which contain vorticity-velocity correlations that are difficult to measure.

The Reynolds number for flow over a hill is sufficiently large that viscosity terms in the equations of motion may be neglected. Thus the equations of motion for two-dimenstional mean flow are:

$$\bar{u}\frac{\partial \bar{u}}{\partial x} + \bar{w}\frac{\partial \bar{u}}{\partial z} = -\frac{\partial p}{\partial x} - \frac{\partial \overline{u^2}}{\partial x} - \frac{\partial \overline{uw}}{\partial z} \tag{2.9}$$

and

$$\bar{u}\frac{\partial \bar{w}}{\partial x} + \bar{w}\frac{\partial \bar{w}}{\partial z} = -\frac{\partial p}{\partial z} - \frac{\partial \overline{w^2}}{\partial z} - \frac{\partial \overline{uw}}{\partial x} \ . \tag{2.10}$$

It is convenient to transform the Cartesian coordinates into von Mises coordinates. In the latter system the independent variables are x and the stream function ψ. The transformation formulae are:

$$\left[\frac{\partial}{\partial x}\right]_z = \left[\frac{\partial}{\partial x}\right]_\psi - \bar{w}\left[\frac{\partial}{\partial \psi}\right]_x \tag{2.11}$$

and

$$\left[\frac{\partial}{\partial z}\right]_x = \bar{u}\left[\frac{\partial}{\partial \psi}\right]_x \ . \tag{2.12}$$

The x, z, and ψ behind the brackets denote that the derivatives are taken when x, z, and ψ respectively are constant. In subsequent equations the subscript is omitted. The equations of motion become

$$\bar{u}\frac{\partial \bar{u}}{\partial x} + \frac{\partial p}{\partial x} - \bar{w}\frac{\partial p}{\partial \psi} = -\frac{\partial \overline{u^2}}{\partial x} + \bar{w}\frac{\partial \overline{u^2}}{\partial \psi} - \bar{u}\frac{\partial \overline{uw}}{\partial \psi} \tag{2.13}$$

$$\bar{u}\frac{\partial \bar{w}}{\partial x} + \bar{u}\frac{\partial p}{\partial \psi} = -\bar{u}\frac{\partial \overline{w^2}}{\partial \psi} - \frac{\partial \overline{uw}}{\partial x} + \bar{w}\frac{\partial \overline{uw}}{\partial \psi} \ . \tag{2.14}$$

The change in total head along a streamline due to the action of Reynolds stresses is easily derived by adding equation (2.13) after multiplication with $\bar{u}$ to equation (2.14) after multiplication with $\bar{w}$. Denoting total head by P, the decrease in total head over a distance from x_o to x_1 is

$$\Delta P = - \int_{x_o}^{x_1} \left[\frac{\partial \overline{u^2}}{\partial x} - \beta \bar{u} \frac{\partial (\overline{u^2} - \overline{w^2})}{\partial \psi} + \beta \frac{\partial \overline{uw}}{\partial x} + \bar{u}(1-\beta^2) \frac{\partial \overline{uw}}{\partial \psi} \right] dx, \qquad (2.15)$$

where $\beta = \frac{\bar{u}}{\bar{w}}$ which is the local flow direction and x_o is an upstream reference point relatively to the crest of the hill.

The additional total head loss is then

$$\Delta P' = \Delta P - \int_{x_o}^{x_1} \frac{\partial p_o}{\partial x} dx \qquad (2.16)$$

where $\frac{\partial p_o}{\partial x}$ is the driving pressure gradient. It is noted that for flow over a flat plate

$$\Delta P' = 0 .$$

An order of magnitude analysis is carried out to determine the maximum losses in the middle region as defined in the previous section. This maximum value is obtained by making the following approximations: Assume flat plate conditions exist upstream from a point defined $x = -L$ where L is the characteristic length of the hill, defined as twice the distance between the crest and the point where the hill height is half the height at the crest, and assume changes in Reynolds stress gradients along streamlines occur a distance up to λL above the surface, if $\lambda L < \delta$ and up to δ, if $\lambda L > \delta$. λ depends on the hill shape and is to be determined empirically. The characteristic change in Reynolds stress will be defined as R, where R may be either

$$R = 0[|\overline{u^2}_{foot} - \overline{u^2}_{crest}|] \qquad (2.17a)$$

or

$$R = 0[\,|\overline{uw}_{foot} - \overline{uw}_{crest}|\,] \qquad (2.17b)$$

whichever is larger. The order of magnitude of the terms of equations (2.15) and (2.16) for $x > -L$ is then,

$$\frac{\partial \overline{u^2}}{\partial x} = 0\ [\frac{R}{L}]$$

$$\beta\bar{u}\ \frac{\partial(\overline{u^2} - \overline{w^2})}{\partial \psi} = 0\ [\frac{hR_m}{L\delta}]$$

where R_m is the maximum Reynolds stress in the flow field.

$$\beta\ \frac{\partial \overline{uw}}{\partial x} = 0\ [\frac{hR}{L^2}]$$

$$\bar{u}(1-\beta^2)\ \frac{\partial \overline{uw}}{\partial \psi} - \frac{\partial p_o}{\partial x} = 0[\frac{R}{\delta}] \quad \text{if} \quad \delta < \lambda L$$

$$= 0[\frac{R}{\lambda L}] \quad \text{if} \quad \delta > \lambda L$$

The order of magnitude of the maximum additional total head loss is then

$$\Delta P' = 0[((1 + \frac{1}{\lambda} + \frac{h}{L})\ \frac{R}{L} + \frac{h}{L}\ \frac{R_m}{\delta})\ (x_1 + L)] \quad \text{if} \quad \delta > \lambda L \qquad (2.18)$$

$$\Delta P' = 0[((1 + \frac{L}{\delta} + \frac{h}{L})\ \frac{R}{L} + \frac{h}{L}\ \frac{R_m}{\delta})\ (x_1 + L)] \quad \text{if} \quad \delta < \lambda L \qquad (2.19)$$

The effect of the hill on $\Delta P'$ is illustrated by applying those approximations to experimental data presented by Rider and Sandborn (1977a). Horizontal and vertical turbulence intensities were measured over triangular hill models where $h/L = 0.17$, 0.25, and 0.33, with $L/\delta = 0.6$, 0.4, and 0.3, respectively. Maximum local turbulence intensities were about 20 percent. It may be expected that for those rather steep and short hills, changes in the Reynolds normal stresses along streamlines are less than changes in the Reynolds shear stresses. The data show that R based upon Reynolds normal stresses is less than 30 percent of R_m and that λ is on the order of 0.5. The maximum additional change in total head at the crest is then

$$\Delta P'_{crest} \simeq 4\%. \qquad (2.20)$$

Further away from the surface, $\Delta P'$ decreases since the most significant changes in the turbulence structure occur in the lowest regions.

The result obtained for flow over the triangular hill models should also be valid for hills with larger ratios of hill length to boundary-layer thickness, since equation (2.18) in particular is not sensitive to this parameter.

The inviscid character of flow over a hill is illustrated also by the following considerations. For weak turbulence and approximately constant Reynolds shear stresses along streamlines, equations (2.13) and (2.14) may be simplified to

$$\bar{u}\,\frac{\partial \bar{u}}{\partial x} + \frac{\partial p}{\partial x} - \bar{w}\,\frac{\partial p}{\partial \psi} = \bar{u}\,\frac{\partial \overline{uw}}{\partial \psi} \tag{2.21}$$

$$\bar{u}\,\frac{\partial \bar{w}}{\partial x} + \bar{u}\,\frac{\partial p}{\partial \psi} = \bar{w}\,\frac{\partial \overline{uw}}{\partial \psi} \quad . \tag{2.22}$$

Eliminating the terms on the right-hand side and presuming that the total head along streamlines stays constant yields the following expression:

$$\frac{\partial \bar{w}}{\partial x} + \frac{\partial p}{\partial \psi} = 0 \tag{2.23}$$

The presumption that total head stays constant may be expressed as

$$\left[\frac{\bar{u}_o^{\,2}}{2}\right]_{\psi=\psi_1} = \left[\frac{\bar{u}^2}{2} + p\right]_{\psi=\psi_1} \quad . \tag{2.24}$$

Elimination of p from equations (2.23) and (2.24) leads to

$$\bar{u}\,\frac{\partial \bar{u}}{\partial \psi} - \frac{\partial \bar{w}}{\partial x} + \frac{\partial \bar{w}}{\partial \psi} = \frac{\frac{1}{2}\partial \bar{u}_o^{\,2}}{\partial \psi} \quad . \tag{2.25}$$

Equation (2.25) represents another property of inviscid flow, namely that the mean vorticity along streamlines stays constant. This justifies the presumption that the total head along streamlines stays constant.

2.3 FLOW SEPARATION OVER RIDGES

The occurrence of flow separation over ridges is from the point of view of wind power undesirable. The wake mixes momentum across streamlines, diminishes longitudinal pressure gradients, and consequently reduces the wind

velocity over the top of the hill. Moreover, separation causes reduced velocities in the surface region downstream of the wake.

At present operational models for flow separation over ridges do not exist. Some semi-empirical models require empirical information, such as the location of the separation point, reattachment point, and base pressure. See the discussion in Appendix E, Section E.4 of Kiya and Arie (1972) and Bitte and Frost (1976). The development of prediction techniques for velocities over hilly terrain must rely heavily on experimental data.

In this section implications of theoretical and experimental separation concepts are reviewed and applied to flow over ridges. A general description of phenomena related to separation from the surface is given by Scorer (1978). The following discussion is a detailed review of existing insights into separation phenomena over ridges. Two separation regions are considered: the separation regions upstream and downstream of the ridge.

The Upstream Separation Region. Upstream separation depends primarily on the upstream slope at the base of the hill. In contrast with the downstream separation region, the upstream region is never very large. The length is of the order of the obstacle hill height. Its effect, however, on the velocity field is quite important, because the separation zone in front of a hill reduces the favorable pressure gradient that normally provides large speedup effects in the lower layers over the crest.

It was shown in Section 2.2 that the flow over hills, if no flow separation occurs, is approximately inviscid. Indeed, even in the presence of separation, the prediction of the occurrence of flow separation may be obtained by an inviscid theory presented by Fraenkel (1962). Fraenkel shows that corner eddies with closed streamlines can be predicted analytically from inviscid flow assumptions. The physical interpretation of this phenomenon is simply that the flow near the front of the obstacle stagnates to the extent that the motion is dominated by the vorticity. Once flow separation occurs, the viscous effects (particularly along the separation streamline) invalidate to some extent the inviscid flow assumption.

A semi-analytical model, based on Fraenkel's theory, was presented by Kiya and Arie (1972) for flow over a fence deeply embedded in a boundary layer (see also Appendix E, Section E.4). Their model requires empirical input parameters to take into account the downstream wake. The flow in the upstream separation region, however, is predicted essentially on a theoretical basis.

Excellent agreement was found between their theoretical results and experimental measurements by Good and Joubert (1968). The success is undoubtedly due to the fact that the vorticity was sufficiently strong.

Conditions similar to those discussed above apply to flow over a ridge embedded in the boundary layer. Hence an inviscid separation model is appropriate. The interaction between main flow and a separation eddy becomes important if the hill height is much larger than boundary-layer thickness. Robertson and Taulbee (1969) conducted an experimental study of turbulent boundary-layer flow over a forward-facing normal step. They evaluated the effect of ratio between the step height and boundary-layer thickness on the extent of the separated flow region. When values of h/δ varied from 0.5 to 2, they found that the location of the separation point upstream of the step extended to $0.8h$ for $h/\delta = 0.5$, and to $1.5h$ for $h/\delta = 2$.

An important phenomenon may occur if the flow is stably stratified. The cooler heavier air in front of a ridge stagnates. That in turn results in a further decrease in temperature. This may lead to a total blocking of the air in front of a mountain range. This phenomenon is the main cause of Föhn winds, in which air descends from an altitude not far from that of a ridge top on the upwind side to the surface on the downwind side. Blocking seems to occur only if (Scorer, 1978)

$$h > \frac{2\Pi}{\ell}$$

where ℓ is the Scorer parameter,

$$\ell = \frac{g}{\bar{u}_o^2} \frac{1}{\theta} \frac{\partial \theta}{\partial z}$$

and θ is the potential temperature.

The Downstream Separation Region. Boundary-layer flow over a flat ground plane driven by a synoptic-pressure system is in equilibrium and does not separate since the pressure drop in the streamwise direction is in balance with the surface shear stress. But the force balance in flow over hills is disturbed due to the increased surface shear stress over the hill. As a result horizontal momentum in the lowest layer is transported downward at a higher rate. Although the momentum along a streamline at the crest is larger than upstream along the same streamline, the momentum may not be large enough to overcome the adverse over-crest pressure gradient. Consequently the flow

tends to separate from the surface, and, depending on the interaction between wake and main flow, a large wake may develop.

The interaction between those two flow regions can be described by considering the flow over a hill model initially at rest and then suddenly in motion at constant speed. (Batchelor (1967, plate 8) illustrated the development of the downstream wake in this way by showing a series of pictures of a flow visualization of the development of the flow patterns around a house model that is pulled in a fluid initially at rest.) In the initial stages when no flow separation has developed, the pressure gradient in the surface region is parallel to the surface. When the flow separates, there is no force that prevents the development of an eddy directly after the separation point. In later stages, however, a pressure gradient across the separating streamline builds up so that futher growth of the eddy is prevented. The equilibrium that is established in the flow is mainly determined by the strength of the eddy and the pressure gradients across the separation streamline. The order of magnitude of those forces suggests that features like location of separation point and hill shape may significantly affect the size of the wake. Indeed, experimental evidence of the importance of the point of separation was given by Huber et al. (1976). They showed that significant increase in the dimensions of the wake downstream of a bell-shaped hill model was created by tripping the boundary layer at the crest.

Depending on the shape of the hill, different flow features may dominate the separation phenomenon. Several aspects of flow separation may be conveniently discussed by considering three different hill types:

- Hills with steep downstream slopes, say $h/L_d \lesssim \frac{1}{2}$, where L_d is the downstream characteristic hill length. For this category of hills the eddy in the separation region is not constrained by the downstream slope. Available information on the flow development downstream of the separation point from studies with vertical backward-facing steps may well be applied.
- Round-crested hills with downstream slopes $\frac{1}{4} < h/L_d < \frac{1}{2}$. For this category, location of the separation point as affected by surface roughness affects the velocity field significantly.
- Sharp-crested hills with downstream slopes $\frac{1}{4} < h/L_d < \frac{1}{2}$. For this hill type, the separation point is fixed. The effect of the ratio h/L_d on the extent of separation region is most marked.

Hills with Downstream Slopes, Say $h/L_d > \frac{1}{2}$

Once separation occurs, two flow regions can be identified. One includes the region around the separation streamline defined as the new shear layer, the other, the region downstream of the reattachment point.

The new shear layer is a free turbulent shear flow similar to the mixing of a uniform-freestream and a quiescent-flow region; hence turbulent half-jet theories are relevant. Some of the first researchers who investigated the flow in this manner were Korst, Page, and Childs (1954) and Chapman, Kuehn, and Larson (1957). Following their methodology, Chang (1966) analyzed the velocity distribution in the new shear layer behind a wedge-shaped hill model with a frontward-facing vertical slope and backward-facing slope of 1/1. He found that the velocity profiles in this layer could be described successfully by the half-jet theory except for the region close to the separation point.

Chang noted that according to half-jet theory the velocity profiles along the separation region may be described by

$$\frac{\bar{u}}{\bar{u}_o} = \frac{1}{2} (1 + \text{erf } \eta), \tag{2.26}$$

where η is a dimensionless coordinate equal to $\sigma z'/x'$, in which σ is a similarity parameter and z' and x' are the coordinates of an intrinsic system. The z' coordinate is determined from measurements, whereas the x' coordinate is the distance from the crest. Experiments have shown that values of σ are approximately constant in ideal flow cases such as the half-jet. In the separated flow region behind a wedge-shaped hill, however, it appears that σ varies with downstream distance from the crest. This deviation may occur because the half-jet theory assumes a uniform incident velocity profile, whereas in the present case a nonuniform velocity distribution exists. Following Kirk (1959), Chang showed that σ may be modified to a constant value, if one displaces the origin in the upstream direction by a distance x_o determined experimentally. Incorporating these considerations into the original equation leads to the following expression for the velocity field downstream of the wedge-shaped hill:

$$\frac{\bar{u}}{\bar{u}_o} = \frac{1}{2} \left(1 + \text{erf } \left(\sigma \frac{z'}{x+x_o}\right)\right) , \tag{2.27}$$

where the curve is a function to be determined experimentally and σ and x_o are empirical constants.

Bradshaw and Wong (1972) reviewed a series of experiments conducted by other researchers [(Tillmann (1945), Arie and Rouse (1956), Tani et al. (1961), Mueller and Robertson (1963), Plate and Lin (1964), and Petryk and Brundrett (1967)]. Based on their results Bradshaw and Wong showed that a strong dependence exists between the length of the downwind separation region and the configuration of the surface upstream of the separation point. The distance between separation and reattachment point varies from 5 to 20 hill heights. The distance is small for simple backward-facing steps and is large for bluff surface obstacles such as fences.

As is well known, the turbulence structure in the new shear layer changes significantly from upstream conditions. Downstream of the separation region the turbulence in the boundary layer is strongly disturbed over the part of the boundary layer that has been exposed to the new shear layer. The thickness depends primarily on the length of the separation region. The longer the separation region, the larger the disturbance of the turbulence and, consequently, the larger the departure of the velocity from the velocity distribution in an equilibrium boundary layer. The return of the boundary layer to an equilibrium structure occurs only after a long distance downstream of the reattachment point.

Some quantitative information on reestablishment of equilibrium flow is presented by Bradshaw and Wong (1972), who further analyzed the data of Petryk and Brundrett (1967). Values of h/δ quoted were in the range of 0.18 and 0.53 where h is the height of a single fence; h as well as δ were varied in Petryk's experiments. Bradshaw and Wong used the Clauser parameter to measure the departure of the boundary layer from equilibrium. The Clauser parameter is defined as:

$$G = \frac{\int_o^\delta (\bar{u}\ (\delta) - u\ (z))^2\ dz/u_*^2\ \delta}{\int_o^\delta (\bar{u}\ (\delta) - u\ (z))\ dz/u_*\ \delta} \qquad (2.28)$$

According to the data of Coles (1962), G is about 6.8 in an equilibrium constant-pressure boundary layer at high Reynolds numbers. Values of G downstream of the reattachment point decreased sharply and then increased slowly to an equilibrium value. The distance x_G where G reaches its minimum could be expressed by the empirical relation

$$x_G \propto \sqrt{\delta h} \ , \qquad (2.29)$$

implying that two length scales are to be considered. This is reasonable, since on one hand the disturbance is caused by the length of the separation region, h ; whereas on the other hand, the recovery of the boundary layer depends on the scale of the turbulence, say δ. The proportionality constant in Equation (2.29) is equal to 100 for a fence, but is certainly less for any hill shape.

Depending on h/δ, the minimum value of G changes, i.e., for $h/\delta = 0.18$, $G_{min} = 5.6$ whereas for $h/\delta = 0.53$, $G_{min} = 4.5$.

Round-Crested Hills with $1/4 < h/L_d < 1$

The force balance in the flow over round-crested hills with $1/4 < h/L_d < 1$ is such that the mean flow field may change significantly due to simple surface features. Flow separation over a hill may be caused by a salient edge; however, if the hill has no salient features, change in surface roughness or significant increase in surface shear stress may affect the location of flow separation and thus the velocity field over the crest.

A popular method to predict the separation point of a turbulent boundary layer in an adverse pressure gradient was developed by Stratford (1959) and Townsend (1962). The basic assumption of the method is that the boundary layer can be divided into two distinct and adjacent regions. The flow in the region adjacent to the wall is determined by the local shear stress distribution and is otherwise independent of the past history of the flow. But the flow in the outer region develops nearly independently of the Reynolds stress, implying that the total head stays constant. In addition it is assumed that the Reynolds shear stress stays constant in the outer region.

Unfortunately, application of the Stratford-Townsend method to predict the point of flow separation over a hill is not possible, since a middle region (see Section 2.3) exists which does not possess the characteristics of the inner and outer region as given above. In the middle region, the flow is locally 'inviscid, but Reynolds shear stress may change significantly due to the strong flow distortion. Only if the Reynolds stresses could be predicted in the lowest layer of the middle region, and if the velocity profile in the inner region at the location of the pressure minimum is known, can a similar approach to that of Stratford and Townsend be developed to predict the separation point.

The prediction becomes even more complicated if the surface roughness changes upstream over the hill. Qualitatively the effect of changing surface roughness on the flow is well understood. For some simple flow cases, analytical solutions have been obtained (Townsend, 1976). In general an increase in surface roughness in the flow direction introduces higher shear stresses in the flow. In turn this causes a larger total head loss in the layer adjacent to the surface and consequently an earlier flow separation. A streamwise decrease in surface roughness has the opposite effect. It may be noted that the installation of extensive windmill hardware on a hill may itself induce earlier flow separation and consequently less speedup of the wind.

The effect of surface roughness on flow separation over a circular cylinder was investigated by Güven, Patel, and Farrell (1976). Although their semi-analytical approach may seem not directly applicable to flow over hills, the experimental results show the effect of surface roughness. Since their approach turbulence is weak and of a large-scale, their results may be interpreted as being the effect of increased surface roughness over a hill relative to upstream conditions. Some of their results for a Reynolds number of 10^7 are presented in the table below.

$\frac{z_o}{d}$	C_{pb}	C_{pm}	ϕ_w	$\frac{U_{pm}}{U_\infty}$
10^{-5}	-0.62	-2.04	111.5	1.74
10^{-4}	-0.80	-1.91	105.6	1.71

where z_o is the equivalent roughness height,
d is the cylinder diameter,
C_{pb} is the base pressure coefficient,
C_{pm} is the minimum pressure coefficient, and
ϕ_w is the approximate angle of beginning of the wake region measured from front stagnation point.

U_{pm}/U_∞ is the relative velocity increase at the pressure minimum. The effect of a change in ϕ_w of 6° causes a 2 percent change in maximum velocity over the cylinder. Although this is not a significant effect over cylinders, for hills the effect of surface roughness on the location of separation point may be much larger because the hill slope at the downstream side decreases in the flow direction.

An interesting illustration of the effects of upwind turbulence (e.g., due to large upwind surface roughness) is offered in an investigation by Halitsky (1965). He noticed that in boundary-layer flow over a ridge ($h/\delta = 3$, $h/L_u \simeq \frac{3}{8}$, $h/L_u \simeq \frac{3}{8}$) downwind flow separation occurred for upwind freestream turbulence intensities of 1 percent, whereas for large upwind turbulence intensities of 15 percent periodic collapse of the wake occurred.

For smooth surfaces, the Reynolds number also influences flow separation. Flow separation is essentially due to viscous effects; thus the separation point will depend on the Reynolds number. Model results may require correction for the effective Reynolds number variation between field and laboratory.

Other than the material previously reviewed, little further material speaks to separation over shapes with salient corners or crests.

Hills with a Salient Edge and with Slopes, Say $\frac{1}{4} < h/L_d < \frac{1}{2}$

The strength of the eddy in the separation region, of course, has an important effect on the size of the wake. If the downstream slope is small, then the eddy stays small causing a weak interaction between wake and mainflow. Quantitative information about the important effect of hill slopes on wake size and velocity speedup over the hill is not available in the literature. In Chapter 3 data is presented that systematically shows the effect of hill slope on the size of the separation region.

2.4 SUMMARY

The following summary of the most important conclusions made in this chapter serves as a review of present understanding of flow over an isolated ridge and provides a basis for the experimental program discussed in the following chapters.

1. Three regions in the flow are distinguished
   a. An Inner Region. In this region Reynolds shear stress gradients are of the same order of magnitude as pressure or inertial gradients. Production and dissipation rates of turbulence are the dominant terms in the turbulence kinetic energy equations. The large mean velocity gradients are characteristic of this region.
   b. A Middle Region. In this region Reynolds stress gradients are locally insignificant but may cause substantial changes in total head downwind of the first flow disturbance. The changes

in total head may be large since extra rates of strain affect Reynolds shear stresses, often one order of magnitude larger than expected. Nevertheless, for relatively short hills ($L < \delta$) with large extra strain ratios, changes in Reynolds stresses are small since it takes time for the stress-bearing eddies to adjust to the mean flow conditions. An order of magnitude analysis and experimental data show that for such flow cases total head changes over the crest are usually less than 4 percent. Generally, the order of magnitude analysis indicates that the flow field upwind of the ridge crest can be predicted accurately by assuming the fluid to be inviscid.

c. An Outer Region. Extra strain rates are small and do not affect the turbulence nor the total head losses.

2. The upwind separation region is small compared with the downwind separation region because interaction between upwind wake and main flow is impeded by the presence of the ridge. For sufficiently large vorticity in the approach flow (in other words, for a sufficiently small ratio h/δ), the upwind separation region is not affected by the interaction between wake and main flow. Otherwise interaction takes place and, with the present understanding of such flow cases, empiricism has to enter analytical-prediction procedures. No quantitative information is available on the amount of vorticity required to avoid interaction.

3. A large wake resulting from main-flow wake interaction affects the mean flow over a hill and downwind of a hill dramatically. The new shear layer causes the boundary layer downwind of the reattachment point to be in strong nonequilibrium. Up to distances of the order of $100\sqrt{h\delta}$ the Clauser parameter decreases, after which a return to equilibrium flow conditions takes place. Therefore prediction of the flow field over a group of ridges is extremely complex. The occurrence of flow separation over downwind ridges may be strongly affected.

4. Existing prediction techniques of flow separation over ridges are not adequate. There exists some experimental evidence that changes in surface roughness affect the occurrence of flow separation over steep ridges ($h/L \tilde{>} .3$) significantly. Qualitatively, the effects

of surface roughness are understood, i.e., an increase in upwind surface roughness causes earlier flow separation whereas a decrease in upwind roughness causes a later flow separation.

5. The length of the downwind separation region is reduced by shallower downwind slopes since the eddy development in this region is impeded by the presence of an elevated surface in the separation region.

3.0 MEAN FLOW OVER RIDGES

The following three chapters discuss laboratory data measurements made under this program and describes quantitatively the effects of ridge shape, turbulence and surface roughness, and moderate stable stratification on the mean flow over ridges. Data are utilized to prepare an empirical wind speed prediction relation in Chapter 4.0. Changes in the turbulence structure over the ridge as a result of the distortion by the mean flow are interpreted using rapid distortion principles in Chapter 5.0. A brief review on the limitations of the physical modeling techniques employed is provided in Appendix F. Flow conditions and hill shapes have been characterized by simple nondimensional parameters defined in that Appendix.

Section 3.1 evaluates the influence of ridge shape on wind speedup over hill crests. The important role of separation on speedup is identified and a criterion for flow separation is provided. The data are used to validate the inviscid approach identified in Section 2.2.

Section 3.2 examines the influence of turbulence and surface roughness on wind speed over hills. An inviscid numerical program described in Appendix E, Section 3.3 was used to extend the results beyond those measured in the laboratory. The influence of turbulence on wind profiles was suggested by the analysis in Chapter 2.0 to be significant only in an inner and middle region near the surface. Comparison of model data against a recent field study revealed the unexpected influence of relaminarization on the inner regions during model measurements.

Section 3.3 considers the influence of stable stratification on the mean velocity profile, the character of the hill crest turbulence, and the extent of separation. Mild stratification appears to result in rather modest perturbations.

Section 3.4 examines the validity of the assumption of two-dimensionality when dealing with real finite-length ridges. A finite hill length reduces hill crest and speedup, modifies the separation region, and results in lateral wind field variations. Nevertheless for the cases considered perturbations were modest.

3.1 EFFECT OF RIDGE SHAPE ON VELOCITY PROFILES

The ridge shape is characterized by 3 parameters, namely h/L_u, h/L_d and h/δ. In addition to these three parameters, the presence of salient features on a ridge is considered in this section.

The effect of ridge shape on wind flow will be considered separately in terms of upwind and downwind slopes, the height of the hill with respect to the atmospheric boundary layer, and the detailed hill profile.

Upwind and Downwind Slopes. The highest ridge in hilly terrain is not necessarily the site where the largest speedup of the wind occurs. At ridge crests where flow separation is present the wind speedup is less than at ridge crests that avoid flow separation. Hence, speedup depends also on the upwind and downwind slopes.

Figures 3.1 to 3.9 show the dramatic changes in mean velocity, static pressure and longitudinal turbulence intensity that accompany flow separation. In these figures and subsequet plots the distance from the crest to the base is 2.5 times the height of the hill (except for Figures 3.7 and 3.9 where it is 5 times the height of the hill). Similar, but enlarged, contour plots of mean velocities and static pressures are presented in Appendix D.

Flow separation occurs for $h/L = 1/2$ and $1/3$; however, no flow separation occurs for $h/L = 1/4$. Static pressure perturbations for the ridges with $h/L = 1/2$, $1/3$ and $1/20$ penetrate deep into the boundary layer, causing slightly higher velocities in the upper region of the boundary layer. Note that the contour lines of the static pressure distribution at the downwind side of the crest for $h/L = 1/2$ and $1/3$ approximately follow the streamlines. This phenomenon is typical for flow separation over ridges. It shows clearly that pressure gradients across streamlines may be much larger than the gradients in the streamwise direction. Therefore, mathematical models in which the $\partial p/\partial z$ term in the equations of motion has been neglected, such as the model of Frost et al., 1977 (see Appendix E, Section E.4) do not represent the flow accurately.

Measurements over various ridge models were performed for two different freestream velocities to identify any Reynolds number flow dependence. Figures 3.1, 3.3, 3.5, 3.7, and 3.9 show contour plots for $U_\infty = 9.14$ m/sec. Figures 3.2, 3.3, 3.4, and 3.6 show contour plots for $U_\infty = 15.24$ m/sec. No significant changes in the flow field occur for different wind velocities. Figures 3.10 to 3.13 are contour plots over two round-crested hills (half-sine

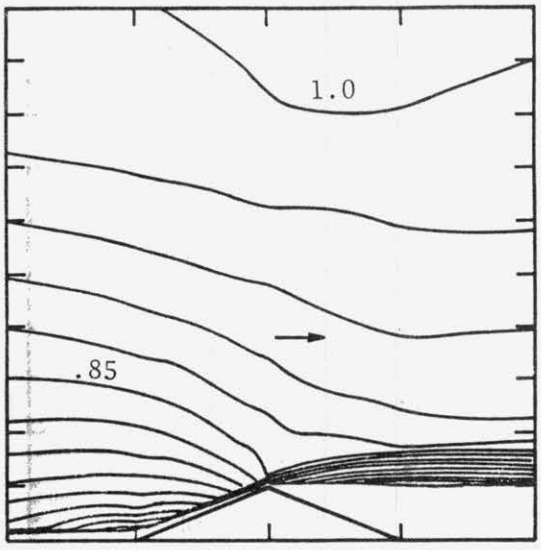

a. Mean longitudinal velocity, $\Delta u/\bar{u}_o$ (δ) = 0.5

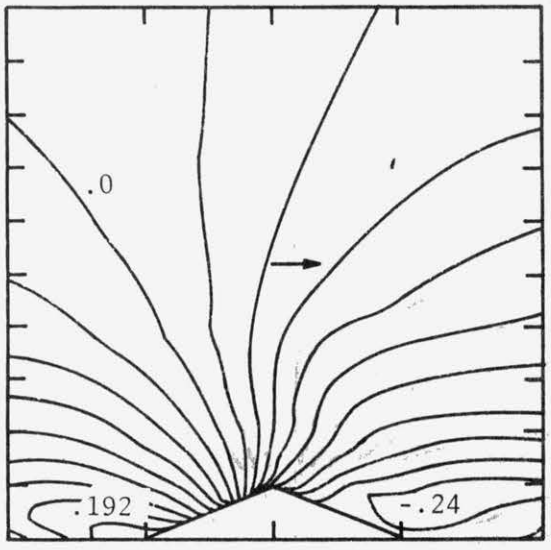

b. Static pressure, ΔC_p = 0.27

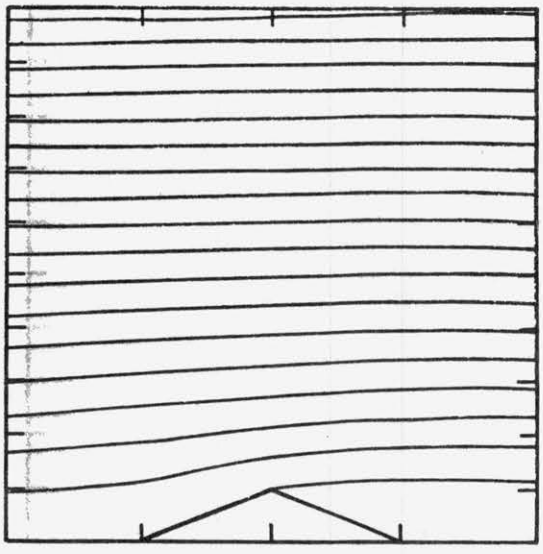

c. Streamlines

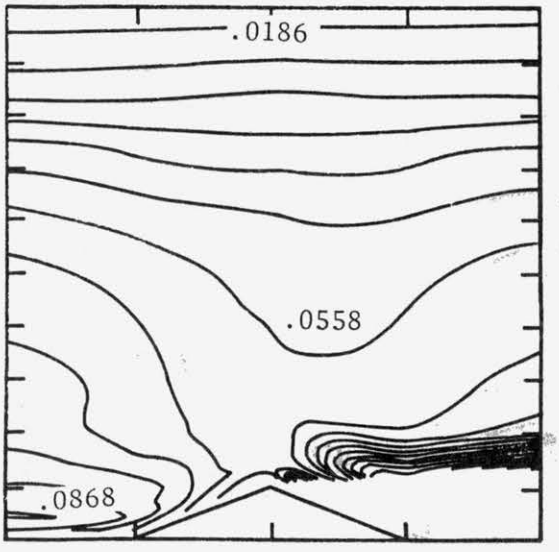

d. Longitudinal turbulence intensity, $\Delta u'/\bar{u}_o$ (δ) = .0062

FIGURE 3.1. Contours of Flow Characteristics Over a Triangular Ridge, h/L = 1/2. Test Case 1

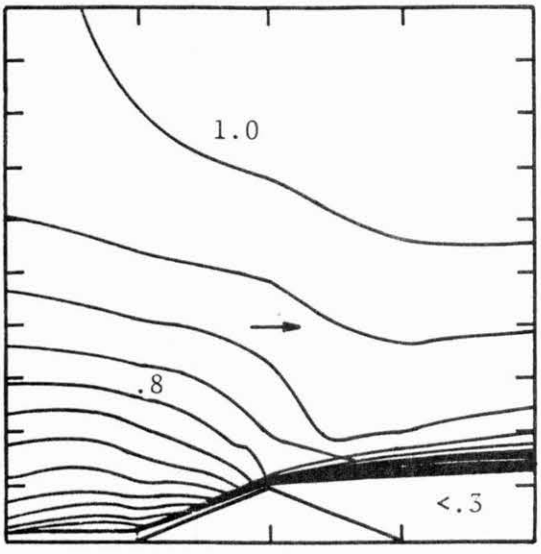

a. Mean longitudinal velocity, $\Delta u/\bar{u}_o$ (δ) = .05

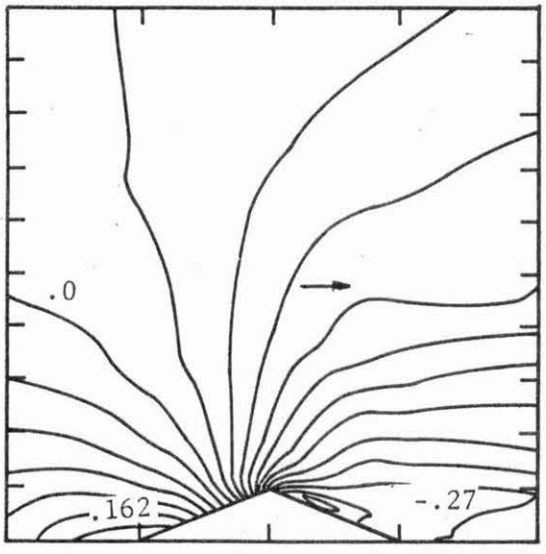

b. Static pressure, ΔC_p = 0.27

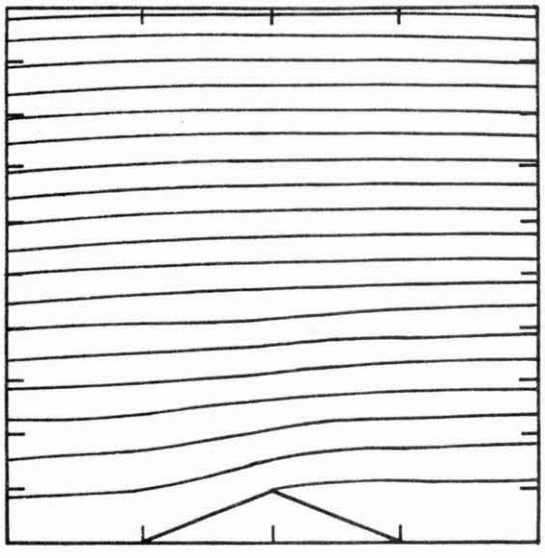

c. Streamlines

FIGURE 3.2. Contours of Flow Characteristics Over a Triangular Ridge, h/L = 1/2. Test Case 2

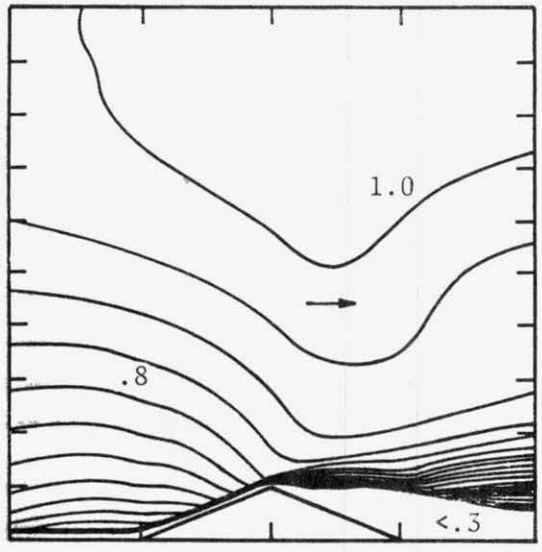

a. Mean longitudinal velocity, $\Delta u/\bar{u}$ (δ) = .05

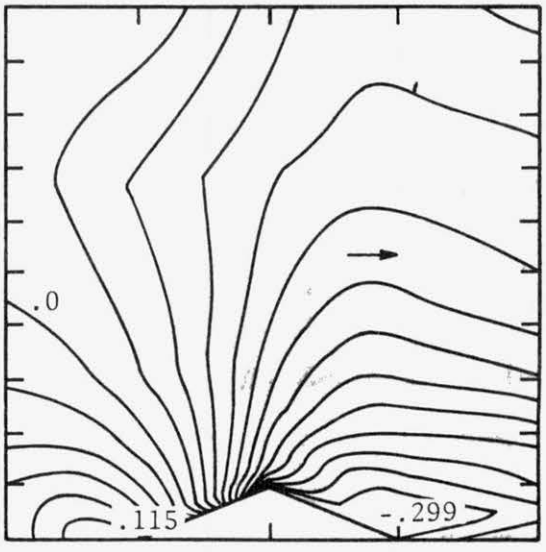

b. Static pressure, ΔC_p = .023

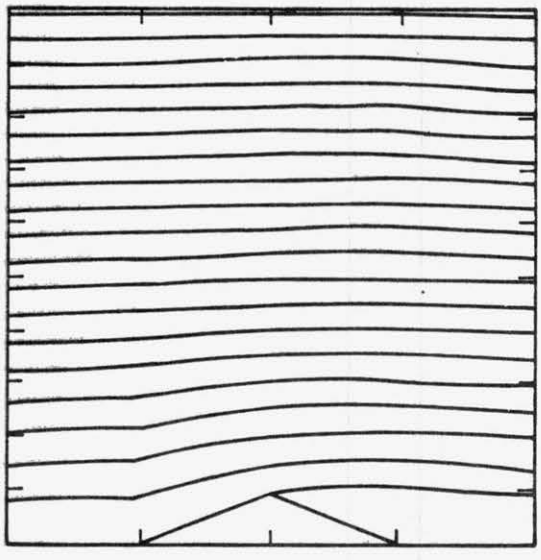

c. Streamlines

FIGURE 3.3. Contours of Flow Characteristics Over a Triangular Ridge, h/L = 1/3. Test Case 3

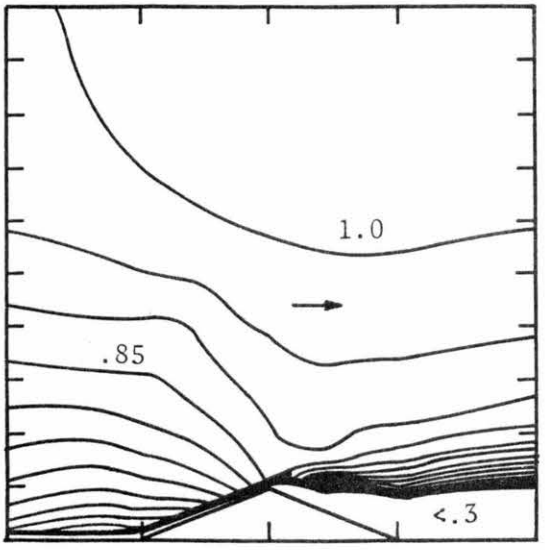

a. Mean longitudinal velocity, $\Delta u/\bar{u}_o$ $(\delta) = 0.5$

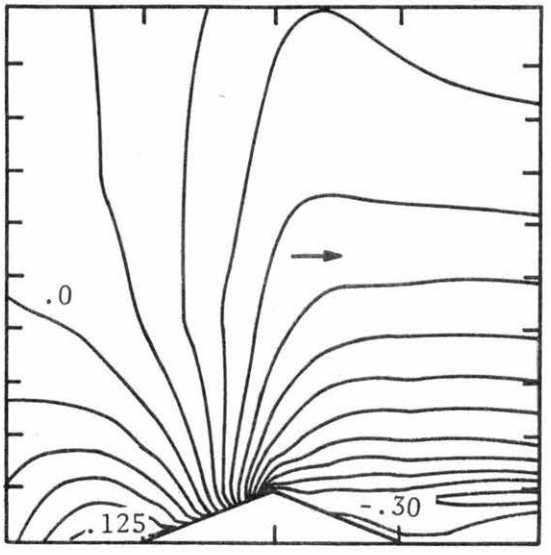

b. Static pressure, $\Delta C_p = .025$

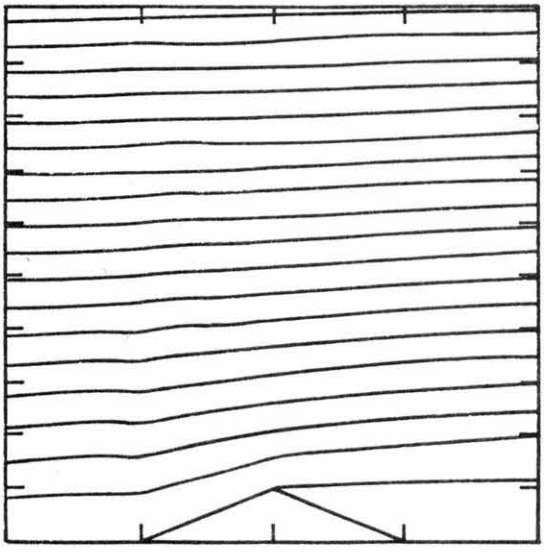

c. Streamlines

FIGURE 3.4. Contours of Flow Characteristics Over a Triangular Ridge, h/L = 1/3. Test Case 4

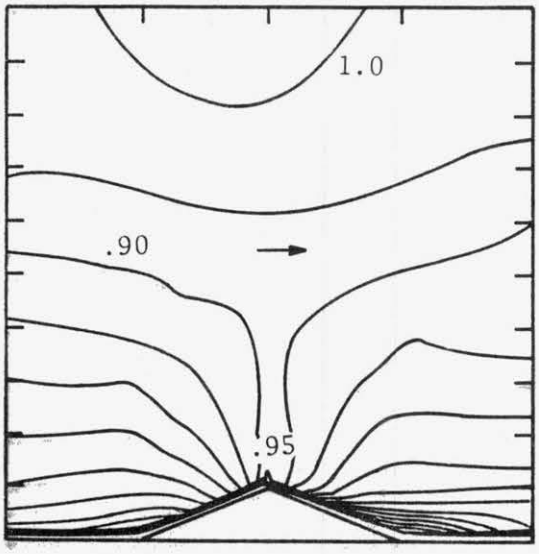

a. Mean longitudinal velocity, $\Delta u/\bar{u}_o$ (δ) = 0.5

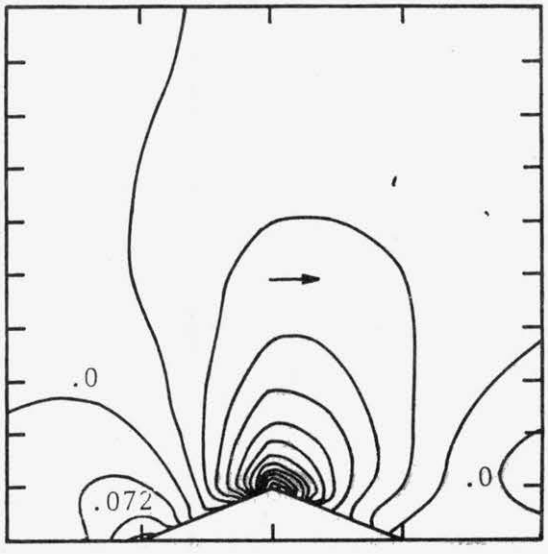

b. Static pressure, ΔC_p = .036

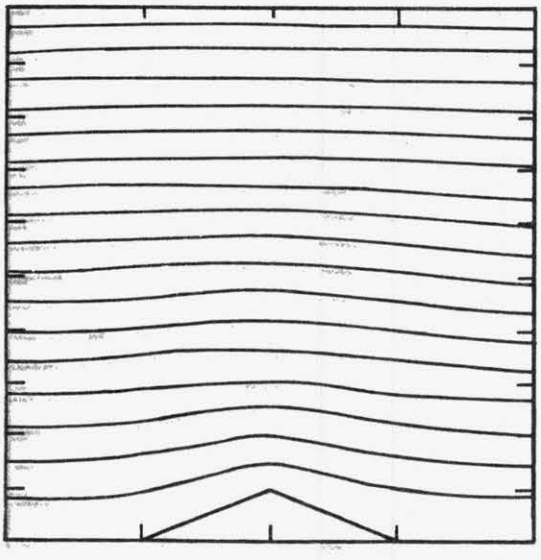

c. Streamlines

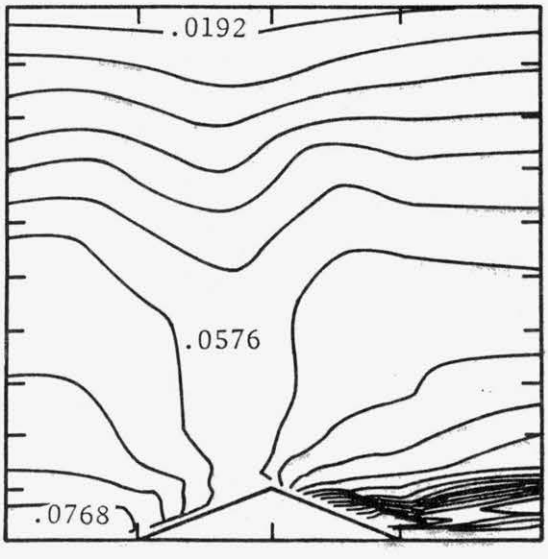

d. Longitudinal turbulence intensity, $\Delta u'/\bar{u}_o$ (δ) = .0064

FIGURE 3.5. Contours of Flow Characteristics Over a Triangular Ridge, h/L = 1/4. Test Case 5

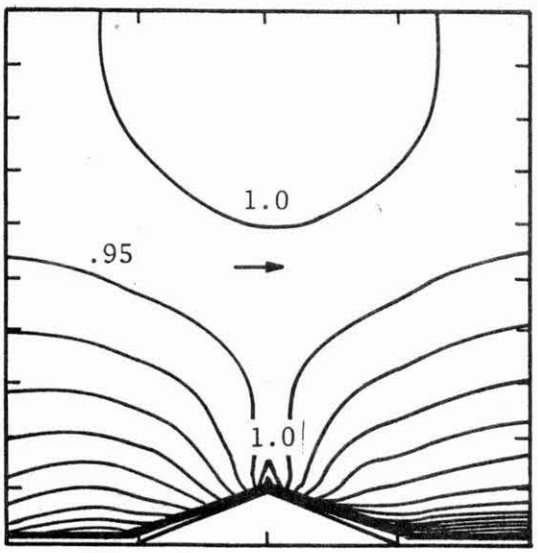

a. Mean longitudinal velocity, $\Delta u/u_o$ (δ) = .05

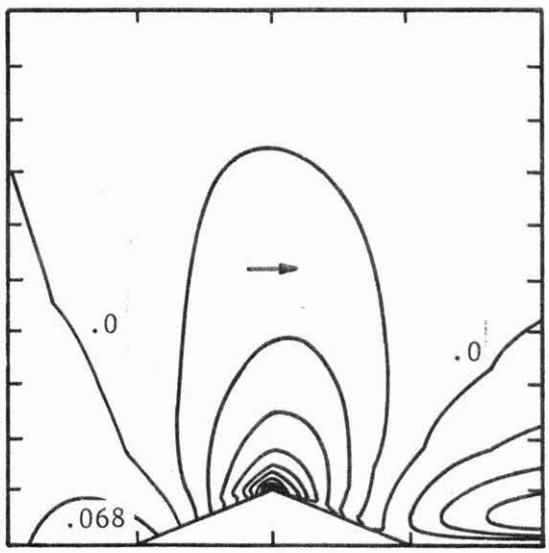

b. Static pressure, ΔC_p = .068

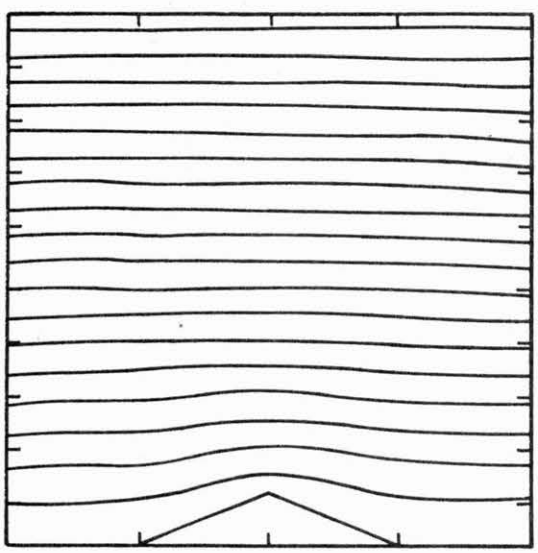

c. Streamlines

FIGURE 3.6. Contours of Flow Characteristics Over a Triangular Ridge, h/L = 1.4. Test Case 6

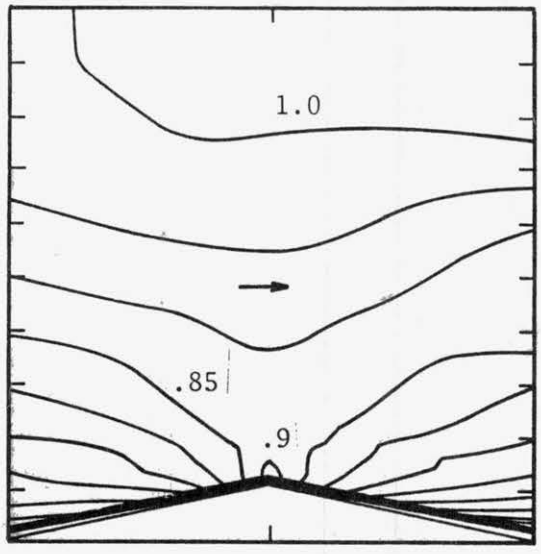

a. Mean longitudinal velocity, $\Delta u/\bar{u}_o$ (δ) = .05

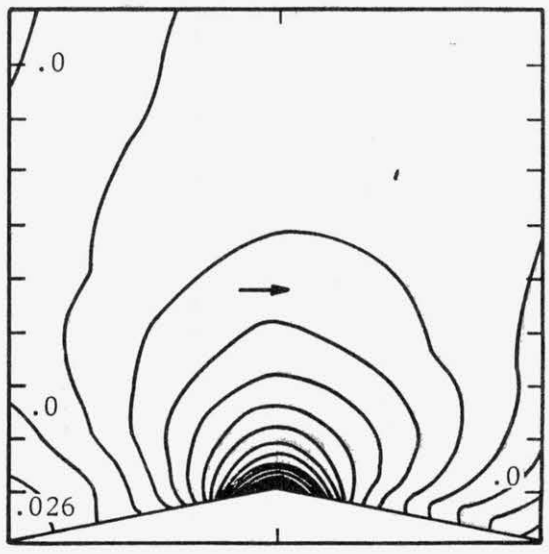

b. Static pressure, ΔC_p = .026

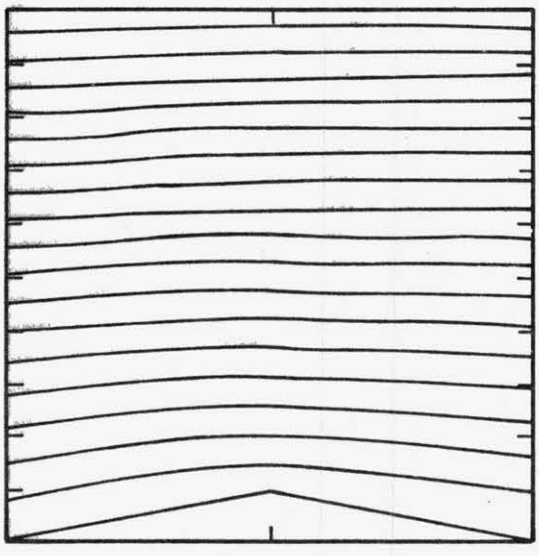

c. Streamlines

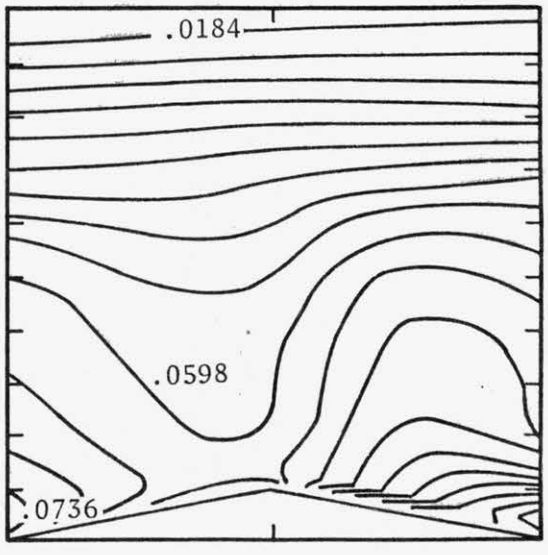

d. Longitudinal turbulence intensity, $\Delta u'/\bar{u}_o$ (δ) = .0046

FIGURE 3.7. Contours of Flow Characteristics Over a Triangular Ridge, h/L = 1/6. Test Case 7

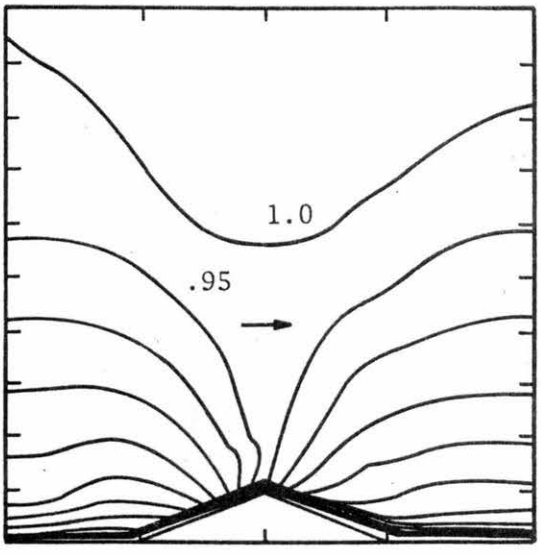

a. Mean longitudinal velocity, $\Delta u/\bar{u}_o$ (δ) = .05

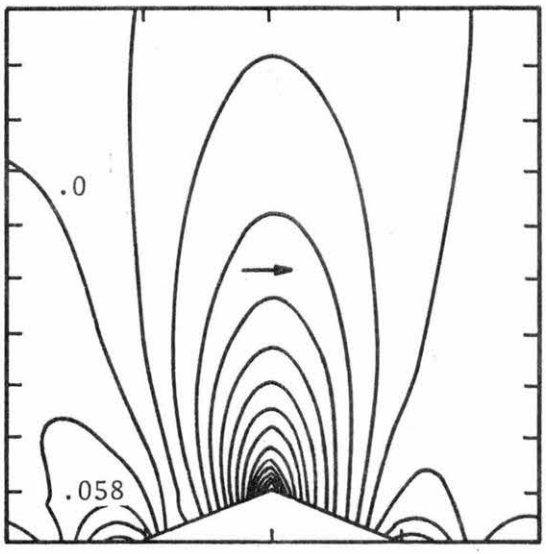

b. Static pressure, ΔC_p = .029

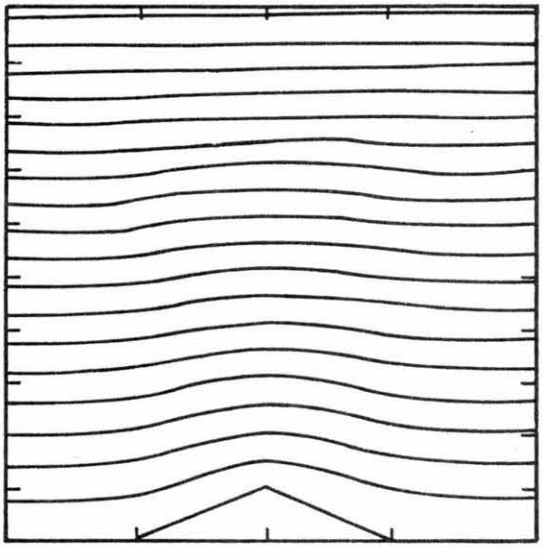

c. Streamlines

FIGURE 3.8. Contours of Flow Characteristics Over a Triangular Ridge, h/L = 1/6. Test Case 8

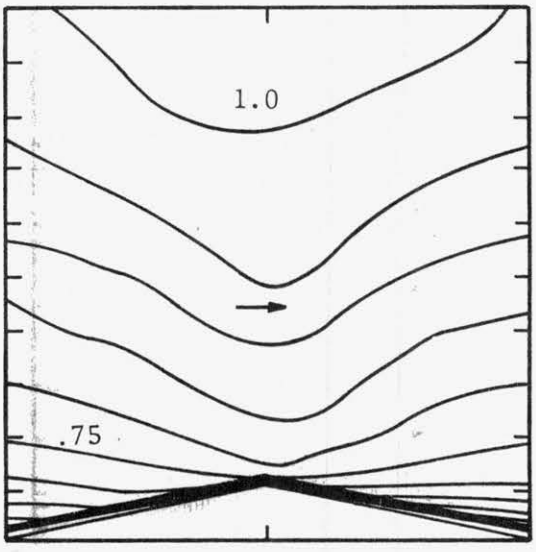

a. Mean longitudinal velocity, $\Delta u/\bar{u}_o$ (δ) = .05

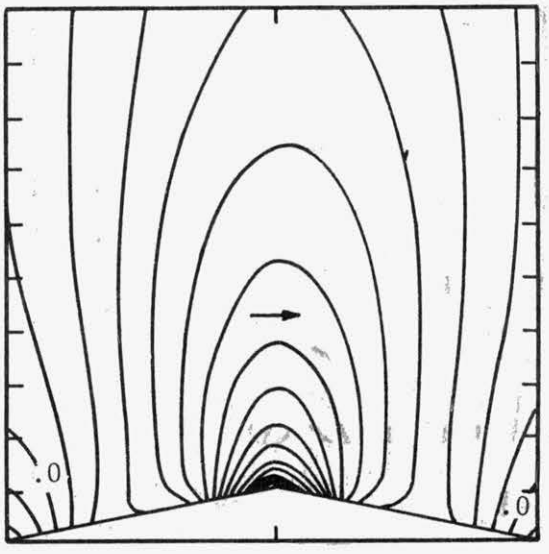

b. Static pressure, ΔC_p = .015

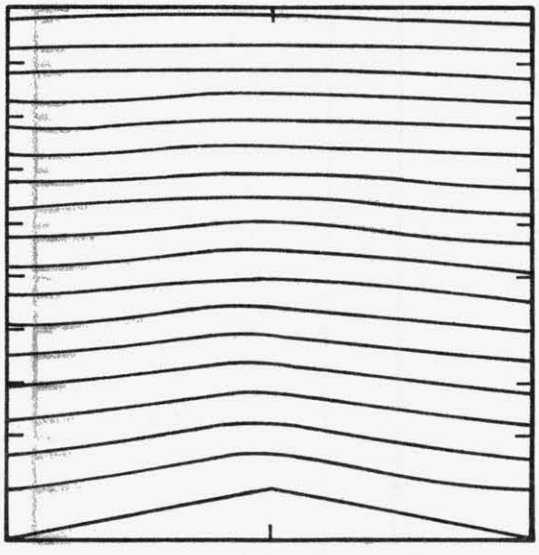

c. Streamlines

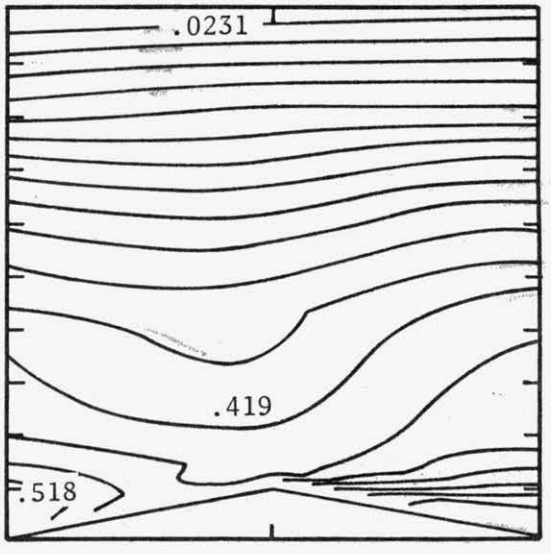

d. Longitudinal turbulence intensity, $\Delta u'/\bar{u}_o$ (δ) = .0033

FIGURE 3.9. Contours of Flow Characteristics Over a Triangular Ridge, h/L = 1/20. Test Case 9

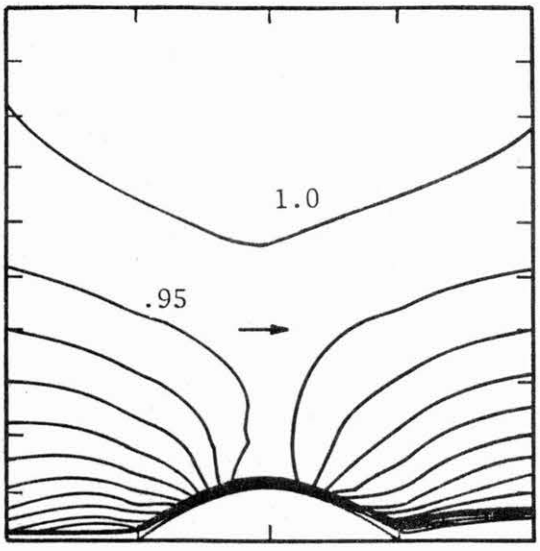

a. Mean longitudinal velocity, $\Delta u/\bar{u}_o$ (δ) = .05

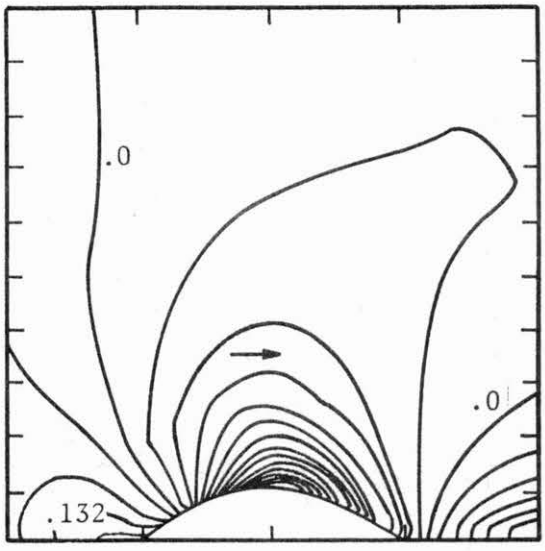

b. Static pressure, ΔC_p = .004

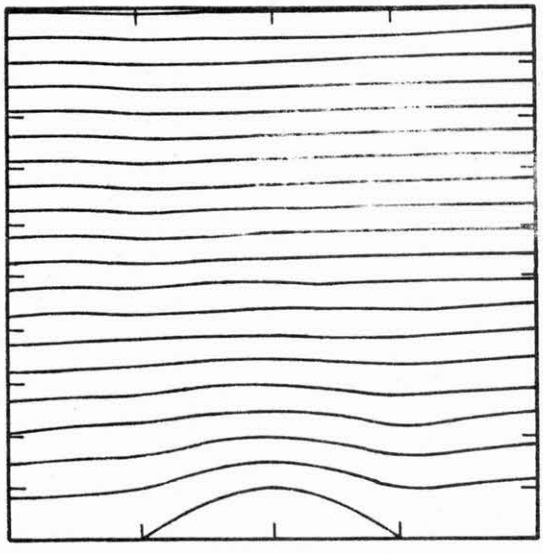

c. Streamlines

FIGURE 3.10. Contours of Flow Characteristics Over a Sinusoidal Ridge, h/L = 1/4. Test Case 10

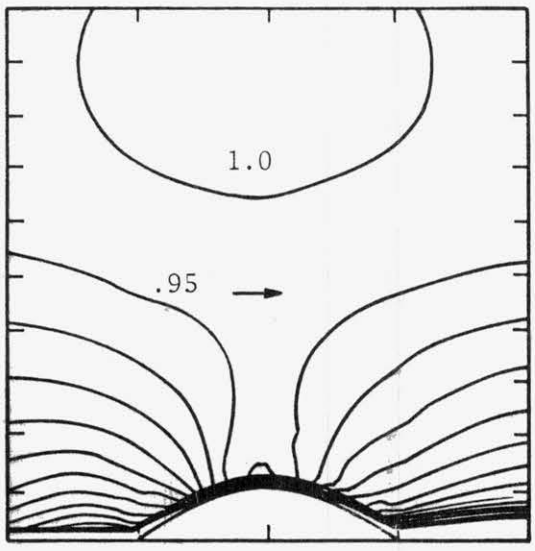

a. Mean longitudinal velocity, $\Delta u/\bar{u}_o$ (δ) = .05

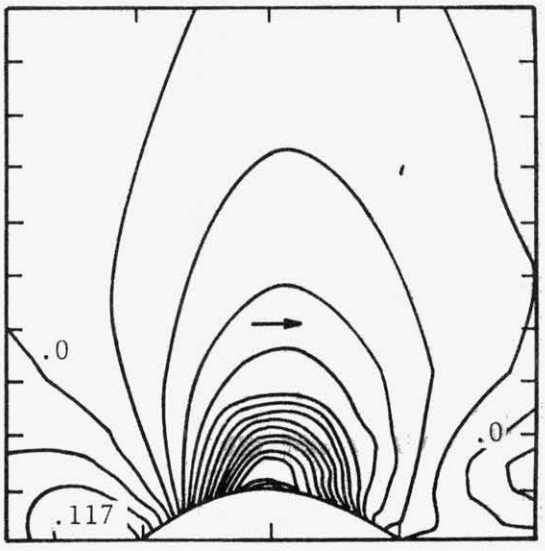

b. Static pressure, ΔC_p = 0.44

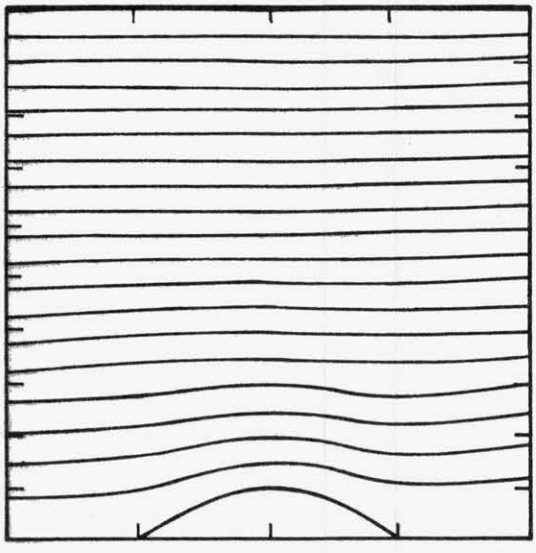

c. Streamlines

FIGURE 3.11. Contours of Flow Characteristics Over a Sinusoidal Ridge, h/L = 1/4. Test Case 11

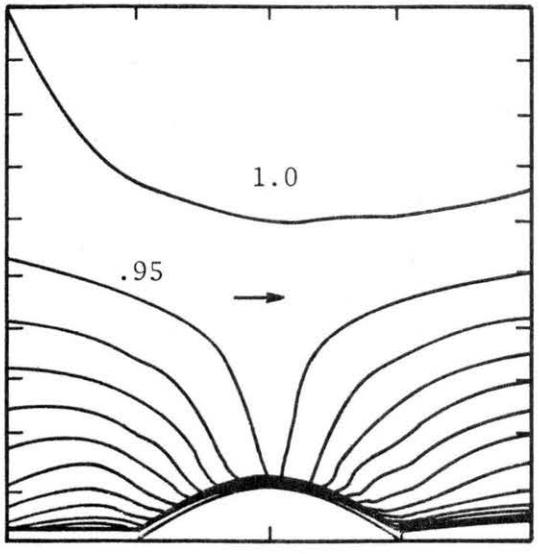

a. Mean longitudinal velocity, $\Delta u/\bar{u}_o$ (δ) = .05

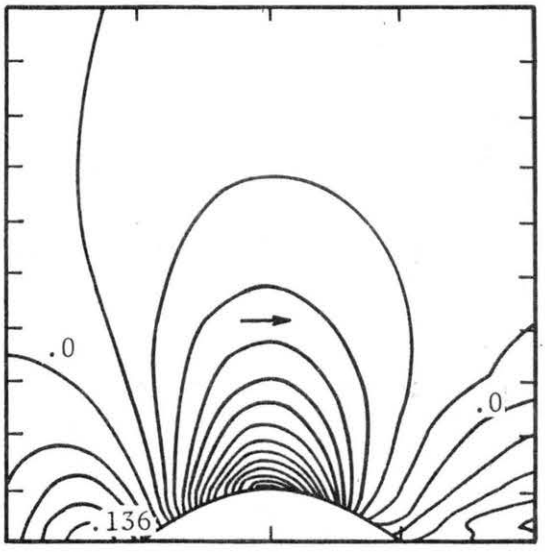

b. Static pressure, ΔC_p = .034

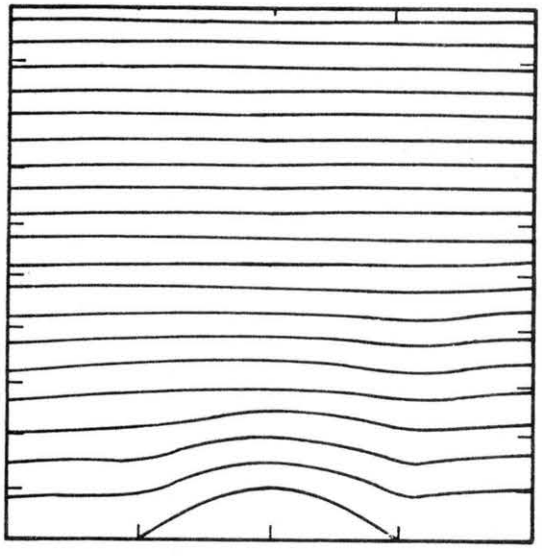

c. Streamlines

FIGURE 3.12. Contours of Flow Characteristics Over a Sinusoidal Ridge, h/L = 3/16. Test Case 12

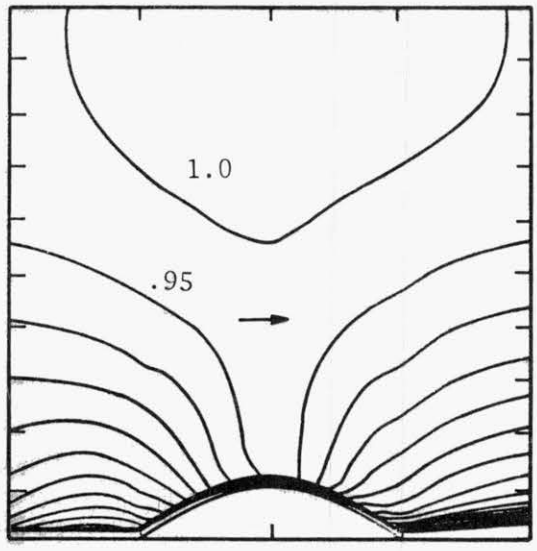

a. Mean longitudinal velocity, $\Delta u/\bar{u}_o$ ($\hat{o}$) = .05

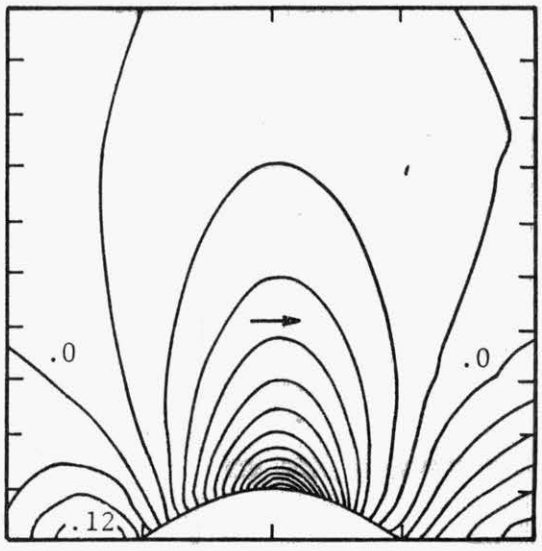

b. Static pressure, ΔC_p = .040

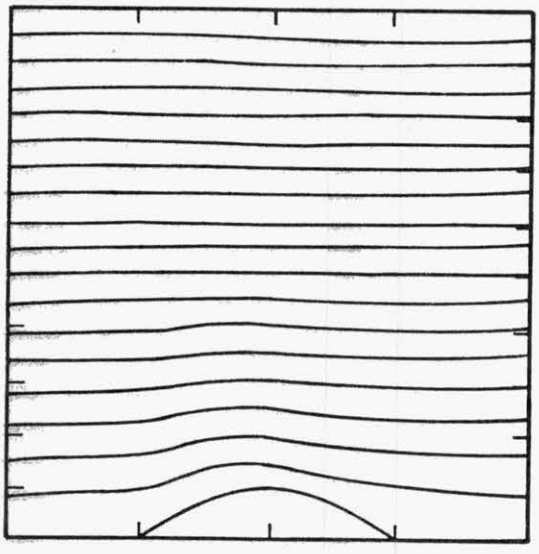

c. Streamlines

FIGURE 3.13. Contour of Flow Characteristics Over a Sinusoidal Ridge, h/L = 3/16. Test Case 13

shaped) for U_∞ = 9.14 m/s and U_∞ = 15.24 m/s. The average slopes defined by h/L_b are 1/3 and 1/4; those defined by h/L are 1/4 and 3/16. Flow separation does not occur in any of these cases. No Reynolds number effects are noticeable. The mean flow fields closely resemble the flow field over the triangular hill h/L = 1/4, but do not resemble the triangular hill h/L = 1/3. Apparently the definition of L characterizes the hill length better than L_b.

Flow separation that may occur upwind of a hill is different from flow separation that may occur downwind. The eddy in the downwind separation region interacts strongly with the main flow, producing an extended wake in the downwind direction. For steep downwind slopes the separation region may extend to a distance of 10 to 20 times the obstacle height. The interaction between eddy and main flow at the upwind side is constrained by the presence of the hill. The upwind separation region, which depends slightly on the parameter h/δ, does not extend further than two hill heights upwind. Flow separation occurs if $h/L_u > 1/2$.

High velocities over the crest result in large static pressure gradients across streamlines just above the separated flow region. These large pressure gradients result in earlier reattachment of the separating streamline. Indeed, Figure 3.14 suggests the separated flow region for h/L_u = 1/2 extended beyond a distance of x = 9h, but that the flow reattached at x = 9h for h/L_u = 1/4 and 1/6. Figures 3.15 and 3.16 display similar trends.

The extent of the downstream separation region depends on the strength of the eddy just downwind of the separation point, which in turn are dependent on both upstream and downstream hill slopes. Figure 3.14 shows vertical mean velocity profiles over the crest and downwind of the crest for three different ridge shapes. In all cases there is a backward-facing step. The upwind slope varies: h/L_u = 1/2, 1/4, and 1/6. Speedup is largest for h/L_u = 1/4, and is slightly less for h/L_u = 1/6. The speedup is smallest for h/L_u = 1/2. For relatively gentle downwind slopes only weak eddies can develop. This causes early reattachment of the separating streamline. The effect of h/L_d on the mean velocity field is illustrated in Figure 3.17 by superimposing vertical velocity profiles at different locations downwind of the hills. For all cases h/L_u = 1/2; the downwind slopes were h/L_d = 1/0, 1/3, 1/4, and 1/6. The boundary layer recovers faster for the smaller values of h/L_d. A significantly larger speedup over the hill crest occurs for h/L_d = 1/6. Similar

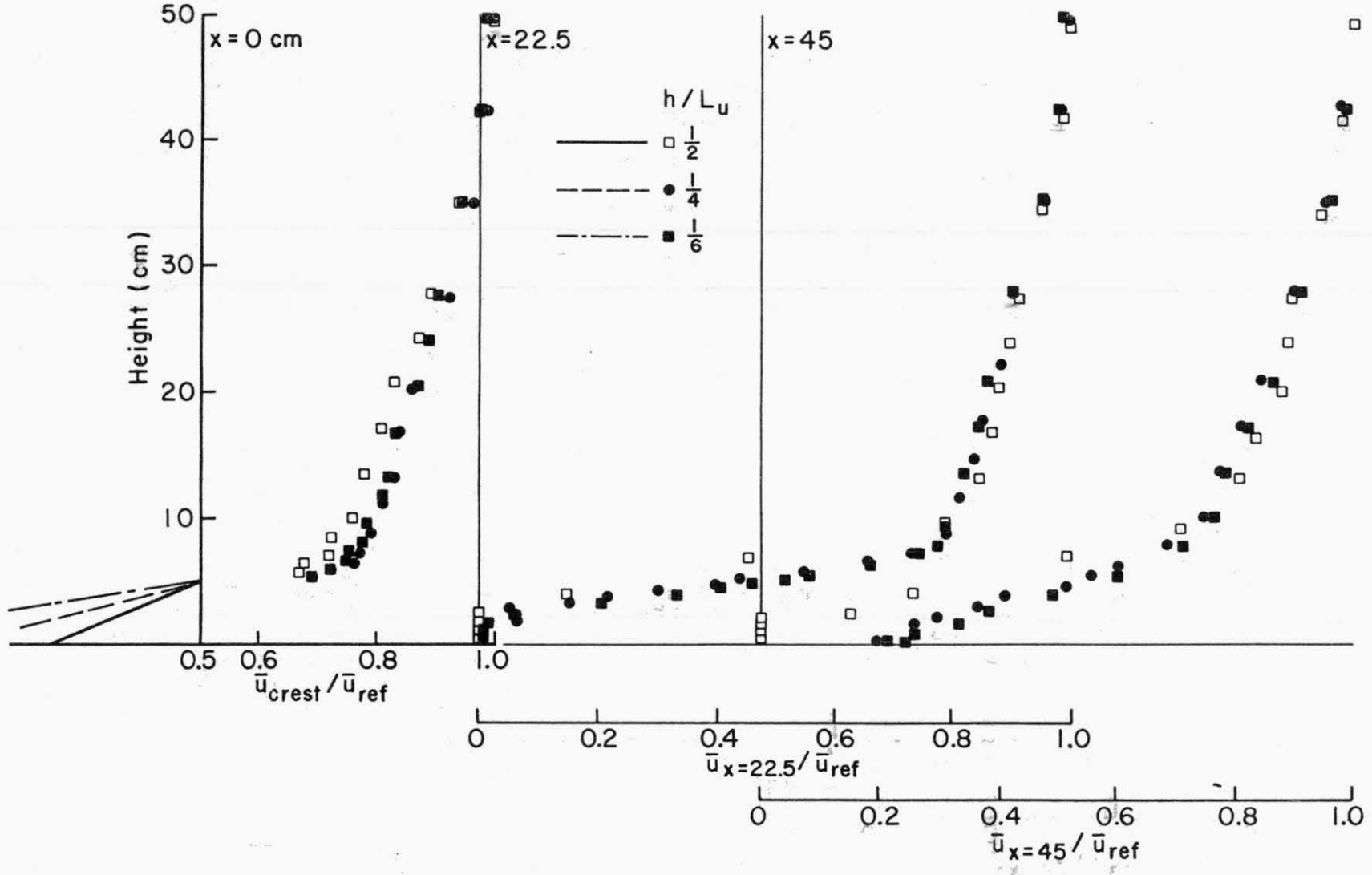

FIGURE 3.14. Mean Velocity Profiles Downwind of a Triangular Hill h/L_d = 1/10 and h/L_u = 1/2, 1/4 and 1/6. Test Cases IX, XI, and X

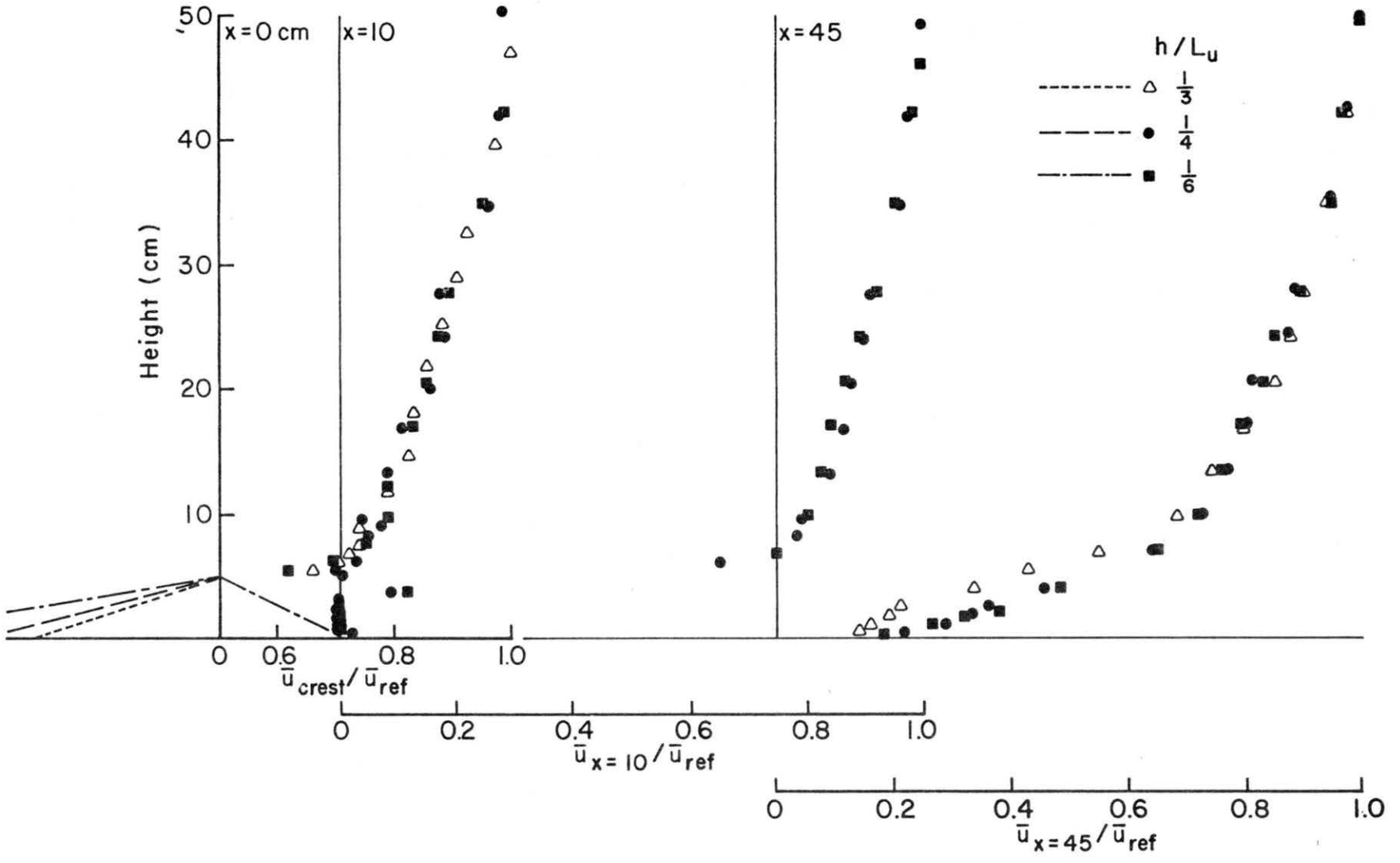

FIGURE 3.15. Mean Velocity Profiles Downwind of a Triangular Hill $h/L_d = 1/2$ and $h/L_u = 1/3$, 1/4 and 1/6. Test Cases VIII, IV, and VI

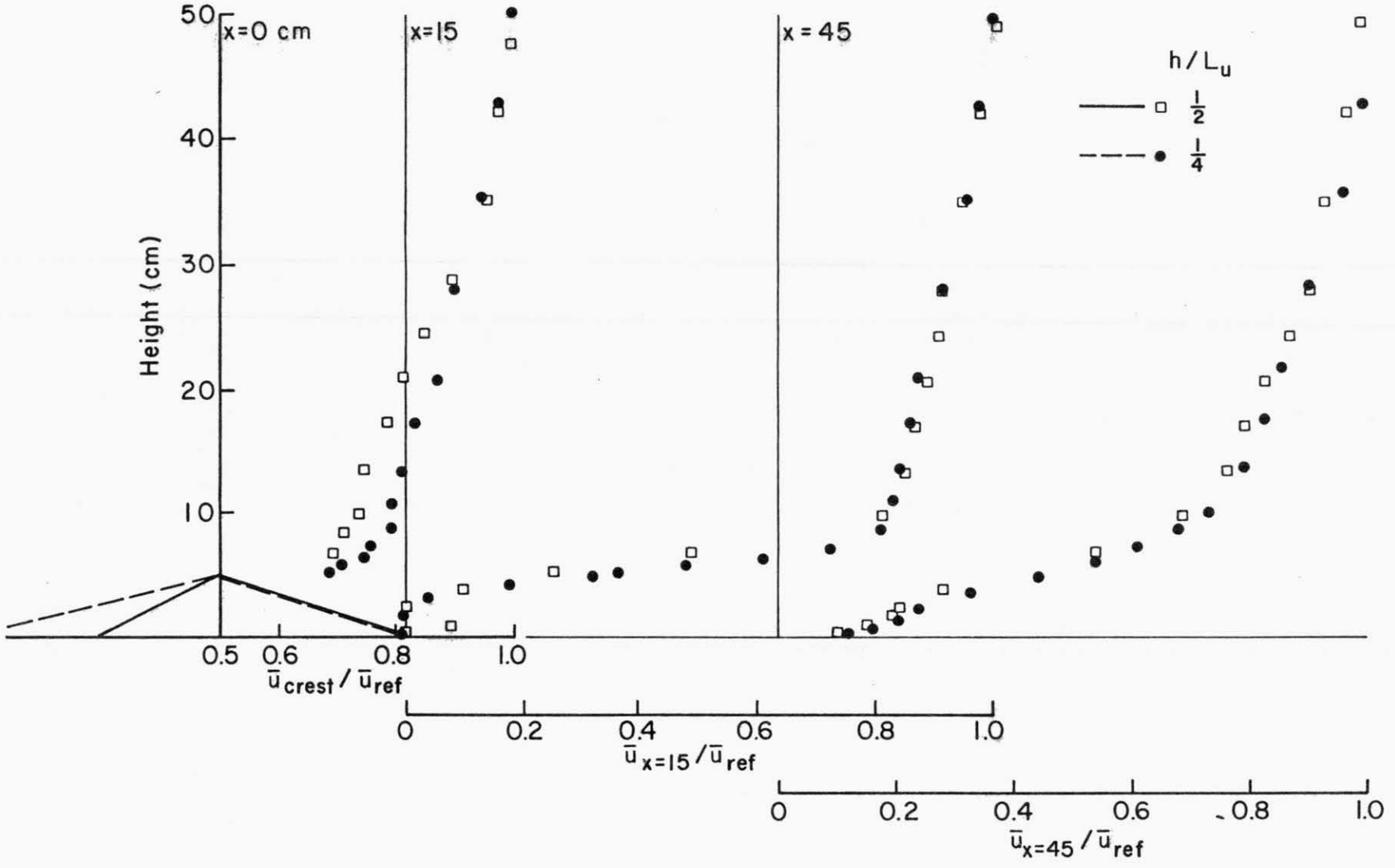

FIGURE 3.16. Mean Velocity Profiles Downwind of a Triangular Hill $h/L_d = 1/3$ and $H/L_u = 1/2$ and $1/4$. Test Cases VII and II

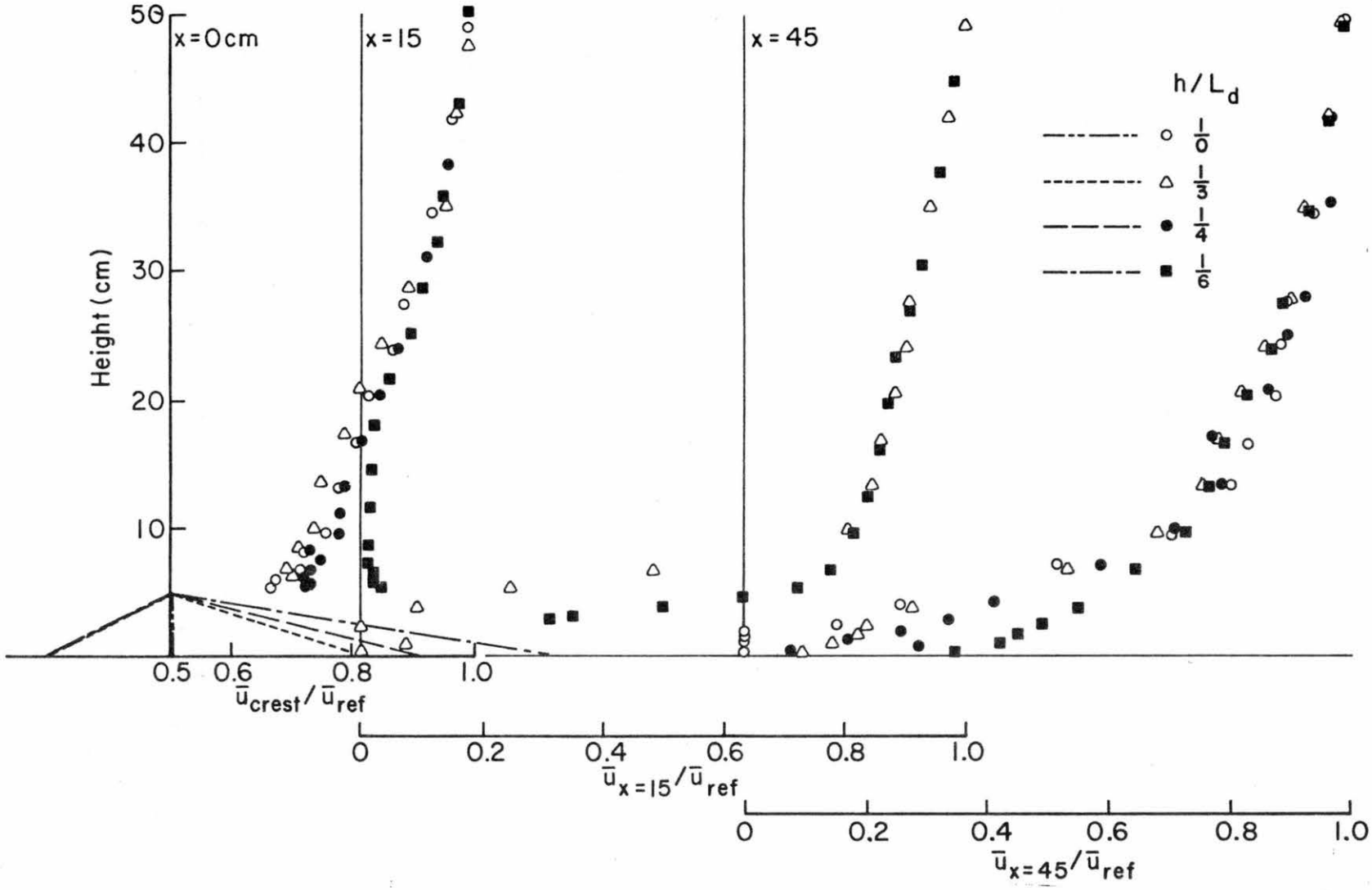

FIGURE 3.17. Mean Velocity Profiles Downwind of a Triangular Hill h/L_u = 1/2 and h/L_d = 1/0, 1/3, 1/4 and 1/6. Test Cases IX, VII, III and V

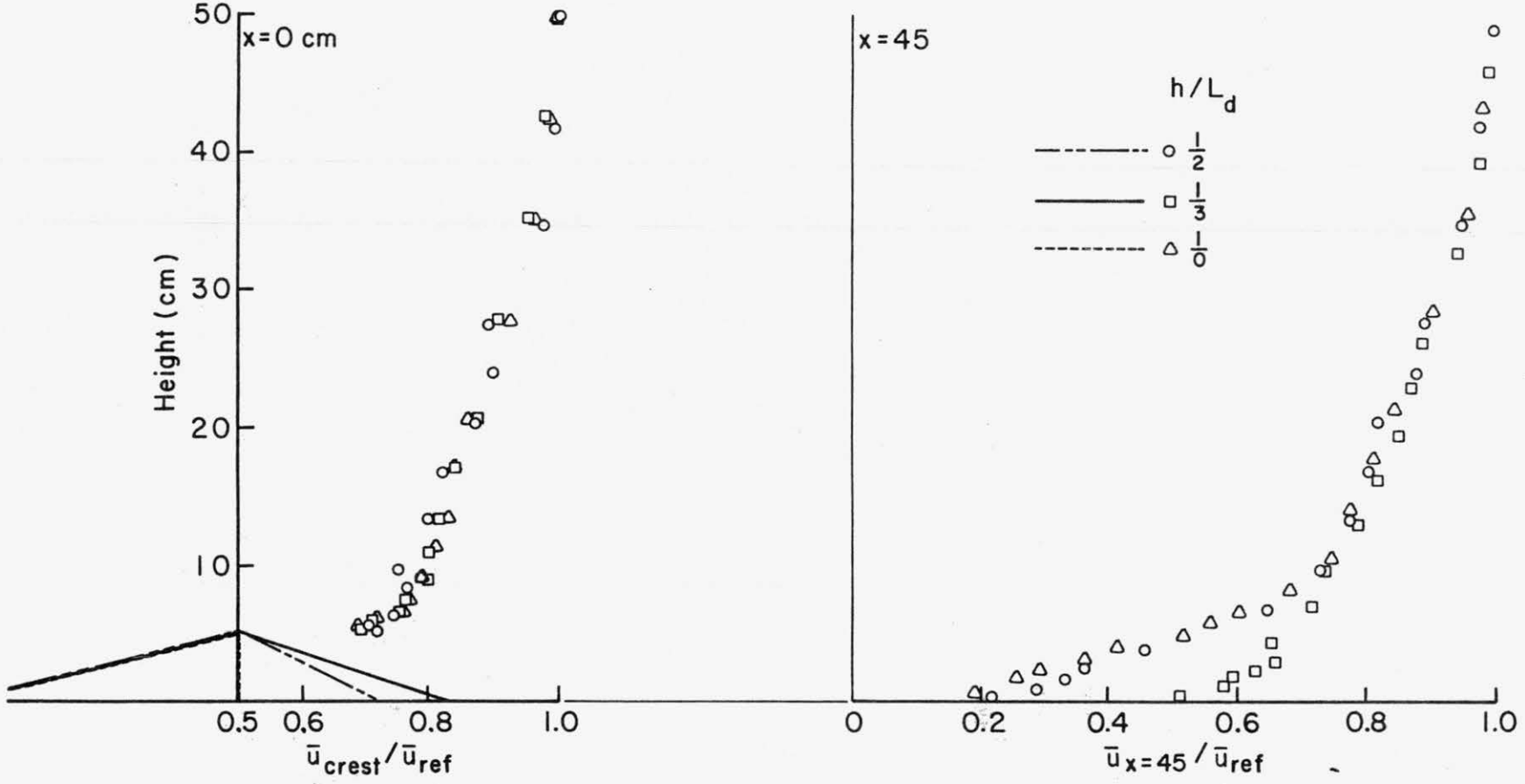

FIGURE 3.18. Mean Velocity Profiles Downwind of a Triangular Hill $h/L_u = 1/4$ and $h/L_d = 1/10$, 1/2, and 1/3. Test Cases XI, IV and II

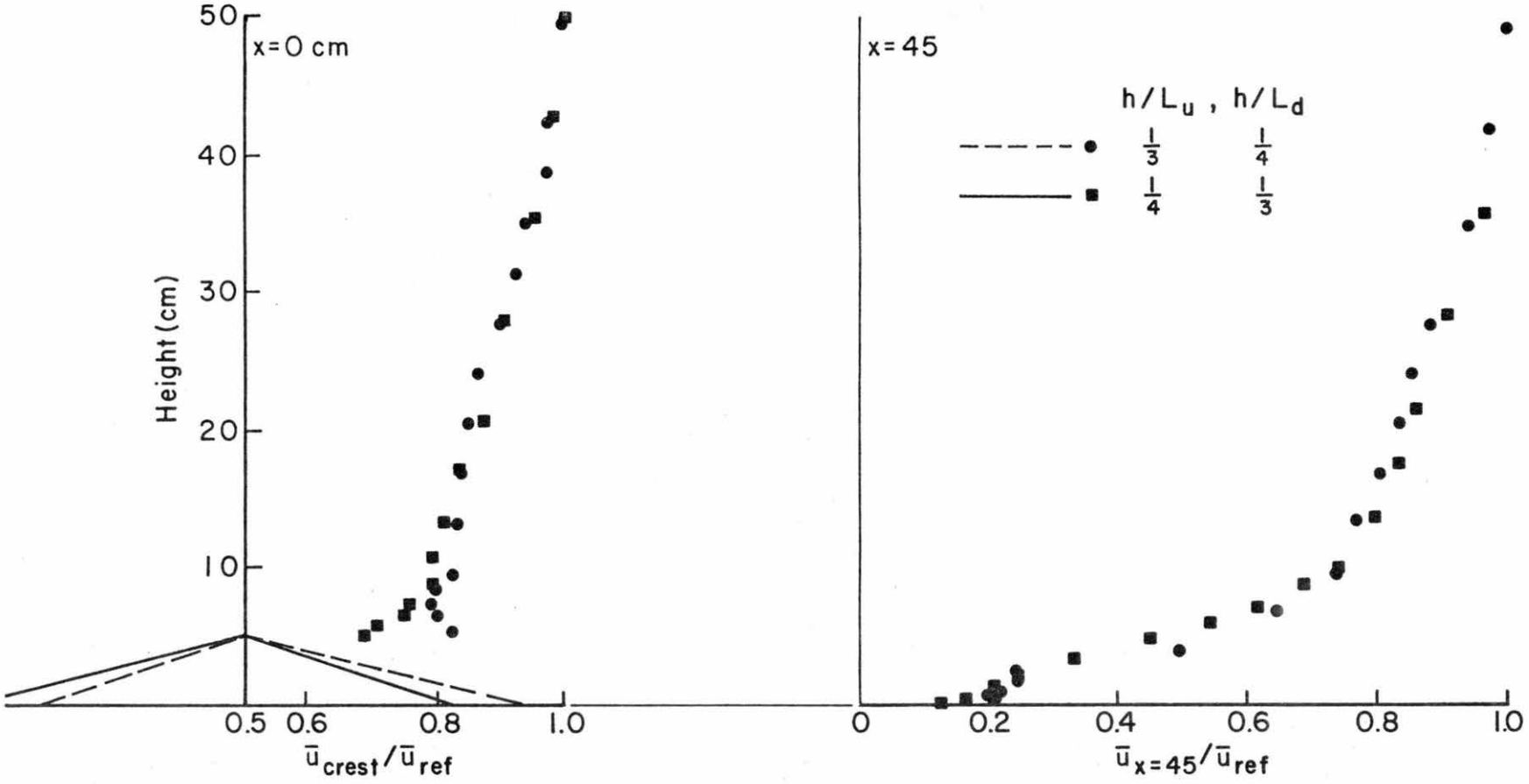

FIGURE 3.19. Mean Velocity Profiles Downwind of a Triangular Hill $h/L_u = 1/3$, $h/L_d = 1/4$ and $h/L_u = 1/4$, $h/L_d = 1/3$. Test Cases I and II

effects may be noticed in Figure 3.18 where vertical velocity profiles are presented at the crest and downwind of hills with $h/L_u = 1/4$, $h/L_d = 1/0$, 1/2, an 1/3.

A given hill may cause quite different crest profiles depending on the approach direction (see Figure 3.19). Although a "jet" effect occurs for the case $h/L_u = 1/3$, $h/L_d = 1/4$, the velocity distributions indicate that a separation cavity has developed downwind of the crest.

All data measured in the current series of measurements to study the effect of upwind and downwind slopes were for $h/\delta = 0.1$. A wider range of conditions was not examined because Huber et al. (1976) found that the separation phenomenon is not affected by the upstream velocity distribution or boundary layer depth. He observed essentially identical downwind separation regions for approach velocity profiles, where $h/\delta = 0.2$ and 0.5. Since the occurrence of flow separation then depends primarily on h/L_d and h/L_u, a generally applicable separation criterion for flow over ridges may be derived from the wind-tunnel data obtained over the triangular ridges. Figure 3.20 suggests an empirical envelope determined between h/L_u and h/L_d that governs the occurrence of flow separation.

Height of the Ridge. It is also desirable to know the effect of hill height to shear layer depth on wind speed when separation does not occur. Jackson and Hunt (1975) define a speedup parameter called a fractional speedup ratio:

$$\Delta S_{crest} = \frac{\bar{u}_{crest}(z) - \bar{u}_o(z)}{\bar{u}_o(z)} ,$$

where $\bar{u}_o$ is the upstream velocity distributon, $\bar{u}_{crest}$ is the velocity profile above the crest, and z is the distance from the surface. By non-dimensionalizing the speedup parameter with the upstream profile, they anticipated that the fractional speedup ratio would not depend strongly on the approach velocity distribution. This would imply that the fractional speedup does not depend strongly on h/δ.

In Chapter 2 and Appendix E it was concluded that mean crest velocities could be predicted accurately with an inviscid flow model. An inviscid model was constructed by Derickson and Merony (1977) and compared with the laboratory data discussed in Sections 3.1 and 3.2. The numerical and

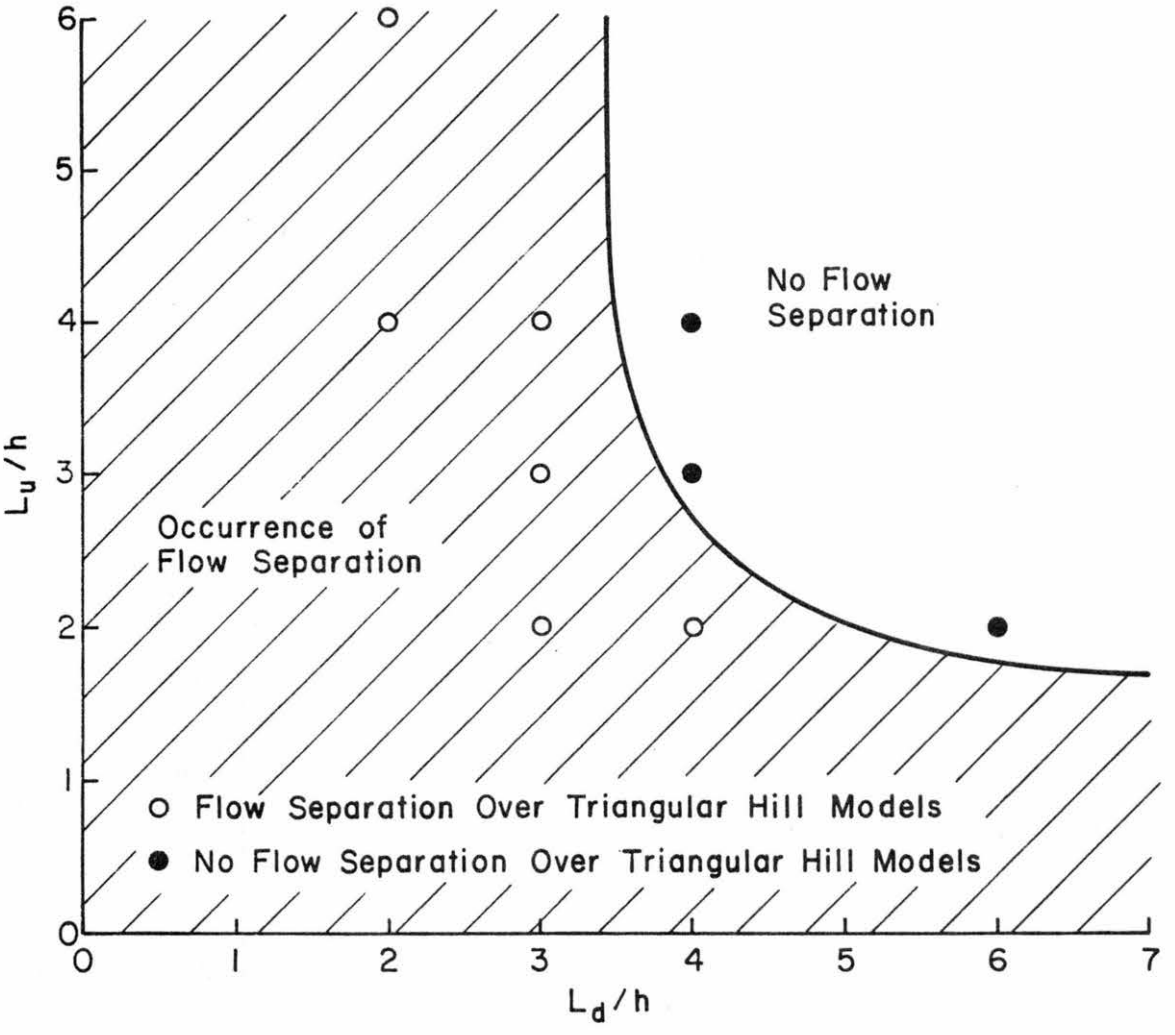

FIGURE 3.20. Criterion for Flow Separation Over Ridges

laboratory and fields were essentially identical. Numerical calculation, using the inviscid flow model as described in Appendix E, Section E.3, can thus give accurate velocity distributions over the crest of a bell-shaped hill with constant h/L and varying h/δ. The hill shape and upwind velocity distribution are defined by Equations (E.20) and (E.21), respectiyely. The parameters considered to predict the influence of the height of the ridge were combined in numerical calculation runs 1, 3, 5, and 14 (see Table E.1). Given a hill slope, $h/L = 0.2$, the values of h/δ used are 0.012, 0.04, 0.4, and 4.0. The surface roughness imposed in each case is approximately the same; hence its perturbation effect on the fractional speedup is assumed to be negligible. Upwind approach velocity profiles and corresponding fractional speedup ratio profiles are given in Figures 3.21 and 3.22.

The calculations suggest that the fracitonal speedup ratios decrease with increasing h/δ. Changes seem to be most significant close to the surface. For $h/\delta < 1$ and $z/h < 1$, fractional speedup ratio ΔS is approximately 30 percent larger than the uniform velocity profile case ($h/\delta >> 1$). For $z/h > 1$ differences approach zero.

Detailed Hill Shape. The effect of detailed hill shape for a given h/L on the velocity field was investigated by comparing velocity fields over symmetric triangular hill models with those measured over sinusoidal-shaped hill models (Figures 3.5, 3.6, 3.10 and 3.11). Almost identical velocity fields were measured. Rider and Sandborn (1977b) in a separate series of tests associated with this test program considered a number of alternate hill shapes with the same height and with the same distance from crest to the base of the hill (L_b). The models include full sine-wave, half sine-wave, triangular, trapezoidal, and box-shaped hills. Speedup effects over the crest of the different hill models varied substantially. For a triangular hill the fractional speedup factor at a height h above the crest was 0.35; for the box-shaped hill this factor was 0.15. This shows again that L_b does not characterize the hill length accurately. The hill length L varied by a factor 2; moreover, separation regions exist upwind and downwind of the box-shaped hill.

3.2 EFFECTS OF TURBULENCE AND SURFACE ROUGHNESS ON VELOCITY PROFILES

The upwind surface roughness induces different approach velocity profiles. The approximate effects of such profile changes on the fractional

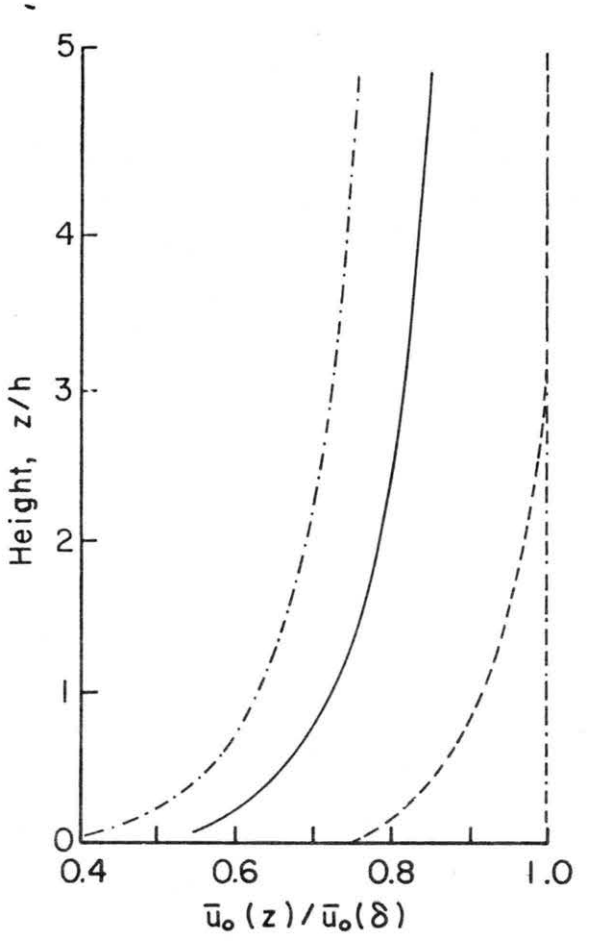

FIGURE 3.21. Upwind Approach Mean Velocity Profiles for Numerical Inviscid Flow Calculations

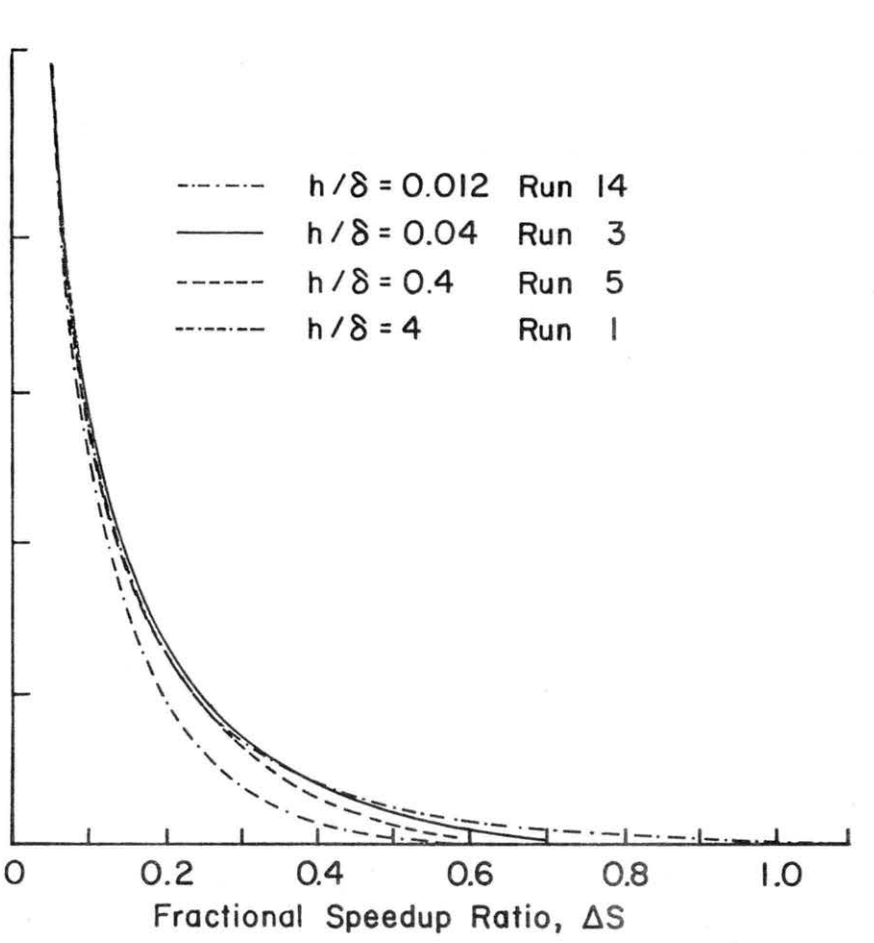

FIGURE 3.22. Fractional Speedup Ratio Profiles at the Crest of a Bell-shaped Hill, h/L = 0.2

speedup were examined utilizing the inviscid flow model described in Appendix E, Section E.3 as well as performing laboratory experiments. The experimental measurements are interpreted in terms of the inner and middle regions previously identified in Chapter 2.0.

The hill shape and upwind velocity distributions are defined, again by Equations (E.20) and (E.21), respectively, The cases considered are listed in Table E.1 as runs 1 to 9. The upwind velocity distributions are given in Figure 3.23 and fractional speedup ration profiles are presented in Figure 3.24. Most values of z_o/δ were too small to represent realistic surface conditions. Nevertheless, the calculations do show some interesting trends. There is only a slight decrease in ΔS as the surface roughness decreases. This change is most significant for small values of h/δ. The latter seems reasonable, because for small values of h/δ, velocities do change significantly with roughness over a surface layer with a thickness of the order of the hill height.

The effect of surface roughness was investigated experimentally by considering the Cases 5 and 14 as listed in Appendix A, Table A.1. In both cases the slopes are 1/4 but surface roughness has changed from $z_o/\delta = 1.2 \times 10^{-4}$ (Case 5) to $z_o/\delta = 1.6 \times 10^{-3}$ (Case 14), representing terrain types varying from crops to rural woods. The fractional speedup ratio profiles at the crest are provided in Figure 3.25. The profiles show the same trend as suggested by the inviscid profiles given in Figure 3.24; however, for these larger, more realistic surface roughnesses the changes are much larger.

The Inner Region. As a result of the large longitudinal pressure gradients developed in the wind-tunnel study, a realistic inner region did not develop. This section identifies the discrepancy through a comparison with recent field data. An examination of the phenomenon reveals that the loss of an inner region may be associated with an relaminarization process previously identified by aerodynamicists.

Bradley (1978) conducted a field study to measure the wind characteristics over a ridge with a shape similar to those tested in the Meteorological Wind Tunnel but with a larger ratio of hill height to boundary-layer thickness. The ridge height was 170 m, the upwind ridge length (L_u) was 550 m, and the downwind length somewhat longer, L_d = 600 m. The hill was covered with trees; surface roughness and the displacement thickness were

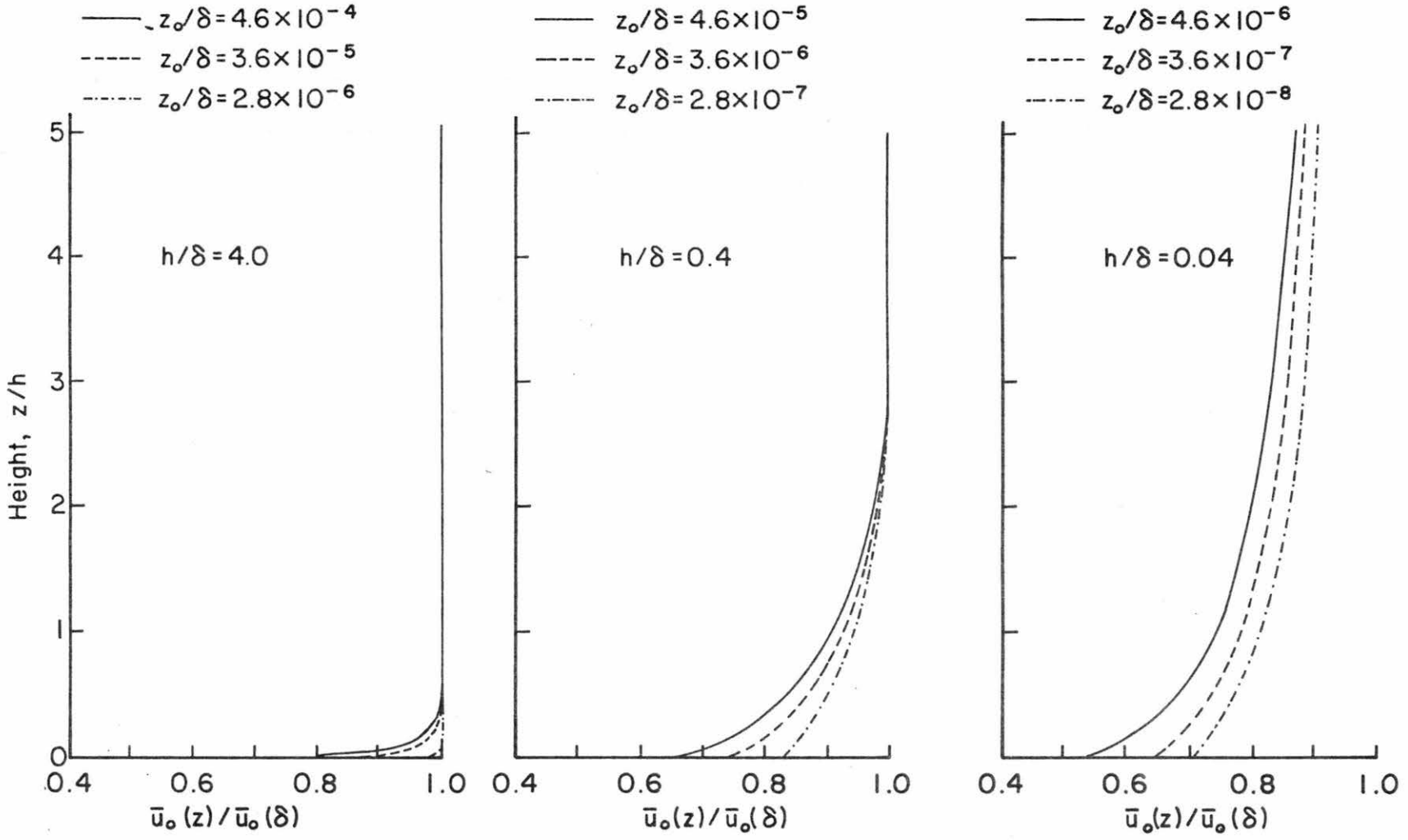

FIGURE 3.23. Upwind Approach Mean Velocity Profiles for Numerical Inviscid Flow Calculations. Runs 1 to 9

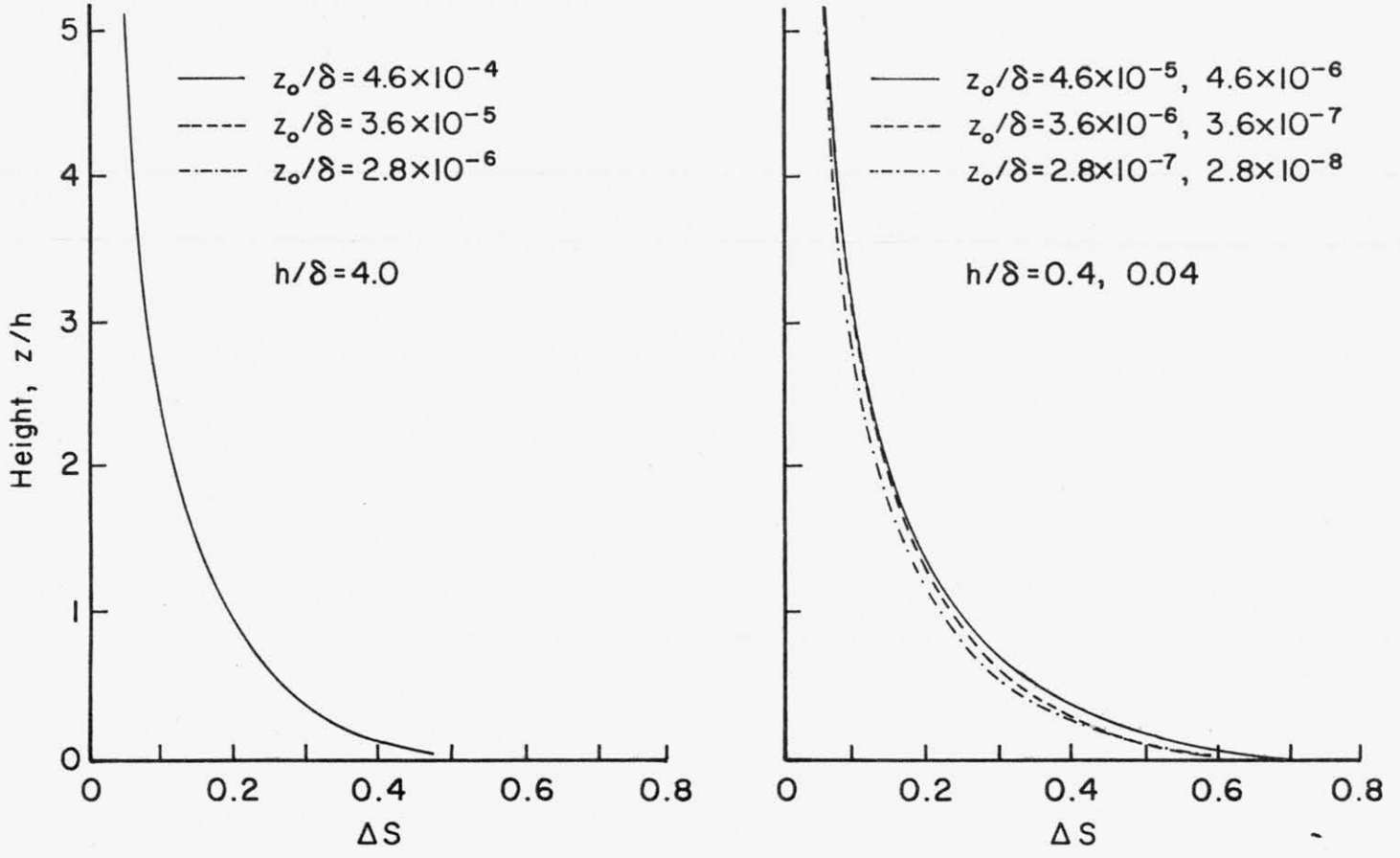

FIGURE 3.24. Fractional Speedup Ratio Profiles at the Crest of a Bell-shaped Hill, h/L = .2. Runs 1 to 9

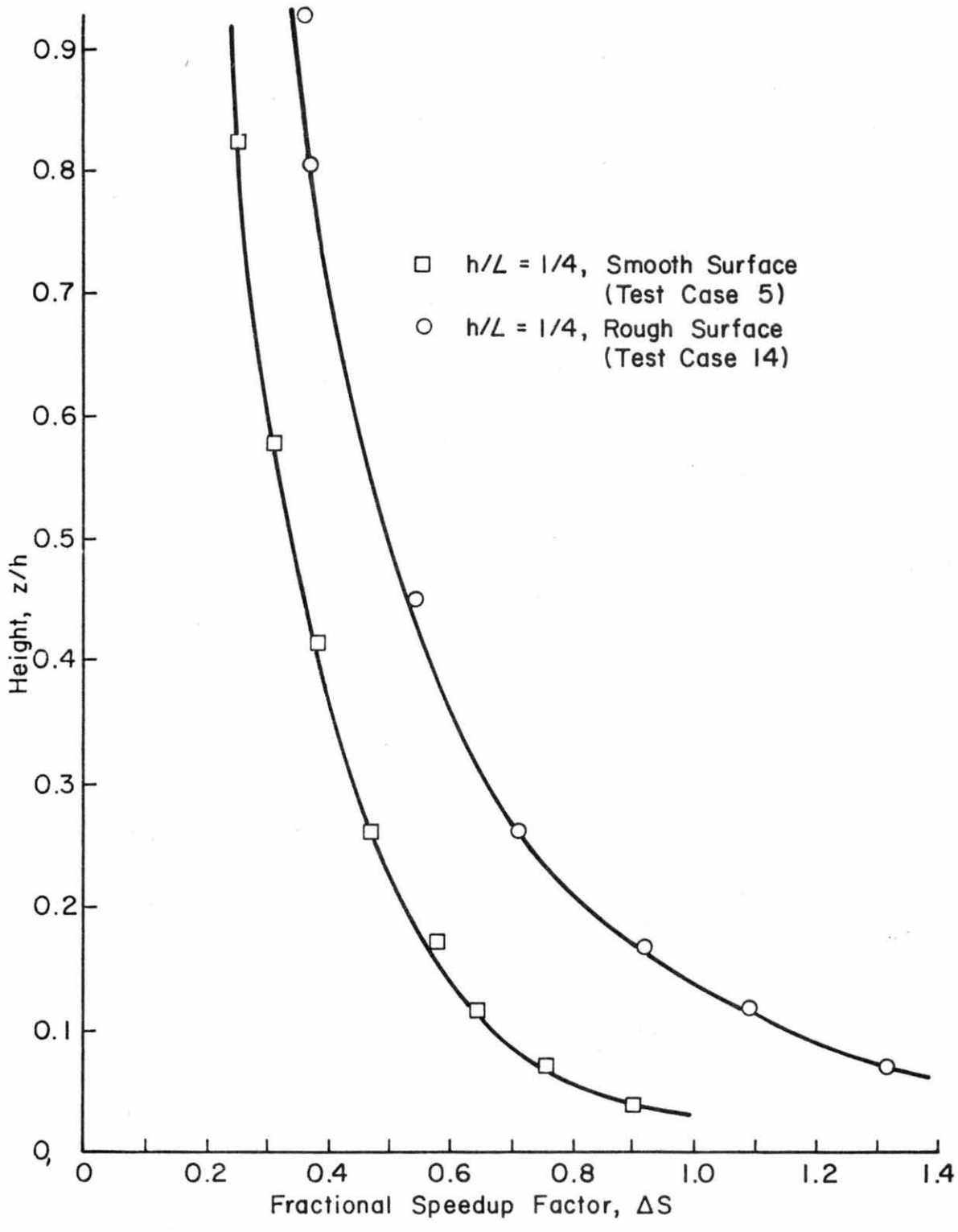

FIGURE 3.25. Comparison of Fractional Speedup Ratio Profiles at the Crest of Triangular Hill, h/L = 1/4 in the Smooth and Rough Surface Boundary Layers. Test Cases 5 and 14

estimated at 1.0 m and at 7.0 m respectively (typical tree height was 10.0 m). The boundary-layer thickness was estimated at 600 to 800 m. Although the ridge was not strictly two-dimensional, it presented a broad face of uniform slope. Data were recorded during periods in which the mean wind direction was within 15° of the normal of the ridge. Bradley obtained wind data at various heights up to 100 m above the crest under neutral conditions. Vertical velocities were measured, and streamline inclinations determined at the top of the ridge. The results indicate that a separation region exists downwind of the crest.

Bradley's measurements have been compared to several laboratory cases via fractional speedup ratio profiles in Figure 3.26. Close to the surface the field data is quite different from the laboratory data. Bradley suggests that an inner region should exist up to a height (h-d) of 28 m, which corresponds to a value of 0.17 on the vertical axis of Figure 3.26. This would imply that in this region

$$\bar{u}\,\frac{\partial \bar{u}}{\partial x} = 0 \quad [\frac{\partial - \overline{uw}}{\partial z}].$$

Bradley measured Reynolds shear stresses at the crest. Values of the shear stress at 9 m were 2.6 times as large as the upwind shear stress, but at 25 m were about the same as upwind values. The upwind shear velocity was 0.52 m/sec. Hence

$$\frac{\partial - \overline{uw}}{\partial z} \simeq .04 \text{ m/sec}^2 .$$

Mean velocities were approximately 6 m/sec so that longitudinal velocity accelerations should be on the order of 1/136 sec^{-1}. Typical measured accelerations were on the order of 4/550 sec^{-1}, which does suggest that the inner region extends to about a distance of 28 m.

However, in the wind-tunnel experiments no inner layer was observed for the steeper hills. If we assume that the hill length is the governing length scale, the inner-layer thickness over the steeper hill models should have been on the order of 0.8 cm. Local destruction of this layer at the sharp-crested triangular hills is unlikely since the fractional speedup ratio profiles over the crest of the sinusoidal hill models are similar. Only for the triangular hill with $h/L = 1/20$ is an inner layer of 0.2h apparent (see Figure 3.26).

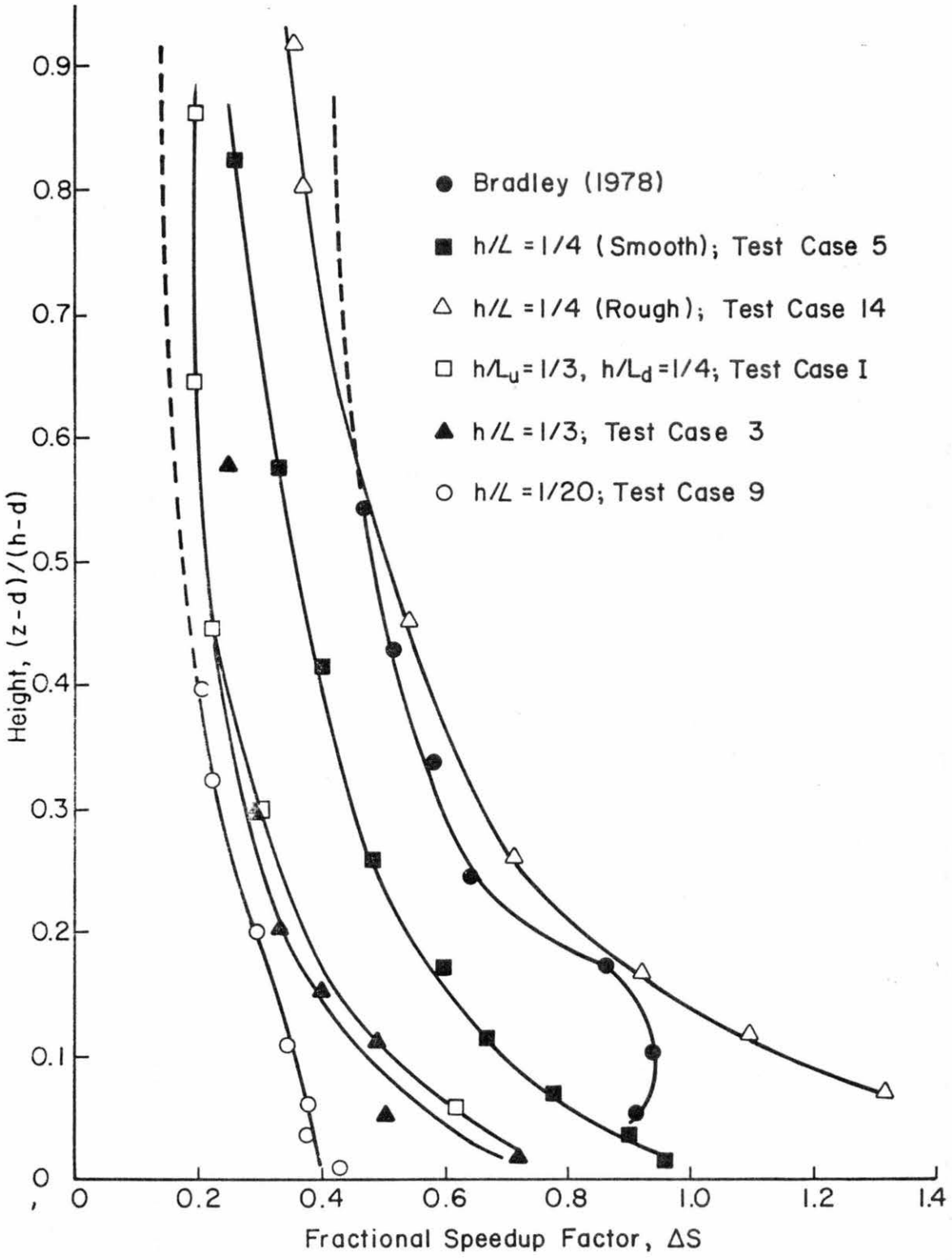

FIGURE 3.26. Comparison of Fractional Speedup Ratio Profiles at the Crest of Triangular Hills with Fractional Speedup Ratios Derived from Field Data. Field Data from Bradley (1978). Test Cases 3, 5, 9, 14 and I

The discrepancy between the field and wind-tunnel data is disconcerting. It may be explained by boundary-layer relaminarization: A turbulent boundary layer reverts towards a laminar state when it undergoes a rapid acceleration through a strongly favorable pressure gradient. The effect is most significant in the surface layer where eddies are sufficiently small to dissipate after being stretched by the longitudinal strain. The result is that above a smooth surface a thickening of the viscous sublayer reduces surface shear stresses. Although relaminarization effects have not been investigated over rough surfaces, it can be argued intuitively that the increased dissipation rate impedes an increase in Reynolds stresses over a rough surface.

Several investigators have sought to explore the relaminarization process in detail. Kline et al. (1967) and Badri Narayanan and Ramjee (1968) found that a critical value of the nondimensional pressure gradient for relaminarization was

$$R_p \equiv \frac{\nu}{\bar{u}_\infty^3} \frac{dp}{dx} \simeq 4 \times 10^{-6},$$

where dp/dx was the longitudinal pressure gradient which was constant across the boundary layers.

Blackwelder and Kovasznay (1972) conducted an experimental study to investigate the turbulence structure of a boundary layer in a strongly favorable pressure gradient. Typical values of R_p were also on the order of 4×10^{-6}. They measured Reynolds shear stresses close to the surface but above the viscous sublayer and showed that the shear stresses remained constant along streamlines. Similar results were reported by Rider and Sandborn (1977a). They presented Reynolds shear stress distributions over the crest of ridges (Cases 1a, 5a and 7a).

It is appropriate to consider the laboratory study of flow over ridges in regard to the parameter suggested by Kline et al. (1967) because pressure gradients across the boundary layer are not constant in flow over low ridges, R_p has been redefined by the following expression:

$$R_p = - \frac{\nu}{\bar{u}_\infty^3} \frac{p_{crest}}{L} \qquad (3.1)$$

It should be pointed out that the velocity scale is evaluated at a height above the crest; therefore, the critical value of R_p according to Equation (3.1) is likely to be less than 4×10^{-6}.

Values of R_p calculated for the different wind-tunnel flow cases are

R_p 3.7×10^{-6} (Case 5) for h/L = 1/4,

$R_p = 1.9 \times 10^{-6}$ (Case 14) for h/L = 1/4,

$R_p = 2.2 \times 10^{-6}$ (Case 3) for h/L = 1/3, and

$R_p = 3.1 \times 10^{-7}$ (Case 9) for h/L = 1/20.

These values of R_p suggest that the flow in the inner region may revert to a laminar state for the wind-tunnel study, except for the 1/20 ridge. Longitudinal pressure gradients in the field study of Bradley (1978) are less by a factor of 3000, so that no reversion was likely to take place.

It was shown in Section 2.2 that for constant shear stress along streamlines and for weak turbulence the flow is effectively inviscid. This theoretical result, combined with the experimental evidence that the shear stresses remain constant, explains the large speedups close to the surface in the flows over the steeper hills when the inner region decays.

An indication of the thickness of the inner layer may be obtained by applying Jackson and Hunt's (1975) formula [Appendix E, Equation (E.12)]. In terms of z_o and L the inner-layer thickness is

$$\ell = 0.067\, z_o^{0.1}\, L^{0.9}$$

Computed values of ℓ for Cases 5, 14, 3, 9, and Bradley (1978) are 0.6 cm, 0.8 cm, 0.5 cm, 2.6 cm, and 19.6 m. respectivley. The "measured" value of ℓ is 0.5 cm for Case 9 and 28 m for Bradley's case. Although these are limited data to validate Equation (E.12), it seems that Jackson and Hunt's expression for ℓ is not unrealistic.

No research has been conducted to study the effect of a stable thermal stratification on boundary-layer relaminarization in a wind-tunnel modeling. Stable stratification may accelerate the relaminarization because velocities in the wind tunnel are usually much less than under neutral test conditions.

In ,summary, it may be concluded that for large pressure gradients in the wind-tunnel study, a realistic inner region does not always develop. Further research is required to validate or modify Equation (E.12), and to investigate the constraint the relaminarization phenomenon places on wind-tunnel simulation.

The Middle Region. Above the inner region the interaction between perturbations of the turbulence and the mean flow are locally insignificant. The effects of the interaction become significant for an air parcel when nonequilibrium* flow conditions persist long enough. The following paragraphs consider whether turbulence significantly influences mean velocity over the middle region for the cases examined.

In Section 2.2 an order of magnitude analysis was presented to estimate the total head losses caused by the distortion of the turbulence. The additional total head losses at the crest can be expressed [Equations (2.18) and (2.19)] as follows:

$$\Delta P'_{crest} = 0 \left[R + \frac{R}{\lambda} + \frac{h}{\delta} R_m\right] \text{ if } \frac{h}{\delta} < \frac{h}{\lambda L_u} , \tag{3.2}$$

$$\Delta P'_{crest} = 0 \left[R + \frac{RL_u}{\delta} + \frac{h}{\delta} R_m\right] \text{ if } \frac{h}{\delta} > \frac{h}{\lambda L_u} , \tag{3.3}$$

where R is the maximum characteristic change in any of the Reynolds stresses along a streamline between a point upstream and a point at the crest, and where R_m is the maximum Reynolds stress existing in the flow field. (An adequate estimate for R_m is the square of the longitudinal turbulence intensity close to the surface.)

To evaluate $\Delta P'$ for a particular hill shape, detailed information of the Reynolds stresses over the hill is required. Rider and Sandborn (1977a) present data on the longitudinal and vertical turbulence intensities and Reynolds shear stresses over ridges (Cases 1a, 5a and 7a). Their data show the following: 1) $\delta > \lambda L_u$; 2) the longitudinal turbulence intensity increases toward the base of the ridge, then decreases over the crest; 3) the vertical turbulence intensity shows a decrease at the base of the ridge and increases over the crest; and 4) changes in Reynolds shear stresses are small. Based on this information, R should be evaluated by considering only longitudinal Reynolds normal stresses, and $\Delta P'$ should be calculated from Equation (3.2).

Contour plots of longitudinal turbulence intensities with the streamline pattern superimposed for triangular hill models $h/\delta = 0.1$, $h/L = 1/2$, $1/4$, $1/6$, and $1/20$ are provided as Figures 3.27 to 3.30. (These models are similar

*Equilibrium flow conditions are defined here as equal momentum transfer to and from a particular streamline.

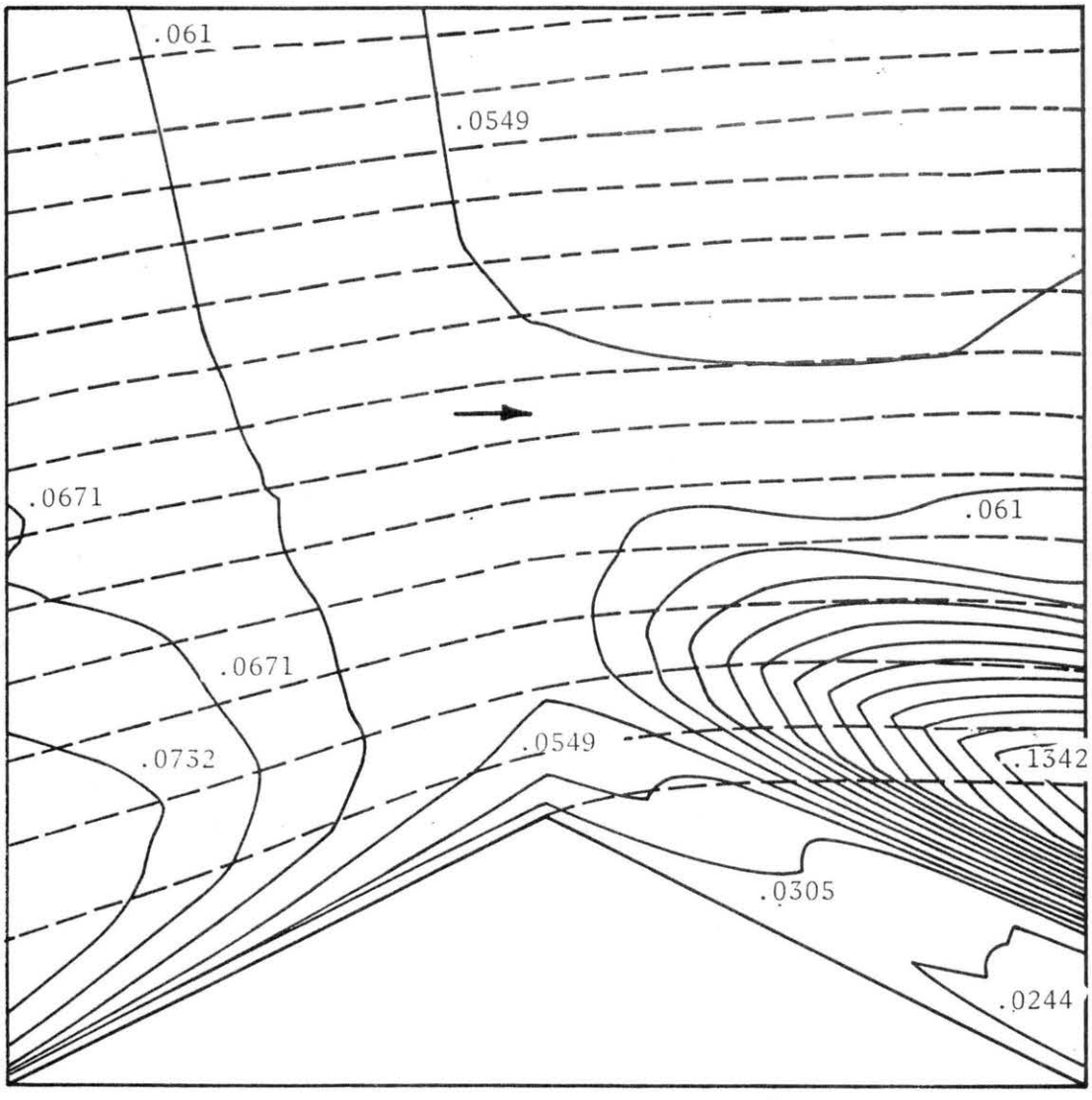

FIGURE 3.27. Contours of Longitudinal Turbulence Intensity Over Triangular Hill h/L = 1/2, with Superimposed Stream-Lines. Contour Interval $\Delta u'/\bar{u}_o$ (δ) = .0061. Test Case 1

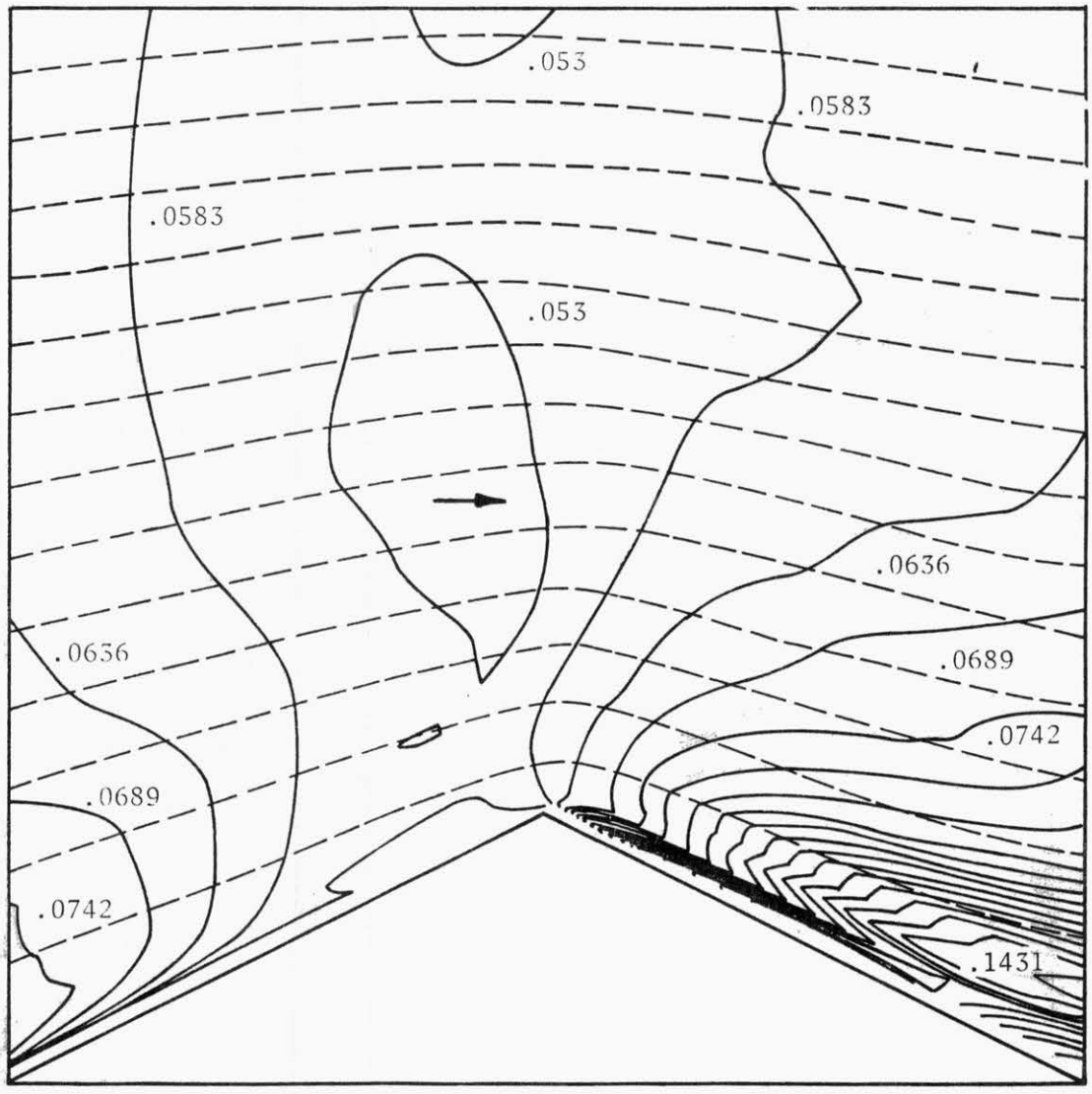

FIGURE 3.28. Contours of Longitudinal Turbulence Intensity Over Triangular Hill h/L = 1/4, with Superimposed Streamlines. Contour Interval $\Delta u'/\bar{u}_o$ (δ) = .0053. Test Case 5

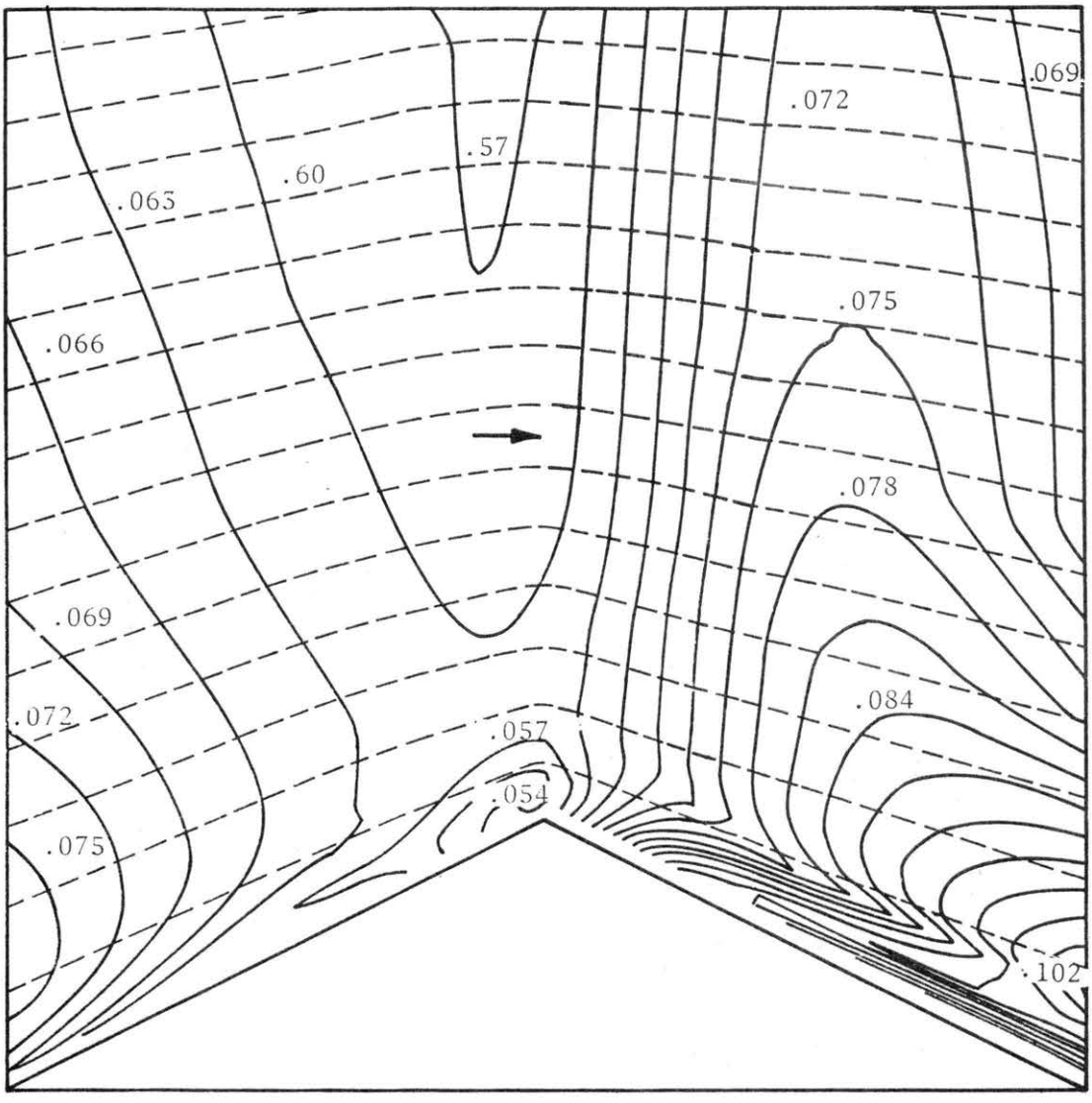

FIGURE 3.29. Contours of Longitudinal Turbulence Intensity Over Trianglar Hill h/L = 1/6, with Superimposed Streamlines. Contour Interval $\Delta u'/u_o$ (δ) = .0030. Test Case 7

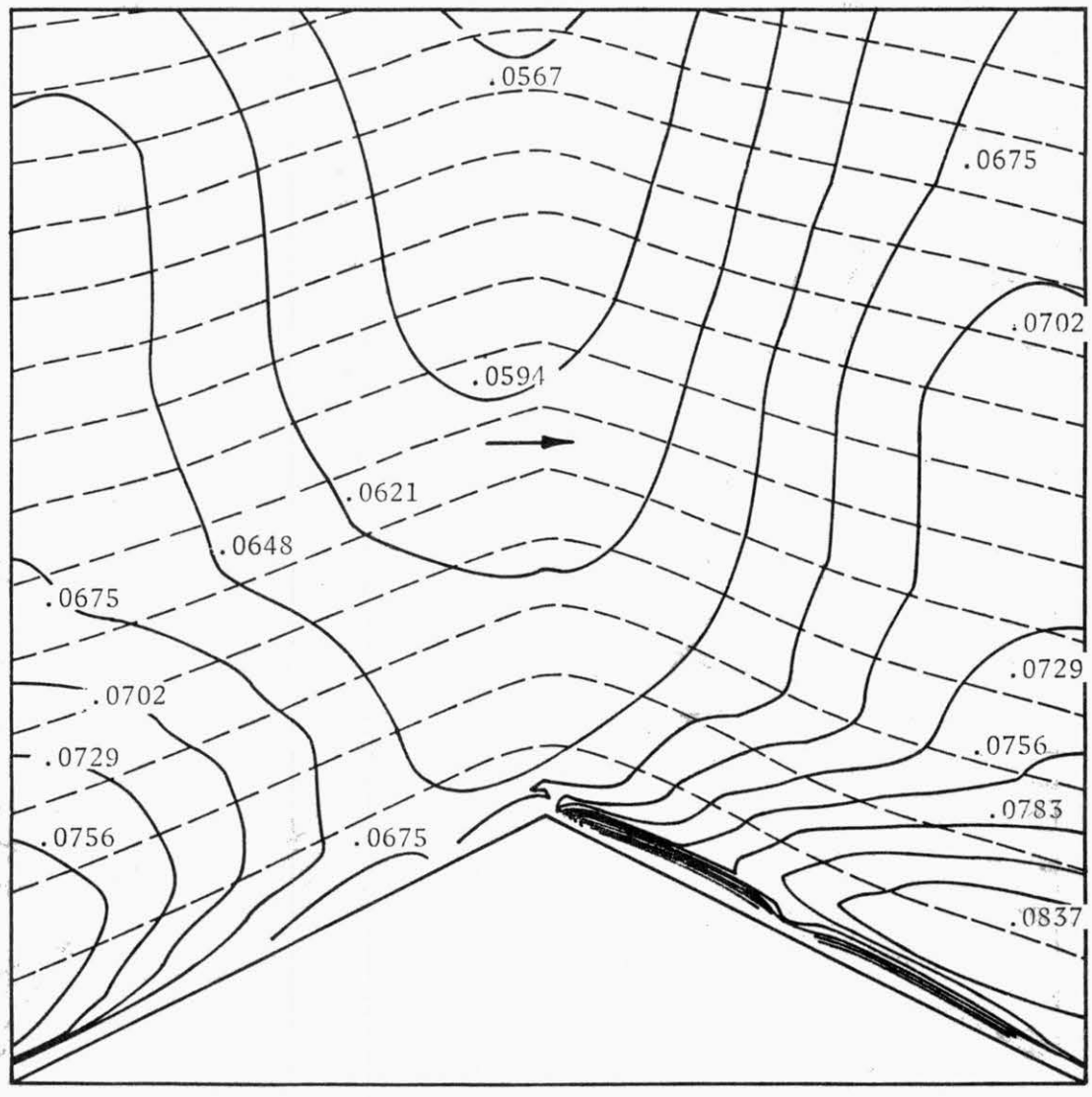

FIGURE 3.30. Contours of Longitudinal Turbulence Intensity Over Triangular Hill h/L = 1/20, with Superimposed Streamlines. Contour Interval $\Delta u'\bar{u}_o$ (δ) = .0027. Test Case 9

to those considered by Rider and Sandborn.) The figures show that the decrease in R between the base and the crest along streamlines close to the surface is 33 percent of R_m for the 1/2-hill, 47 percent for the 1/4-hill, 42 percent for the 1/6-hill, and 27 percent for the 1/20-hill. The parameter λ varies between 0.3 and 1.0. R_m = 0.6 percent of $\bar{u}_o (\delta)^2$. Resulting changes in additional total head are then at most two times R_m. Increases in dynamic head may be as large as 300 percent; even for the 1/20-hill the increase in dynamic head is 100 percent. Supposing that the change of additional total head causes an equal change in dynamic head, it may be concluded that the effect of turbulence on the mean flow at the crest is not significant at least for $h/\delta < h/\lambda L_u$. The effects of turbulence may be expected to be somewhat larger for hills with $h/\delta > h/\lambda L_u$ (long hills).

An increased surface roughness will further increase the additional total head losses. If $z_o/\delta = 1.6 \times 10^{-3}$, then R = 63 percent of R_m, and R_m = 0.1 percent of $\bar{u}_o (\delta)^2$ (see Figure 3.31). However, since R_m and R do not change by orders of magnitude, it may be concluded that the inviscid flow theory will predict the mean flow field outside the inner region accurately upwind of the crest even for a large surface roughness.

Downwind of the crest, turbulence production increases, and turbulence intensities in this region exceed upwind intensities. As a result, additional total head changes become larger. The relative effect of the turbulence perturbations on the dynamic head increases downwind of the crest, since the dynamic head returns to values approximately equal to upwind values.

The effects of turbulence downwind of the crest are illustrated by considering flow over a symmetric hill. According to inviscid flow theory, the velocity and static pressure fields over a symmetric hill are also symmetric. Therefore, the measured degree of flow symmetry indicates the effects of turbulence on the mean flow.

Contour plots of mean velocity and static pressure over symmetric hill models are presented in Figures 3.1 to 3.13 and in Appendix D. Excluding the first four cases for which flow separation occurs, slightly asymmetric contour plots may be observed. At the downwind base of the hills, velocities are smaller than they are at the upwind base, and the positive static pressures downwind are smaller than they are upwind. The static pressure plots indicate that the downwind static pressures return very slowly to upwind values. Some of the apparent static pressure variation may be caused by the turbulence,

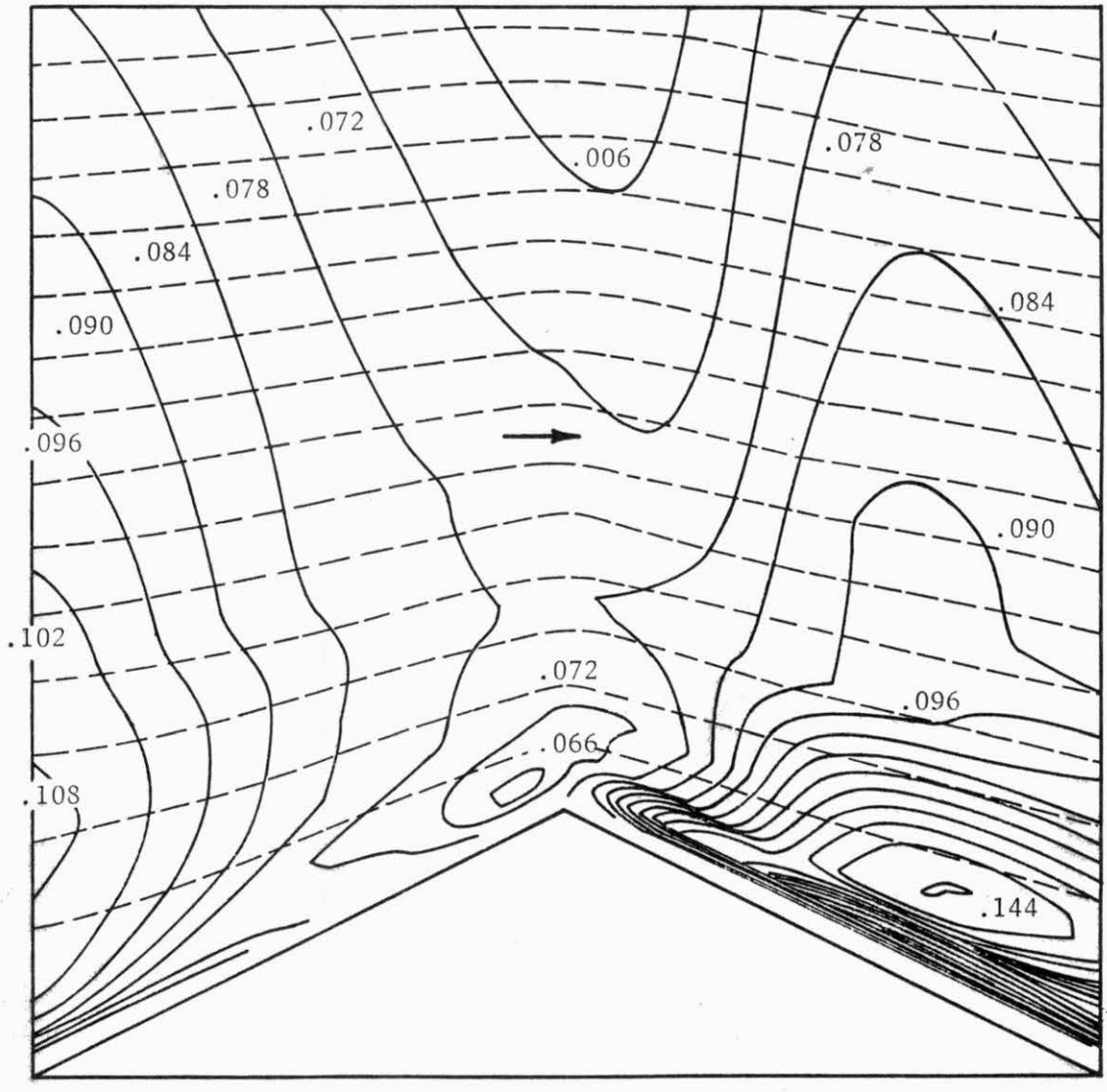

FIGURE 3.31. Contours of Longitudinal Turbulence Intensity Over Triangular Hill h/L = 1/4, with Superimposed Streamlines. Contour Interval $\Delta u'/\bar{u}_o$ (δ) = .0060. Test Case 14

since static pressures were not corrected for the relatively large turbulence intensities downwind. For example, for the 1/6-hill (Case 8) downwind turbulence intensities are $0.1\bar{u}_o(\delta)$. The resulting errors may be as large as 10 percent of the static pressure variation at the base over a surface layer of thickness h.

The downwind mean flow is strongly affected by the upwind turbulence intensities. This is demonstrated in contour plots of mean velocities for 1/4-hills with different surface roughness conditions (Figure 3.32). Asymmetry is more significant for the rough flow case. The ratios of the upwind to the downwind maximum turbulence intensities are 1.33 for the rough surface case, and 1.11 for the smooth surface case. One concludes that wind fields downwind of a hillcrest are not governed by an inviscid physics; nonetheless, in the absence of separation the inviscid numerical model may give quite adequate results.

3.3 EFFECTS OF THERMAL STRATIFICATON ON VELOCITY PROFILES

A stably stratified boundary layer was simulated to study its effect on the velocity field over ridges. Triangular ridges with $h/L = 1/4$, $1/6$ and $h/\delta = 0.1$ were used. The freestream approach velocity was varied from 2.8 to 8.9 m/sec with a corresponding variation in Richardson number, as defined by

$$Ri = \frac{g}{T} \frac{\Delta T}{\Delta U_z^2} h ,$$

from 0.004 to 0.021. Details of the measurements of the mean and turbulent velocities and temperatures are given in Meroney et al. (1978b, Appendix C).

The effect of stable thermal stratification on the fractional speedup ratio above the crest is shown in Figures 3.33a and b for the 1/4-hill and the 1/6-hill, respectively. There is some evidence that the experimental ΔS increases slightly as the stratification becomes more stable. However, it is probable the effect is caused by changes in approach profile shape with stability. Similar effects were found for different approach profiles under neutral thermal flow conditions. Calculations by Derickson and Meroney (1977) suggest that ΔS will normally decrease slightly with stability for a given approach profile.

It is likely a wider range of experimental stability conditions must be considered to resolve this discrepancy. Since stable stratification also

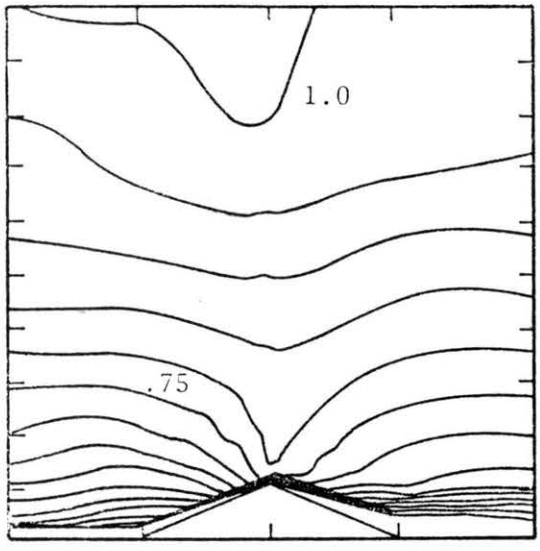

Rough surface

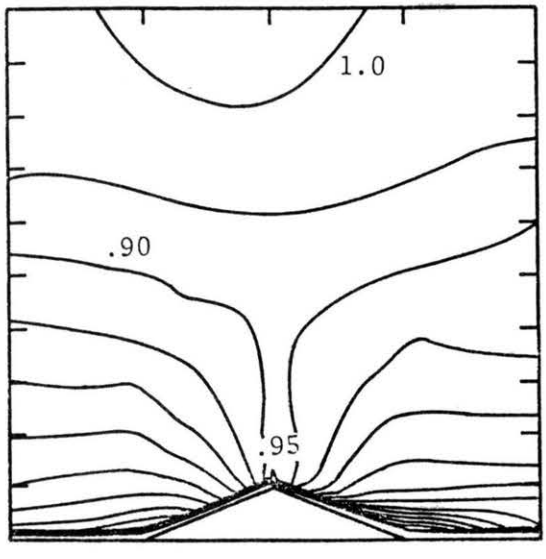

Smooth surface

FIGURE 3.32. Comparison of Mean Velocity Fields Over a Triangular Hill h/L = 1/4 in the Smooth and Rough Surface Boundary Layers. Test Cases 5 and 14

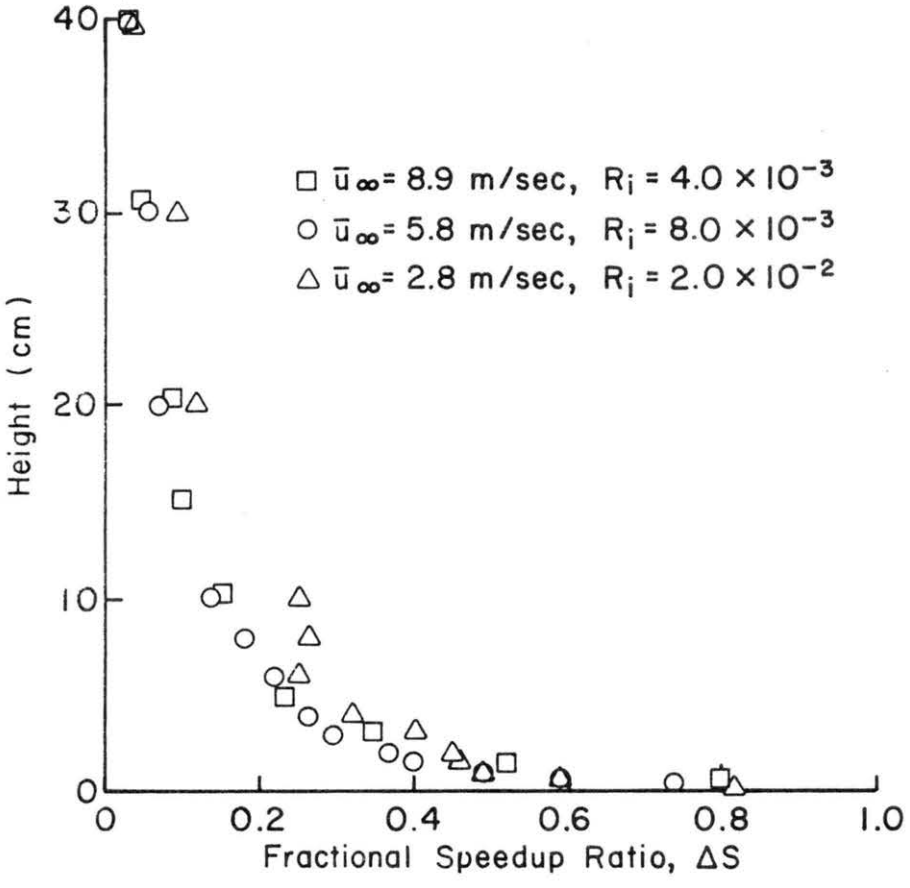

FIGURE 3.33a. Fractional Speedup Ratio Profiles Over a Triangular Hill h/L = 1/4 in Neutral and Stable Stratified Boundary Layers. Test Cases S1, S2, and S3

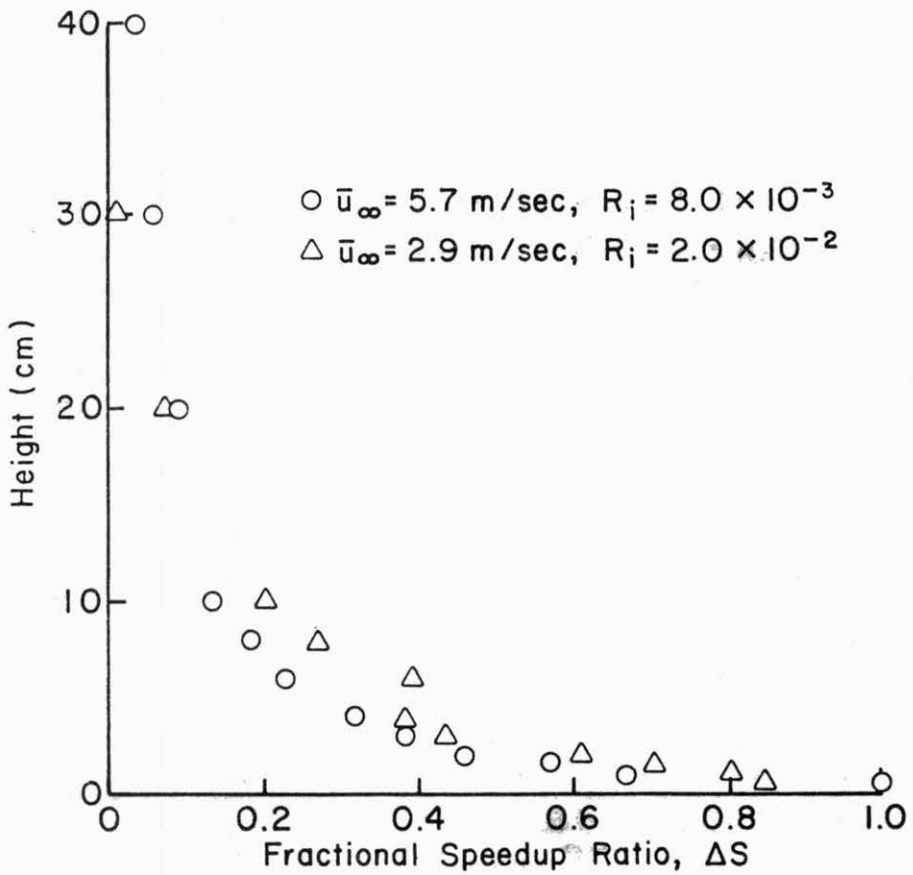

FIGURE 3.33b. Fractional Speedup Ratio Profiles Over a Triangular Hill h/L = 1/6 in Neutral and Stable Stratified Boundary Layers. Test Cases S4 and S5

influences the approach wind profile it will be difficult to separate the influence of profile and buoying in the laboratory.

The effect of stably stratified flow on the turbulence is to further reduce the longitudinal velocity component over that originally observed in the neutral flow case for the same ridge shapes. The temperature fluctuation behaves as a passive scalar quantity and does not change as it is convected over the ridge (see Meroney et al. (1978b, Appendix C).

The effect of stratified flow on the extent of a separation region is significant, although speedup over the crest is not strongly affected. Measurements of mean velocities downwind of a triangular hill with $h/L_u = 1/4$ and $h/L_d = 1/0$ (an escarpment) show that the downwind separation region is much longer under stable conditions than under neutral conditions (Figure 3.34). The temperature in the separation region is low as a result of the low wind velocities in this region; therefore, the heavier air in the separation region resists reattachment of the separation streamline.

3.4 EFFECT OF FINITE RIDGE WIDTH ON VELOCITY PROFILES

In the previous sections, ridges with infinite width were considered. Additional experiments were conducted over ridges with limited lateral extent to study the effects of finite width. The ridge shapes were identical to those employed in the two-dimensional ridge study, namely: $h/L_u = 1/4$, $h/L_d = 1/3$, and $h/L_u = 1/4$, $h/L_d = 1/0$. Total ridge widths (2b) were 9h and 18h. Sets of velocity profiles at the crest of these ridges are displayed in Figures 3.35 to 3.38. The deviation from the two-dimensional velocity profiles at the crest is indicated by the solid curve at each measuring station. In all four cases, the velocities at the center of the ridge are less than for the two-dimensional case, especially if a large separated flow region exists downwind. At the extreme ends, the velocities are about equal for the case $h/L_u = 1/4$, $h/L_d = 1/0$. The large speedups at the ends of the ridge crest for $h/L_u = 1/4$ and $h/L_d = 1/3$ apparently result from a reduced separated flow region at the sides of the downwind slope.

These data confirm the calculated conclusions of Hunt (1978) who reported amplification factors over the top of an ellipsoid based on a potential flow model. Hunt's results suggest that for $b/L_b > 5$ the amplifications are essentially constant regardless of the slopes, and that for $b/L_b < 5$, changes

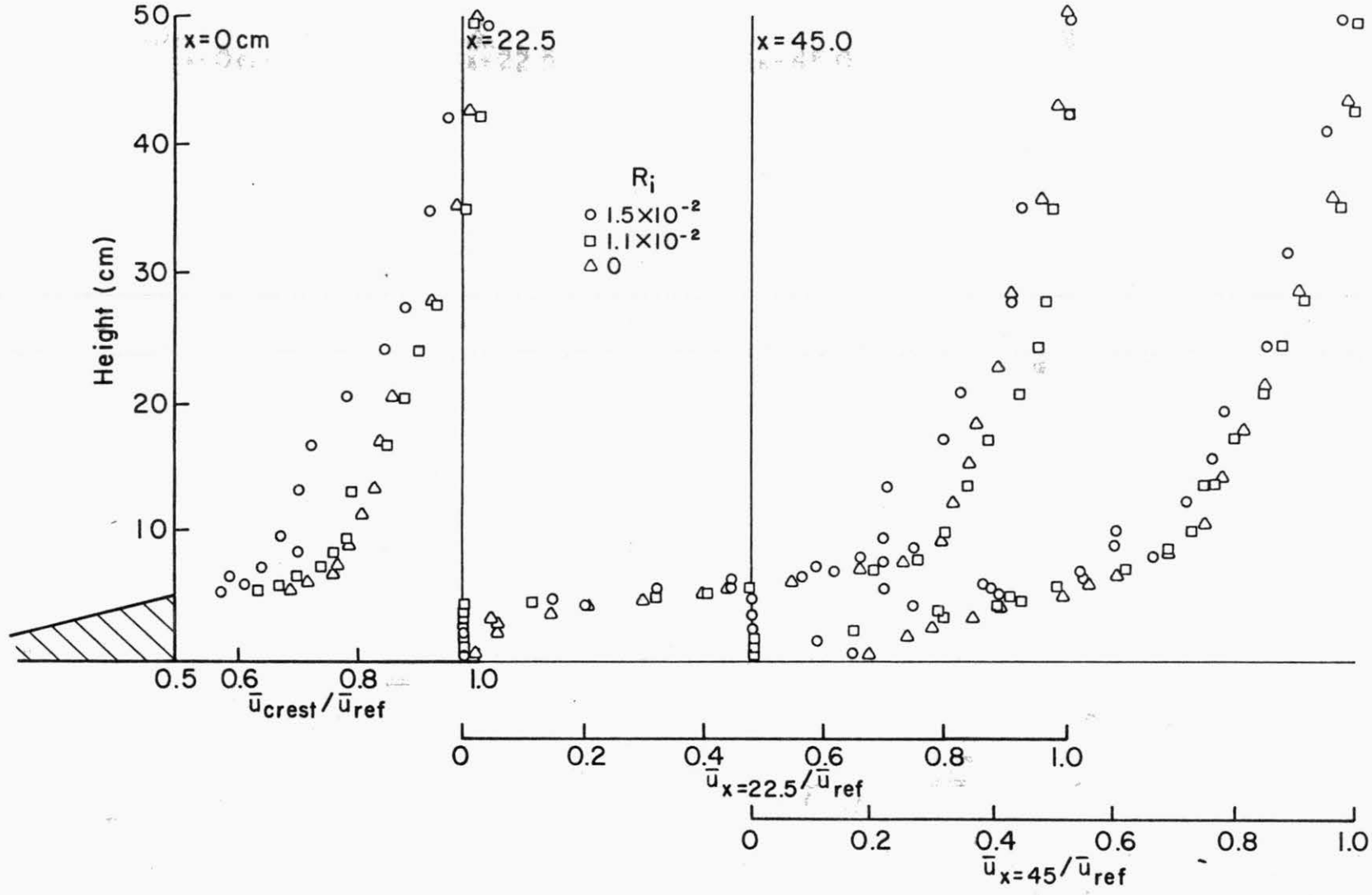

FIGURE 3.34. Mean Velocity Profiles Downwind of a Triangular Ridge $h/L_u = 1/4$ and $h/L_d = 1/10$ in Neutral and Stable Stratified Boundary Layers. Test Cases XI, XVII and XVIII

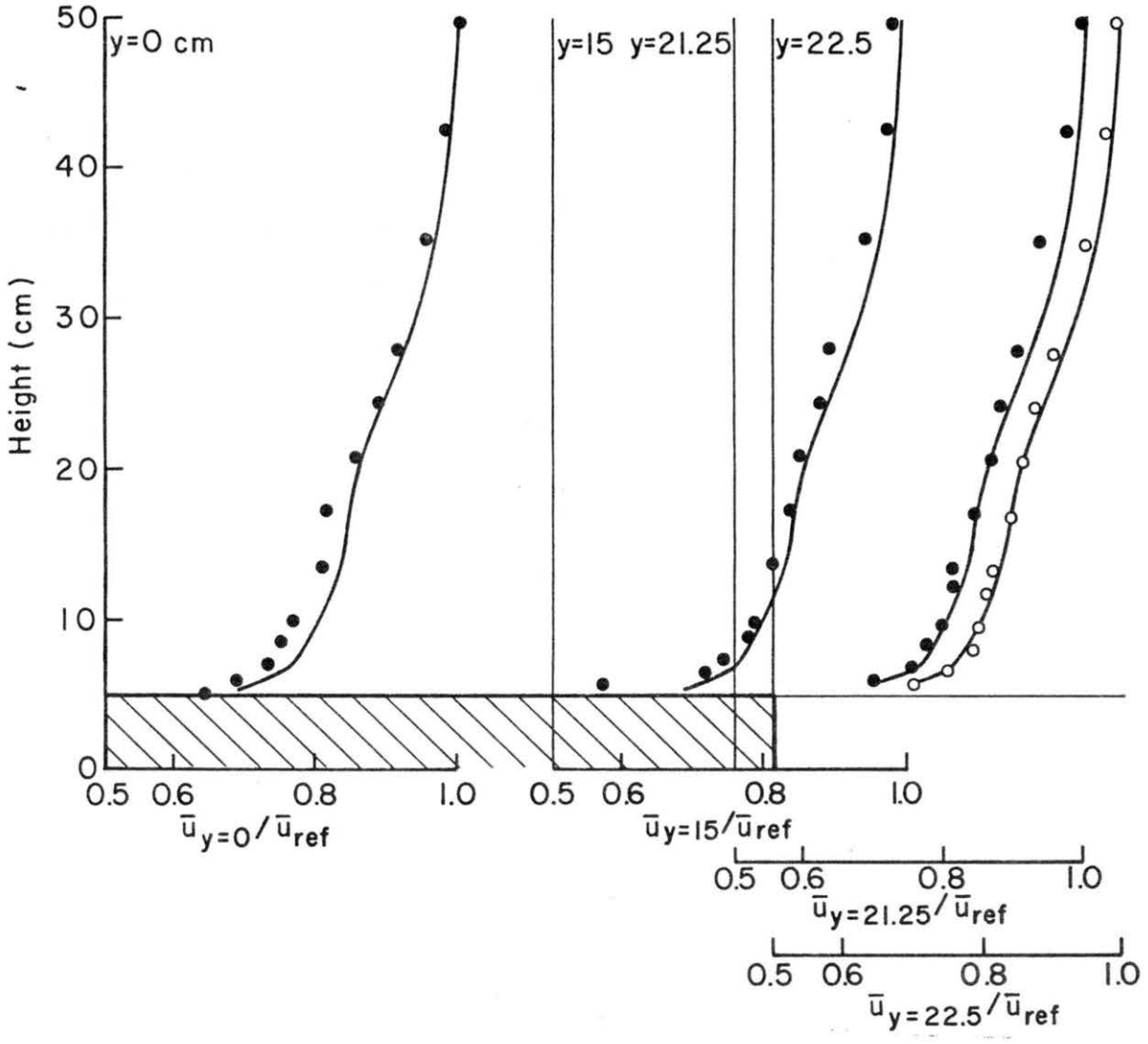

FIGURE 3.35. Mean Velocity Profiles Along the Crest of a Finite Width Ridge, b = 22.5 cm $h/L_u = 1/4$, $h/L_d = 1/0$. Test Case XIII

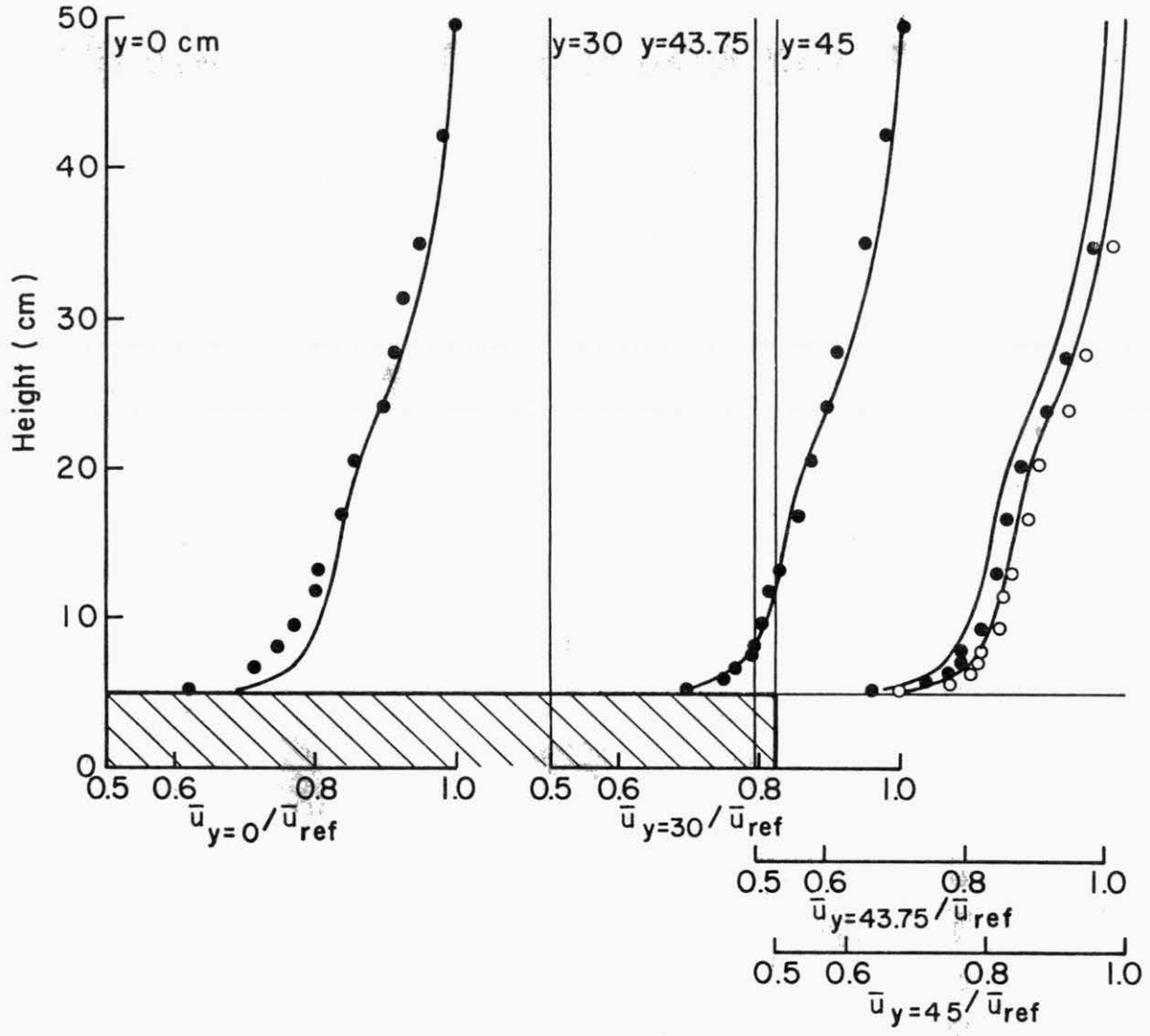

FIGURE 3.36. Mean Velocity Profiles Along the Crest of a Finite Width Ridge, b = 45 cm h/L_u = 1/4, h/L_d = 1.0. Test Case XIV

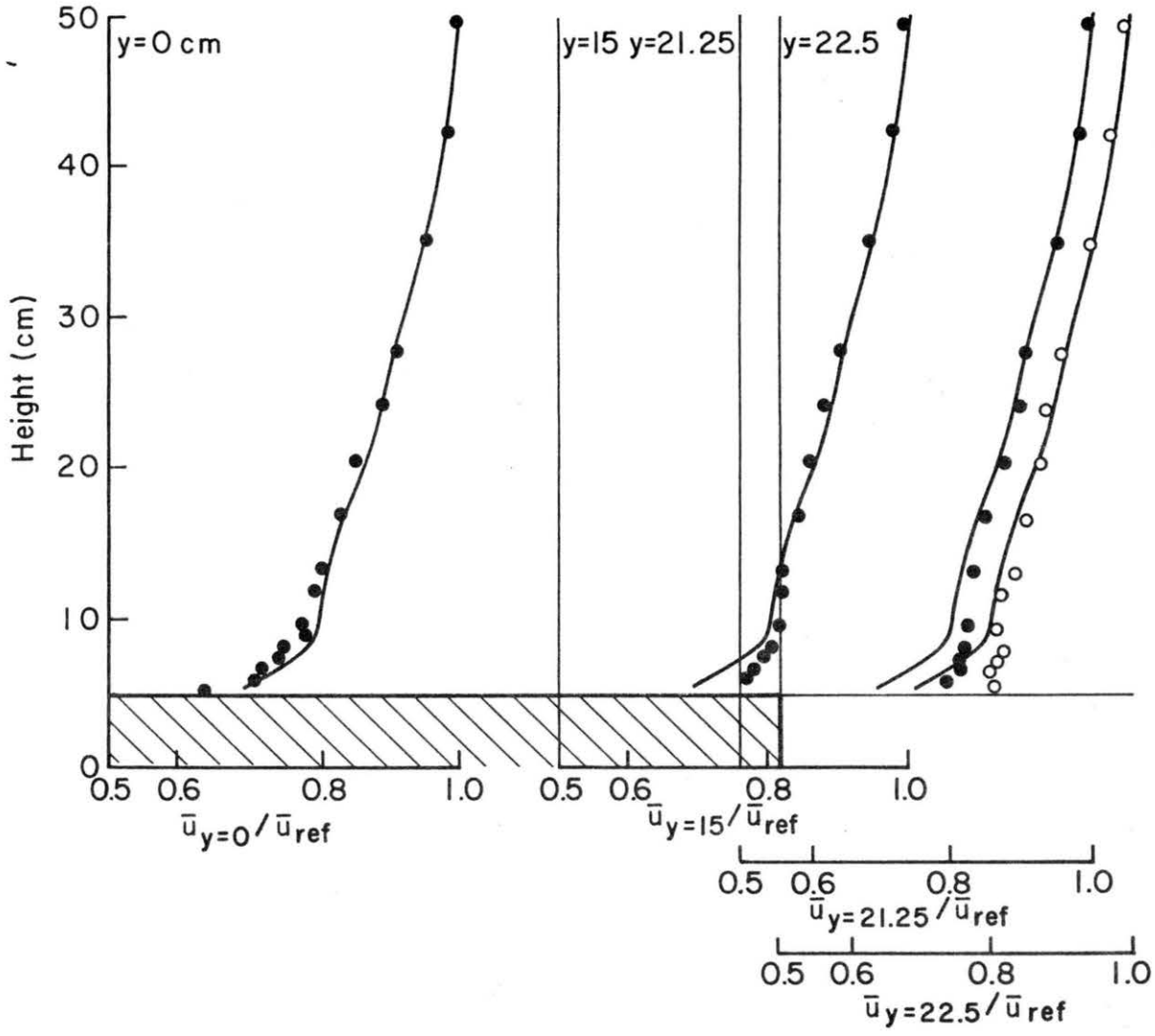

FIGURE 3.37. Mean Velocity Profiles Along the Crest of a Finite Width Ridge, b = 22.5 cm h/L_u = 1/4, h/L_d = 1/3. Test Case XV

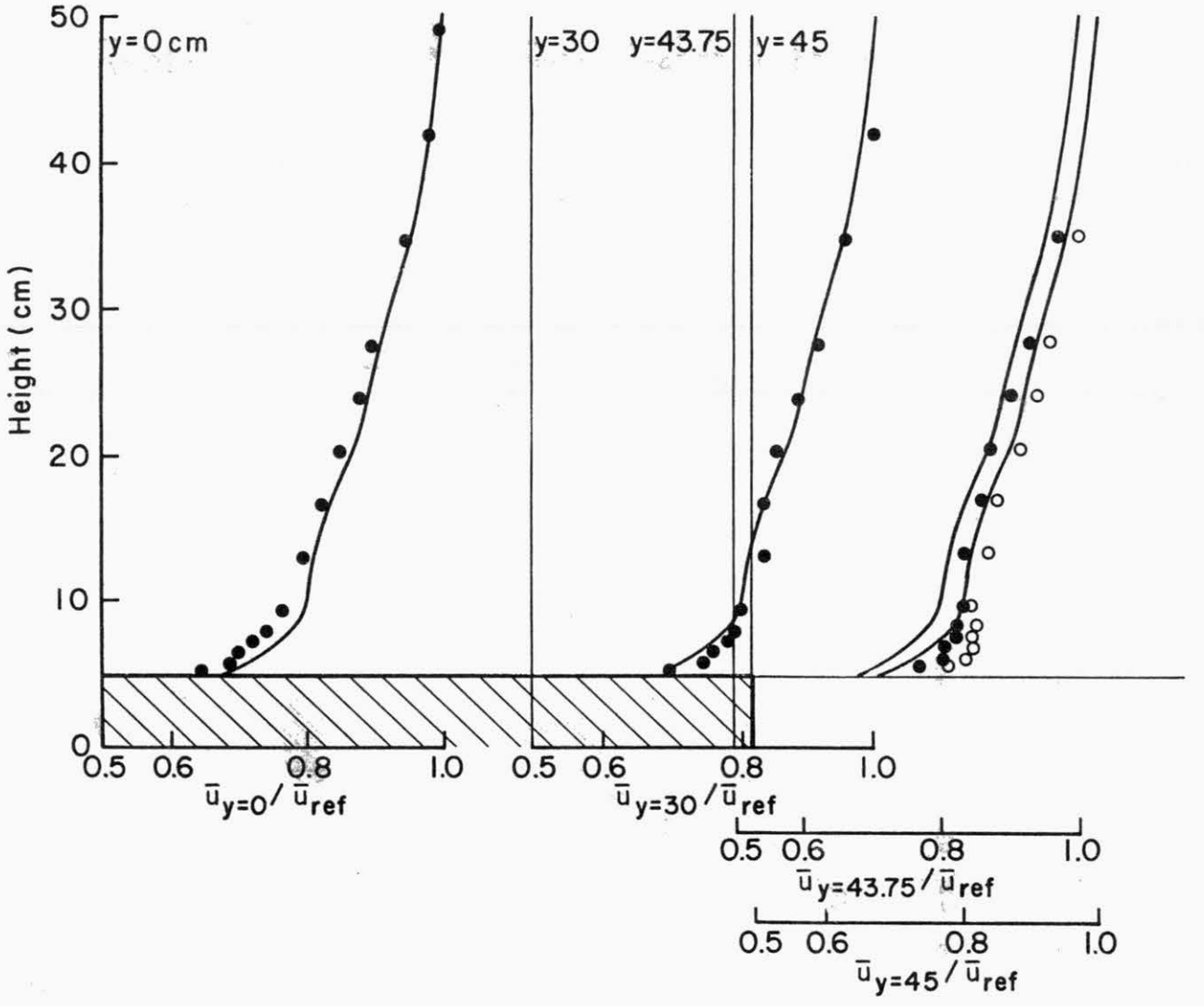

FIGURE 3.38. Mean Velocity Profiles Along the Crest of a Finite Width Ridge, b = 45 cm h/L_u = 1/4, h/L_d = 1/3. Test Case XVI

in the amplification factor become increasingly less as h/L_b decreases; e.g., the parameter, A increases from 1.055 to 1.062, as b/L_b varies from 1 to ∞, for $h/L_b = 0.1$.

Speedups over a finite-width ridge in a stable stratified boundary layer are significantly less than those over the same ridge under neutral conditions. Figure 3.39 shows a set of velocity profiles at different locations at the crest. The ridge shape is identical to that of Figure 3.35 ($h/L_u = 1/4$, $h/L_d = 1/0$). Particularly at the ends of the crest the speedup is much less. This is caused by the tendency of the air to go around the ridge rather than over it. Relatively large speedup effects are obtained above the center of the crest.

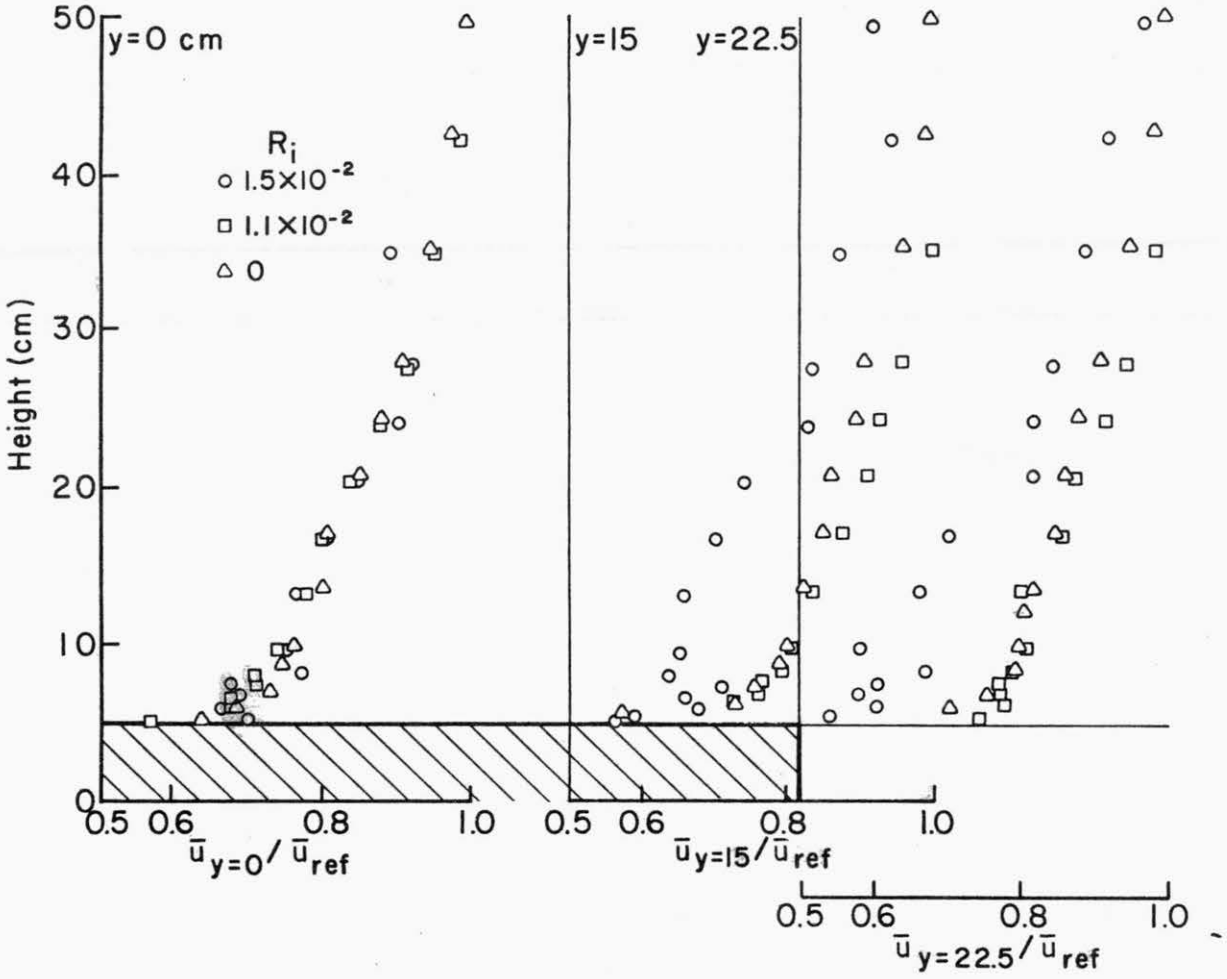

FIGURE 3.39. Comparison of Mean Velocity Profiles Along the Crest of a Finite Width Ridge, b = 22.5, h/L_u = 1/4, h/L_d = 1/0 in Neutral and Stable Stratified Boundary Layers. Test Case XX

4.0 A PREDICTION TECHNIQUE FOR THE VELOCITY PROFILE AT A RIDGE CREST

Analysis of the measured data indicates that wind speedups at hill crest is a complicated nonlinear function of approach profile, upwind hill slope, and downwind hill slope. Neither linearized perturbation analysis nor primitive equation numeral models are currently capable of predicting speedup effects over a wide range of these parameters. In this chapter an emperical model has been prepared to perform the prediction task of hill crest wind speed prediction. In section 4.1 the empirical model is developed and adjustable constants specified. In section 4.2 the model is tested against the independent field data of Bradley (1978). Probable error bands are specified based on the scatter of comparisons against the laboratory measurements. Section 4.3 recommends a step-by-step procedure for the use of this new model. Two example cases are produced.

4.1 EMPIRICAL MODEL FOR HILL CREST VELOCITY AMPLIFICATION

It is common practice to approximate boundary-layer velocity profiles by a power law distribution. This approach has been very successful particularly over flat terrain. In the present study the crest profile has been approximated by a power law formula to obtain a simple relation between upwind conditions and ridge shape on the one hand and crest profile on the other hand. This implies that certain crest-profile features, such as local maximum velocities ("jets"), cannot be reproduced, but that the large features of the profile will be predicted.

The factorial increase in velocity is defined by an amplification factor

$$A(z) = \frac{\bar{u}_c(z)}{\bar{u}_o(z)} \quad . \tag{4.1}$$

Substitution of the power law expressions into this equation give

$$, \quad A(z) = A(z_{ref}) \left(\frac{z}{z_{ref}}\right)^{\alpha_c - \alpha_o} , \tag{4.2}$$

where α_o and α_c are the power law exponents of the velocity profiles at the crest and upwind, respectively, and z_{ref} is the reference height where velocities are known.

By defining variables, s and a , as

$$s = \frac{z}{h} \quad \text{and} \quad a = \frac{z_{ref}}{h} \tag{4.3a,4.3b}$$

and by selecting a value, s , such that

$$A(sh) = 1 \tag{4.4}$$

the following expression is derived from equation (4.1):

$$A(ah) = \left(\frac{s}{a}\right)^{\alpha_o - \alpha_c} . \tag{4.5}$$

Let a = 1; then it appears from test cases selected from Table A.1 that $\alpha_o - \alpha_c$ and A are highly correlated (see Figure 4.1). The relation between A(h) and $\alpha_o - \alpha_c$ as defined by equation (4.5) is displayed for s = 7 and s = 10. Almost all data fall in this s-value range, implying that speedups are practically zero for heights larger than 7h. Selecting s = 8.5 yields an expression for A(z) which only depends on the difference in power law exponents, $\alpha_c - \alpha_o$, namely

$$A(z) = \left(\frac{z}{8.5h}\right)^{\alpha_c - \alpha_o} . \tag{4.6}$$

If the amplification factor would be known at the reference height, the exponent, α_c, can be calculated from equation (4.5), namely

$$\alpha_c = \alpha_o - \frac{\log A(ah)}{\log \frac{8.5}{a}} \tag{4.7}$$

An alternative expression for A(z) may be obtained by the following relation between $\alpha_o - \alpha_c$ and A(h) (see Figure 4.1):

$$\alpha_o - \alpha_c = \frac{A(h) - 1}{2.3} . \tag{4.8}$$

Substitution of equation (4.8) into equation (4.2) gives

$$A(z) = A(ah) \left(\frac{z}{ah}\right)^{\frac{1 - A(h)}{2.3}} , \tag{4.9}$$

where A(h) can be calculated iteratively from the expression

$$A(h) = 1 + \frac{2.3}{\log a} \log \left(\frac{A(h)}{A(ah)}\right) . \tag{4.10}$$

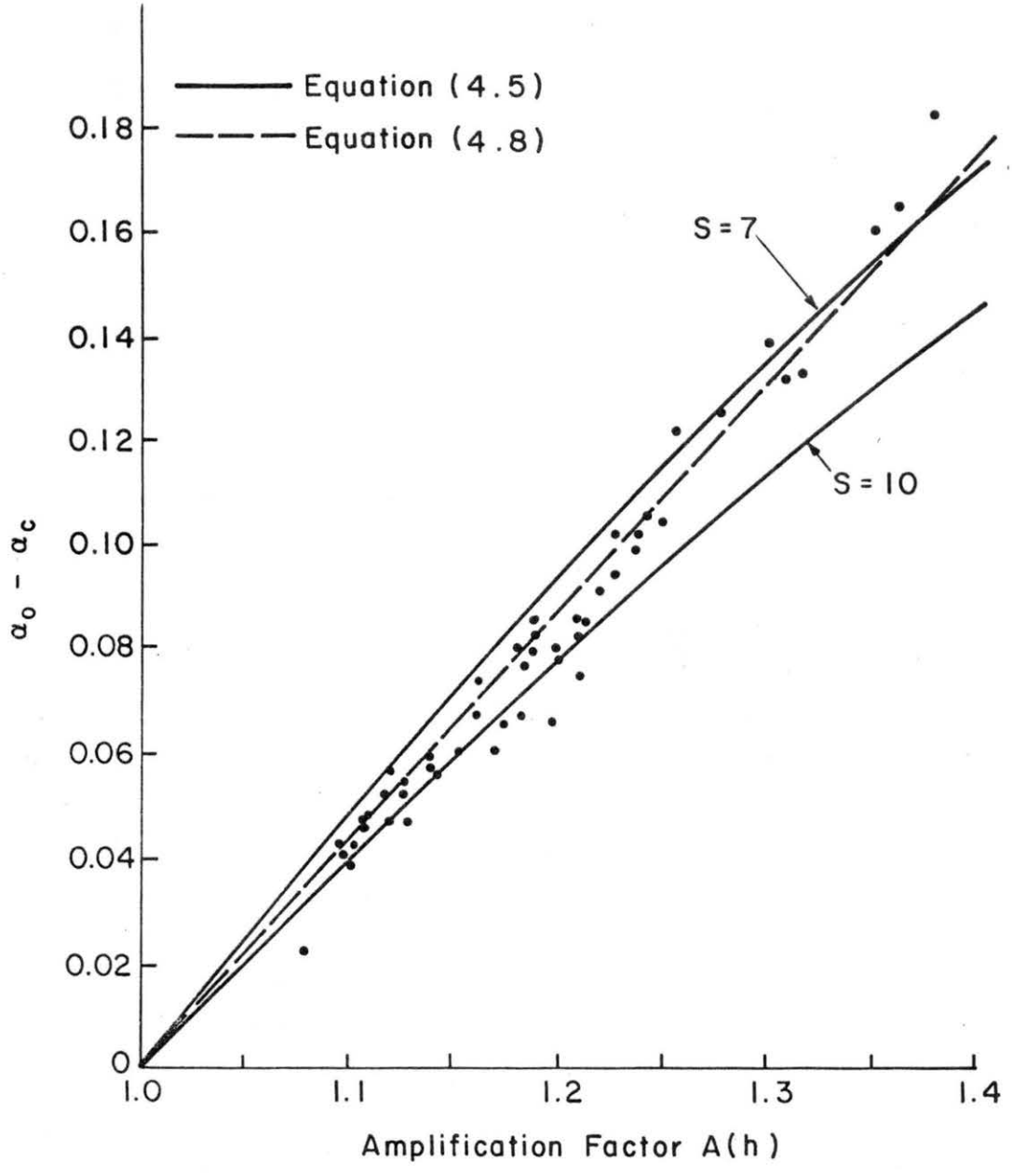

FIGURE 4.1. Correlation Between $\alpha_o - \alpha_c$ and Crest-amplification Factor at z=h Obtained from Wind Tunnel Experiments

The power law profile approach may also be applied to establish a criterion for the height at which the streamlines are approximately horizontal. For numerical calculations, such a criterion may be of practical value for the specificiation of the height of the top boundary condition. Stipulating that at a height th , the streamlines are not affected by the topography (streamlines are horizontal), the following expression is obtained after integrating the upwind and crest power law profiles:

$$\frac{\alpha_c+1}{\alpha_o+1} = \left(\frac{t-1}{t}\right)\left(\frac{t-1}{t}\right)^{\alpha_c} \quad . \tag{4.11}$$

Since $t>>1$ and $\alpha_c \lesssim 0.25$, the factor t may be approximated by

$$t \simeq \frac{1+\alpha_o}{\alpha_o-\alpha_c} \quad . \tag{4.12}$$

Expression (4.12) suggests that for large differences between α_o and α_c (large speedup) t is relatively small. Hence, low hills require a relatively much larger spatial domain during numerical calculations than steep hills with the same height (provided no flow separation occurs).

It has been shown that the speedup over a hill can be characterized by a single parameter, namely the amplification factor at a selected height, preferably above the inner region. By relating this amplification factor to the three most important characteristics, namely α_o , h/L_u and h/L_d , it is possible to predict the amplification distribution from the upwind velocity distribution (α_o) and ridge characteristics.

The dependency between α_o and A is given in Figure 4.2 for two sets of values of h/L_u and h/L_d. These data suggest the following relation between α_o and A.

$$A(\alpha_o) = A(\alpha_o') \frac{1.15 + \alpha_o}{1.15 + \alpha_o'} \tag{4.13}$$

where α_o and α_o' are two different upwind power law exponents. For more gentle hills, however, the effect of α_o on A decreases. Note that for flat terrain $A(\alpha_1) = A(\alpha_o')$.

The relations between A(h) and different combinations of h/L_u and h/L_d for $\alpha_o = 0.13$ are given in Figures 4.3 and 4.4. Measured amplification factors for $\alpha_o \neq 0.13$ were corrected using equation (4.13). Since

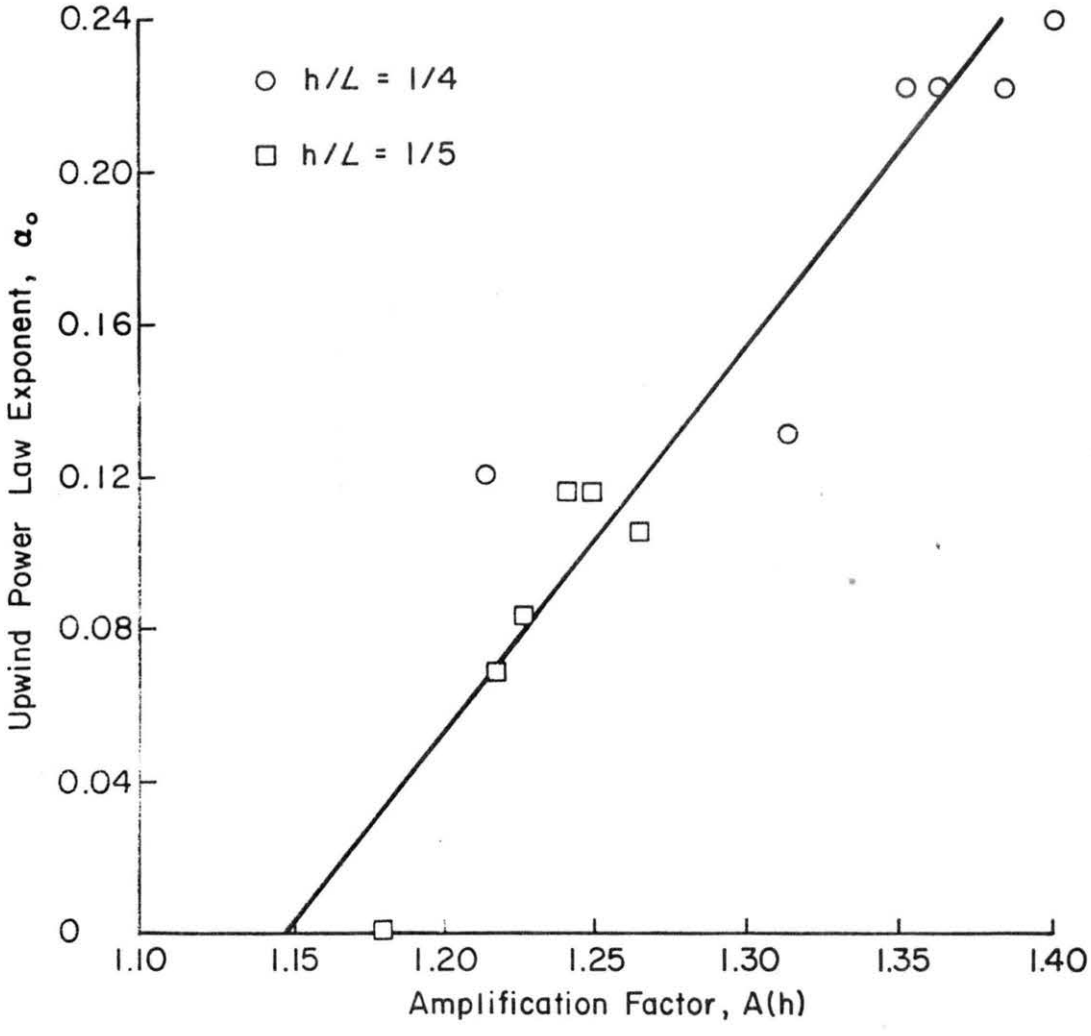

FIGURE 4.2. Correlation Between Upwind Power Law Exponent and Crest-amplification Factor at z=h

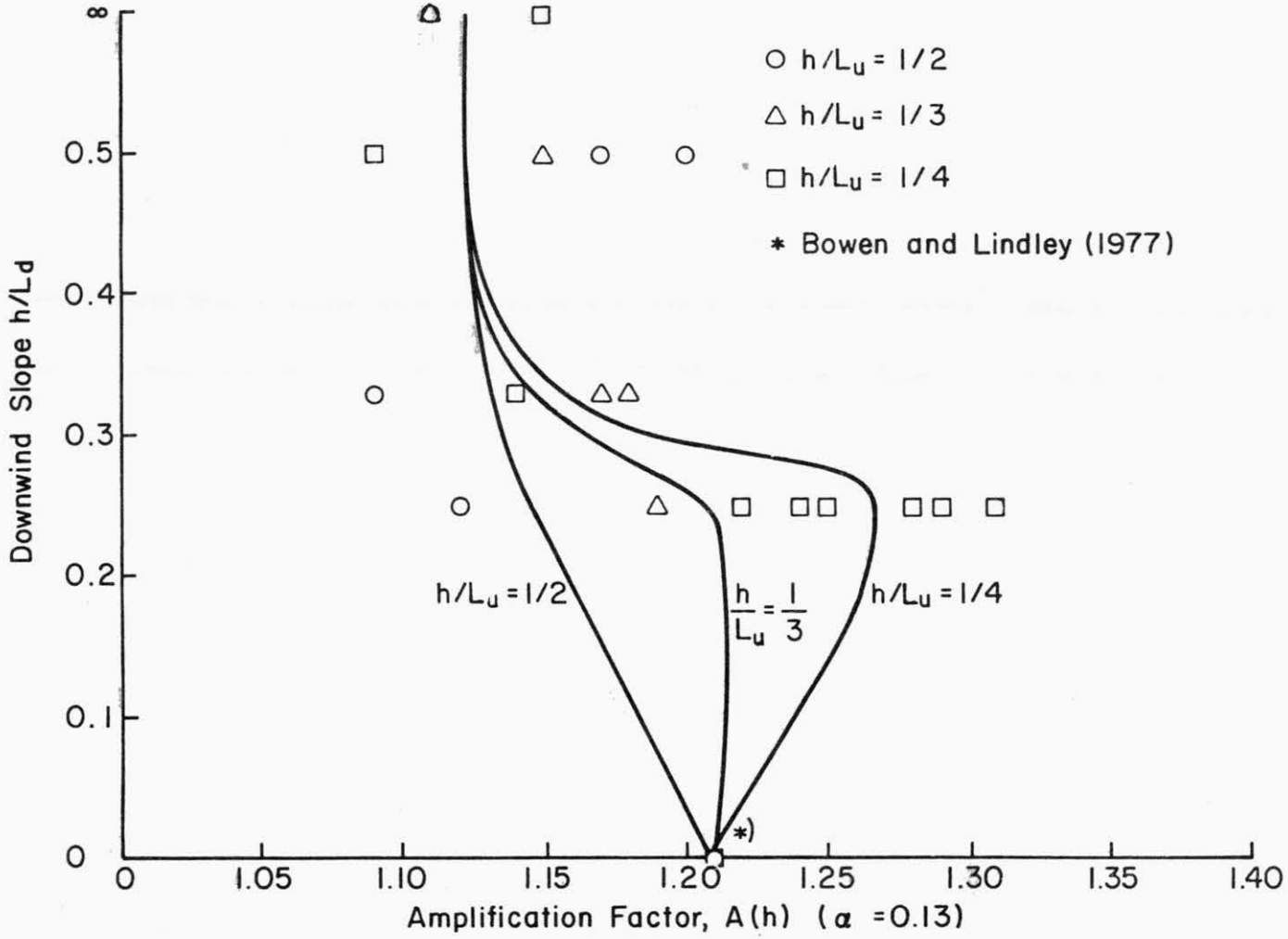

FIGURE 4.3. Dependency of Crest-amplification Factor on Downwind Slope for h/L_u = 1/2, 1/3, and 1/4; α_o = 0.13

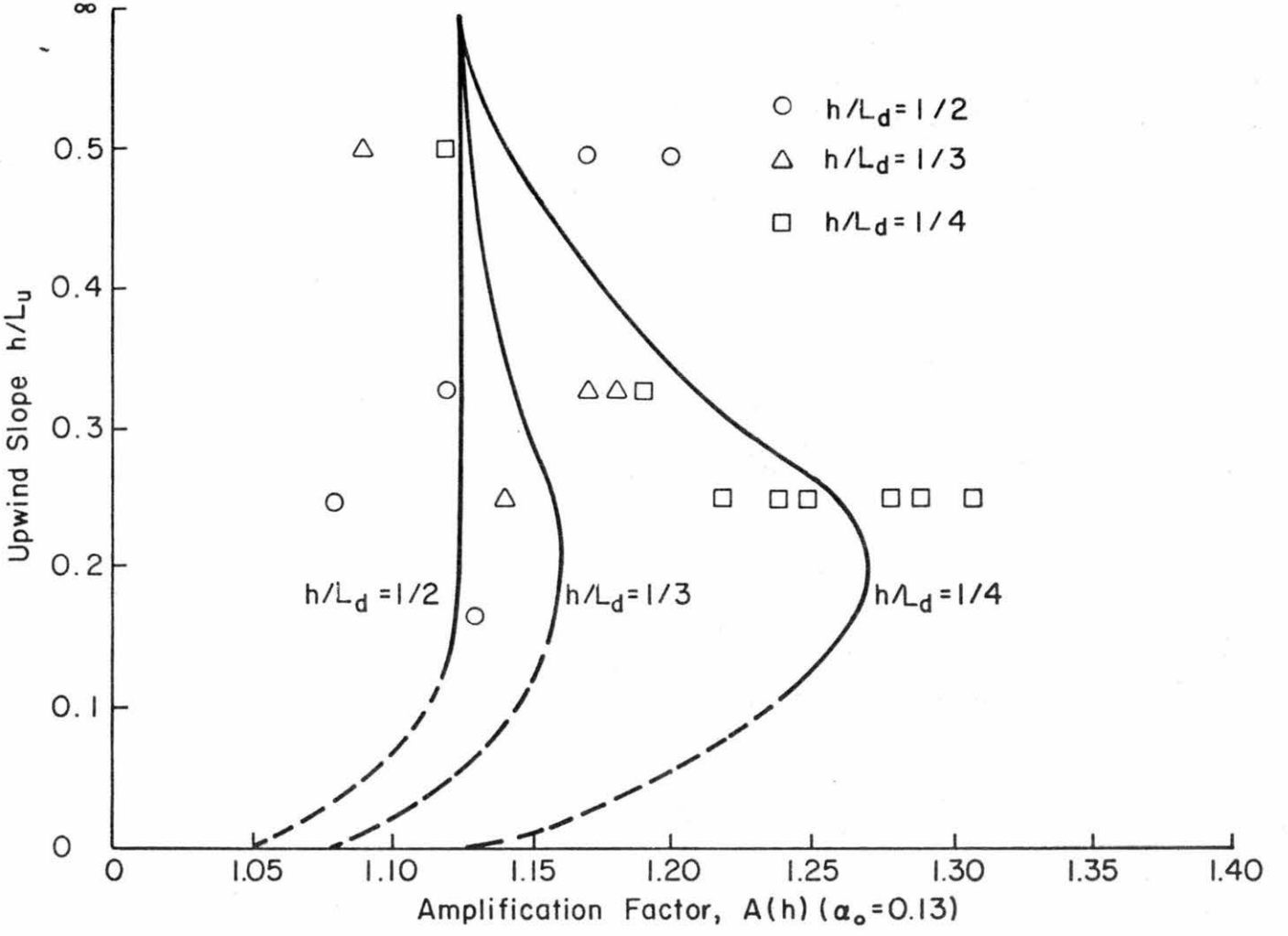

FIGURE 4.4. Dependency of Crest-amplification Factor on Upwind Slope for h/L_d = 1/2, 1/3 and 1/4; α_o = 0.13

there is considerable scatter in the data, the curves given in Figure 4.3 and 4.4 were selected on the basis of the available data and an understanding of the effects of flow separation on the mean flow over the hill.

In this section a methodology has been developed to predict the mean velocity distribution above a ridge crest. The prediction technique has been applied to an example problem in the following section.

4.2 MODEL COMPARISON AGAINST FIELD DATA

The amplification factors calculated from Bradley's (1978) velocity measurements were compared with predicted amplifications using equations (4.6) and (4.7), and, alternatively, using equations (4.9) and (4.10). A representative upwind velocity distribution was obtained for Bradley's case by extrapolating the velocity data upwards from 25 m by assuming a logarithmic velocity profile. A power law exponent was then estimated by fitting the power law formula over a layer between 10 m and 100 m. It was found that $\alpha_o = 0.26$, which is in good agreement with Counihan's estimate of 0.24 for flat terrain with a roughness length $z_o = 1$ m. Values of α_c and A(z) have been calculated for various reference heights. Results are presented in Tables 4.1 and 4.2. The amplification distribution was also calculated using equations (4.9) and (4.10). Results for various reference heights are given in Table 4.3.

A comparison between predicted and measured amplification factors indicates that equation (4.6) leads to an average error of about 15 percent. Better results were obtained with equation (4.9), particularly for reference heights above the inner region. The errors in predicted amplification factors are less than 10 percent. For reference heights above the inner region, errors are less than 5 percent. When equation (4.9) was applied to the wind-tunnel data, average errors in the predicted A-values deviated less than 5 percent from the measured amplification factor.

4.3 EXAMPLE CALCULATIONS

In Section 4.1 of this report empirical expressions were developed to predict mean velocities above a ridge crest. The following paragraphs suggest a rate methodlogy to follow when estimating wind speed over hill crests.

TABLE 4.1. Field Data of Bradley (1978) and Calculation of A(ah) and α_c

z (m)	$\bar{u}_o$ (m/s)	$\bar{u}_c$ (m/s)	A(ah)	a	α_c
9	2.84	5.45	1.92	0.055	0.13
17	3.70	7.16	1.94	0.104	0.11
28	4.36	8.13	1.86	0.172	0.10
40	4.82	7.93	1.64	0.245	0.12
55	5.25	8.29	1.58	0.337	0.12
70	5.57	8.50	1.52	0.429	0.12
89	5.89	8.66	1.47	0.546	0.12

TABLE 4.2. Comparison of Measured and Calculated Amplification Factors, A, Using Equation (4.6)

Field Data		Calculated A Using Equation (4.6)			
z (m)	A(z)	$\alpha_c = 0.13$	$\alpha_c = 0.11$	$\alpha_c = 0.10$	$\alpha_{c'} = 0.12$
9	1.92	1.92	1.74	1.57	1.83
17	1.94	1.77	1.62	1.55	1.70
28	1.86	1.66	1.54	1.48	1.60
40	1.64	1.59	1.48	1.43	1.53
55	1.58	1.52	1.43	1.38	1.47
70	1.52	1.47	1.39	1.35	1.43
89	1.47	1.43	1.35	1.32	1.39

TABLE 4.3. Comparison of Measured and Calculated Amplification Factors, A, Using Equation (4.9)

Field Data		Calculated A Using Equation (4.9) z_{ah}						
z (m)	A(z)	9 m	17 m	28 m	40 m	55 m	50 m	89 m
9	1.92	1.92	2.14	2.25	2.04	2.07	2.06	2.07
17	1.94	1.76	1.94	2.02	1.86	1.88	1.87	1.88
28	1.86	1.65	1.79	1.86	1.73	1.75	1.74	1.75
40	1.64	1.57	1.70	1.75	1.64	1.66	1.65	1.66
55	1.58	1.51	1.61	1.66	1.57	1.58	1.58	1.58
70	1.52	1.47	1.55	1.60	1.51	1.52	1.52	1.52
89	1.47	1.42	1.50	1.53	1.46	1.47	1.47	1.47

Prediction Procedures

a) Available data: ridge shape, upwind surface roughness, and upwind topography.

1) Determine characteristic ridge lengths L_u and L_d.

2) Determine the upwind power law exponent α_o.

For a uniform and homogeneous upwind surface roughness, a good estimate of the power law exponent may be obtained from Counihan (1975). He proposed the following relation between surface roughness z_o and α_o:

$$\alpha_o = 0.096 \log_{10} z_o + 0.016 (\log_{10} z_o)^2 + 0.24 \qquad (4.14)$$

The following values of z_o are typical for different terrain types:

snow and short grass	0.1 cm
crops	5 cm
rural	20 cm
rural and woods	50 cm
woods	100 cm

Alternatively, α_o may be obtained by matching the powerlaw velocity distribution to the atmospheric velocity distribution for stable conditions, given by

$$\bar{u}_o(z) = \frac{u_*}{k} \ln \frac{z+z_o}{z_o} + \beta \frac{z}{L_{mo}} \quad , \qquad (4.15)$$

where L_{mo} is the Monin-Obukhov length parameter. The powerlaw exponent α_o as a function of height is then

$$\alpha_o = \frac{1 + \frac{z}{L_{mo}}}{\ln \frac{z}{z_o} + \beta \frac{z}{L_{mo}}} \quad . \qquad (4.16)$$

A representative value of z is $z = 0.7h$, so that

$$\alpha_o = \frac{1 + 0.7 \frac{h}{L_{mo}}}{\ln \frac{0.7h}{z_o} + 0.7 \beta \frac{h}{L_{mo}}} \quad . \qquad (4.17)$$

If upwind topography is close to the ridge, it creates high turbulence levels; hence, one has to increase α_o to say $\alpha_o = 0.3$.

Generally this correction must be applied if the upwind topography has steep downwind slopes $h/L_d < 1/4$ and if the distance to an upwind hill is less than 15 times the height of the upwind hill.

3) Determine the power law exponent correction factor from

$$f \equiv \frac{A(\alpha_o)}{A(\alpha_o=0.13)} = \frac{1.28}{1.15+\alpha_o} \quad . \tag{4.18}$$

4) Estimate $A(h;\ \alpha_o = 0.13)$ for h/L_u, h/L_d from Figures 4.3 and 4.4, and multiply this value with f.

5) Calculate the amplification distribution using the following expression

$$A(z) = A(h)\ (\frac{z}{h})^{\frac{1-A(h)}{2.3}} \quad . \tag{4.19}$$

6) Determine the velocity profile from

$$\frac{\bar{u}_c(z)}{\bar{u}_o(z_{ref})} = A(z)\ (\frac{z}{z_{ref}})^{\alpha_o} \quad . \tag{4.20}$$

b) Available data: ridge shape, upwind surface roughness, and upwind topography, and $\overline{u_o}(z_{ref})$ and $\overline{u_c}(z_{ref})$.

1) Determine α_o as indicated under a, point 2.

2) Calculate

$$A(z_{ref}) = \frac{\overline{u_c}(z_{ref})}{\overline{u_o}(z_{ref})} \quad . \tag{4.21}$$

The reference height, z_{ref}, should be preferably above the inner region: $(z_{ref} > 0.067\ z_o^{0.1}\ L^{0.9})$.

3) Calculate the amplification distribution

$$A(z) = A(z_{ref})(\frac{z}{z_{ref}})^{\frac{1-A(h)}{2.3}} \quad , \tag{4.22}$$

where $A(h)$ follows from

$$A(h) = 1 + \frac{2.3}{\log}\left(\frac{z_{ref}}{h}\right) \log \left(\frac{A(h)}{A(z_{ref})}\right) \quad . \tag{4.23}$$

Examples

a) The following data is available:

$L_u = 550$ m; $L_d = 600$ m; $h = 163$ m;
uniform surface roughness, woods; no upwind hills.
(Bradley, 1978).

According to Figures 4.3 and 4.4 $A(h; \alpha_o = 0.13) = 1.20$. From equation (4.14) it follows that $\alpha_o = 0.24$ ($z_o = 1$ m). The A correction factor is then 1.09, so that

$$A(h) = A(h; \alpha_o = 0.13) \quad f = 1.31.$$

Thus the velocity distribution at the crest is

$$\frac{\bar{u}_c(z)}{\bar{u}_o(z_{ref})} = 1.31 \left(\frac{z}{z_{ref}}\right)^{0.24} .$$

b) The following data is available:

$L_u = 550$ m; $L_d = 600$ m; $h = 163$ m; uniform surface roughness, woods; no upwind hills; $\bar{u}_o(17\text{ m}) = 3.70$ m/sec; $\bar{u}_c(17\text{ m}) = 7.16$ m/sec.

The amplification factor at $z = 17$ m is

$$A(h) = 1.36,$$

so that (equation (4.22))

$$A(z) = 1.94 \left(\frac{z}{17}\right)^{-0.16} .$$

The velocity distribution at the crest is then

$$\frac{\bar{u}_c(z)}{\bar{u}_o(z_{ref})} = 1.94 \left(\frac{z}{17}\right)^{-0.16} \left(\frac{z}{z_{ref}}\right)^{0.24} .$$

The velocity distribution is expressed in terms of $\bar{u}_o(z_{ref})$ and z_{ref} to indicate that any height may be selected. For example, one may select the annual mean velocity at 10 m.

5.0 TURBULENCE CHARACTERISTICS OVER TWO DIMENSIONAL RIDGES

The implications of ridge presence on boundary layer turbulence structure is discussed in Section 5.1 in terms of rapid distortion theory. Section 5.2 reveals that the terrain influence of turbulent energy distribution over narrow eddy scales is small for inseparated flow fields.

5.1 DIRECTIONAL DISTRIBUTION OF TURBULENT ENERGY OVER RIDGES

The turbulence structure over a ridge is distorted by the additional strains induced by the ridge. In the inner region the turbulence interacts strongly with the mean flow, whereas in the middle region the turbulence-main flow interaction is weak. The inner and middle regions will be considered separately to discern this difference.

The Inner Region. Section 3.2 indicated that the Reynolds stresses in a thin layer adjacent to the hill-model surface did not always accurately simulate field conditions. Nevertheless, it is possible to approximate the shear stress distribution at the crest by making a number of assumptions, namely: 1) equation (E.12) provides a realistic value for the inner-layer thickness, 2) the Reynolds shear stress at the outer edge of the inner layer is constant and equal to its unwind value, 3) the decrease of shear stress with height is linear, and 4) the longitudinal inertial stress gradient at a height ℓ is of the same order of magnitude as the vertical shear stress gradient. The shear stress distribution above the crest may then be expressed as

$$\frac{\overline{uw}(z)}{\overline{u}_o(\ell)} = \frac{\ell - z}{L}\,\Delta S(\ell) + \frac{u_*^2}{\overline{u}_o(\ell)} \qquad o < z < \ell \tag{5.1}$$

Turbulence shear stresses measured by Bradley (1978) above the crest of a prototype ridge correspond closely to those predicted from equation (5.1). Bradley also reported measurements of the three components of the turbulence intensity in the inner region. His data suggest that all turbulence components above the crest are approximately 50 percent larger than at comparable heights upwind.

The Middle Region. In the middle region the turbulence is affected by the history of the airparcels. Particularly, if the eddy-decay time-scale is

less than the time it takes an airparcel to travel over a distnace L, history or rapid distortion effects dominate turbulence production and dissipation effects. In Section 2.1 it was shown that this is generally the case if $L < \delta$.

Figures 3.1d, 3.5d, 3.7d, 3.9d and 3.27 to 3.31 show contour plots of longitudinal turbulence intensities. In all cases a slight increase exists along streamlines toward the upwind base and a decrease exists towards the crest. Rider and Sandborn (1977a) reported measurements of vertical turbulence intensities for almost identical flow cases. Their data show that the relative vertical component of turbulence increases at hill crest.

For all flow cases considered herein $L < \delta$. Therefore the turbulence is "rapidly distorted" by the mean flow. An increase in vertical turbulence intensity and a decrease in longitudinal turbulence intensity were predicted around a circular cylinder by a Rapid Distortion Theory (Hunt, 1973). Hunt's approach flow was irrotational; whereas the approach boundary layer in the wind tunnel is rotational. Apparently the mean vorticity of the boundary-layer flow is, at least qualitatively, not different from irrotational distortion. Even in the surface region, where the vorticity is relatively large and the eddy-decay time-scale relatively short, a continuous decrease of longitudinal turbulence towards the crest is noticeable (except for the 1/20 hill). For $L > \delta$ the effects of turbulence production, dissipation and diffusion become more significant. These effects reduce the degree of anisotropy of the turbulence.

5.2 TURBULENT SPECTRAL DISTRIBUTION OVER RIDGES

The turbulence eddy structure was investigated by measuring the frequency distribution of the longitudinal fluctuating velocity component. Power spectra of the velocity signal were generated at several locations along streamlines over the 1/4-ridge (Case 5). The locations are indicated in Figure 5.1. The spectra are reproduced in Figures 5.2 and 5.3. (After normalization, the spectra were shifted in the vertical for ease of comparison.) The differences between the spectra are not large. The only systematic deviation noted was irregularity of spectra along the streamline going through the points 1, 2, and 3.

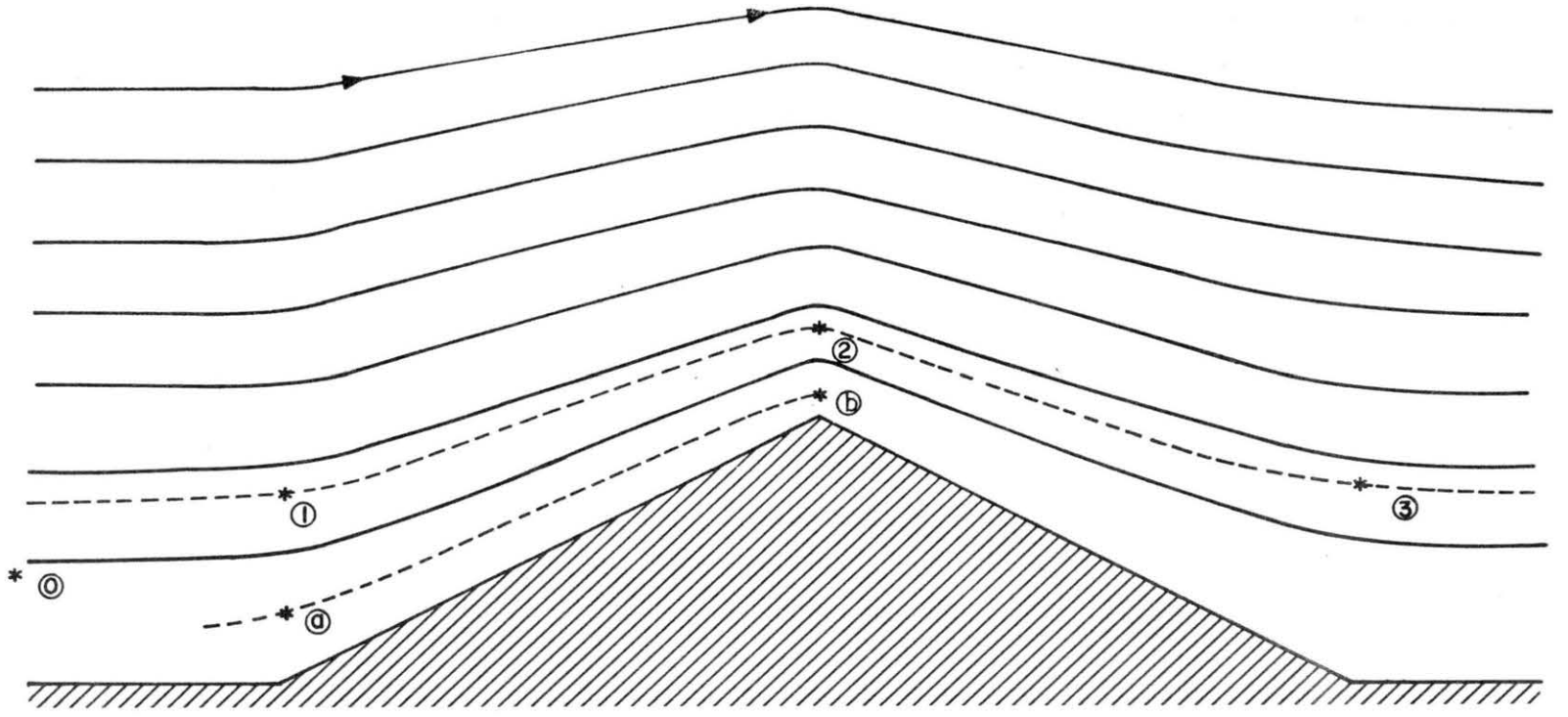

FIGURE 5.1. Locations in the Flow over Triangular Hill, h/L = 1/4, where Velocity Time Signals were Taken

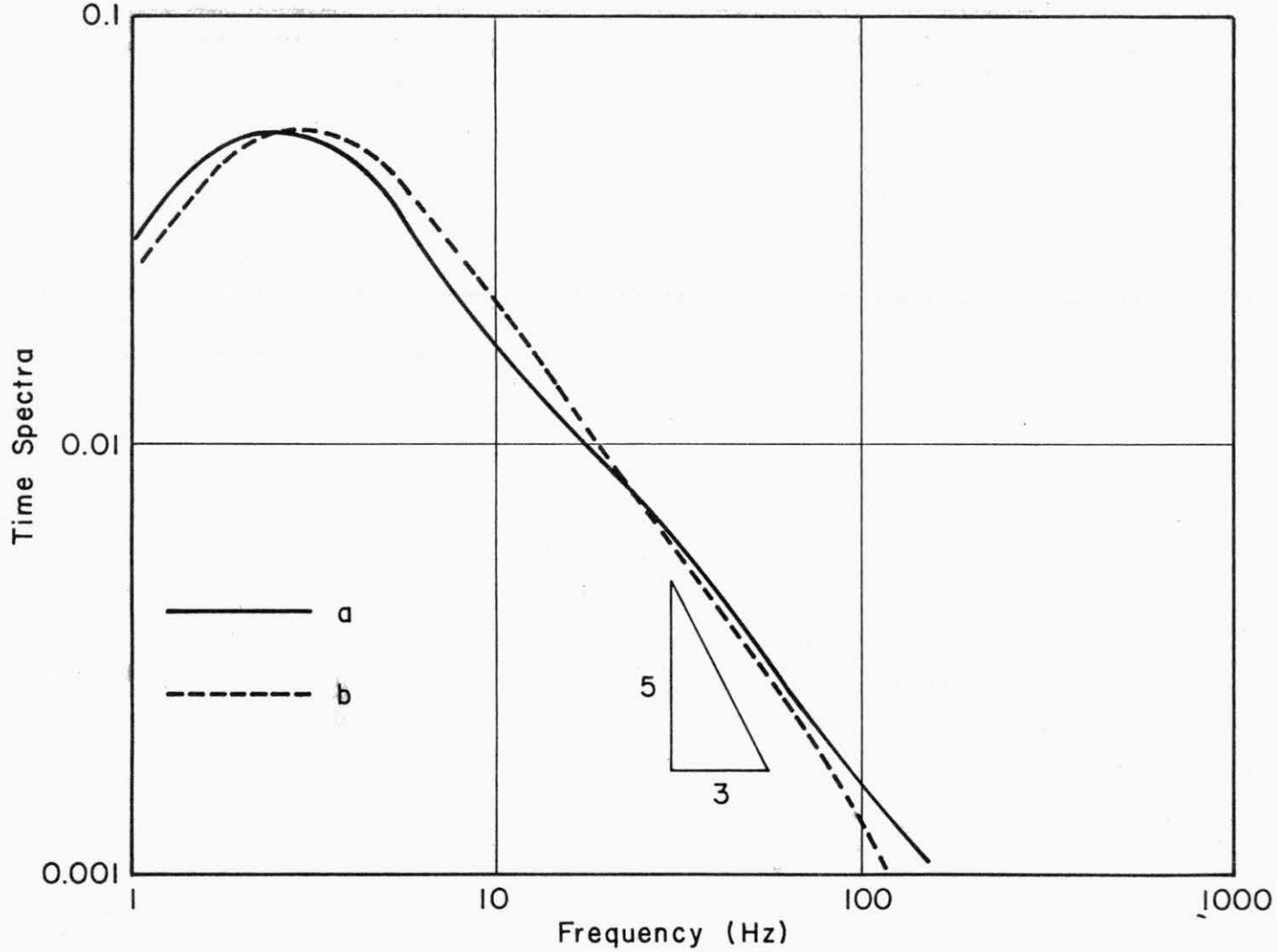

FIGURE 5.2. Comparison of One-dimensional Turbulent Energy Spectra at Different Locations along a Streamline in the Flow over a Triangular Ridge h/L = 1/4

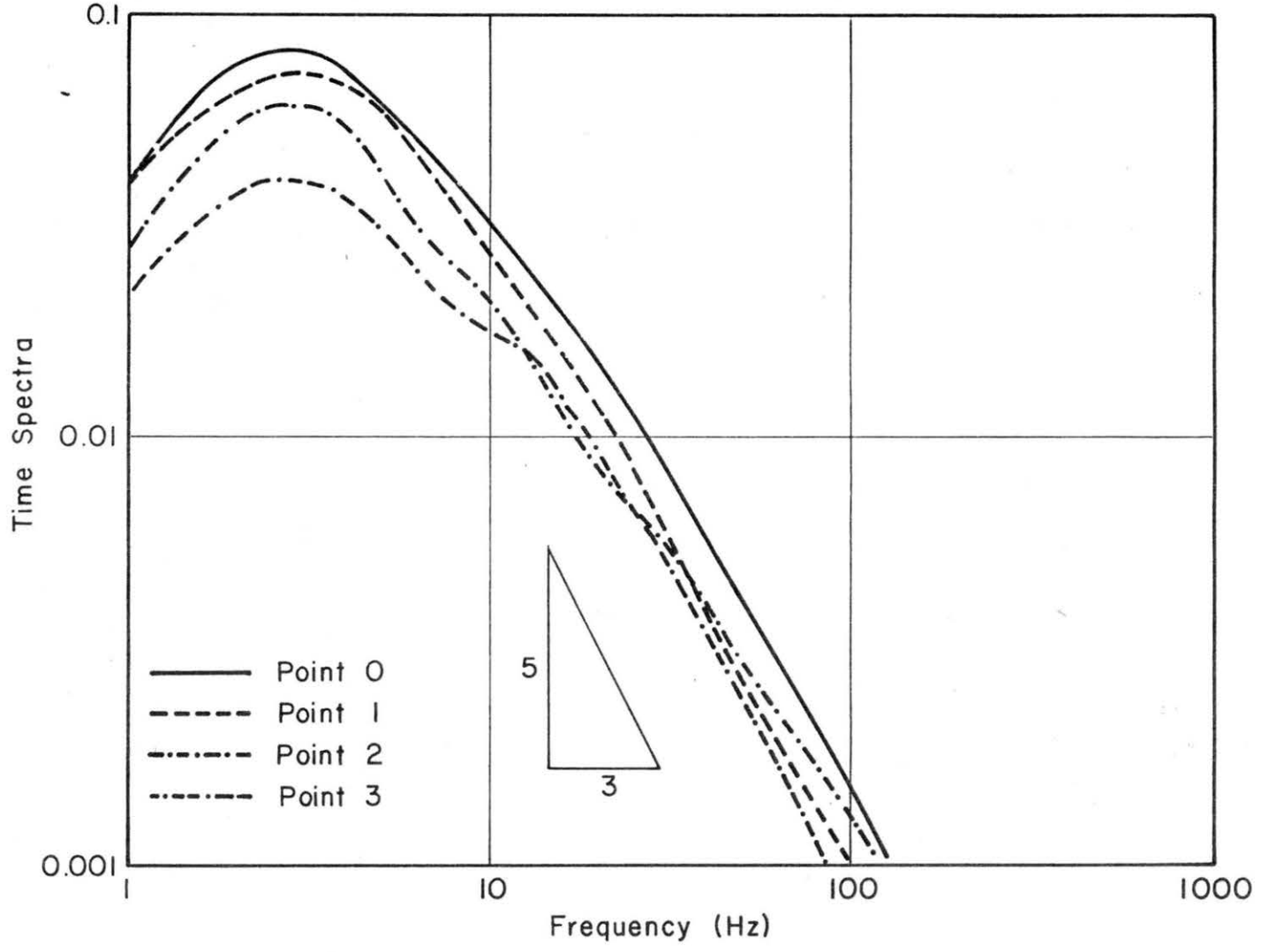

FIGURE 5.3. Comparison of One-dimensional Turbulent Energy Spectra at Different Locations along a Streamline in the Flow over a Triangular Ridge h/L = 1/4

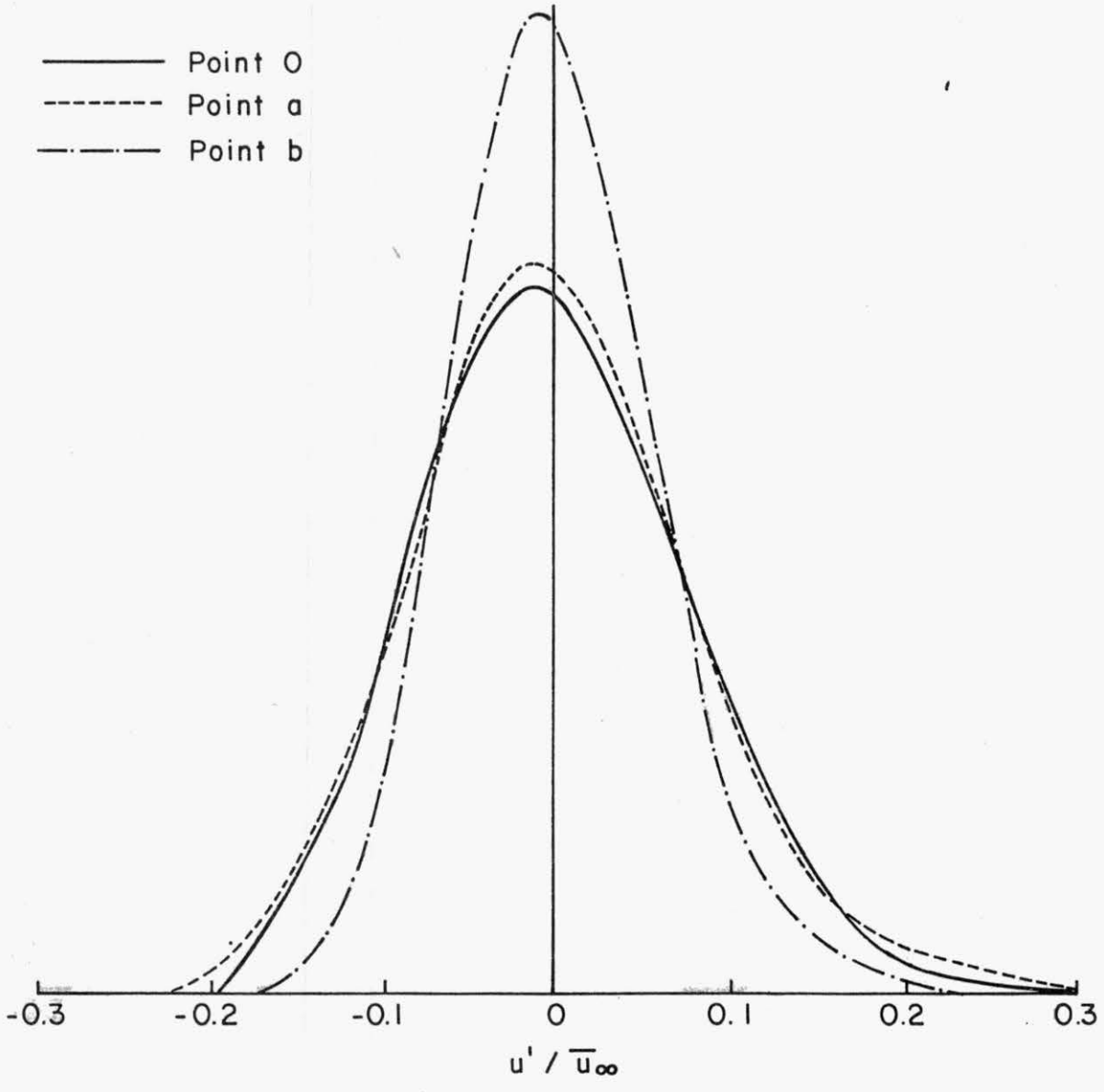

FIGURE 5.4. Probability Density Function of a Velocity Time Signal at Different Locations along a Streamline in the Flow over a Triangular Ridge h/L = 1/4

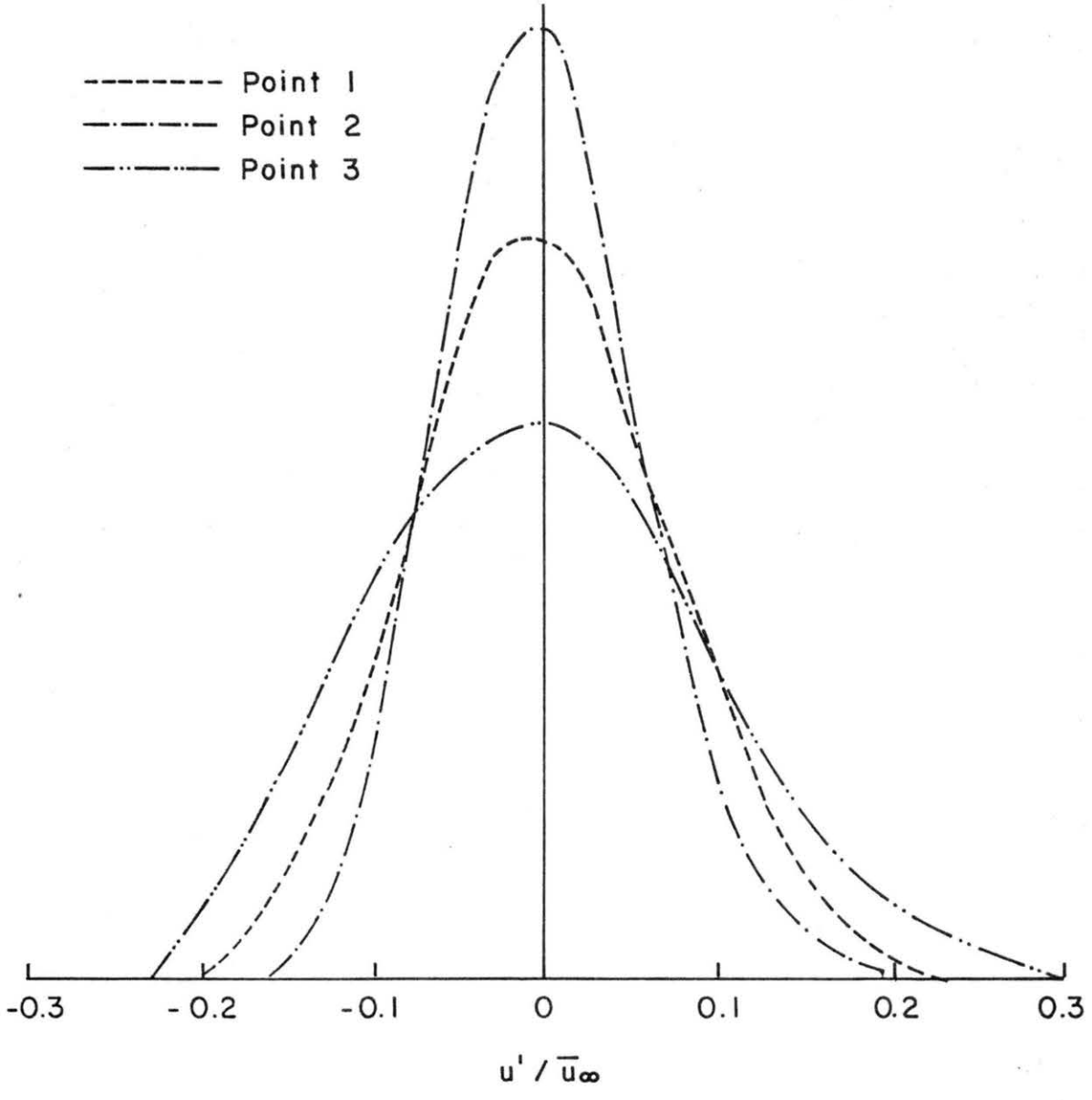

FIGURE 5.5. Probability Density Function of a Velocity Time Signal at Different Locations along a Streamline in the Flow over a Triangular Ridge h/L = 1/4

Probability density functions of the longitudinal velocity fluctuations were generated for the points 0, a, b, 1, 2, and 3 (Figure 5.1). The density functions as displayed in Figures 5.4 and 5.5 show clearly the effects of increase and decrease of turbulence intensities along streamlines. The shape, however, remains essentially the same, except for point 3. Skewness and flatness factors of the probability density function are provided in Table 5.1. The skewness factor decreases at the upwind base of the ridge and then increases over the ridge to values approximately equal to those upwind. The initial sharp decrease is caused by changes in minimum peak velocities and not by those in maximum peak velocities. The flatness factor at the crest is about 3 and less at the upwind and downwind base. This indicates that the extreme velocity fluctuations in these regions are relatively small.

In summary it may be concluded that the directional redistribution of the turbulence kinetic energy along a streamline is the most significant phenomenon. The frequency distributions and probability density function of the velocity fluctuations change only slightly.

TABLE 5.1. Statistical Characteristics of Longitudinal Velocity Fluctuations (Case 5)

Point (Figure 5.44)	Turbulence Intensity	Skewness Factor	Flatness Factor
0	0.080	0.33	3.15
a	0.079	0.26	3.09
b	0.058	0.30	3.12
1	0.074	0.18	2.80
2	0.058	0.23	2.95
3	0.096	0.27	2.74

6.0 CONCLUSIONS

In this chapter final conclusions are drawn concerning the implications of this experimental program for WECS-siting procedures. The conclusions listed here are general rather than specific, which reflects the complicated and nonlinear behavior of the phenomena studied. Many specific sub-conclusions which will be valuable to meteorologists, engineers, and numerical specialists are contained within the subsections of Chapters 3.0, 4.0 and 5.0.

Some of the remarks included below may seem obvious or trivial; however, the reader should recall that due to the lack of data many perturbations proposed have been only conjecture until now. Indeed, the most recent review on flow over topography prepared by the World Meteorological Organization (Davidson, 1964) was unable to conclude with any assurance whether speedup or speeddown was most likely to occur over ridges. The conclusions are grouped in three sections to reflect the objectives of this study as listed in Section 1.1.

6.1 WIND CHARACTERISTICS OVER RIDGES

Wind characteristics over ridges are affected to some degree by ridge shape, surface roughness and upwind turbulence, and thermal stratification. Specifically this study reveals:

1. The occurrence of flow separation at the downwind side of a ridge depends on both upwind and downwind slopes and is independent of the ratio of ridge height to boundary-layer thickness. Flow separation is delayed if upwind surface roughness is larger over the ridge, or if turbulence levels in the approach wind are high due to upwind topography. Flow separation may occur for more gentle slopes if the upwind surface roughness is less than that over the ridge or if the flow has a stable stratification.
2. The downwind separation region is in general large as a result of a strong interaction between the main flow and the separated flow region. Crest velocities are reduced significantly. Static pressure gradients above the separated region are largest across streamlines. If no flow separation occurs the static pressure gradients are largest parallel to the streamlines.

3. The downwind separated flow region may extend to a distance of 15 h from the crest. For relatively gentle slopes the separation region is shorter. The downwind flow remains in nonequilibrium after reattachment. Return to equilibrium flow conditions depends on the length of the separation region; it is on the order of 100 h for steep downwind slopes.

4. Upwind flow separation depends primarily on the upwind slope. Separation will occur for $h/L_u < 1/2$. The separated flow region upwind is generally much smaller than the separated region downwind because the interaction between wake and main flow is impeded by the presence of the ridge. The interaction may vanish for sufficiently large vorticity.

5. The effect of the turbulence on the mean flow is very small, except for the inner region. In the inner region Reynolds shear stress gradients are the same order of magnitude as pressure gradients. A realistic estimate for the inner-layer thickness could be obtained from

$$\ell = 0.067\ z_o^{0.1}\ L^{0.9} \qquad \text{(Jackson and Hunt, 1975).}$$

However, it is recommended that further research be conducted to validate this expression (see also point 1 in Section 6.3). The turbulence above the inner region, downwind of the crest affects the mean flow most significantly. An estimate for total head losses resulting from nonequilibrium flow conditions over a hill may be obtained from equations (2.18) and (2.19).

6. The turbulence structure changes along streamlines in the flow field over hills. In the inner region, where turbulence length scales are small, the turbulence dissipation and production rates are the dominant terms in the turbulence kinetic energy equation. Consequently, the turbulence intensities and shear stresses increase towards the crest. In the middle region for $L < \delta$ the turbulence characteristics at the crest behave as those predicted for turbulence undergoing a contraction. The longitudinal turbulence intensity reduces in magnitude towards the crest, while the vertical turbulence intensity increases. For $L > \delta$ distortion effects are still important; in addition turbulence production, dissipation, and diffusion affect

the turbulence structure. In general, turbulence characteristics in the middle region, other than turbulence intensities, do not deviate significantly from upwind conditions.

6.2 FUNCTIONAL DEPENDENCY BETWEEN UPWIND AND RIDGE-CREST MEAN VELOCITIES

A simple relation has been obtained for upwind and ridge-crest mean velocities by systematically varying the pertinent ridge and flow characteristics (see Section 5.4 and Appendix E). The method incorporates the most important parameters which affect the wind velocity amplification at a ridge crest. The following conclusions may be drawn with respect to speedup:

1. Largest speedups occur over ridges which just avoid flow separation and which are symmetrically shaped (See Figures 3.20, 4.3 and 4.4).
2. Amplification (not necessarily speedup) is largest for large upwind power law exponents.
3. Measurements and theory suggest that mild stable or unstable stratification decrease or increase wind velocities slightly at hill crests, respectively, for equivalent approach velocity profiles. This, of course, assumes no elevated inversion of "lid" that lies directly above a hill crest. When airflow is constrained to move between a ridge and an elevated inversion then exactly opposite wind effects are likely.
4. Speedup over round-crested and sharp-crested ridges are essentially equal for ridges with the same parameters, h/L_u and h/L_d. If flow separation occurs speedups may be larger over round-crested ridges because of later flow separation.
5. Speedups over ridges of finite width ($b = 9\ h$ and $18\ h$) are approximately the same as those over infinite-width ridges. Under neutral flow conditions, wind velocities are slightly larger at the ends of the crest and slightly less at the center. Under stable flow conditions speedups are larger in the center and significantly less at the ends of the ridge. Potential flow calculations (Hunt, 1978) suggest that for $b/L > 5$ the amplifications are essentially constant irrespective of the slopes and for $b/L < 5$ changes in the amplification factor become increasingly less as h/L decreases.

6.3 PHYSICAL AND NUMERICAL MODELING

Physical modeling requirements of the turbulent approach flow were met as specified in Appendix F. As a result dynamics and kinematics in the middle region replicated the atmosphere accurately. It appeared, however, that physical similarity in the inner region could not be met under certain conditions.

Based on a categorization of flow regimes criteria for the applicability of simple closure models were developed. In Appendix E a comparison was made between mathematical models to investigate the effects of the turbulence closure equations on the surface shear stress. In addition mathematical modeling techniques of flow over ridges including flow separation were discussed.

In this section conclusions are drawn that summarize the most significant limitations of specific modeling techniques.

1. The flow in the inner region over ridge models may be affected by boundary-layer relaminarization if pressure gradients are sufficiently large. It appears that in the present wind-tunnel study the pressure gradients over the steeper ridges were such that this phenomenon affected the thickness of the inner region. Further research is required to investigate the constraint the relaminarization phenomenon places on wind-tunnel simulation.
2. Realistic representation of the turbulence effects on the mean flow in the middle region by simple closure models, i.e., mixing length model, modified mixing length model taking into account streamline-curvature effects (Bradshaw, 1969), and the turbulence kinetic energy model, is rather limited. In Appendix E, Section E.1 the conditions are summarized under which the closure assumptions may be applied.
3. A comparison between surface shear stress distributions over bell-shaped hills computed by different mathematical models showed considerable discrepancies. No clear correspondence existed between numerical nonlinear models. Research is required to establish criteria for the proper discretization of the mathematical model in the surface region.
4. Linear models may be applied to flow over low hills. Results of Jackson and Hunt (1975) suggest that linear models may be applied to

hills with $h/L < 0.01$. However, Jackson and Hunt found also agreement between theory and experiments for hills with slopes too steep for the theory to be strictly valid.

5. Existing mathematical models of flow over surface obstacles that include flow separation require a substantial amount of, empirical information and are difficult to apply to other than very simple surface obstacle shapes.

REFERENCES

Alexander, A. J. and Coles, C. F. (1971), "A Theoretical Study of Wind Flow over Hills," 3rd Int. Congress on Wind Loads on Buildings and Structures, Tokyo, Japan.

Arie, M. and Rouse, H. (1956), "Experiments on a Two-Dimensional Flow over a Normal Wall," Journal of Fluid Mechanics, Vol. 1, pp. 129-141.

Arya, S. P. S. (1968), "Structure of Stably Stratified Turbulent Boundary Layer," Fluid Dynamics and Diffusion Laboratory Report CER68-69SPSA10.

Astley, J., Bowen, A. J., Lindley, D., and Flay, R. (1977), "Aspects of Wind Flow in Urban and Rural Boundary Layers," Royal Meteorological Society Summer Conference on Urban Meteorology, McQuarrie University, Sydney, Australia, p. 20.

Badri Narayanan, M. A. and Ramjee, V. (1968), Indian Institute of Science, Bangalore, India, Report AE 68FMI.

Batchelor, G. K. (1967), An Introduction to Fluid Dynamics, Cambridge University Press: London, United Kingdom.

Bernstein, A. B. (1965), "Dimensional Analysis Applied to the Wind Distribution in the Planetary Boundary Layer," Monthly Weather Review, Vol. 93, No. 10, pp. 579-585.

Bitte, J. and Frost, W. (1976), "Atmospheric Flow over Two-Dimensional Bluff Surface Obstructions," NASA CR-2750, p. 207.

Blackwelder, R. F. and Kovasznay, L. S. G. (1972), "Large-Scale Motion of a Turbulent Boundary Layer During Relaminarization," Journal of Fluid Mechanics, Vol. 53, pp. 61-83.

Bowen, A. J., and Lindley, D. (1977), "A Wind Tunnel Investigation of the Wind Speed and Turbulence Characterstics Close to the Ground over Various Escarpment Shapes," Boundary-Layer Meteorology, 12, pp. 259-271.

Bradley, E. F. (1978), "An Experimental Study of the Profiles of Wind Speed, Shearing Stress and Turbulence at the Crest of a Large Hill," Division of Environmental Mechanics, CSIRO, Canberra, Australia.

Bradshaw, P. (1969), "The Analogy between Streamline Curvature and Buoyancy in Turbulent Shear Flow," Journal of Fluid Mechanics, Vol. 36, pp. 177-191.

Bradshaw, P. (1973a), "Effects of Streamline Curvature on Turbulent Flow," AGARDograph 169, NATO, Paris, France, p. 80.

Bradshaw, P. (1973b), "The Strategy of Calculation Methods for Complex Turbulent Flows," Imperial College, Aero Report 73.05, London, United Kingdom, p. 20.

Bradshaw, P., Ferris, D. H. and Atwell, P. (1967), "Calculation of Boundary-Layer Development Using the Turbulent Energy Equation," Journal of Fluid Mechanics, Vol. 28, pp. 593-616.

Bradshaw, P. and Wong, F. Y. F. (1972), "The Reattachment and Relaxation of a Turbulent Shear Layer," Journal of Fluid Mechanics, Vol. 52, pp. 113-135.

Bradshaw, P. (editor) (1976), "Turbulence," Topics in Applied Physics, Vol. 12, p. 335.

Castro, I. P. and Bradshaw, P. (1976), "The Turbulence Structure of a Highly Curved Mixing Layer," Journal of Fluid Mechanics, Vol. 73, Pt. 2, pp. 265-304.

Cermak, J. E., et al. (1966), "Simulation of Atmospheric Motion by Wind-Tunnel Flows," Technical Report for DA-AMC-28-043-G20, Fluid Dynamics and Diffusion Laboratory, Colorado State University, Fort Collins, Colorado (CER66JEC-VAS-ESP-GJB-HC-RNM-S117).

Cermak, J. E. (1975), "Application of Fluid Mechanics to Wind Engineering," 1974 Freeman Scholar Lecture, ASME Journal of Fluids Engineering, Vol. 97, Series 1, No. 1, March, Colorado State University, Fort Collins, Colorado (CEP74-75JEC7).

Chang, S. C. (1966), "Velocity Distributions in the Separated Flow behind a Wedge-Shaped Model Hill," Technical Report, Grant DA-AMC-28-043-G20, March, Colorado State University, Fort Collins, Colorado (CER65SCC66), p. 101.

Chien, H., Meroney, R. N., Sandborn, V. A. and Bouwmeester, R. J. B. (1978), "Preliminary Measurements of Flow Over Model, Three-Dimensional Hills," Fluid Dynamics and Diffusion Laboratory, Colorado State University Research Memorandum No. 29, CEM-77-78HCC-VAS-RNM-RJBB29, p. 34. (This report is included in Meroney et al., 1978b.)

Coles, D. (1962), R. A. N. D. Corp. Rep. R-403-PR.

Cook, N. J. (1977/1978), "Determination of the Model Scale Factor in Wind-Tunnel Simulations of the Adiabatic Atmospheric Boundary Layer," Journal of Industrial Aerodynamics, Vol. 2, pp. 311-321.

Counihan, J. (1969), "An Improved Method for Simulating an Atmospheric Boundary Layer in a Wind Tunnel," Atmospheric Environment, Vol. 3, pp. 197-214.

Counihan, J. (1973), "Simulation of an Adiabatic Urban Boundary Layer in a Wind Tunnel," Atmospheric Environment, Vol. 7, pp. 673-689.

Counihan, J. (1975), "Review Paper: Adiabatic Atmospheric Boundary Layers: A Review and Analysis of Data from the Period 1880-1972," Atmospheric Environment, Vol. 9, pp. 871-905.

Davidson, B. (1964), " Sites for Wind-Power Installations," World Meteorological Organization, Technical Note No. 63, WMO No. 156, TP-76, Geneva, Switzerland.

Davis, R. E. (1970), "On Turbulent Flow Over a Wavy Boundary," Journal of Fluid Mechanics, Vol. 42, pp. 721-731.

Davis, R. E. (1972), "On the Prediction of the Turbulent Flow over a Wavy Boundary," Journal of Fluid Mechanics, Vol. 52, pp. 287-306.

Deaves, D. M. (1975), "Wind Over Hills: A Numerical Approach," Journal of Industrial Aerodynamics, Vol. 1, pp. 371-391.

Derickson, R. G. and Meroney, R. N. (1977), "A Simplified Physics Airflow Model for Evaluating Wind Power Sites in Complex Terrain," Proceedings of Summer Computer Simulation Conference, July 18-20, Chicago, Illinois, p. 14.

Dobson, F. W. (1971), "Measurements of Atmospheric Pressure on Wind-Generated Sea Waves," Journal of Fluid Mechanics, Vol. 48, pp. 91-127.

Fraenkel, L. E. (1961), "On Corner Eddies in Plane Inviscid Shear Flow," Journal of Fluid Mechanics, Vol. 11, pp. 400-406.

Frost, W., Maus, J. R., and Simpson, W. R. (1973), "A Boudnary Layer Approach to the Analysis of Atmospheric Motion over a Surface Obstruction," NASA CR-2182, p. 141.

Gartshore, I. S. and de Croos, K. A. (1976), "Roughness Element Geometry Required for Wind Tunnel Simulations of the Atmospheric Wind," ASME Technical Paper, 76-WA/FE-18, p. 7.

Good, M. C. and Joubert, P. M. (1968), "The Form Drag of Two-Dimensional Bluff--Plates Immersed in Turbulent Boundary Layers," Journal of Fluid Mechanics, Vol. 31, pp. 547-582.

Güven, O., Patel, V. C. and Farell, C. (1976), "A Model for High-Reynolds-Number Flow Past Rough-Walled Circular Cylinders," ASME Technical Paper, 76-WA/FE-14.

Halistsky, J., Magony, G. A., Halpern, P. (1965), "Turbulence Due to Topographical Effects, Report No. 2," New York University, School of Engineering and Science Report No. TR66-5.

Huber, A. H., Snyder, W. H., and Lawson, R. E. (1976), "Stack Placement in the Lee of a Mountain Ridge: A Wind Tunnel Study," Environmental Sciences Research Lab., Research Triangle Park, NC, p. 44.

Hunt, J. C. R. (1973), "A Theory of Turbulent Flow and Two-Dimensional Bluff Bodies," Journal of Fluid Mechanics, Vol. 61, pp. 625-706.

Hunt, J. C. R. (1977), "A Review of the Theory of Rapidly Distorted Turbulent Flow and its Applications," Biennial Fluid Dynamics Symposium, Sept. 5-10, 1977, Poland.

Hunt, J. C. R. (1978), "Wind Over Hills," Survey paper for NOAA-NSF Workshop, Boulder, Colorado.

International Mathematical and Statistical Libraries, Inc., (1975) IMSL LIB3-0005, Revised November, 1975.

Jackson, P. S. and Hunt, J. C. R. (1975), "Turbulent Wind Flow over a Low Hill," Quarterly Journal of the Royal Meteorological Society, Vol. 101, pp. 292-955.

Kendahl, J. M. (1970), "The Turbulent Boundary-Layer over a Wall with Progressive Surface Waves," Journal of Fluid Mechanics, Vol. 41, pp. 259-281.

Kirk, F. N. (1959), "An Approximate Theory of Base Pressure in Two-Dimensional Base Flow at Supersonic Speeds," Great Britain Royal Aircraft Establishment, Technical Note Aero. 2377.

Kiya, M. and Arie, M. (1972), "A Freestreamline Theory for Bluff Bodies Attached to a Plane Wall," Journal of Fluid Mechanics, Vol. 56, pp. 201-219.

Kline, S. J., Reynolds, W. C., Schraub, F. A., and Rundstadtler, P. W. (1967), "The Structure of Turbulent Boundary Layers," Journal of Fluid Mechanics, Vol. 30, pp. 741-773.

Korst, H. H., Page, R. H. and Childs, M. E. (1954), "Compressible Two-Dimensional Jet Mixing at Constant Pressure," University of Illinois, ME-TN-392-1, OSR-TN-54-82.

Kuhn, G. D. and Nielsen, J. N. (1974), "Prediction of Turbulent Separated Boundary Layers," AIAA Journal, Vol. 12, No. 7, pp. 881-882.

Launder, B. E. and Spalding, D. B. (1972), Mathematical Models of Turbulence, Academic Press, Inc., (London) Ltd., p. 169.

McVehil, G. E., Ludwig, G. R., and Sundaram, T. R. (1967), "On the Feasibility of Modeling Small Scale Atmospheric Motions," Cornell AeroLab Report ZB-2328-P-1, Buffalo, New York.

Melbourne, W. H. (1977), "Development of Natural Wind Models at Monash University," 6th Australian Hydraulics and Fluid Mechanics Conference, Adelaide, Australia, December 5-9, pp. 190-194.

Meroney, R. N., Sandborn, V. A., Bouwmeester, R. J. B., and Rider, M. A. (1976a), "Sites for Wind Power Installations: Wind Tunnel Simulation of the Influence of Two-Dimensional Ridges on Wind Speed and Turbulent," Annual Report: First Year, NSF/RANN Contract (CSU CER76-77RNM-VAS-RJBB-MAR-5), p. 80.

Meroney, R. N., Sandborn, V. A., Bouwmeester, R. J. B. and Rider, M. A. (1976b), "Sites for Wind Power Installations - Tabulated Experimental Data," Progress Report June-November 1976, ERDA Wind Energy Program Report ERDA/Y-76-S (CSU CER76-77RNM-VAS-RJBB-MAR-29), p. 60.

Meroney, R. N., Bowen, A. J., Lindley, D., and Pearse, J. R., (1978a), "Wind Characteristics over Complex Terrain: Laboratory Simulation and Field Measurements at Rakaia Gorge, New Zealand," Colorado State University Research Report No. CER77-78RNM29, May, p. 219.

Meroney, R. N., Sandborn, V. A., Bouwmeester, R. J. B., Chien, H. C., and Rider, M. A. (1978b), "Sites for Wind Power Installations: Physical Modeling of the Influence of Hills, Ridges and Complex Terrain on Wind Speed and Turbulence: Final Report, Part III," Colorado State University Research Report No. CER77-78RNM-VAS50a and 50b, p. 91, and p. 197.

Miles, J. W. (1957), "On the Generation of Surface Waves by Shear Flows," Journal of Fluid Mechanics, Vol. 6, p. 568.

Miles, J. W. (1967), "On the Generation of Surface Waves by Shear Flows," Journal of Fluid Mechanics, Vol. 30, p. 163.

Mueller, T. J. and Robertson, J. M. (1963), Modern Developments in Theoretical Applied Mechanics, Vol. 1, p. 326.

Parkinson, G. V. and Jandali, T. (1970), "A Wake Source Model for Bluff Body Potential Flow," Journal of Fluid Mechanics, Vol. 40, pp. 577-594.

Petryk, S. and Brundrett, E. (1967), Department of Mechanical Engineering, University of Waterloo, Res. Rep. No. 4.

Plate, E. J. and Cermak, J. E. (1963), "Micrometeorological Wind Tunnel Facility, Description and Characterstics," Fluid Dynamics and Diffusion Laboratory Report CER63EJP-JEC9, Colorado State University, Fort Collins, Colorado.

Plate, E. J. and Lin, C. W. (1965), "The Velocity Field Downstream from a Two-Dimensional Model Hill--Part 2," Colorado State University, Fort Collins, Colorado (CER65EJP-CWL41).

Reinsch, C. H. (1967), "Smoothing by Spline Functions," Numerische Mathematik, Vol. 10, pp. 177-183.

Rider, M. A. and Sandborn, V. A. (1977a), "Boundary Layer Turbulence over Two-Dimensional Hills," Colorado State University Technical Report No. CER77-78MAR-VAS4, p. 125. (This report is included in Meroney et al., 1978b, Appendix B.)

Rider, M. A. and Sandborn, V. A. (1977b), "Measurements of the Mean and Longitudinal Turbulent Velocities over Varying Hill Shapes," Colorado State University, CEM77-78MAR-VAS28, p. 30. (This report is included in Meroney et al., 1978b, Appendix A.)

Robertson, J. M. and Taulbee, D. B. (1969), "Turbulent Boundary Layer and Separation Flow Ahead of a Step," Developments in Mechanics, Vol. 5, Proceedings of the 11th Midwestern Mechanics Conference, pp. 171-183.

Sacre, C. (1975), "Numerical Method for the Calculation of the Excess Velocity of the Wind on a Hill," Centre Scientifique et Technique du Batement, Nantes, France, p. 26.

Scorer, R. S. (1978), "Environmental Aerodynamics," Ellis Horwood Limited, Chichester, p. 487.

Snyder, R. L. and Cox, C. S. (1966), "A Field Study of the Wind Generation of Ocean Waves," Journal of Marine Research, Vol. 24, pp. 141-178.

Snyder, W. H. (1972), "Similarity Criteria for the Application of Fluid Models to the Study of Air Pollution Meteorology," Boundary Layer Meteorology, Vol. 3, pp. 113-134.

Stewart, R. H. (1970), "Laboratory Studies of the Velocity of Field over Deep-Water Waves," Journal of Mechanics, Vol. 42, p. 733.

Stratford, B. S. (1959), "The Prediction of Separation of the Turbulent Boundary Layer," Journal of Fluid Mechanics, Vol. 5, pp. 1-16.

Tani, I., Iuchi, M. and Komoda, (1961), Aeronautical Research Institute, Tokyo, Japan, Report No. 364.

Taylor, P. A. and Gent, P. R. (1974), "A Model of Atmospheric Boundary-Layer Flow on Isolated Two-Dimensional 'Hill'; an Example of Flow Above 'Gentle Topography'," Boundary-Layer Meteorology, Vol. 7, pp. 349-362.

Tillman, W. (1945), Vokenrode Translation MAP-VG34-45T. British Ministry of Aircraft Production, London, England.

Townsend, A. A. (1961), "Equilibrium Layers and Wall Turbulence," Journal of Fluid Mechanics, Vol. 11, pp. 97-120.

Townsend, A. A. (1962), "The Behavior of a Turbulent Boundary Layer Near Separation," Journal of Fluid Mechanics, Vol. 12, pp. 536-554.

Townsend, A. A. (1972), "Flow in a Deep Turbulent Boundary-Layer over a Surface Distorted by Water Waves," Journal of Fluid Mechanics, Vol. 55, pt. 4, pp. 719-735.

Townsend, A. A. (1976), The Structure of Turbulent Shear Flow, Cambridge University Press, Cambridge, United Kingdom, p. 430.

Yamada, T. (1978), "A Three-Dimensional Numerical Study of Complex Atmospheric Circulations Produced by Terrain," Proceedings Conf. on Sierra Nevada Meteorology, American Meteorological Society, Boston, Mass., June 19-21, Lake Tahoe, p. 7.

Zoric, D. L. (1969), "Approach of Turbulent Boundary Layer to Similarity," Colorado State University, Fort Collins, Colorado (CER68-69DLZ9).

Zoric, D. and Sandborn, V. A. (1972), "Similarity of Large Reynolds Number Boundary Layers," Boundary-Layer Meteorology, Vol. 2, No. 3, pp. 326-333.

APPENDIX A

EXPERIMENTAL PROGRAM AND INSTRUMENTATION

APPENDIX A EXPERIMENTAL PROGRAM AND INSTRUMENTATION

A.0 INTRODUCTION

Laboratory simulation permits the systematic evaluation of the influence of simple combinations of approach flow wind characteristics and of topographical features on the resultant flow field over model topography. In this Appendix the test conditions, the methods used to make measurements, and the techniques employed in converting raw measurements to meaningful physical quantities are discussed. Attention is drawn to the limitations in the techniques in order to prevent misinterpretations or misunderstandings of the results.

A number of reports have been prepared under this research program (Meroney et al., 1976a, 1976b, Rider and Sandborn, 1977a, 1977b, and Meroney et al., 1978a, 1978b). A large portion of the data was obtained in the flow field over two-dimensional ridges. In this Appendix such information is consolidated by reviewing test conditions, measuring techniques, etc.

A.1 THE WIND-TUNNEL FACILITY

The experiments were performed in the Meteorological Wind Tunnel (MWT) located in the Fluid Dynamics and Diffusion Laboratory at Colorado State University. A plan view of the wind tunnel is shown in Figure A.1. The tunnel is a closed-circuit facility driven by a 250 hp variable-pitch, variable-speed propeller. The test section is nominally 2 m square and 27 m long fed through a 9:1 contraction ratio. The test-section walls diverge 0.01 m/m and the roof is adjustable to maintain a zero pressure gradient along the test section. The mean velocity can be adjusted continuously from 0.3 to 37 m/sec. The wind speed in the test section does not deviate from that set by the speed controller by more than one percent. The tunnel is equipped with a heating and cooling system to simulate thermally stratified boundary layers. The floor is cooled by circulating brine through coils insulated in the floor. Thermocouples imbedded in the floor were used to maintain a uniform preselected temperature. The freestream temperature was controlled by a heat exchanger in the return-flow leg of the tunnel. Under neutral flow conditions the heat exchanger was used to maintain the air temperature at a constant

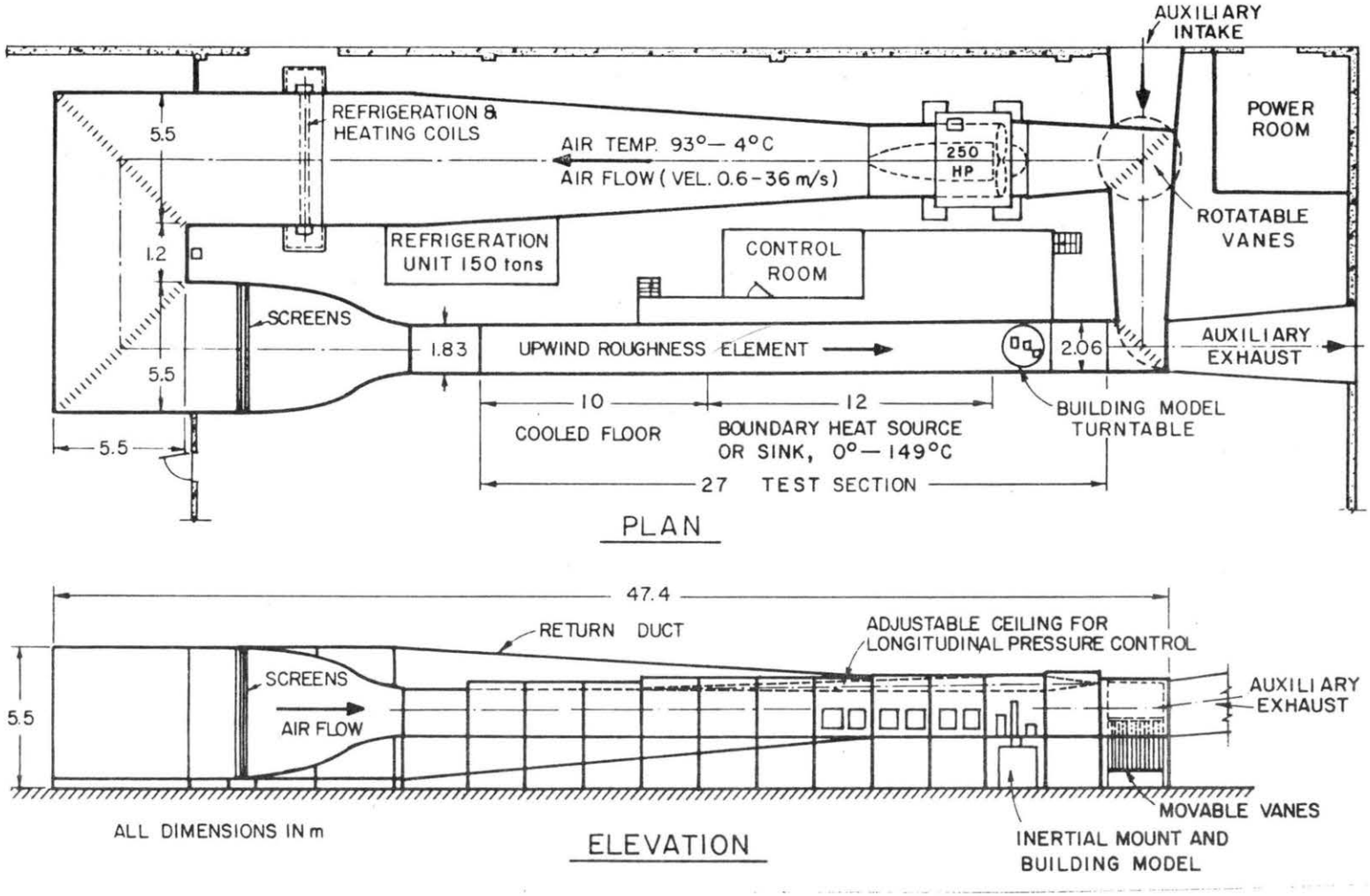

FIGURE A.1. Meteorological Wind Tunnel, Fluid Dynamics and Diffusion Laboratory, Colorado State University

level ($\pm \frac{1}{2}^{\circ}$C). All tests reported in this report used a neutral or stable boundary-layer stratification. The facility is described in detail by Plate and Cermak (1963).

At the entrance to the wind-tunnel test section a 0.038 m high saw-tooth boundary-layer trip was installed to insure prompt formation and growth of a turbulent boundary layer. The boundary-layer thickness increases with distance from the entrance. Over the smooth plate the thickness of the boundary layer increases in proportion to $x^{0.48}$ (Zoric 1969).

A.2 TEST CONDITIONS

A series of 15 hill models were constructed for tests in the meteorological wind-tunnel:

- symmetric triangular hill models with a width of 1.83 m, a height of 5.08 m, and slopes (h/L_b) of 1/2, 1/3, 1/4, 1/6, and 1/20;
- symmetric sinusoidal hill models with a width of 1.83 m, a height of 5.08 cm, and slopes (h/L_b) of 1/3 and 1/4;
- triangular hill models with a width of 1.83 m, a height of 5.08 cm, one vertical face, and one slope (h/L_b) of 1/2, 1/3, 1/4, and 1/6;
- triangular hill models with a width of 0.90 m, a height of 5.08 cm, one vertical face, and one slope (h/L_b) of 1/3 and 1/4;
- triangular hill models with a width of 0.45 m, a height of 5.8 cm, one vertical face, and one slope (h/L_b) of 1/3 and 1/4.

The symmetric models were constructed by placing a 0.32 cm thick Plexiglas skin over 9 support ribs. The models were equipped with static pressure holes and preston tubes. The asymmetric models were constructed in a similar manner, but the material was wood and masonite, 0.32 cm thick.

The experiments were carried out in three phases. In each phase, somewhat different experimental procedures were applied as suggested by differing accuracy or resolution requirements (see next section). Upwind conditions for Phase I were different from Phase II and III.

Upward Conditions, Phase I. The hills were mounted in the wind tunnel with a false floor upstream. The false floor was placed 5.60 m directly downwind of the initial boundary layer trip and was 10.75 m in length, (Figure A.2a). The false floor consisted of three sections: an approach ramp, a plywood testing base, and a trailing ramp behind the hill. The horizontal

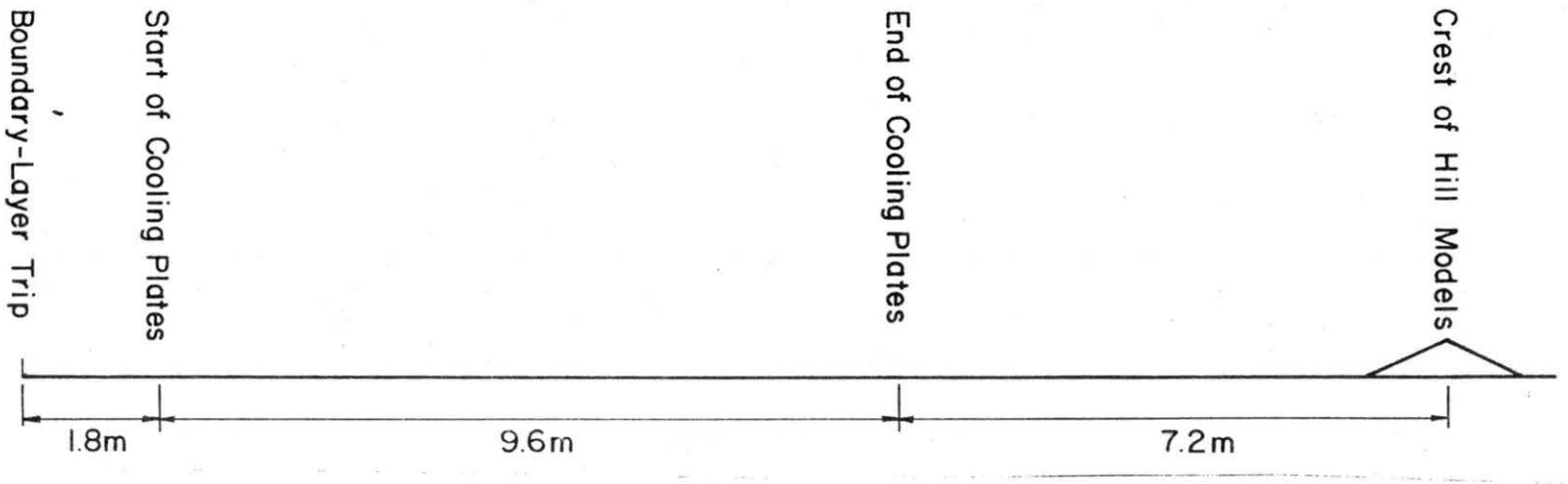

FIGURE A.2a. Test Configuration during Phase I

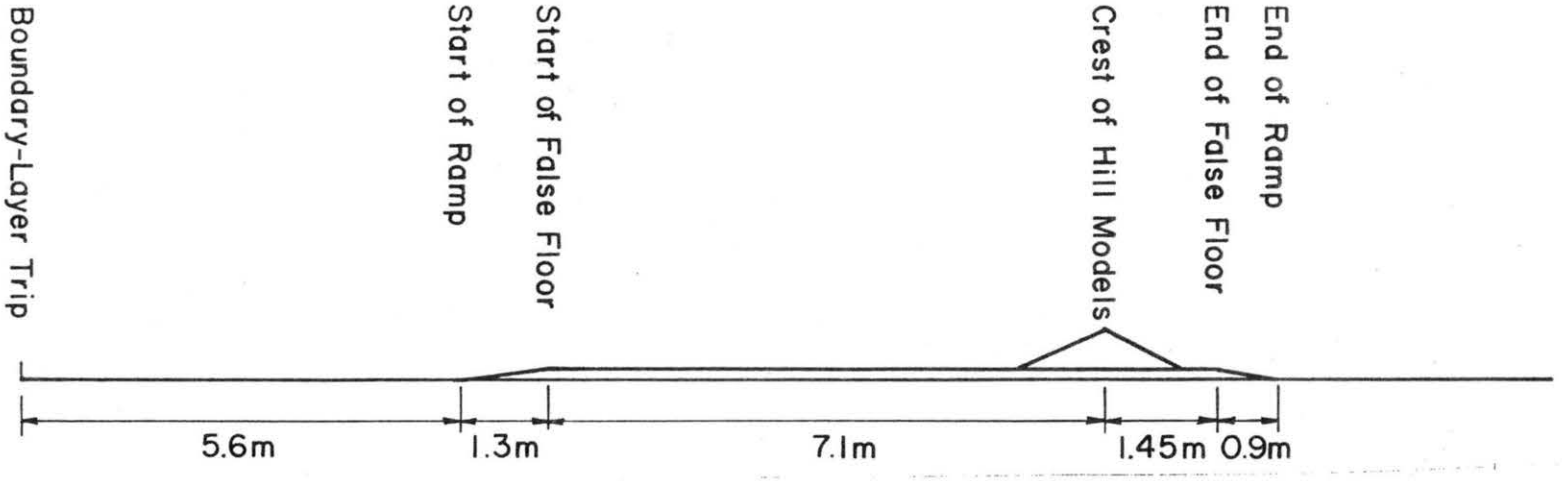

FIGURE A.2b. Test Configuration during Phase II and III

length of approach ramp was 1.3 m. The plywood testing base was that section of false floor positioned adjacent to and flush with the approach ramp. Plywood, 1.91 cm thick, was used to maintain a horizontal surface on which designated models could be placed. The testing based covered 8.55 m in length. The trailing ramp was the final section of false floor located furthest downstream. The ramp was positioned flush with and sloping downward from the testing base. This final section of false floor was 0.90 m in length. The approach and trailing ramp formed an angle of about 1° with the horizontal. The center of the model was set 14.0 m from the entrance (Figure A.2b). During Phase I freestream wind velocities were set at 9.1 m/sec and 15.2 m/sec. For a detailed description of the upwind flow characteristics, the reader is referred to Section A.6.

Upwind Conditions Phase II and III. The models were mounted directly on the aluminum floor of the wind tunnel. During stratified flow measurements, cooling plates were installed beginning at 1.83 m from the saw-tooth fence and ending at 11.93 m. The surface of the cooling plates was varigated as a result of cooling channels. The coolant channel ribs were 0.16 m in height and were spaced both normally and parallel to the flow. The center of the models was set at 18.6 m from the entrance.

For one of the runs in Phase II, a uniformally rough surface was obtained by glueing graded rock particles, having an average diameter of 0.25 cm spaced approximately 1.0 cm on center, to 1.91 cm plywood support boards. The particle size and distribution was designed by the method of Gartshore and de Croos (1976) to produce a $z_o/\delta \simeq 1.5 \times 10^{-4}$. Roughness was also applied to the hill utilizing double-sided sticky tape. The roughness extended 7.2 m upwind of the hill crest and 2.4 m downwind of the crest. On the upwind side of the rough boards, an approach ramp was installed flush with the board.

During all tests (Phases I, II and III) the wind tunnel ceiling was kept horizontal, including the section in which the hill models were installed. No measurable changes in static pressure gradients along the ceiling were observed before or after installation of the hills.

An overview of all test conditions is presented in Table A.1. For detailed information on upwind flow characteristics, the reader is referred to Section A.4.

TABLE A.1. Identification of Test Cases Including Locations of Tabulated Data

Case	Shape[7]	h/L_u	h/L_d	h/δ	Phase	$\bar{u}_o(10h)$ (m/sec)	Ri	z_o/δ	$u_*/\bar{u}(10h)$	Tabulated Data: $\bar{u}$	P	P_s	u'	w'	$\overline{uw}$	T	t'
1	tr	1/2	1/2	.09	II	9.1	0	1.2×10^{-4}	.027	1	1		1			n.a.	n.a.
1a	tr	1/2	1/2	.11	I	9.1	0	1.2×10^{-4}	.034	2		3	3	3	3	n.a.	n.a.
2	tr	1/2	1/2	.11	I	15.2	0	7.5×10^{-5}	.034	1	1					n.a.	n.a.
3	tr	1/3	1/3	.11	I	9.1	0	1.2×10^{-4}	.034	1	1					n.a.	n.a.
4	tr	1/3	1/3	.11	I	15.2	0	7.5×10^{-5}	.034	1	1					n.a.	n.a.
5	tr	1/4	1/4	.09	II	9.1	0	1.2×10^{-4}	.027	1	1		1[5]			n.a.	n.a.
5a	tr	1/4	1/4	.11	I	9.1	0	1.2×10^{-4}	.034	3		3	3	3	3	n.a.	n.a.
6	tr	1/4	1/4	.11	I	15.2	0	7.5×10^{-5}	.034	1	1					n.a.	n.a.
7	tr	1/6	1/6	.09	II	9.1	0	1.2×10^{-4}	.027	1	1	3	1			n.a.	n.a.
7a	tr	1/6	1/6	.11	I	9.1	0	1.2×10^{-4}	.034	3		3	3	3	3	n.a.	n.a.
8	tr	1/6	1/6	.11	I	15.2	0	7.5×10^{-5}	.034	1	1					n.a.	n.a.
9	tr	1/20	1/20	.09	II	9.1	0	1.2×10^{-4}	.027	1	1		1			n.a.	n.a.
10	sn	1/4[1]	1/4[1]	.11	I	9.1	0	1.2×10^{-4}	.034	1	1					n.a.	n.a.
11	sn	1/4[1]	1/4[1]	.11	I	15.2	0	7.5×10^{-5}	.034	1	1					n.a.	n.a.
12	sn	3/16[2]	3/16[2]	.11	I	9.1	0	1.2×10^{-4}	0.34	1	1					n.a.	n.a.
13	sn	3/16[2]	3/16[2]	.11	I	15.2	0	7.5×10^{-4}	.034	1	1					n.a.	n.a.
14	tr	1/4	1/4	.09	II	9.1	0	1.6×10^{-3}	.048	1	1		1			n.a.	n.a.
S1	tr	1/4	1/4	.09	II	9.0	.004		-	4			4			4	4
S2	tr	1/4	1/4	.09	II	6.0	.008		-	4			4			4	4
S3	tr	1/4	1/4	.09	II	3.0	.021		-	4			4			4	4
S4	tr	1/6	1/6	.09	II	6.0	.008		-	4			4			4	4
S5	tr	1/6	1/6	.09	II	3.0	.021		-	4			4			4	4
I	tr	1/3	1/4	.09	III	9.1	0	1.2×10^{-4}	.027	2			2			n.a.	n.a.
II	tr	1/4	1/3	.09	III	9.1	0	1.2×10^{-4}	.027	2	2		2			n.a.	n.a.
III	tr	1/2	1/4	.09	III	9.1	0	1.2×10^{-4}	.027	2	2		2			n.a.	n.a.
IV	tr	1/4	1/2	.09	III	9.1	0	1.2×10^{-4}	.027	2	2		2			n.a.	n.a.
V	tr	1/2	1/6	.09	III	9.1	0	1.2×10^{-4}	.027	2	2		2			n.a.	n.a.
VI	tr	1/6	1/2	.09	III	9.1	0	1.2×10^{-4}	.027	2	2		2			n.a.	n.a.
VII	tr	1/2	1/3	.09	III	9.1	0	1.2×10^{4}	.027	2	2		2			n.a.	n.a.
VIII	tr	1/3	1/2	.09	III	9.1	0	1.2×10^{-4}	.027	2	2		2			n.a.	n.a.
IX	tr	1/2	1/0	.09	III	9.1	0	1.2×10^{-4}	.027	2	2		2			n.a.	n.a.
X	tr	1/3	1/0	.09	III	9.1	0	1.2×10^{-4}	.027	2	2		2			n.a.	n.a.
XI	tr	1/4	1/0	.09	III	9.1	0	1.2×10^{-4}	.027	2	2		2			n.a.	n.a.
XII	tr	1/6	1/0	.09	III	9.1	0	1.2×10^{-4}	.027	2	2		2			n.a.	n.a.
XIII	tr[3]	1/4	1/0	.09	III	9.1	0	1.2×10^{-4}	.027	2						n.a.	n.a.
XIV	tr[4]	1/4	1/0	.09	III	9.1	0	1.2×10^{-4}	.027	2						n.a.	n.a.
XV	tr[3]	1/4	1/3	.09	III	9.1	0	1.2×10^{-4}	.027	2						n.a.	n.a.
XVI	tr[4]	1/4	1/3	.09	III	9.1	0	1.2×10^{-4}	.027	2						n.a.	n.a.
XVII	tr	1/4	1/0	.09	III	3.0	.015	1.2×10^{-4}	-	2	2					2	
XVIII	tr	1/4	1/0	.09	III	6.0	.011	1.2×10^{-4}	-	2	2					2	
XIX	tr[3]	1/4	1/0	.09	III	3.0	.015	1.2×10^{-4}	-	2						2	
XX	tr[4]	1/4	1/0	.09	III	6.0	.011	1.2×10^{-4}	-	2						2	

1) Equivalent to $h/L_b = 1/3$
2) Equivalent to $h/L_b = 1/4$
3) Ridge with finite width 2b = 45cm
4) Ridge with finite width 2b = 90cm
5) Spectra and probability density functions are presented in Figures 5.1-5.5 of this report
6) Numbers refer to reports listed below
7) tr: triangular, sn: sinusoidal, n.a.: not applicable

Tabulated Data Reported In:

1. Meroney et al. (1976b)
2. Appendix B of this report
3. Rider Sandborn (1977) (positive x-direction points in upwind direction)
4. Meroney et al. (1978b), Appendix C (positive x-direction points in upwind direction)

A.3 MEASURING PROCEDURES

All measurements in the flow field over the hill models were carried out over a grid of points determined by vertical surveys (z-direction) at particular longitudinal points (x-direction) along the center of the tunnel. The MWT carriage can be positioned at any desired point in the x-direction. A control unit outside the tunnel monitors the vertical movement of the probe support and probes through the boundary layers. This actuator system provided a constant voltage change for a particular change in height. The probe support was attached to the carriage by a 1.00 m extension bar. The length of this bar was sufficiently long that the flow distortion due to carriage was negligible at the measuring location (Figure A.3a).

In the tests, a stop rod attached tightly to the probe support made contact with the floor prior to the other instruments. The purpose of the stop rod was to protect the probes from being driven into the floor and to accurately determine the vertical distance between the surface and the probes. During Phase I an electric indicator triggered when the stop rod contacted the floor. During Phases II and III a 0.00254 cm dial indicator was employed to determine more accurately the z-locations of the probes within 0.5 cm of the wall. A schematic of the probe support is given in Figure A.3b.

The freestream velocity was monitored throughout the tests with a pitot-static probe affixed to the ceiling upstream of the hill locations.

The instrumentation employed during Phases I, II and III is listed in Table A.2.

Mean Velocity Measurements. During Phase I, mean velocity measurements above the hills were made with commerical probes. Dynamic pressures were measured from the pressure differential between the total-head hole of a kiel probe 0.16 cm in diameter and the static holes of a pitot-static tube 0.18 cm in diameter. The kiel probe is insensitive to flow angles over a range of at least ± 40 degrees. For the range of velocities measured in the present study the kiel probes agreed with the total pressure measured by the laboratory standard probe. In the region near the hill surface where relatively large flow angles were encountered the pitot-static probe was pointed in the direction of the flow. However, due to uncertainty about the precise flow direction, misalingment of the probe has occurred. Errors in mean velocity caused by misalingment may have been as large as 4 percent of the local mean velocity.

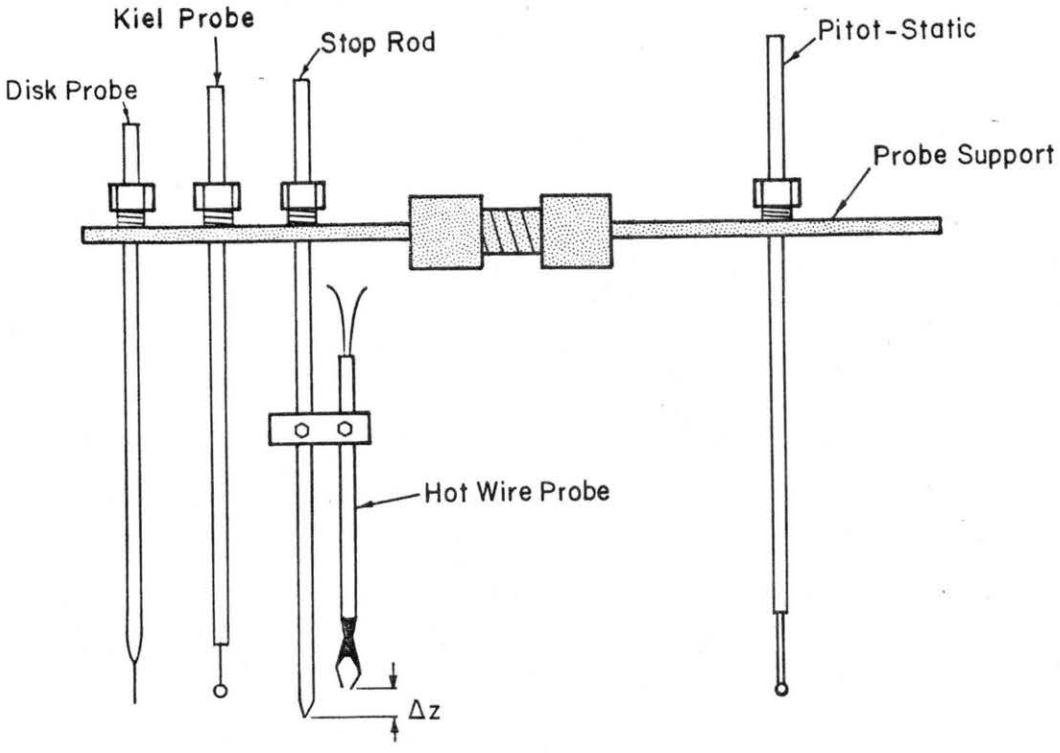

FIGURE A.3a. Schematic of Probes

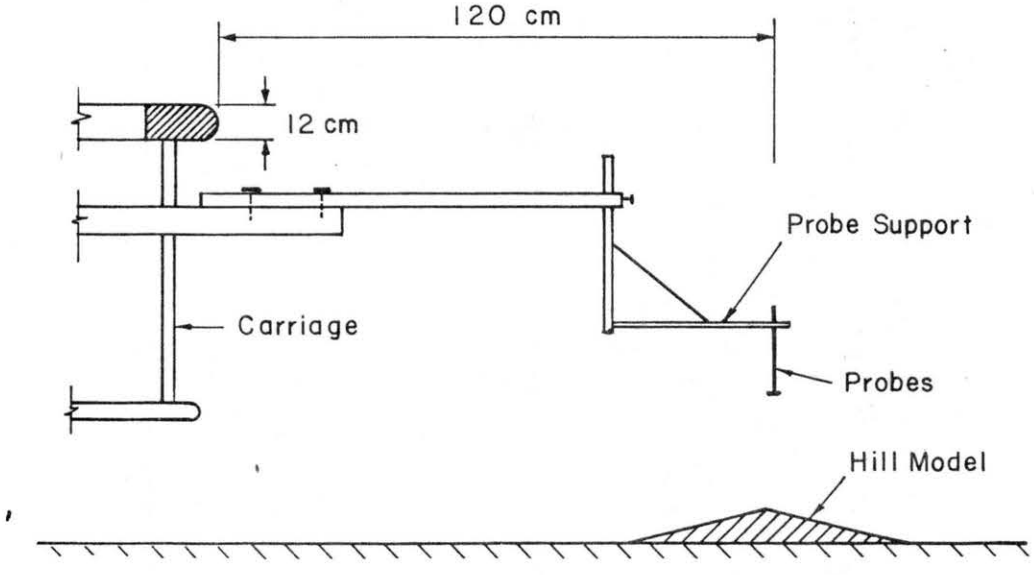

FIGURE A.3b. Schematic of Carriage and Probe Support

TABLE A.2. Instrumentation

PHASE I

A. PROBES

Freestream:

- Total and static pressure: pitot-static tube (United Sensor, Type PAC)

Flow Field over Hills:

- Total pressure: kiel probe (United Sensor, Type KB)
- Static pressure: static holes of a pitot-static tube (United Sensor, Type PBA)
- Velocity signal: single hot-wire probe and X-wire probe (both non-commerical): wires 80 percent platinum and 20 percent iridium, 1.2×10^{-3} cm in diameter, length $\tilde{\sim}$ 0.16 cm.

B. Surface Static Pressure Gauges

- Static taps on models; sharp edged, 0.064 cm in diameter, drilled perpendicular to the model
- Static pressure probes on the wind-tunnel floor; brass tubing 0.079 cm i.d. and 0.139 cm o.d. (end of tubes closed and small holes drilled in a circle around circumference)

C. Transducers and Anemometers

- Pressure transduces (MKS Baratron Pressure Meters, Type 77)
- Constant temperature anemometers (TSI, Model 1051-2)

D. Readout and Time Averaging Instruments

- Pressure meter outputs: digital voltmeters (TSI, Model 1076); outputs averaged by 10 seconds averaging circuits of digital voltmeters
- Anemometer outputs (d.c. and a.c.): digital voltmeters (TSI, Model 1076); outputs averaged by 10 seconds averaging circuits of digital voltmeters; X-wire anemometer outputs (a.c.): outputs multiplied by an analog multiplier (non-commercial)

E. Calibration Pressure Transducer

- Water manometer (Dwyer, Microtector)

TABLE A.2. (Continued)

PHASE II

A. Probes

Freestream:

- Total and static pressure; pitot-static tube (United Sensor, Type PAC)

Flow Field over Hills, Neutrally Thermal Stratification:

- Total pressure: kiel probe (United Sensor, Type KB)
- Static pressure: disk probe (non-commercial); disk diameter 0.62 cm
- Mean temperature: thermistor (YSI)
- Temperature signal: hot-wire probe (non-commercial): wire 90 percent platinum and 10 percent rhodium, wire diameter 5×10^{-5} cm
- Velocity-temperature signal: hot-wire probe (non-commercial); wire 80 percent platinum and 20 percent irridum, 1.2×10^{-3} cm in diameter, length $\tilde{\sim}$ 0.16 cm

B. Transducers and Anemometers

- Pressures transducers (MKS Baratron Pressure Meters, Type 77)
- Constant temperature anemometers (TSI Model 1051-2)
- Temperature transducer (YSI, Model 42 SC)

C. Readouts and Time Averaging Instruments

- Pressure meter outputs: integrating digital voltmeters (DYMEC, Model 2401C); outputs integrated over 60 seconds
- Anemometers outputs (d.c. and rms): digital voltmeters (TSI, Model 1076); outputs averaged by a 10 second averaging circuit
- Temperature outputs read from needle position

D. Spectra and Probability Density Functions

- Correlation and probability density function (Honeywell, Model SA1 43A)
- Spectra (Honeywell, Model SAI 470)

E. Calibration of Pressure Transducers

- Water manometer (Dwyer, Microtector)

TABLE A.2. (Continued)

PHASE III

A. Probes

Freestream:

- Total and static pressure: pitot-static tube, (United Sensor, Type PAC)

Flow Field over Hills, Neutrally Thermal Stratification:

- Total pressure: kiel probe (United Sensor, Type KB)
- Static pressure: disk probe (non-commercial): disk diameter 0.62 cm
- Velocity signal: hot-wire probe (non-commercial): wire 80 percent platinum and 20 percent iridium, 1.2×10^{-3} cm in diameter, length $\simeq$ 0.16 cm

Flow Field over Hills, Stably Thermal Stratification:

- Total pressure: kiel probe (United Sensor, Type KB)
- Static pressure: disk probe (non-commercial): disk diameter 0.62 cm
- Mean temperature: thermistor (YSI)
- Velocity signal: hot-film probe (TSI-10)

B. Transducers and Anemometers

- Pressure transducers (MKS Baratron Pressure Meters, Type 7)
- Constant temperature anemometer (TSI, Model 1051-2)
- Temperature transducer (YSI, Model 42SC)

C. Readouts and Time Averaging Instruments

- Pressure meter outputs: minicomputer (HP 1000); outputs digitized and integrated over 10 seconds
- Anemometer outputs: minicomputer (HP 1000); outputs digitized, converted to velocities and integrated over 10 seconds to calculate mean velocities and rms of the velocity fluctuations
- Temperature outputs: output read from needle position

D. Calibration of Pressure Transducers

- Water manometer (Dwyer, Microtector

During Phases II and III the pitot-static probe was replaced by a disk type probe to reduce errors in flow direction. The disk probe is similar to the Elliott rotating probe used for atmospheric static pressure measurements. The disk is positioned vertically and parallel to the flow direction. Holes are drilled through the center of the disk. The pressure at the holes is somewhat larger than the static pressure in the absence of the probe due to speed up effects. It was found that dynamic pressures using the kiel-disk system could be calculated from

$$p_{dyn} = (p_{pitot} - p_{disk}) * C_{disk} \qquad (A.1)$$

where C_{disk} is a constant to be determined experimentally. For the range of velocities measured in this study, C_{disk} was approximately 0.9 and was evaluated daily by calibration against a standard pitot-static probe in the freestream.

Another error in the dynamic pressure measurements was caused by the effects of turbulence. In the measurements over the surface with rock particles and downwind of the crest, this error could be significant, because the turbulence intensity here was of the order of 20 to 30 percent of the local mean velocity. Thus the maximum error in the mean velocity is estimated to be of the order of three percent. Typical systematic errors were approximately one to two percent. Random errors were reduced by time averaging circuits of 10 seconds during Phase I, of 60 during Phase II, and 10 seconds of Phase III.

Some data is presented which was obtained in the separated wake of the hill using the apparatus and techniques just described. This data is presented only for completeness and for the useful qualitative view it presents of the flow. The values given are not accurate.

Static Pressure Measurements. Static pressure measurements were taken on the surface of the symmetric hill models and on the floor of the tunnel during Phases I and II. Each of the models tested contained a set of pressure holes distributed over the centerline of the hill. On the floor of the tunnel just upwind of the hills static probes were constructed from 0.079 o.d. and 0.139 o.d. brass tubing. Detailed specification of the surface pressure sensors is given by Rider and Sandborn (1977a).

Static pressures in the flow over the hill were measured along with the velocity measurements. During Phase I readings of pressure differentials between the static holes of a pitot-static tube and the surface static pressure

holes at the same x-location were monitored. After the vertical traverses were completed, the pressure differentials between the surface static pressure and the freestream static pressure were measured. The static pressures, p_{stat}, in the flow field over the hill were obtained simply by subtraction, namely

$$p_{stat} = p_{p.t.} - p_{surf} + p'_{surf} - p_{ref} \tag{A.2}$$

This procedure was followed to eliminate some of the spatial static pressure variation. However, it turned out that errors in the static pressure measurements were still quite large because of dirt in the surface static pressure holes. Another source of error was the misalignment of the pitot-static probe. Errors were sometimes as large as 10 percent of the freestream dynamic pressure.

During Phases II and III, static pressure readings were obtained by monitoring the difference between the static pressure at the static pressure holes of the freestream pitot-static probe and the static pressure at the disk probe. Static pressure was calculated using the following expression:

$$p_{stat} = p_{disk}\ p_{ref} + (1 - C_{disk})\, p_{dyn} \tag{A.3}$$

Systematic errors were caused by the effect of turbulence and are of the order of two percent.

Turbulence Intensity Measurements. During Phase I constant temperature hot wire anemometers were employed to measure longitudinal and vertical velocity fluctuations. The cross wire used was not of the usual X-wire type, but had one wire normal and one wire yawed to the flow. The yawed wire is sensitive to two turbulent velocities, u, w plus the correlation between the components, $\overline{uw}$. A detailed discussion of the experimental procedure as well as the evaluation of the hot-wire output is given by Rider and Sandborn (1977a).

During Phases II and III, longitudinal turbulence intensities were measured using constant temperature anenometers. The hot wires (Phase II) and hot film (Phase III) were calibrated daily by placing them in the freestream of the wind tunnel. The flow velocity was measured directly with a pitot-static probe.

Calibration data were fit to a variable exponent form of King's Law:

$$\bar{e}^2 = A + B\,\bar{u}^m \tag{A.4}$$

using a least square fitting program. From this equation it can be shown that the local turbulence intensity is given by

$$\frac{u'}{\bar{u}} = \frac{2\bar{e}\,e'}{m\,(\bar{e}^2 - A)} \tag{A.5}$$

On many days of testing, the hot wire or hot film was calibrated several times per day. This was done to reduce the errors due to drifting of the anemometer system and also to obtain an indication of the system accuracy and repeatibility. Repeatibility in longitudinal turbulence intensities was of the order of one percent and was never observed greater than three percent.

Some data is presented which was obtained in the downwind wake of the hill model. The values given are not accurate because of the low mean velocities and relatively high velocity fluctuations. The data should be used only to determine trends along the new shear layer.

Probability Density and Spectra Measurements. The longitudinal velocity signal was recorded over a symmetric triangular hill $h/L_b = 1/4$, with an aerodynamically smooth surface. Upwind surface was flat and aerodynamically smooth. The distance between boundary layer trip and the center of the hill model was 14.0 m. The turbulence signal was obtained with a commercial hot-film anenometer system. The unit was operated without linearization or filtering. According to manufacturer's specifications the film had a frequency response up to 16 KH_z. This was more than adequate in these measurements as the maximum frequency of interest was of the order of 300 H_z.

Measurements of power spectra and probability density functions were made with a commerical digital data acquisition system. Probability density functions (p.d.f.) and spectra were computed after multiplying the a.c. signal by a factor 10. The system produces a 400 point p.d.f. analysis. The sample rate was 2000 sps and the sampling time was 33 seconds. Before the p.d.f. was generated, it was insured that the amplitude of signal would lie within selected bounds.

Power spectra were generated by a Fourier analysis of a 400 point autocorrelation function (a.c.f.). The a.c.f. was determined simultaneously

at 400 incremental lag points. The sampling rate was 1000 sps. Hence the maximum time lag was 0.4 seconds. Point averaging was applied over 327 cycles. The power spectrum was computed by a Fourier analysis of the averaged a.c.f. Although theoretical constraints dictate that from 400 available data points only one half as many independent frequency points can be obtained, the system incorporates an interpolation scheme which provides a 1000 point interpolated output. In actual frequency, the maximum value is 500 H_z (Nyquist frequency).

The computed p.d.f. and a.c.f. were available as hard copy plots in less than a minute after the signal was recorded. The method has the advantage that repeatability of the functions could be checked while the tests were conducted.

A.4 DATA REPORTING

In this section a review is given of all data of flow characteristics over two-dimensional ridges obtained in the Meteorological Wind Tunnel. The purpose is to make access to the data easier. The identification of the data location is organized according to the three phases of the measuring program. In Table A.1, the report location of all available data is tabulated. There is some inconsistency in the choice of the two-dimensional coordinate system. The standard coordinate system is such that the origin of the x-axis is located at the crest with its positive side pointed in the downwind direction. The z-axis is pointed upwards with its origin at the base of the upwind flat surface. Deviant coordinate systems, etc., are indicated in the table.

A.5 DATA REDUCTION

The reduction of data obtained during Phases I and II was directed toward mapping the complete pressure, velocity and turbulence fields above the hills in the form of contour plots by employing the computer. The procedure includes data smoothing techniques reducing random errors associated with the original data. In the generation of contour plots, the original data is checked for internal consistency. In some cases it was necessary to exclude certain data points and in a few cases vertical data profiles. As a result the accuracy of the contour plots is at least as high as the original data. An unusual feature of the contour plotting route is that the two-dimensional domain over the hill may be specified arbitrarily.

All available data points are included, even if they fall outside the boundaries of the contour plot domain. Space increments Δx and Δz are equal in both x and z direction, but Δx may be different from Δz. The contour plots presented in this report have been generated by 50 increments in x- and z-direction. The generation of such contour plots is described in detail in Appendix C.

APPENDIX B

TABULATED EXPERIMENTAL DATA OF FLOW OVER TRIANGULAR RIDGES

TABLE B.1. Locator Table: Identification of Tables for Test Condition in Phase III

Case	h/L_u	h/L_d	b (cm)	$\bar{u}(10h)$ (m/sec)	Ri	Table number	Upwind condition (See Table 1)
I	1/3	1/4	180.[1)]	9.0	0.0	B.3a	A
II	1/4	1/3	180.	9.0	0.0	B.3b	A
III	1/2	1/4	180.	9.0	0.0	B.3c	A
IV	1/4	1/2	180.	9.0	0.0	B.3d	A
V	1/2	1/6	180.	9.0	0.0	B.3e	A
VI	1/6	1/2	180.	9.0	0.0	B.3f	A
VII	1/2	1/3	180.	9.0	0.0	B.3g	A
VIII	1/3	1/2	180.	9.0	0.0	B.3h	A
IX	1/2	1/0	180.	9.0	0.0	B.3i	A
X	1/3	1/0	180.	9.0	0.0	B.3j	A
XI	1/4	1/0	180.	9.0	0.0	B.3k	A
XII	1/6	1/0	180.	9.0	0.0	B.3l	A
XIII	1/4	1/0	45.	9.0	0.0	B.3m	A
XIV	1/4	1/0	90.	9.0	0.0	B.3n	A
XV	1/4	1/3	45.	9.0	0.0	B.3o	A
XVI	1/4	1/3	90.	9.0	0.0	B.3p	A
XVII	1/4	1/0	180.	3.0	0.07	B.3q	C
XVIII	1/4	1/0	180.	6.0	0.0012	B.3r	B
XIX	1/4	1/0	45.	3.0	0.07	B.3s	C
XX	1/4	1/0	45.	6.0	0.0012	B.3t	B

1) b = 180, this hill width represents the two-dimensional flow case.

TABLE B.2. Upwind Conditions in Phase III

CASE A		CASE B			CASE C		
Z	U	Z	T	U	Z	T	U
.30	4.41	.30	7.2	.81	.31	12.5	2.42
.72	4.85	.80	15.5	1.13	.71	15.0	2.70
1.29	5.14	1.38	15.5	1.18	1.23	18.0	2.97
1.92	5.46	2.04	16.5	1.47	1.94	20.0	3.16
2.86	5.62	3.06	17.5	1.34	2.71	21.0	3.34
4.42	5.81	4.16	19.0	1.58	4.11	21.5	3.52
5.89	6.15	5.93	20.0	1.78	5.93	23.0	3.69
8.29	6.39	8.13	21.5	1.79	8.05	24.0	3.60
10.41	6.69	10.30	22.5	2.03	10.20	24.5	3.98
13.87	7.03	13.81	23.5	1.96	13.79	25.0	3.99
17.46	7.17	17.39	24.5	2.08	17.37	25.5	4.37
21.03	7.47	21.05	25.0	2.37	20.96	26.5	4.62
28.34	7.92	24.64	25.5	2.48	24.57	26.5	4.81
35.65	8.28	28.20	25.5	2.49	28.14	27.0	4.74
42.73	8.49	35.39	25.7	2.74	35.32	27.0	5.08
49.73	8.64	42.54	26.0	2.87	42.53	27.5	5.21
56.90	8.64	49.73	26.3	2.88	49.70	28.0	5.39
		56.90	26.5	2.85	56.89	28.0	5.21

T TEMPERATURE IN DEGREES CELCIUS
U LONGITUDINAL VELOCITY IN M/SEC
Z HEIGHT ABOVE UPWIND SURFACE-LEVEL IN CM

TABLE B.3a. Triangular Hill Model, Height 5.08 cm, Upwind Slope 1/3, Downwind Slope 1/4, Surface Roughness Smooth, Freestream Velocity 9. m/sec, Neutral Thermal Stratification

****

X= 0.00

Z	U	URMS
5.38	7.40	.66
6.60	7.17	.70
7.33	7.11	.70
8.39	7.18	.69
9.46	7.40	.69
13.13	7.47	.60
16.78	7.54	.58
20.40	7.62	.58
24.07	7.76	.59
27.68	8.08	.58
31.34	8.27	.54
35.00	8.42	.53
38.69	8.71	.44
42.32	8.73	.37
45.92	8.99	.21
49.58	8.93	.34
56.90	8.97	.41

X= 10.00

Z	U	URMS	P
2.84	1.09	.74	-.12
3.52	2.03	.81	-.13
4.23	3.34	.77	-.14
5.69	6.00	1.27	-.13
8.26	7.25	1.06	-.11
9.69	7.34	.71	-.10
13.34	7.51	.60	-.09
16.96	7.65	.58	-.07
20.62	7.71	.59	-.06
24.19	7.86	.56	-.05
27.47	7.87	.53	-.04
31.50	8.19	.54	-.05
35.12	7.87	.53	-.04
35.12	8.25	.49	-.04
42.36	8.51	.37	-.03
49.69	8.63	.28	-.02
56.90	8.68	.09	-.02

X= 20.00

Z	U	URMS	P
.30	.00	.01	-.07
.74	1.07	.01	-.08
.95	.59	.04	-.07
1.69	1.70	.70	-.08
2.42	2.55	.80	-.09
3.88	4.24	1.06	-.09
6.79	6.62	2.10	-.10
9.71	7.22	1.13	-.08
13.32	7.58	.68	-.08
16.92	7.61	.58	-.07
20.56	7.83	.58	-.06
24.22	7.98	.57	-.05
27.89	8.20	.54	-.03
35.13	8.79	.51	-.08
42.36	8.93	.35	-.07
49.66	9.12	.14	-.07
56.90	9.09	.25	-.06

X= 45.00

Z	U	URMS	P
.30	1.92	1.14	-.07
.57	1.82	1.14	-.07
.92	2.02	1.21	-.10
1.63	2.24	1.35	-.10
2.36	2.21	1.40	-.11
3.81	4.59	1.51	-.03
6.70	5.97	1.93	-.03
9.53	6.84	1.72	-.03
13.15	7.13	1.03	-.02
16.72	7.50	.66	-.03
20.28	7.76	.64	-.03
23.93	7.93	.63	-.03
27.51	8.18	.60	-.02
34.67	8.74	.53	-.02
41.88	9.04	.39	-.02
49.05	9.27	.23	-.02
56.20	9.31	.24	-.01

U LONGITUDINAL VELOCITY IN M/SEC
URMS RMS OF LONG. VELOCITYFLUCT. IN M/SEC
P STATIC PRESSURES IN NT/DM2
X DOWNWIND DISTANCE FROM CREST IN CM
Z HEIGHT ABOVE UPWIND SURFACE-LEVEL IN CM

TABLE B.3b. Triangular Hill Model, Height 5.08 cm, Upwind Slope 1/4, Downwind Slope 1/3, Surface Roughness Smooth, Freestream Velocity 9. m/sec, Neutral Thermal Stratification

****

X= 0.00

Z	U	URMS	P
5.28	6.19	.62	-.07
5.83	6.36	.66	-.07
6.54	6.71	.75	-.07
7.38	6.81	.71	-.07
8.80	7.11	.69	-.07
10.78	7.12	.63	-.06
13.31	7.27	.66	-.05
17.08	7.49	.65	-.05
20.63	7.81	.67	-.05
27.87	8.08	.62	-.04
35.25	8.50	.55	-.03
42.69	8.74	.43	-.03
49.89	8.93	.26	-.03
56.90	8.95	.23	-.02

X= 7.50

Z	U	URMS	P
2.74	.38	.55	-.12
3.15	.72	.52	-.12
3.55	.00	.62	-.11
3.98	.27	.75	-.13
4.47	1.42	1.50	-.12
4.84	2.60	1.80	-.12
5.26	4.20	1.88	-.12
6.01	6.47	1.06	-.11
5.67	5.68	1.71	-.12
6.47	6.84	.75	-.10
8.19	7.28	.72	-.10
10.67	7.46	.63	-.09
13.31	7.54	.66	-.07
16.66	7.63	.71	-.06
20.58	7.88	.66	-.06
27.66	8.17	.65	-.04
35.29	8.60	.53	-.04
42.46	8.76	.43	-.03
49.63	8.95	.33	-.03
56.90	9.04	.25	-.03

X= 15.00

Z	U	URMS	P
.20	.00	.00	-.11
1.85	.00	.00	-.11
3.34	.39	.00	-.12
4.32	1.61	2.32	-.12
4.87	2.89	2.66	-.12
5.31	3.27	4.36	-.13
5.84	4.33	4.91	-.13
7.13	6.53	6.76	-.12
6.44	5.50	6.22	-.12
8.68	7.31	7.24	-.10
11.06	7.49	7.50	-.09
13.54	7.60	7.71	-.08
17.28	7.74	7.72	-.07
20.81	7.86	7.86	-.06
27.97	8.21	8.21	-.05
35.21	8.58	8.61	-.04
42.74	8.77	8.86	-.03
49.76	8.97	9.07	-.03
56.90	8.99	9.07	-.02

X= 45.00

Z	U	URMS	P
.20	1.10	1.07	-.01
.58	1.44	1.24	-.02
1.29	1.83	1.52	-.02
2.25	2.16	1.65	-.02
3.37	2.92	1.72	-.04
4.83	3.98	1.71	-.05
5.97	4.80	1.43	-.04
7.09	5.44	1.42	-.04
8.57	6.08	1.16	-.04
9.90	6.54	.89	-.04
13.48	7.07	.70	-.03
17.46	7.40	.69	-.04
21.27	7.64	.70	-.04
28.06	8.06	.65	-.03
35.57	8.55	.56	-.03
42.69	8.86	.47	-.03
50.26	9.03	.32	-.03
56.91	9.05	.33	-.02

U LONGITUDINAL VELOCITY IN M/SEC
URMS RMS OF LONG. VELOCITYFLUCT. IN M/SEC
P STATIC PRESSURES IN NT/DM2
X DOWNWIND DISTANCE FROM CREST IN CM
Z HEIGHT ABOVE UPWIND SURFACE-LEVEL IN CM

TABLE B.3c. Triangular Hill Model, Height 5.08 cm, Upwind Slope 1/2, Downwind Slope 1/4, Surface Roughness Smooth, Freestream Velocity 9. m/sec, Neutral Thermal Stratification

****

X= 0.00			
Z	U	URMS	P
5.38	6.33	.71	-.09
5.69	6.38	.68	-.08
6.11	6.28	.60	-.08
6.72	6.40	.65	-.07
7.53	6.53	.71	-.07
8.24	6.37	.62	-.06
9.68	6.80	.67	-.06
11.15	6.83	.63	-.05
13.28	6.90	.54	-.05
16.88	7.11	.58	-.04
20.47	7.38	.51	-.04
24.02	7.64	.49	-.03
31.20	8.04	.47	-.03
38.36	8.35	.43	-.02
45.59	8.75	.32	-.03
52.76	8.74	.34	-.02
56.32	8.69	.38	-.01

X= 10.00			
Z	U	URMS	P
2.84	1.18	.69	-.15
3.26	.00	.75	-.13
3.82	.87	.72	-.15
4.03	.65	.68	-.14
6.19	4.31	1.75	-.14
8.34	7.14	.82	-.12
10.46	7.30	.60	-.10
13.37	7.44	.54	-.09
16.93	7.51	.56	-.07
24.09	7.86	.48	-.05
31.26	8.28	.45	-.04
38.46	8.51	.37	-.03
45.66	8.80	.37	-.03
52.83	8.85	.36	-.02
56.43	8.90	.37	-.02

X= 20.00			
Z	U	URMS	P
.30	.00	.70	-.11
1.15	.51	.69	-.12
1.88	1.06	.75	-.12
2.61	.71	.74	-.12
3.33	.98	.96	-.13
4.79	3.02	1.27	-.13
6.22	4.14	1.74	-.13
7.62	5.89	1.82	-.13
9.77	7.16	.90	-.11
13.38	7.45	.58	-.09
16.98	7.66	.51	-.08
24.14	7.89	.48	-.06
31.35	8.28	.41	-.04
38.50	8.59	.28	-.04
45.73	8.84	.16	-.03
52.90	8.89	.26	-.03
54.30	8.88	.26	-.03
56.60	8.84	.30	-.02

X= 45.00			
Z	U	URMS	P
.30	.69	.86	-.01
.84	2.55	.90	-.05
1.20	1.52	.88	-.03
1.92	2.30	1.11	-.04
2.72	3.02	1.22	-.05
4.06	3.67	1.39	-.06
7.01	5.22	1.64	-.06
9.82	6.28	1.31	-.06
13.41	7.00	.71	-.05
17.05	6.84	.53	-.01
20.60	7.88	.52	-.05
24.19	8.04	.49	-.05
27.78	8.38	.45	-.06
34.98	8.77	.34	-.05
42.16	8.91	.25	-.03
49.33	9.11	.15	-.03
56.50	8.78	.03	.01

U LONGITUDINAL VELOCITY IN M/SEC
URMS RMS OF LONG. VELOCITYFLUCT. IN M/SEC
P STATIC PRESSURES IN NT/DM2
X DOWNWIND DISTANCE FROM CREST IN CM
Z HEIGHT ABOVE UPWIND SURFACE-LEVEL IN CM

TABLE B.3d. Triangular Hill Model, Height 5.08 cm, Upwind Slope 1/4, Downwind Slope 1/2, Surface Roughness Smooth, Freestream Velocity 9. m/sec, Neutral Thermal Stratification

****

X= 0.00

Z	U	URMS	P
5.38	6.40	.72	-.08
6.02	6.31	.74	-.07
6.75	6.67	.81	-.07
8.17	6.74	.80	-.06
8.89	6.95	.84	-.07
9.64	6.66	.77	-.04
13.21	7.11	.77	-.04
16.81	7.31	.72	-.05
20.38	7.77	.71	-.06
23.99	8.00	.65	-.04
27.55	7.91	.64	-.02
34.74	8.06	.46	-.05
41.90	8.79	.05	-.03
49.09	8.84	.28	-.01
56.17	9.03	.43	-.02

X= 5.00

Z	U	URMS	P
2.84	.00	.30	.00
3.47	.00	.37	-.00
4.18	.00	.41	-.01
5.65	4.08	.75	-.02
7.05	7.10	1.19	-.02
8.47	7.22	.86	-.02
9.94	7.40	.81	-.01
13.51	7.46	.76	-.01
17.10	7.72	.66	-.00
20.69	8.07	.71	-.01
24.27	8.07	.64	-.00
27.86	8.36	.58	-.01
35.08	8.67	.49	-.00
42.26	8.85	.31	-.00
49.41	9.06	.14	.00
56.62	9.15	.33	-.00

X= 10.00

Z	U	URMS	P
.30	.00	.26	.00
.55	.00	.39	.01
.92	.00	.40	.00
1.65	.00	.39	.01
2.37	.00	.44	.00
3.08	.00	.47	.01
3.77	.84	.40	.00
5.96	5.92	1.70	-.01
8.13	7.12	.84	-.01
9.53	7.21	.76	-.01
13.13	7.61	.74	-.01
16.69	7.84	.70	-.01
20.32	7.94	.63	-.00
23.88	8.13	.64	-.00
27.48	8.22	.63	-.00
34.64	8.69	.46	-.00
41.82	8.84	.21	.00
49.03	9.02	.33	.00
56.20	9.09	.40	-.00

X= 45.00

Z	U	URMS	P
.50	1.98	.80	.02
.97	2.61	.91	.01
1.71	3.02	1.06	.01
2.45	3.29	1.30	.01
3.83	4.15	1.68	.00
6.74	5.69	1.98	.00
9.61	6.64	1.34	.00
13.20	7.06	.85	.00
16.79	7.31	.74	-.00
20.38	7.44	.73	.00
23.99	7.97	.71	-.00
27.57	8.10	.64	.00
34.71	8.61	.48	-.00
41.90	8.88	.23	-.00
49.11	9.06	.29	.00
56.29	9.15	.36	.00

U LONGITUDINAL VELOCITY IN M/SEC
URMS RMS OF LONG. VELOCITYFLUCT. IN M/SEC
P STATIC PRESSURES IN N1/DM2
X DOWNWIND DISTANCE FROM CREST IN CM
Z HEIGHT ABOVE UPWIND SURFACE-LEVEL IN CM

TABLE B.3e. Triangular Hill Model, Height 5.08 cm, Upwind Slope 1/2, Downwind Slope 1/6, Surface Roughness Smooth, Freestream Velocity 9. m/sec, Neutral Thermal Stratification

****

X= 0.00			
Z	U	URMS	P
5.38	7.63	.66	-.74
5.75	7.50	.62	-.18
6.43	7.50	.66	-.15
7.18	7.44	.67	-.14
8.64	7.45	.68	-.11
11.49	7.45	.59	-.08
14.38	7.50	.56	-.07
17.98	7.54	.56	-.06
21.57	7.75	.55	-.05
25.15	8.06	.58	-.04
28.72	8.24	.55	-.04
32.34	8.45	.52	-.04
35.89	8.55	.47	-.03
43.07	8.79	.35	-.03
50.25	8.92	.24	-.02
56.17	8.96	.17	-.02

X= 15.00			
Z	U	URMS	P
2.84	2.68	1.08	-.23
3.16	3.03	1.33	-.25
3.89	4.29	1.76	-.27
4.61	5.44	1.87	-.30
5.32	6.24	1.59	-.33
6.76	6.70	.94	-.33
9.61	7.03	.63	-.32
12.50	7.24	.60	-.32
16.08	7.44	.60	-.31
19.70	7.55	.54	-.27
23.26	7.66	.53	-.26
26.86	7.83	.52	-.24
30.47	8.04	.53	-.23
37.64	8.28	.41	-.22
44.83	8.49	.33	-.21
52.02	8.62	.24	-.21
55.82	8.64	.20	-.20

X= 30.00			
Z	U	URMS	P
.30	2.21	1.05	-.05
.62	2.61	1.12	-.07
1.33	3.14	1.27	-.09
2.07	3.67	1.32	-.10
3.50	4.57	1.63	-.12
4.95	5.53	1.58	-.15
6.36	6.01	1.20	-.14
7.77	6.30	1.10	-.15
9.25	6.54	.75	-.18
12.82	6.88	.64	-.19
16.43	7.15	.56	-.19
20.01	7.30	.55	-.19
23.60	7.59	.57	-.21
27.18	7.70	.53	-.20
34.39	8.06	.48	
41.56	8.45	.38	- 20
48.77	8.58	.27	- 20
55.91	8.54	.15	- 18

X= 45.00			
Z	U	URMS	P
.30	3.07	1.03	-.03
1.00	3.69	1.06	-.06
1.70	3.97	1.22	-.07
2.43	4.30	1.36	-.08
3.88	4.82	1.36	-.09
6.73	5.64	1.39	-.08
9.60	6.34	.87	-.12
13.22	6.69	.68	-.14
16.78	6.83	.59	-.12
20.40	7.20	.54	-.15
23.94	7.53	.54	-.15
27.55	7.74	.51	-.17
34.74	8.07	.46	-.17
41.90	8.37	.38	-.18
49.12	8.54	.24	-.19
56.28	8.59	.13	-.18

U LONGITUDINAL VELOCITY IN M/SEC
URMS RMS OF LONG. VELOCITYFLUCT. IN M/SEC
P STATIC PRESSURES IN NT/DM2
X DOWNWIND DISTANCE FROM CREST IN CM
Z HEIGHT ABOVE UPWIND SURFACE-LEVEL IN CM

TABLE B.3f. Triangular Hill Model, Height 5.08 cm, Upwind Slope 1/6, Downwind Slope 1/2, Surface Roughness Smooth, Freestream Velocity 9. m/sec, Neutral Thermal Stratification

****

X= 0.00

Z	U	URMS	P
5.38	5.32	.69	- 07
6.03	6.03	.62	- 06
7.48	6.44	.70	- 07
9.67	6.81	.65	- 07
11.80	6.79	.55	- 06
16.80	7.18	.57	- 05
20.42	7.39	.59	- 05
23.98	7.53	.57	- 04
27.57	7.71	.55	- 04
34.77	8.23	.49	- 03
41.95	8.48	.37	- 02
49.13	8.67	.28	- 02
56.30	8.66	.30	- 02

X= 5.00

Z	U	URMS	P
2.84	.00	.34	-.10
3.59	.00	.41	-.10
4.43	.77	.63	-.10
5.42	5.22	1.30	-.09
6.54	6.73	.68	-.09
9.37	7.22	.68	-.08
13.00	7.38	.61	-.06
16.60	7.52	.62	-.06
20.18	7.91	.59	-.06
23.77	8.07	.60	-.05
27.31	8.19	.55	-.04
34.52	8.57	.48	-.04
41.73	8.75	.32	-.03
48.92	8.94	.13	-.02
56.04	8.95	.19	-.02

X= 10.00

Z	U	URMS	P
.30	.00	.30	-.10
1.04	.00	.47	-.11
1.72	.00	.47	-.10
2.43	.00	.46	-.10
3.84	1.05	.68	-.10
6.73	6.67	.76	-.10
9.58	7.14	.64	-.09
13.21	7.35	.59	-.08
16.80	7.49	.63	-.07
20.40	7.75	.57	-.06
23.97	7.95	.57	-.05
27.54	8.20	.57	-.05
34.72	8.49	.47	-.04
41.89	8.75	.31	-.03
45.92	8.87	.07	-.02
56.24	8.95	.28	-.03

X= 45.00

Z	U	URMS	P
.30	1.62	.98	-.00
1.05	2.35	1.16	-.01
1.70	2.85	1.28	-.02
2.10	3.39	1.41	-.02
3.88	4.32	1.63	-.02
6.76	5.78	1.40	-.03
9.58	6.45	.75	-.02
13.17	6.78	.63	-.03
16.83	7.09	.58	-.03
20.38	7.40	.61	-.03
24.00	7.58	.62	-.03
27.59	7.96	.56	-.03
34.75	8.43	.49	-.03
41.91	8.64	.35	-.02
49.10	8.85	.17	-.02
56.26	8.91	.26	-.02

U LONGITUDINAL VELOCITY IN M/SEC
URMS RMS OF LONG. VELOCITYFLUCT. IN M/SEC
P STATIC PRESSURES IN NT/DM2
X DOWNWIND DISTANCE FROM CREST IN CM
Z HEIGHT ABOVE UPWIND SURFACE-LEVEL IN CM

TABLE B.3g. Triangular Hill Model, Height 5.08 cm, Upwind Slope 1/2, Downwind Slope 1/3, Surface Roughness Smooth, Freestream Velocity 9. m/sec, Neutral Thermal Stratification

X= 0.00				X= 7.50			
Z	U	URMS	P	Z	U	URMS	P
5.38	.00	.69	-.03	2.64	.00	.45	-.04
5.91	6.39	.59	-.00	3.82	.65	.46	-.04
6.65	6.36	.69	.00	5.22	1.25	.55	-.04
8.09	6.60	.70	.00	6.70	4.97	1.62	-.03
9.54	6.81	.66	.01	9.54	7.28	.65	-.00
13.09	6.97	.56	.01	13.12	7.55	.59	.00
16.67	7.19	.55	.02	16.70	7.71	.57	.01
20.30	7.38	.58	.02	20.31	7.87	.56	.01
23.85	7.73	.54	.02	23.92	7.90	.55	.02
27.45	8.09	.54	.02	27.51	8.16	.51	.02
34.61	8.47	.48	.03	34.64	8.61	.45	.03
41.81	8.72	.42	.03	41.84	8.79	.37	.03
49.01	8.95	.31	.04	49.01	9.07	.13	.03
56.18	9.03	.33	.03	56.19	9.09	.20	.04

X= 15.00				X= 45.00			
Z	U	URMS	P	Z	U	URMS	P
.30	.00	.44	-.04	.30	.88	.56	-.01
1.00	.68	.65	-.04	.97	1.35	.71	-.01
2.45	.00	.58	-.04	1.69	1.75	.83	-.01
3.88	.88	.66	-.04	2.40	1.86	.86	-.02
5.31	2.25	.61	-.04	3.85	2.55	1.26	-.01
6.76	4.40	1.57	-.03	6.71	4.95	1.78	-.01
9.64	7.36	.62	-.01	9.60	6.32	1.49	.00
13.20	7.71	.64	.00	13.22	7.03	.81	.01
16.83	7.86	.58	.01	16.78	7.30	.61	.01
20.40	8.04	.57	.01	20.35	7.63	.55	.01
24.02	8.20	.52	.01	23.96	8.01	.61	.02
27.58	8.25	.54	.02	27.58	8.34	.59	.02
34.80	8.55	.52	.03	34.76	8.56	.49	.03
41.97	8.84	.37	.03	41.94	8.91	.40	.03
49.11	9.07	.04	.03	49.11	9.12	.13	.03
56.30	9.07	.13	.04	56.28	9.23	.24	.03

U LONGITUDINAL VELOCITY IN M/SEC
URMS RMS OF LONG. VELOCITYFLUCT. IN M/SEC
P STATIC PRESSURES IN NT/DM2
X DOWNWIND DISTANCE FROM CREST IN CM
Z HEIGHT ABOVE UPWIND SURFACE-LEVEL IN CM

TABLE B.3h Triangular Hill Model, Height 5.08 cm, Upwind Slope 1/3, Downwind Slope 1/2, Surface Roughness Smooth, Freestream Velocity 9. m/sec, Neutral Thermal Stratification

****

X= 0.00			
Z	U	URMS	P
5.38	5.96	.59	-.25
5.73	6.35	.59	-.28
6.46	6.52	.67	-.27
7.18	6.69	.71	-.27
8.58	6.70	.73	-.24
11.51	7.13	.62	-.25
14.39	7.44	.64	-.25
17.94	7.53	.59	-.23
21.57	7.70	.55	-.23
25.13	7.95	.56	-.23
28.72	8.18	.54	-.23
32.33	8.33	.47	-.22
39.47	8.76	.39	-.23
46.67	8.99	.24	-.23
53.84	9.02	.14	-.21
56.18	9.05	.16	-.22

X= 5.00			
Z	U	URMS	P
2.64	.00	.39	-.37
3.20	.00	.44	-.37
3.93	.00	.37	-.37
4.62	.00	.39	-.38
6.09	4.38	1.11	-.40
8.97	7.42	.77	-.41
11.86	7.60	.68	-.35
19.07	7.77	.55	-.30
22.63	7.94	.56	-.27
26.22	8.13	.54	-.27
29.82	8.30	.51	-.26
33.43	8.46	.51	-.25
40.60	8.88	.41	-.25
47.76	9.00	.18	-.22
55.00	9.09	.22	-.23

X= 10.00			
Z	U	URMS	P
.30	.00	.27	-.12
.68	.00	.41	-.12
1.62	.00	.47	-.12
2.32	.00	.51	-.12
3.76	.00	.51	-.12
6.63	2.78	1.34	-.14
9.50	4.17	.69	-.13
13.08	4.23	.63	-.12
16.69	4.36	.58	-.11
20.26	4.47	.56	-.10
23.86	4.55	.51	-.09
27.47	4.63	.52	-.09
34.65	4.83	.52	-.09
41.81	5.01	.38	-.08
48.99	9.06	.06	-.25
56.15	9.08	.24	-.24

X= 45.00			
Z	U	URMS	P
.30	1.32	.44	-.03
.93	1.49	.52	-.04
1.67	1.78	.63	-.05
2.34	1.96	.71	-.05
3.82	3.14	.96	-.05
5.21	4.01	1.23	-.06
6.65	5.10	1.54	-.08
9.53	6.37	1.73	-.05
13.12	6.92	1.10	-.05
16.75	7.41	.64	-.05
20.29	7.90	.60	-.05
23.94	8.12	.60	-.05
27.51	8.35	.59	-.05
34.68	8.69	.50	-.04
41.84	9.04	.42	-.03
49.07	9.29	.28	-.03
56.25	9.27	.22	-.03

U LONGITUDINAL VELOCITY IN M/SEC
URMS RMS OF LONG. VELOCITYFLUCT. IN M/SEC
P STATIC PRESSURES IN NT/DM2
X DOWNWIND DISTANCE FROM CREST IN CM
Z HEIGHT ABOVE UPWIND SURFACE-LEVEL IN CM

TABLE B.3i. Triangular Hill Model, Height 5.08 cm, Upwind Slope 1/2, Downwind Slope 1/0, Surface Roughness Smooth, Freestream Velocity 9. m/sec, Neutral Thermal Stratification

**********,

X= 0.00				X= 22.50			
Z	U	URMS	P	Z	U	URMS	P
5.38	5.86	.56	-.05	.30	.00	.63	-.12
5.98	5.93	.62	-.05	1.03	.00	.69	-.12
6.68	6.30	.71	-.05	1.74	.00	.64	-.12
8.10	6.33	.66	-.04	2.45	.00	.62	-.12
9.57	6.64	.71	-.05	3.95	1.31	.68	-.13
13.16	6.84	.70	-.04	6.90	4.03	1.59	-.12
16.72	7.07	.57	-.04	9.70	6.95	1.07	-.11
20.35	7.26	.62	-.03	13.27	7.46	.64	-.10
23.92	7.60	.55	-.03	20.44	7.74	.55	-.08
27.52	7.77	.51	-.03	16.84	7.64	.63	-.09
34.68	8.18	.37	-.03	24.05	7.90	.57	-.07
41.84	8.47	.36	-.02	27.63	8.03	.51	-.06
49.05	8.68	.35	-.03	34.77	8.36	.47	-.05
56.21	8.70	.33	-.02	42.00	8.66	.42	-.04
				49.13	8.75	.41	-.04
				56.33	8.80	.43	-.03

U LONGITUDINAL VELOCITY IN M/SEC
URMS RMS OF LONG. VELOCITYFLUCT. IN M/SEC
P STATIC PRESSURES IN NT/DM2
X DOWNWIND DISTANCE FROM CREST IN CM
Z HEIGHT ABOVE UPWIND SURFACE-LEVEL IN CM

TABLE B.3j. Triangular Hill Model, Height 5.08 cm, Upwind Slope 1/3, Downwind Slope 1/0, Surface Roughness Smooth, Freestream Velocity 9. m/sec, Neutral Thermal Stratification

****

X= 0.00				X= 22.50			
Z	U	URMS	P	Z	U	URMS	P
				.30	.00	.49	-.11
5.38	6.06	.42	-.07	.93	.00	.46	-.11
5.88	5.85	.43	-.07	1.65	.00	.42	-.11
6.61	6.26	.47	-.06	2.34	.00	.44	-.11
8.04	6.57	.45	-.06	3.80	1.38	.48	-.11
9.46	6.75	.44	-.05	6.67	4.91	1.09	-.11
13.06	7.03	.43	-.04	9.52	7.03	.53	-.09
16.64	7.17	.41	-.04	13.16	7.27	.47	-.08
20.26	7.33	.43	-.03	16.69	7.49	.42	-.07
23.83	7.54	.41	-.04	20.30	7.74	.42	-.07
[illegible]	[illegible]	.41	-.03	23.91	7.63	.39	-.06
34.61	8.44	.36	-.03	27.45	7.81	.41	-.05
41.80	8.82	.28	-.03	34.65	8.27	.38	-.05
49.00	8.56	.24	-.02	41.84	8.42	.28	-.04
56.17	8.78	.22	-.02	48.99	8.62	.21	-.04
				56.17	8.60	.15	-.03

U LONGITUDINAL VELOCITY IN M/SEC
URMS RMS OF LONG. VELOCITYFLUCT. IN M/SEC
P STATIC PRESSURES IN NT/DM2
X DOWNWIND DISTANCE FROM CREST IN CM
Z HEIGHT ABOVE UPWIND SURFACE-LEVEL IN CM

TABLE B.3k. Triangular Hill Model, Height 5.08 cm, Upwind Slope 1/4, Downwind Slope 1/0, Surface Roughness Smooth, Freestream Velocity 9. m/sec, Neutral Thermal Stratification

****

X= 0.00

Z	U	URMS	P
5.38	6.09	.69	-.07
5.94	6.35	.61	-.07
6.50	6.70	.64	-.07
7.28	6.77	.63	-.07
8.89	6.93	.61	-.06
11.20	7.12	.59	-.06
13.25	7.29	.56	-.06
16.95	7.36	.53	-.05
20.34	7.53	.55	-.05
27.67	8.09	.53	-.05
35.05	8.43	.46	-.04
42.45	8.63	.29	-.03
49.85	8.72	.05	-.03
56.90	8.76	.27	-.03

X= 22.50

Z	U	URMS	P
.30	.19	.62	-.08
2.18	.51	.57	-.09
2.56	.52	.55	-.08
3.01	.44	.70	-.08
3.39	1.27	.76	-.09
3.98	1.84	.94	-.09
4.44	2.58	1.10	-.09
4.95	3.43	1.32	-.09
5.42	3.79	1.41	-.08
5.94	4.73	1.41	-.09
6.80	5.69	1.18	-.08
7.46	6.34	.95	-.08
9.06	6.84	.67	-.07
11.80	7.03	.59	-.06
14.91	7.23	.55	-.06
17.99	7.36	.54	-.05
22.44	7.64	.51	-.05
28.09	7.81	.50	-.04
35.41	8.25	.44	-.03
42.58	8.48	.34	-.03
49.83	8.62	.23	-.02
56.90	8.67	.26	-.02

X= 45.00

Z	U	URMS	P
.30	1.68	.70	-.01
1.72	2.21	.95	-.01
2.28	2.54	1.08	-.01
3.13	3.13	1.22	-.02
3.95	3.56	1.41	-.02
4.79	4.43	1.39	-.02
5.62	4.80	1.42	-.02
6.34	5.20	1.31	-.02
7.99	5.92	1.11	-.02
10.28	6.44	.69	-.02
13.84	6.68	.64	-.02
17.51	6.98	.49	-.02
21.08	7.27	.61	-.02
28.24	7.75	.53	-.02
35.37	8.21	.49	-.02
43.03	8.42	.36	-.02
49.85	8.63	.31	-.02
56.90	8.61	.35	-.01

U LONGITUDINAL VELOCITY IN M/SEC
URMS RMS OF LONG. VELOCITYFLUCT. IN M/SEC
P STATIC PRESSURES IN NT/DM2
X DOWNWIND DISTANCE FROM CREST IN CM
Z HEIGHT ABOVE UPWIND SURFACE-LEVEL IN CM

TABLE B.31. Triangular Hill Model, Height 5.08 cm, Upwind Slope 1/6, Downwind Slope 1/0, Surface Roughness Smooth, Freestream Velocity 9. m/sec, Neutral Thermal Stratification

****

X= 0.00			
Z	U	URMS	P
5.20	6.21	.67	-.07
5.85	6.53	.63	-.07
6.56	6.75	.64	-.07
7.31	6.79	.71	-.07
8.00	7.00	.66	-.07
9.48	7.05	.69	-.06
11.68	7.29	.67	-.05
13.13	7.40	.64	-.05
16.75	7.51	.64	-.05
20.43	7.86	.60	-.05
24.07	8.01	.60	-.04
27.71	8.16	.63	-.04
35.02	8.51	.55	-.03
42.33	8.85	.46	-.03
49.60	8.89	.39	-.02
56.90	9.00	.36	-.02

X= 22.50			
Z	U	URMS	P
.30	.00	.57	-.08
1.05	.00	.56	-.09
1.77	.12	.66	-.09
2.54	.53	.91	-.09
3.21	1.84	1.21	-.09
3.95	2.99	1.37	-.09
4.38	3.63	1.49	-.09
4.69	4.14	1.41	-.09
5.07	4.64	1.43	-.09
5.40	5.02	1.33	-.09
6.13	5.97	1.15	-.09
6.91	6.72	.88	-.09
7.61	7.01	.78	-.08
9.02	7.10	.66	-.07
13.39	7.40	.64	-.06
17.06	7.63	.64	-.06
20.66	7.77	.61	-.05
27.88	8.15	.59	-.04
35.14	8.61	.57	-.03
42.40	8.85	.47	-.03
49.66	8.93	.41	-.02
56.90	9.03	.38	-.02

X= 45.00			
Z	U	URMS	P
.20	1.88	.86	.02
.77	2.28	1.00	.01
1.61	2.95	1.09	.01
2.58	3.39	1.29	.00
3.99	4.33	1.49	.00
5.46	5.30	1.49	.00
7.69	6.27	1.04	.00
9.91	6.74	.78	-.00
13.57	6.92	.67	-.01
17.14	7.23	.67	-.00
20.74	7.61	.65	-.01
27.92	8.02	.66	-.01
35.20	8.48	.54	-.01
42.49	8.69	.45	-.01
49.90	8.88	.30	-.00
56.90	8.91	.25	-.00
56.89	8.87	.25	.00
56.89	8.91	.26	-.00
56.88	8.77	.30	.01

U LONGITUDINAL VELOCITY IN M/SEC
URMS RMS OF LONG. VELOCITYFLUCT. IN M/SEC
P STATIC PRESSURES IN NT/DM2
X DOWNWIND DISTANCE FROM CREST IN CM
Z HEIGHT ABOVE UPWIND SURFACE-LEVEL IN CM

TABLE B.3m. Triangular Hill Model, Height 5.08 cm, Upwind Slope 1/4, Downwind Slope 1/0, Surface Roughness Smooth, Freestream Velocity 9. m/sec, Neutral Thermal Stratification

****

Y= 0.00			Y= 15.00		
Z	U	URMS	Z	U	URMS
5.24	6.02	.65	5.50	5.30	.71
6.03	6.45	.60	6.19	6.72	.63
7.15	6.87	.66	7.10	6.98	.68
8.59	7.05	.66	8.71	7.29	.63
10.00	7.21	.66	9.74	7.38	.63
13.62	7.57	.61	13.43	7.61	.61
17.21	7.64	.62	17.01	7.84	.62
20.83	8.02	.64	20.64	7.94	.65
24.40	8.30	.64	24.24	8.24	.63
28.00	8.55	.62	27.88	8.39	.61
35.26	8.92	.54	35.13	8.84	.49
42.48	9.17	.46	42.41	9.14	.39
49.71	9.36	.37	49.67	9.23	.37
56.90	9.38	.35	56.90	9.32	.35

Y= 21.25			Y= 22.50		
Z	U	URMS	Z	U	URMS
5.74	6.47	.66	5.74	6.48	.69
6.72	6.98	.62	6.69	6.93	.63
8.18	7.17	.59	8.11	7.26	.64
9.58	7.38	.63	9.66	7.31	.61
11.97	7.49	.61	11.81	7.41	.61
13.22	7.49	.60	13.28	7.50	.57
16.85	7.79	.60	16.85	7.77	.58
20.53	8.01	.59	20.52	7.91	.58
24.15	8.12	.57	24.16	8.07	.57
27.78	8.37	.54	27.75	8.34	.58
35.07	8.66	.50	35.09	8.71	.47
42.34	9.01	.41	42.36	9.00	.39
49.67	9.19	.37	49.65	9.15	.35
56.90	9.24	.33	56.90	9.23	.35

U LONGITUDINAL VELOCITY IN M/SEC
URMS RMS OF LONG. VELOCITYFLUCT. IN M/SEC
Y LATERAL DISTANCE FROM CENTER CREST IN CM
Z HEIGHT ABOVE UPWIND SURFACE-LEVEL IN CM

TABLE B.3n. Triangular Hill Model, Height 5.08 cm, Upwind Slope 1/4, Downwind Slope 1/0, Surface Roughness Smooth, Freestream Velocity 9. m/sec, Neutral Thermal Stratification

Y= 0.00

Z	U	URMS
5.24	5.66	.66
6.61	6.53	.68
8.06	6.83	.68
9.50	7.04	.65
11.72	7.31	.61
13.19	7.34	.60
16.83	7.64	.63
20.48	7.81	.66
24.08	8.19	.58
27.73	8.34	.56
31.41	8.43	.58
35.02	8.66	.51
42.32	8.95	.45
49.61	9.11	.33
56.90	9.14	.31

Y= 15.00

Z	U	URMS
5.24	5.77	78.50
5.66	6.02	70.50
6.37	6.30	72.39
7.45	6.60	81.39
8.18	6.61	74.31
9.63	6.90	68.07
11.87	7.12	69.22
13.29	7.18	68.92
16.92	7.48	60.75
20.51	7.59	65.52
24.16	7.74	61.09
27.84	8.05	58.62
35.10	8.45	47.11
42.39	8.76	36.47
49.62	8.91	23.68
56.90	8.95	18.57

Y= 30.00

Z	U	URMS
5.24	6.17	.63
5.98	6.64	.59
6.66	6.78	.63
7.42	6.99	.59
8.10	7.08	.58
9.59	7.13	.59
11.76	7.23	.61
13.24	7.35	.57
16.88	7.59	.54
20.48	7.72	.54
24.13	7.92	.52
27.76	8.07	.50
35.07	8.40	.44
42.36	8.66	.32
49.65	8.86	.25
56.90	8.91	.20

Y= 43.75

Z	U	URMS
5.23	6.53	.71
5.81	7.28	.73
6.49	7.58	.68
7.23	7.74	.69
7.93	7.73	.64
9.42	8.03	.65
13.04	8.24	.67
16.65	8.38	.68
20.29	8.56	.68
23.97	8.92	.64
27.51	9.17	.62
34.81	9.55	.49
42.04	9.80	.42
49.32	9.87	.37
56.54	9.76	.36

Y= 45.00

Z	U	URMS
5.20	5.97	.65
5.73	6.61	.63
6.43	6.89	.61
7.16	6.98	.62
7.91	7.03	.63
9.39	7.25	.65
11.58	7.30	.59
13.05	7.38	.61
16.69	7.60	.59
20.34	7.72	.57
23.99	8.10	.57
27.66	8.30	.51
34.96	8.55	.42
42.27	8.86	.28
49.61	8.91	.20
56.90	8.80	.23

U LONGITUDINAL VELOCITY IN M/SEC
URMS RMS OF LONG. VELOCITYFLUCT. IN M/SEC
Y LATERAL DISTANCE FROM CENTER CREST IN CM
Z HEIGHT ABOVE UPWIND SURFACE-LEVEL IN CM

TABLE B.3o. Triangular Hill Model, Height 5.08 cm, Upwind Slope 1/4, Downwind Slope 1/3, Surface Roughness Smooth, Freestream Velocity 9. m/sec, Neutral Thermal Stratification

****

Y= 0.00			Y= 15.00		
Z	U	URMS	Z	U	URMS
5.20	6.30	.75	5.20	1.01	.24
5.96	7.03	.70	5.91	7.61	.69
6.68	7.14	.67	6.62	7.71	.65
7.38	7.37	.71	7.36	7.84	.74
8.11	7.46	.72	8.06	7.95	.67
8.89	7.75	.71	9.52	8.06	.67
9.55	7.70	.72	11.70	8.09	.67
11.74	7.87	.65	13.19	8.11	.64
13.24	7.99	.66	16.80	8.32	.64
16.87	8.23	.64	20.44	8.49	.63
20.52	8.43	.69	24.11	8.69	.61
24.16	8.81	.64	27.76	8.93	.62
27.77	9.03	.65	35.04	9.34	.53
35.08	9.45	.58	42.34	9.65	.45
42.32	9.75	.45	49.60	9.82	.38
49.60	9.89	.35	56.90	9.91	.34
56.90	9.95	.28			

Y= 21.25			Y= 22.50		
Z	U	URMS	Z	U	URMS
5.20	.88	.20	5.20	5.06	.91
5.89	7.77	.75	5.76	7.90	.76
6.61	7.95	.74	6.49	7.83	.68
7.34	7.95	.68	7.23	7.93	.66
8.14	8.02	.69	7.96	8.02	.68
9.55	8.07	.69	9.42	7.93	.63
13.21	8.16	.65	11.59	7.98	.61
16.86	8.31	.59	13.10	8.18	.61
20.46	8.58	.61	16.71	8.32	.64
24.12	8.78	.61	20.39	8.55	.60
27.77	8.86	.60	24.04	8.61	.62
35.03	9.29	.52	27.71	8.63	.57
42.33	9.61	.43	35.02	9.23	.49
49.63	9.72	.39	42.30	9.51	.44
56.90	9.81	.37	49.59	9.70	.36
			56.90	9.77	.36

U LONGITUDINAL VELOCITY IN M/SEC
URMS RMS OF LONG. VELOCITYFLUCT. IN M/SEC
Y LATERAL DISTANCE FROM CENTER CREST IN CM
Z HEIGHT ABOVE UPWIND SURFACE-LEVEL IN CM

TABLE B.3p. Triangular Hill Model, Height 5.08 cm, Upwind Slope 1/4, Downwind Slope 1/3, Surface Roughness Smooth, Freestream Velocity 9. m/sec, Neutral Thermal Stratification

Y= 0.00

Z	U	URMS
5.23	6.28	.69
5.78	6.67	.62
6.49	6.78	.69
7.20	7.00	.69
7.95	7.20	.70
9.42	7.41	.68
13.03	7.71	.62
16.66	7.97	.64
20.33	8.20	.66
23.97	8.47	.60
27.51	8.64	.64
34.80	9.11	.54
42.10	9.44	.39
49.32	9.59	.24
56.57	9.59	.20

Y= 15.00

Z	U	URMS
5.23	6.52	.67
5.80	6.94	.65
6.47	7.02	.66
7.24	7.26	.66
7.99	7.43	.66
9.41	7.69	.64
13.04	7.93	.64
16.64	8.18	.59
20.30	8.39	.62
23.95	8.60	.61
27.52	8.74	.59
34.78	9.20	.49
42.08	9.48	.40
49.27	9.66	.28
56.60	9.63	.23

Y= 30.00

Z	U	URMS
5.23	6.73	.66
5.75	7.21	.62
6.51	7.34	.69
7.25	7.56	.65
7.95	7.65	.66
9.37	7.74	.63
13.04	8.06	.62
16.68	8.08	.61
20.31	8.26	.61
23.91	8.57	.60
27.54	8.62	.59
34.77	9.21	.49
42.05	9.59	.36
49.30	9.69	.32
56.55	9.65	.30

Y= 43.75

Z	U	URMS
5.23	7.51	.69
5.80	7.82	.71
6.47	7.84	.71
7.24	8.00	.69
7.99	8.01	.70
9.44	8.12	.69
13.07	8.14	.67
16.63	8.39	.68
20.31	8.50	.62
23.94	8.81	.60
27.56	9.06	.58
34.77	9.45	.52
42.10	9.73	.37
49.28	9.74	.36
56.61	9.67	.32

Y= 45.00

Z	U	URMS
5.23	7.53	.72
5.77	7.81	.77
6.54	7.91	.67
7.20	7.90	.71
7.99	7.95	.72
9.39	7.89	.69
13.02	8.13	.66
16.64	8.26	.66
20.29	8.55	.65
23.89	8.82	.64
27.57	8.99	.59
34.83	9.43	.49
42.06	9.71	.39
49.31	9.74	.32
56.59	9.63	.30

U LONGITUDINAL VELOCITY IN M/SEC
URMS RMS OF LONG. VELOCITYFLUCT. IN M/SEC
Y LATERAL DISTANCE FROM CENTER CREST IN CM
Z HEIGHT ABOVE UPWIND SURFACE-LEVEL IN CM

TABLE B.3q. Triangular Hill Model, Height 5.08 cm, Upwind Slope 1/4, Downwind Slope 1.0, Surface Roughness Smooth, Freestream Velocity 3. m/sec, Stable Thermal Stratification

****

X= 0.00		
Z	T	U
5.38	15.0	1.71
5.97	15.5	1.80
6.58	15.5	1.76
7.29	17.0	1.90
8.35	18.0	2.06
9.50	19.0	1.98
13.16	21.0	2.06
16.78	22.5	2.12
20.39	23.5	2.30
24.08	24.0	2.46
27.72	24.5	2.56
35.02	25.2	2.72
42.32	25.7	2.75
49.61	26.2	2.91
56.90	26.5	2.90

X= 22.50		
Z	T	U
.30	3.0	.00
2.09	10.7	.00
4.12	13.2	.50
4.63	14.2	.40
5.35	14.5	.86
5.73	15.5	1.18
6.07	16.0	1.19
6.81	17.0	1.65
6.43	16.5	1.51
7.15	17.5	1.59
7.54	10.0	1.86
7.88	18.5	1.77
8.60	19.0	2.00
9.36	19.5	1.86
13.32	21.0	1.87
16.98	23.0	2.14
20.64	24.0	2.20
27.84	25.0	2.44
35.10	26.0	2.47
42.38	26.5	2.69
49.62	27.0	2.69
56.90	27.5	2.70

X= 45.00		
Z	T	U
1.21	12.2	.00
1.34	13.5	.00
2.14	14.0	.00
3.35	14.5	.00
4.07	15.0	.00
4.60	15.5	.00
4.96	15.5	1.10
5.34	15.5	1.10
5.37	15.5	.60
5.72	15.7	1.00
6.71	18.0	1.50
6.12	17.5	1.50
7.91	19.0	1.78
8.70	19.5	1.61
9.91	20.0	1.63
12.16	21.0	1.92
15.45	22.6	2.04
19.19	23.5	2.09
24.27	24.5	2.28
31.51	25.5	2.37
41.03	25.7	2.53
49.67	26.0	2.59
56.90	26.5	2.69

T TEMPERATURE IN DEGREES CELCIUS
U LONGITUDINAL VELOCITY IN M/SEC
X DOWNWIND DISTANCE FROM CREST IN CM
Z HEIGHT ABOVE UPWIND SURFACE-LEVEL IN CM

TABLE B.3r. Triangular Hill Model, Height 5.08 cm, Upwind Slope 1/4, Downwind Slope 1.0, Surface Roughness Smooth, Freestream Velocity 6. m/sec, Stable Thermal Stratification

****

X= 0.00		
Z	T	U
5.38	19.0	3.47
5.80	19.5	3.65
6.52	20.5	3.81
7.26	21.0	4.04
8.35	22.5	4.14
9.44	23.0	4.27
13.08	24.5	4.30
16.75	25.5	4.60
20.39	26.0	4.76
24.02	26.5	4.87
27.68	27.0	5.05
34.99	27.6	5.28
42.26	27.5	5.40
49.59	28.0	5.32
56.90	28.5	5.42

X= 22.50		
Z	T	U
.30	7.0	.00
.62	13.0	.00
1.34	14.5	.00
2.08	15.5	.00
3.16	16.0	.00
3.52	16.0	.00
3.89	17.0	.00
4.64	17.0	.62
4.25	17.0	1.71
4.99	18.0	2.15
5.32	18.0	2.51
6.75	20.0	3.62
7.49	21.0	4.01
9.68	23.0	4.22
13.25	24.0	4.42
16.86	25.0	4.60
20.47	25.5	4.87
24.10	26.0	5.02
27.69	26.5	5.09
34.91	27.0	5.14
42.13	27.5	5.32
49.35	28.0	5.42
56.54	28.5	5.33

X= 45.00		
Z	T	U
.30	12.5	.00
.60	14.8	.00
1.35	18.0	.00
2.08	19.0	.92
3.18	19.3	1.73
3.54	19.7	1.68
3.90	20.0	2.18
4.30	20.2	2.42
4.66	20.3	2.31
5.34	21.0	2.72
6.76	21.8	3.31
8.22	22.4	3.70
9.68	23.3	3.92
13.26	24.5	4.10
16.89	25.2	4.29
20.47	26.1	4.55
24.08	27.0	4.71
27.69	27.2	4.91
34.91	27.6	5.21
42.13	28.0	5.33
49.36	28.2	5.40
56.55	28.5	5.42

T TEMPERATURE IN DEGREES CELCIUS
U LONGITUDINAL VELOCITY IN M/SEC
X DOWNWIND DISTANCE FROM CREST IN CM
Z HEIGHT ABOVE UPWIND SURFACE-LEVEL IN CM

TABLE B.3s. Traingular Hill Model, Height 5.08 cm, Upwind Slope 1/4, Downwind Slope 1/0, Surface Roughness Smooth, Freestream Velocity 3. m/sec, Stable Thermal Stratification

****

Y= 0.00

Z	T	U
5.10	21.0	1.67
5.80	21.5	1.58
6.57	21.4	1.64
7.28	21.7	1.62
8.03	21.8	1.84
9.47	22.1	1.80
13.08	23.0	1.82
16.67	24.5	1.92
20.33	25.3	2.03
23.95	26.0	2.16
27.54	26.5	2.20
34.81	27.0	2.13
42.08	27.5	2.40
49.30	27.9	2.56
56.56	28.0	2.39

Y= 15.00

Z	T	U
5.10	20.0	1.36
5.84	19.9	1.63
6.51	20.3	1.59
7.23	21.0	1.71
7.99	21.3	1.54
9.44	21.9	1.58
13.06	23.0	1.59
16.67	24.0	1.70
20.32	25.0	1.79
23.92	25.7	2.01
27.52	26.0	2.02
34.81	26.8	2.11
42.08	27.2	2.28
49.29	27.5	2.22
56.54	27.7	2.42

Y= 22.50

Z	T	U
5.20	16.0	1.33
5.89	16.3	1.49
6.65	17.5	1.42
7.34	18.4	1.49
8.09	19.3	1.65
9.50	20.3	1.43
13.15	21.9	1.64
16.74	23.3	1.73
20.39	24.1	2.02
23.99	25.0	2.02
27.61	25.5	2.09
34.86	26.3	2.19
42.08	26.8	2.26
49.31	26.9	2.38
56.55	27.2	2.48

T TEMPERATURE IN DEGREES CELCIUS
U LONGITUDINAL VELOCITY IN M/SEC
X DOWNWIND DISTANCE FROM CREST IN CM
Z HEIGHT ABOVE UPWIND SURFACE-LEVEL IN CM

TABLE B.3t. Triangular Hill Model, Height 5.08 cm, Upwind Slope 1/4, Downwind Slope 1/0, Surface Roughness Smooth, Freestream Velocity 6. m/sec, Stable Thermal Stratification

****

Y= 0.00		
Z	T	U
5.20	19.5	3.05
5.95	20.0	3.64
6.63	21.3	3.64
7.38	22.0	3.81
8.09	22.9	3.80
9.55	23.7	3.97
13.14	24.9	3.20
16.82	26.0	4.32
20.38	27.0	4.51
24.01	27.1	4.73
27.61	27.6	4.92
34.87	28.0	5.08
42.12	28.4	5.26
49.31	28.9	5.39
56.54	28.6	5.37

Y= 15.00		
Z	T	U
5.21	22.5	3.08
5.95	23.0	3.78
6.65	23.5	3.94
7.35	23.7	3.97
8.08	24.0	4.12
9.51	24.3	4.18
13.13	25.1	4.36
16.77	25.9	4.54
20.37	26.1	4.77
24.00	26.9	4.85
27.63	27.1	5.00
34.88	27.6	5.22
40.64	27.8	5.30
49.34	28.0	5.27
56.54	28.5	5.26

Y= 22.50		
Z	T	U
5.20	22.9	3.94
5.95	23.0	4.11
6.64	23.1	4.09
7.34	23.4	4.09
8.07	23.7	4.18
9.56	24.0	4.27
13.15	25.1	4.22
16.76	25.6	4.53
20.41	26.1	4.63
24.01	26.8	4.85
27.63	26.8	4.99
34.87	27.4	5.21
42.11	27.8	5.36
49.30	28.0	5.34
56.54	28.1	5.32

T TEMPERATURE IN DEGREES CELCIUS
U LONGITUDINAL VELOCITY IN M/SEC
X DOWNWIND DISTANCE FROM CREST IN CM
Z HEIGHT ABOVE UPWIND SURFACE-LEVEL IN CM

APPENDIX C

CONTOUR PLOTTING PROCEDURES

APPENDIX C CONTOUR PLOTTING PROCEDURES

When measuring flow characteristics there is always some deviation from the true value. The error is partly random and partly systematic. Systematic errors are usually caused by inaccurate calibration data. Typically random errors are caused by the "drift" of the measuring system and by insufficient time-averaging. Least-square curve-fitting techniques may be used to reduce the degree of random error provided there is sufficient data available. This appendix describes the procedures developed to interpolate and smooth the data in order that accurate contour plots of the measured quantity could be generated.

C.1 GENERAL PROCEDURE

A spatial domain was selected for which contour plots are to be generated. The domain was defined by the upwind distance from the crest, D_u, the downwind distance, D_d, and the top, H. Additional consideration was given to horizontal interpolation of data close to the surface of irregular terrain by performing a transformation of the vertical coordinates for the measured data points. The following transformation was used:

$$\bar{z} = \frac{H}{H-z_s} (z-z_s), \tag{C.1}$$

where z_s represents the local surface elevation. Subsequently each vertical profile was smoothed and interpolated by a least-squares fit using cubic spline functions. The computer subroutine used for the data-fitting is part of the Tubesna Library (IMSL) and is named ICSSCU.

The algorithm of ICSSCU was developed by Reinsch (1967). The formulation is as follows. Let $\bar{z}_i$, q_i, $(i = 1,\ldots,N_k)$ be the transformed vertical coordinates and corresponding measured magnitudes respectively, where N_k is the number of data points of data profile k. A smoothing function $g_k(\bar{z})$ is constructed which minimizes the integral

$$\int_{\bar{z}_1}^{\bar{z}_{N_k}} g_k''(z)\, dz \tag{C.2}$$

such that

$$\sum_{i=1}^{N_k} \left[\frac{g_k(\bar{z}_i) - q_i}{dy_i}\right]^2 \leq S \qquad (C.3)$$

The constants $S \geq 0$ and $dy_i \geq 0$ $(i = 1,\ldots,N_k)$ are numbers to be specified. The function $g_k(z)$ is taken as a third degree polynomial. The constant S allows for an implicit rescaling of the quantities dy_i and is introduced only for convenience. The constants dy_i control locally the extent of the smoothing. Choosing S equal to zero leads to interpolation by cubic spline functions. Some difficulty was encountered in applying this technique to the vertical data profiles. These problems and the subsequent program modifications will be discussed in Section C.2.

Once the spline functions $g_k(\bar{z})$, $(k = 1,\ldots,N_p)$, (N_p is the number of data profiles) were specified values $g_k(\bar{z_j})$, $(j = 1,\ldots,N_z)$ were evaluated. N_z is the number of intervals in the z-direction and

$$z_j = \frac{j}{N_z} H \qquad (C.4)$$

The same procedure as that applied to the data profiles was then used to determine cubic spline functions $h_j(x)$, $(j = 1,\ldots,N_z)$. These spline functions were specified such that the points x_i, $g_i(\bar{z}_j)$ were smoothed and interpolated accurately. Once a satisfactory fit was obtained values $h_j(x_i)$, $(i = 0,\ldots,N_x)$, $(j = 0,\ldots,N_2)$ were calculated. (N_x is the number of intervals in the x-direction and

$$x_i = \frac{i}{N_x} (D_d - D_u)) \qquad (C.5)$$

Given now a uniform grid of data values in the $x\text{-}\bar{z}$ system, two-dimensional arrays $(x_i, z_i)_j$, $(i = 1,\ldots,N_s)$, $(j = 1,\ldots,N_c)$ containing the coordinates of the j^{th} contour line were generated using subroutine CALCNT. This program was a linear contour routine in the Fortran Library available at the Colorado State University Computer Center. (N_s is the array dimension, and N_c is the number of contour lines to be plotted.) Prior to plotting the contour lines a back transformation was applied such that

$$(x_i, z_i)_j = \left(x_i,\ z_s + \frac{H - z_s}{H}\,(\bar{z}_i)\right)_j \quad . \tag{C.6}$$

A flowchart summarizing the procedure is presented in Figure C.1.

C.2 MODIFICATIONS

a) Vertical Velocity Profiles

The magnitude of the velocity changes drastically close to the surface and in the wake-main flow interface. These regions required the following special attention in the data-reduction procedure.

Surface region: The vertical coordinates $\bar{z}$ were transformed to a logarithmic scale; thus the data to be smoothed was more or less equally spaced in the transformed space.

Wake interface region: Smoothing of a vertical profile through a wake using the procedure described above results in an oscillating interpolating function. This results because at the wake-main flow interface large second derivatives, $g''(\bar{z})$ are calculated. A rotation of the coordinates (velocity and elevation) eliminates this undesired phenomenon.

Consistency of the velocity data is improved by including the option to multiply the velocity interpolating function by a factor such that at $z = 10\ h$ the resulting streamline is horizontal. The adjustment was made if the variation in velocities generated at that height corresponded closely with measurements obtained from a horizontal traverse at that elevation.

b) Static Pressure and Turbulence Intensity Profiles

Large second derivatives were calculated by curve-fitting the turbulence intensity profiles using subroutine ICSSCU. Relatively large errors in the original static pressure measurements did not justify the use of a sophisticated curve-fitting procedure. Adequate data fitting of turbulence intensity and static pressure profiles were provided by simple linear interpolation. This procedure was followed only for the vertical data profiles.

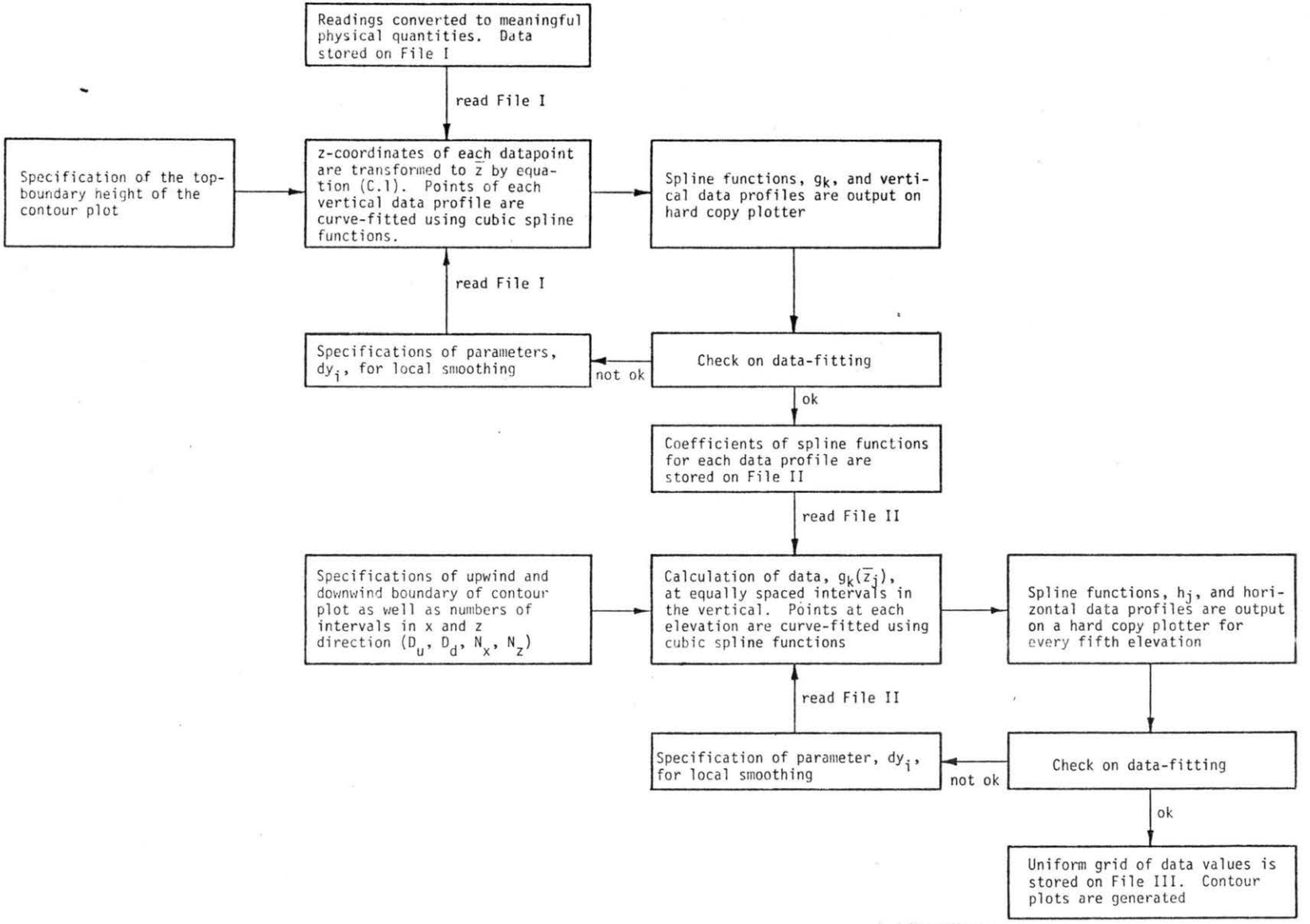

FIGURE C.1. Flow Chart of Contour Plotting Procedure

APPENDIX D

CONTOUR PLOTS OF LONGITUDINAL VELOCITIES AND STATIC PRESSURES

TABLE D.1. Locator Table of Contour Plots

CASE	Phase	h/L	$\bar{u}(10h)$ (m/sec)	Figure numbers of contour plots	
				Longitudinal velocity	Static pressure
1	II	1/2	9.1	D.1a	D.2a
2	I	1/2	15.2	D.1b	D.2b
3	I	1/3	9.1	D.1c	D.2c
4	I	1/3	15.2	D.1d	D.2d
5	II	1/4	9.1	D.1e	D.2e
6	I	1/4	15.2	D.1f	D.2f
7	II	1/6	9.1	D.1g	D.2g
8	I	1/6	15.2	D.1h	D.2h
9	II	1/20	9.1	D.1i	D.2i
10	I	1/4(sine)	9.1	D.1j	D.2j
11	I	1/4(sine)	15.2	D.1k	D.2k
12	I	3/16(sine)	9.1	D.1l	D.2l
13	I	3/16(sine)	15.2	D.1m	D.2m
14	II(rough)	1/4	9.1	D.1n	D.2n

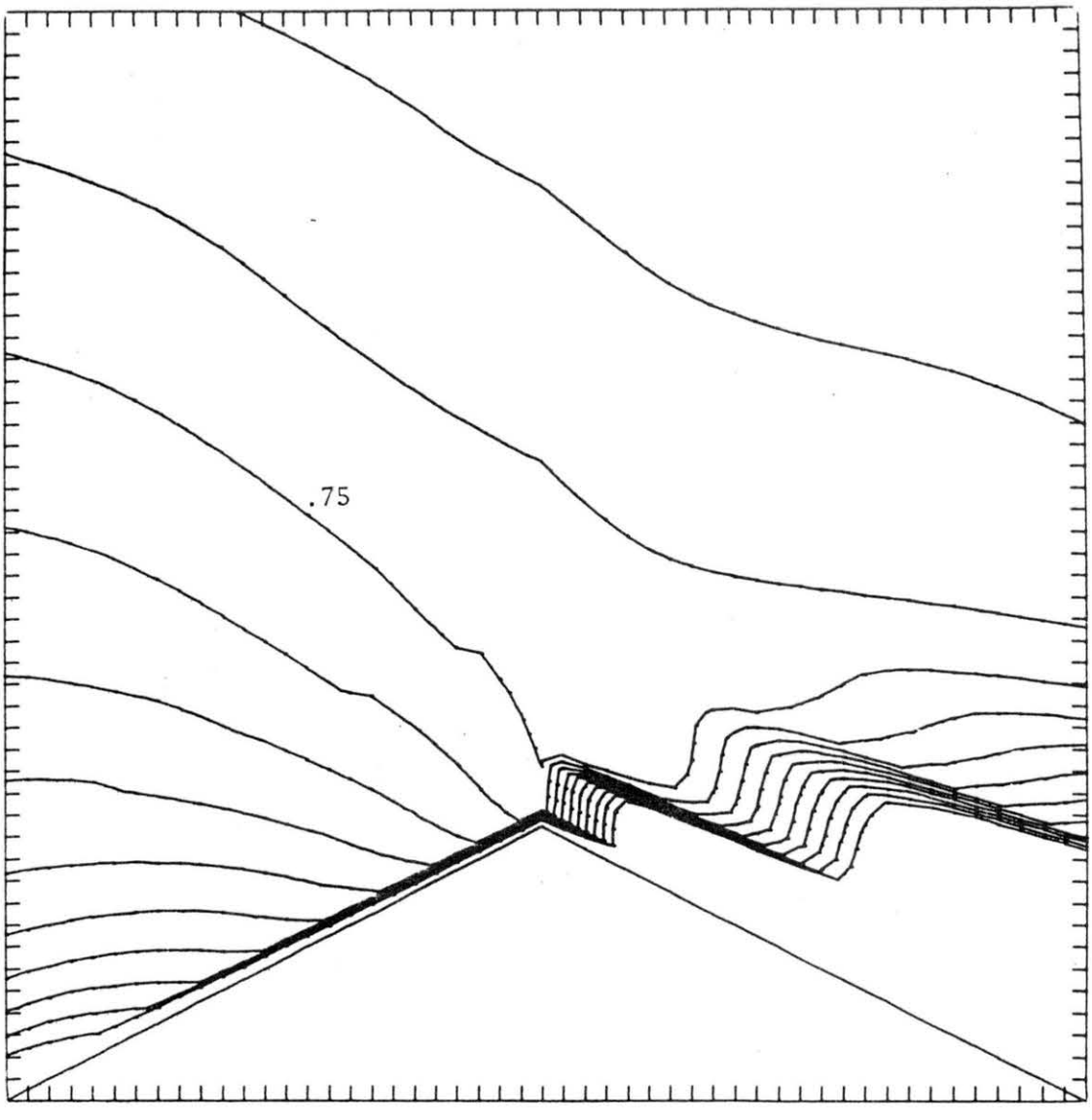

FIGURE D.1a. Contours of Mean Longitudinal Velocities over Triangular ridge h/L = 1/2. Contour Interval $\Delta u/\bar{u}(10h) = 0.05$

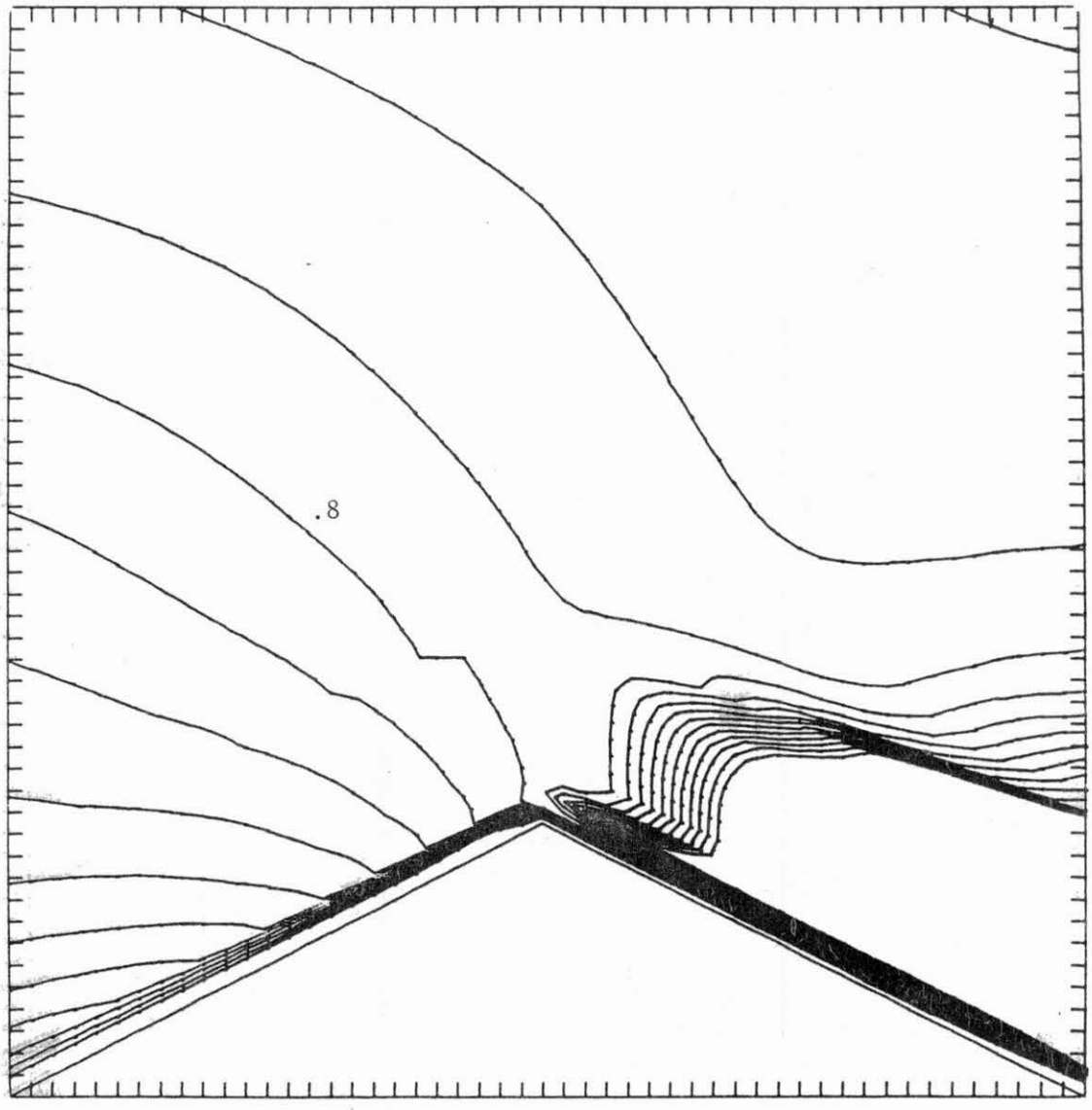

FIGURE D.1b. Contours of Mean Longitudinal Velocities over Triangular Ridge h/L = 1/2. Contour Interval $\Delta u/\bar{u}(10h) = 0.05$

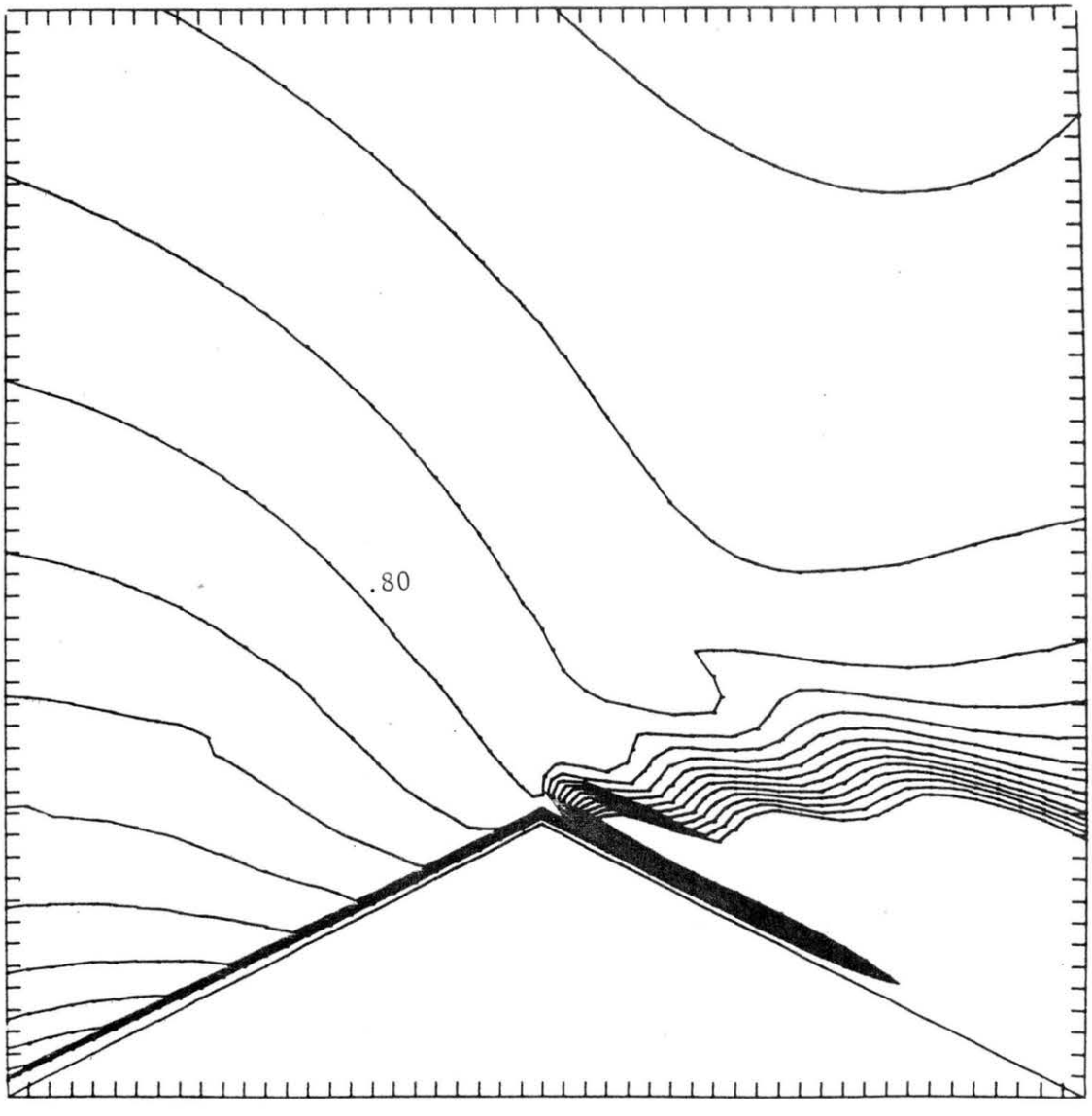

FIGURE D.1c. Contours of Mean Longitudinal Velocities over Triangular Ridge h/L = 1/3. Contour Interval $\Delta u/\bar{u}(10h) = 0.05$

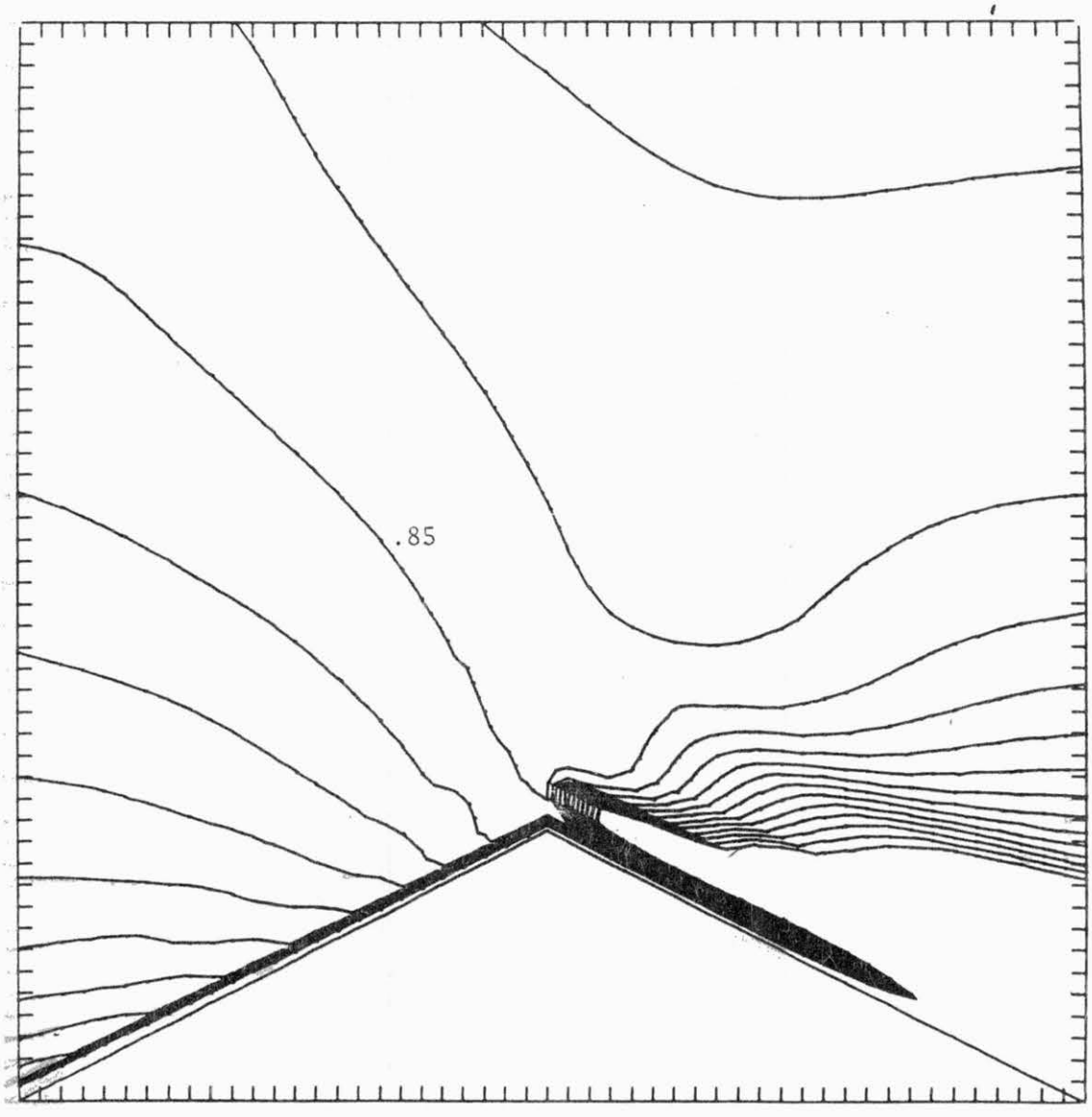

FIGURE D.1d. Contours of Mean Longitudinal Velocities over Triangular Ridge h/L = 1/3. Contour Interval $\Delta u/\bar{u}(10h) = 0.05$

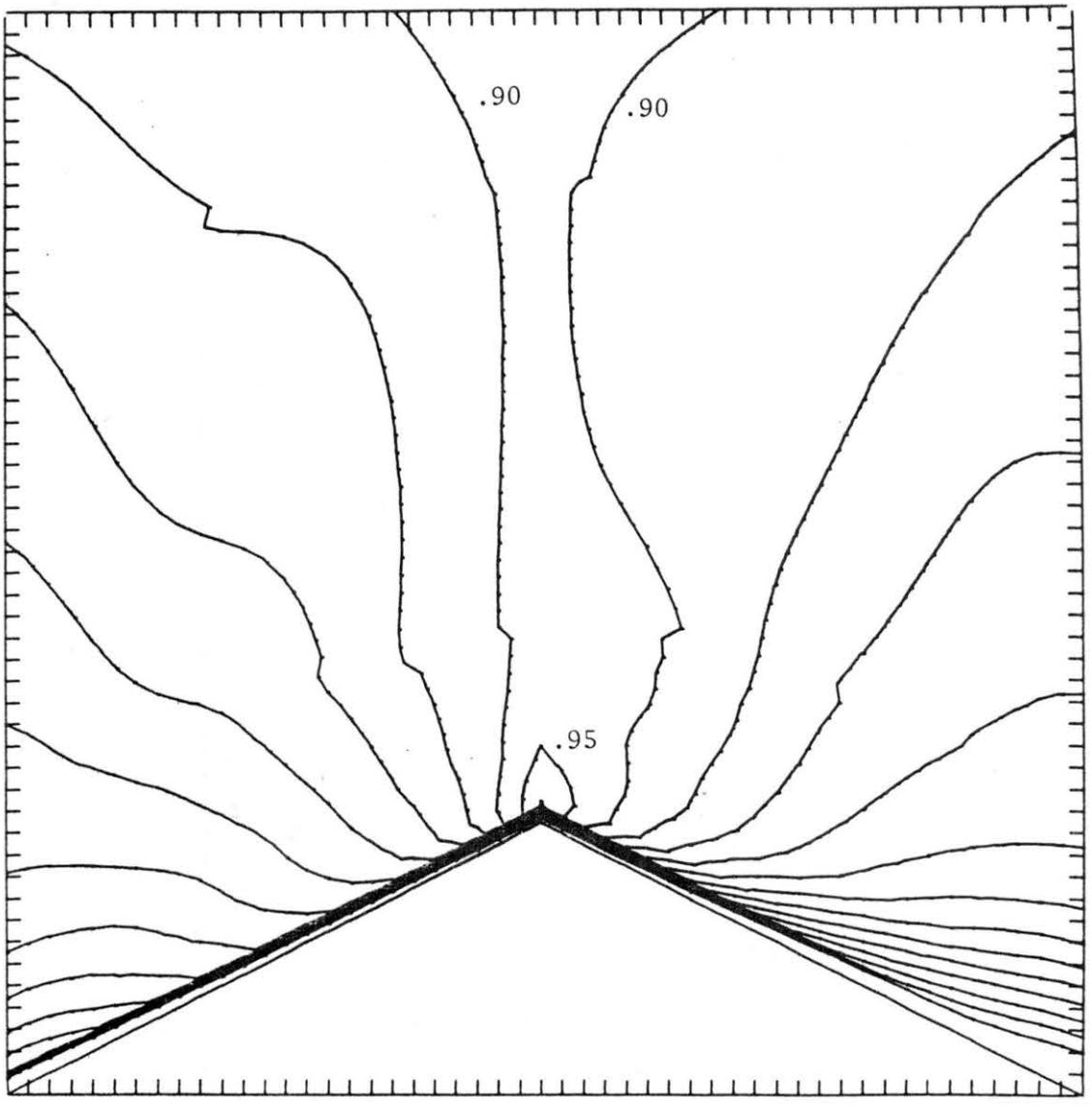

FIGURE D.1e. Contours of Mean Longitudinal Velocities over Triangular Ridge h/L = 1/4. Contour Interval $\Delta u/\bar{u}(10h) = 0.05$

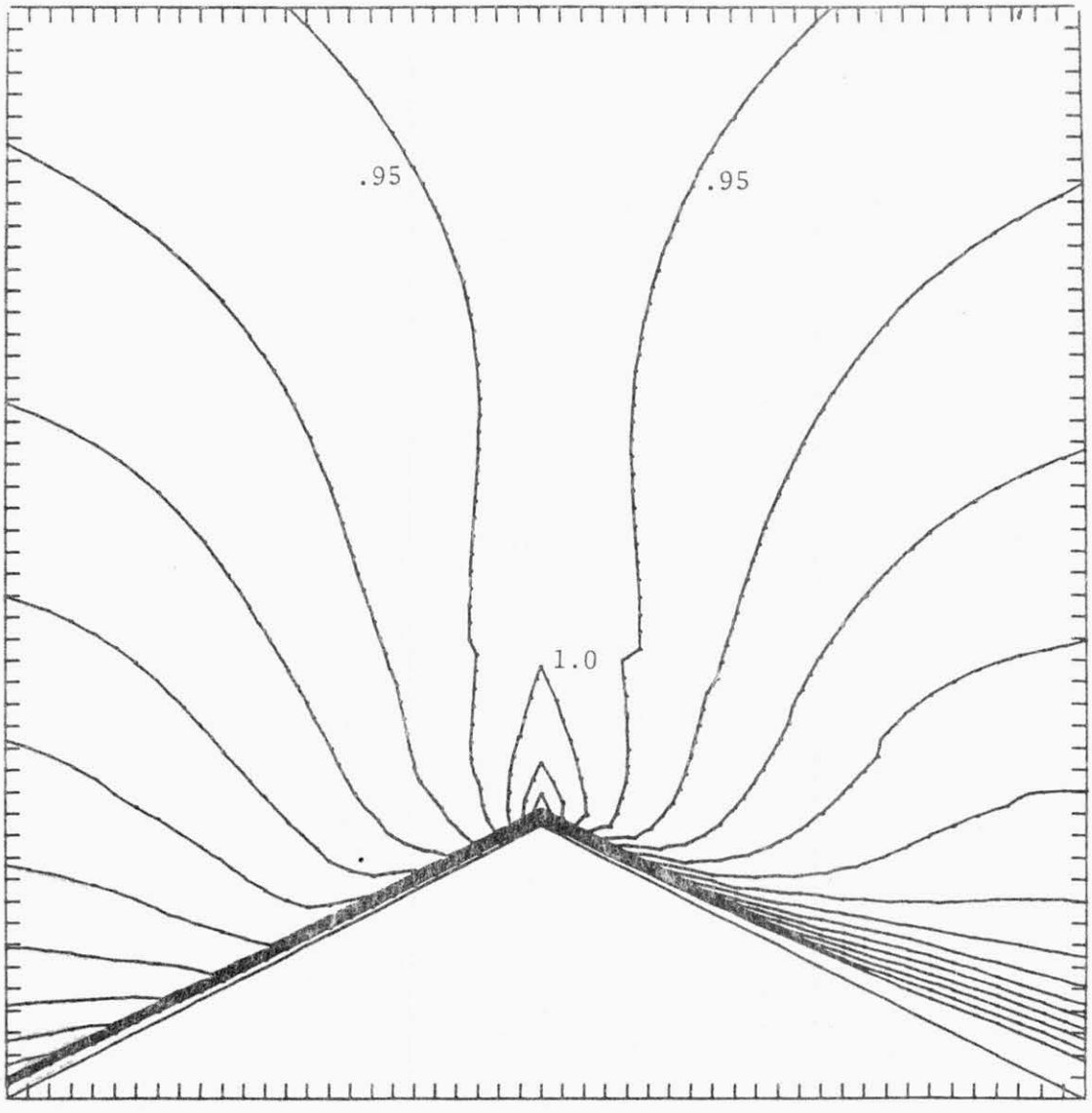

FIGURE D.1f. Contours of Mean Longitudinal Velocities over Triangular Ridge h/L = 1/4. Contour Interval $\Delta u/\bar{u}(10h) = 0.05$

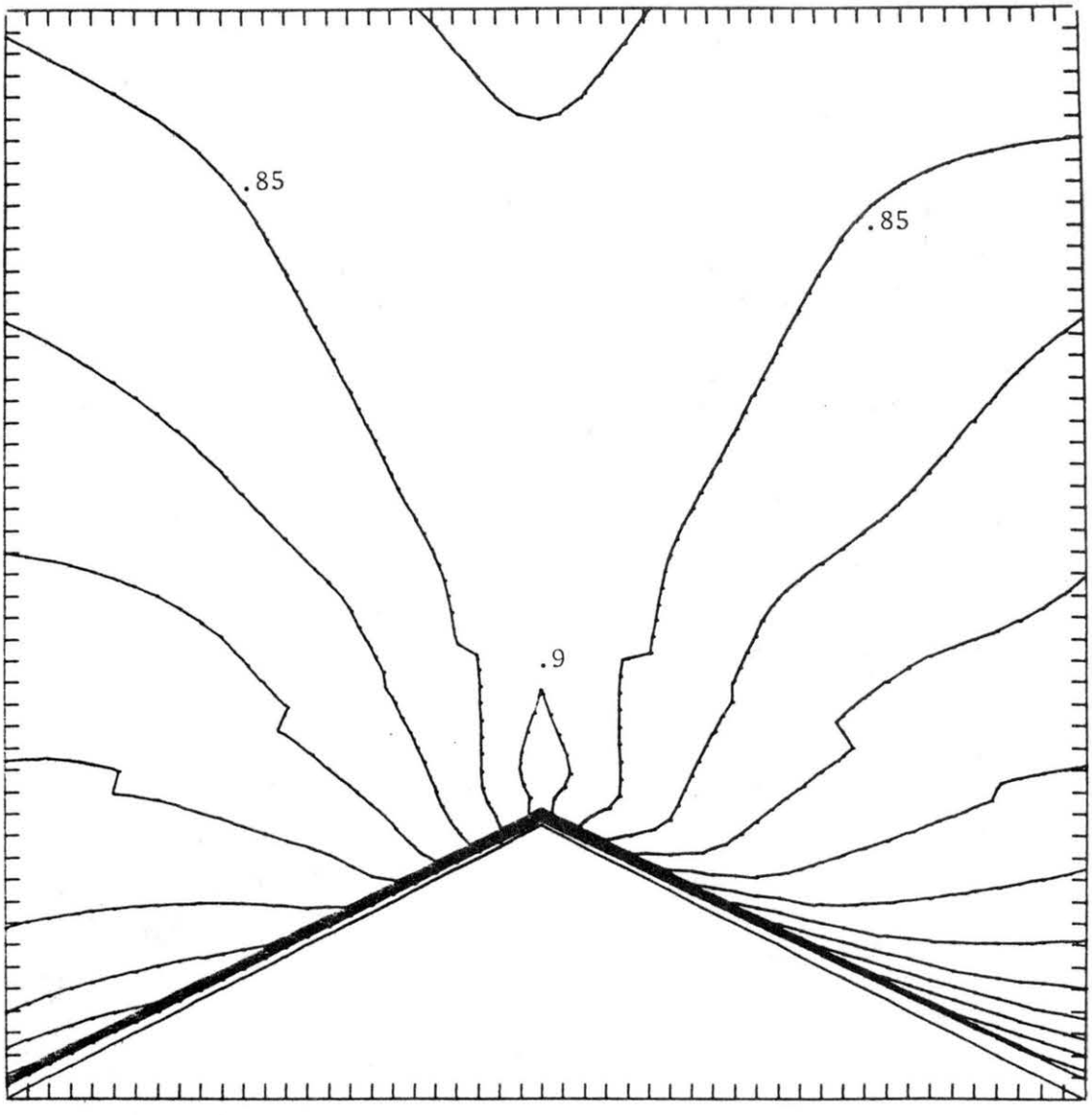

FIGURE D.1g. Contours of Mean Longitudinal Velocities over Triangular Ridge h/L = 1/6. Contour Interval $\Delta u/\bar{u}(10h) = 0.05$

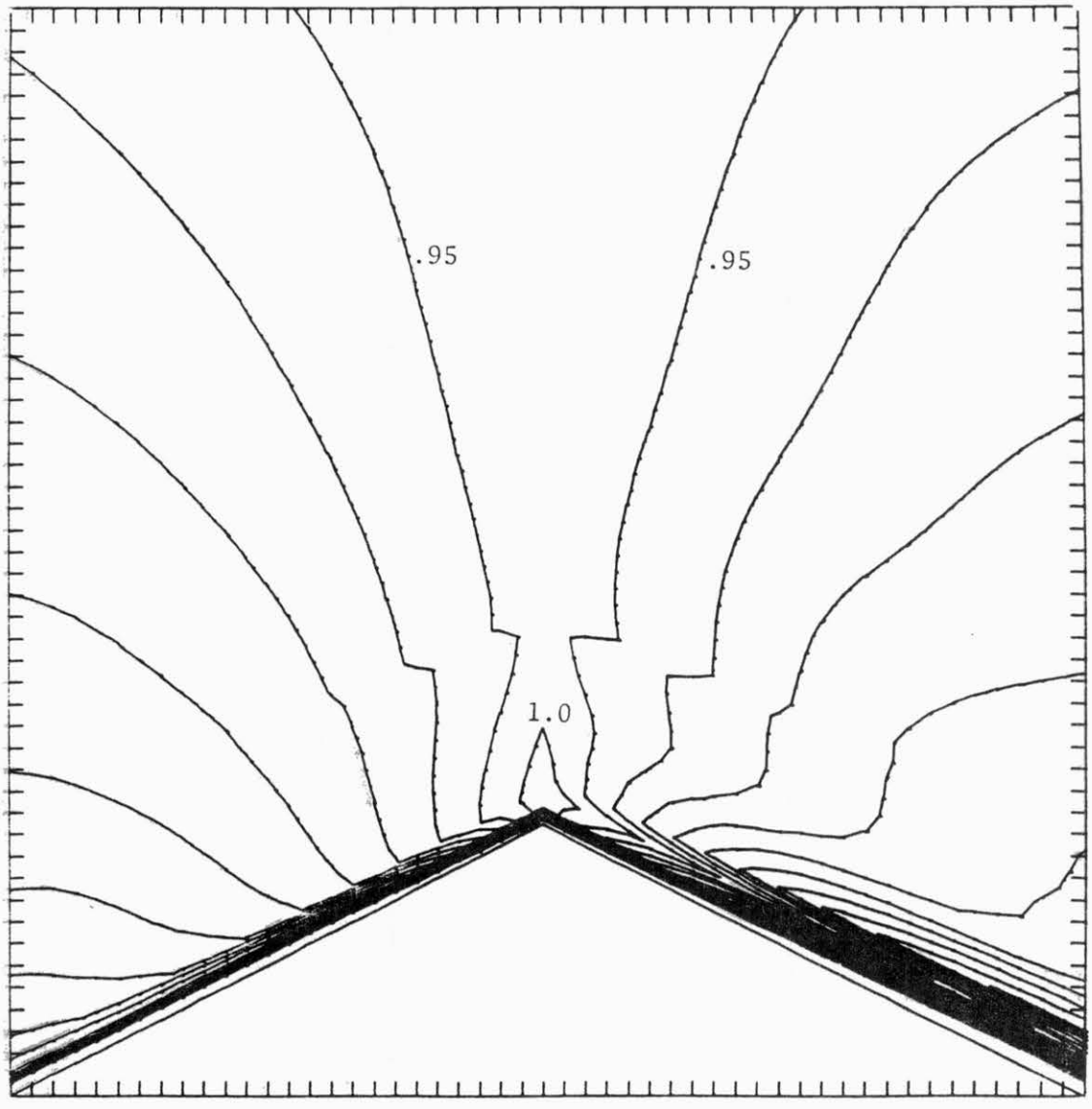

FIGURE D.1h. Contours of Mean Longitudinal Velocities over Triangular Ridge h/L = 1/6. Contour Interval $\Delta u/\bar{u}(10h) = 0.05$

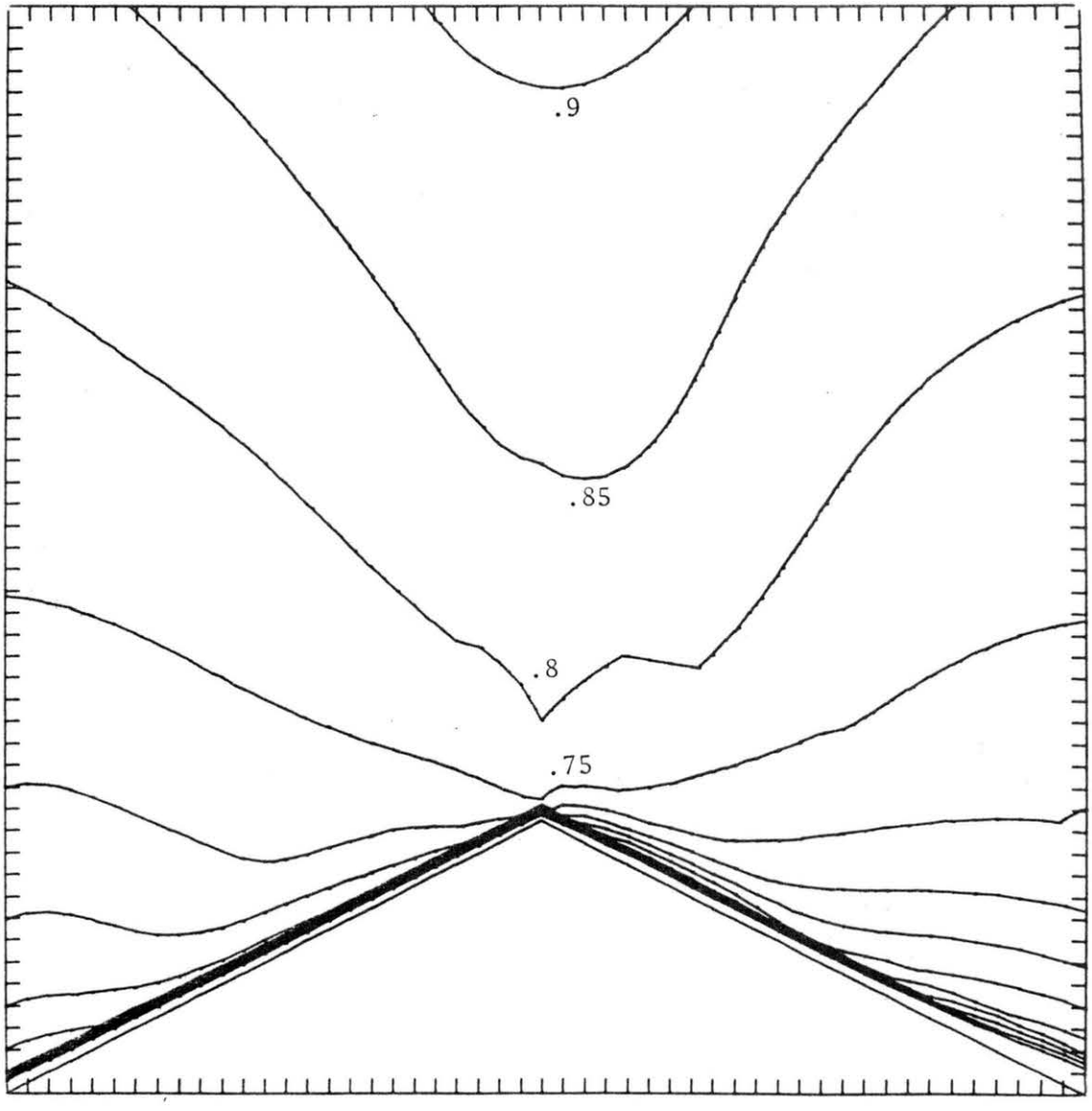

FIGURE D.1i. Contours of Mean Longitudinal Velocities over Triangular Ridge h/L = 1/20. Contour Interval $\Delta u/\bar{u}(10h) = 0.05$

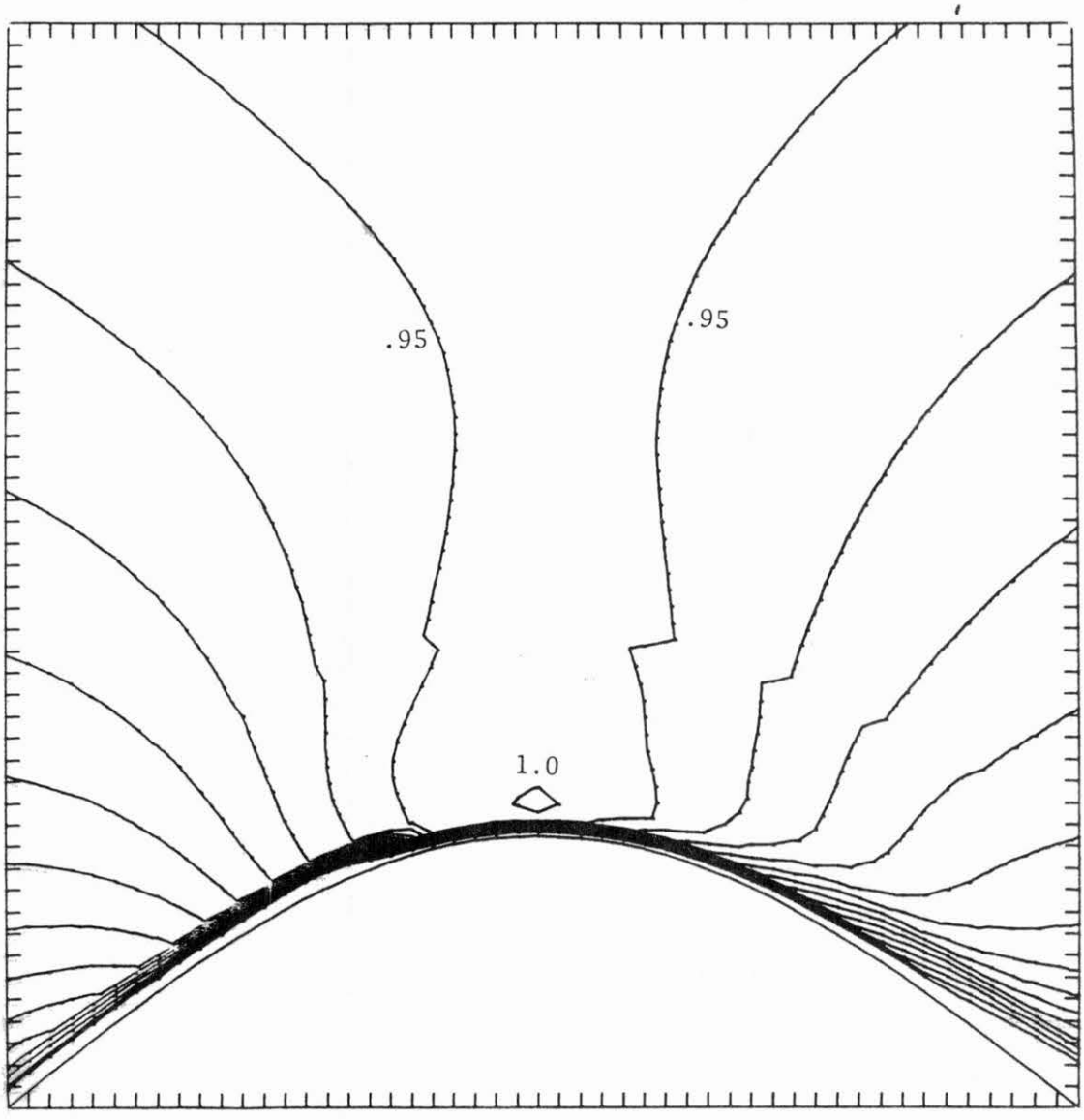

FIGURE D.1j. Contours of Mean Longitudinal Velocities over Sinusoidal Ridge h/L = 1/4. Contour Interval $\Delta u/\bar{u}(10h) = 0.05$

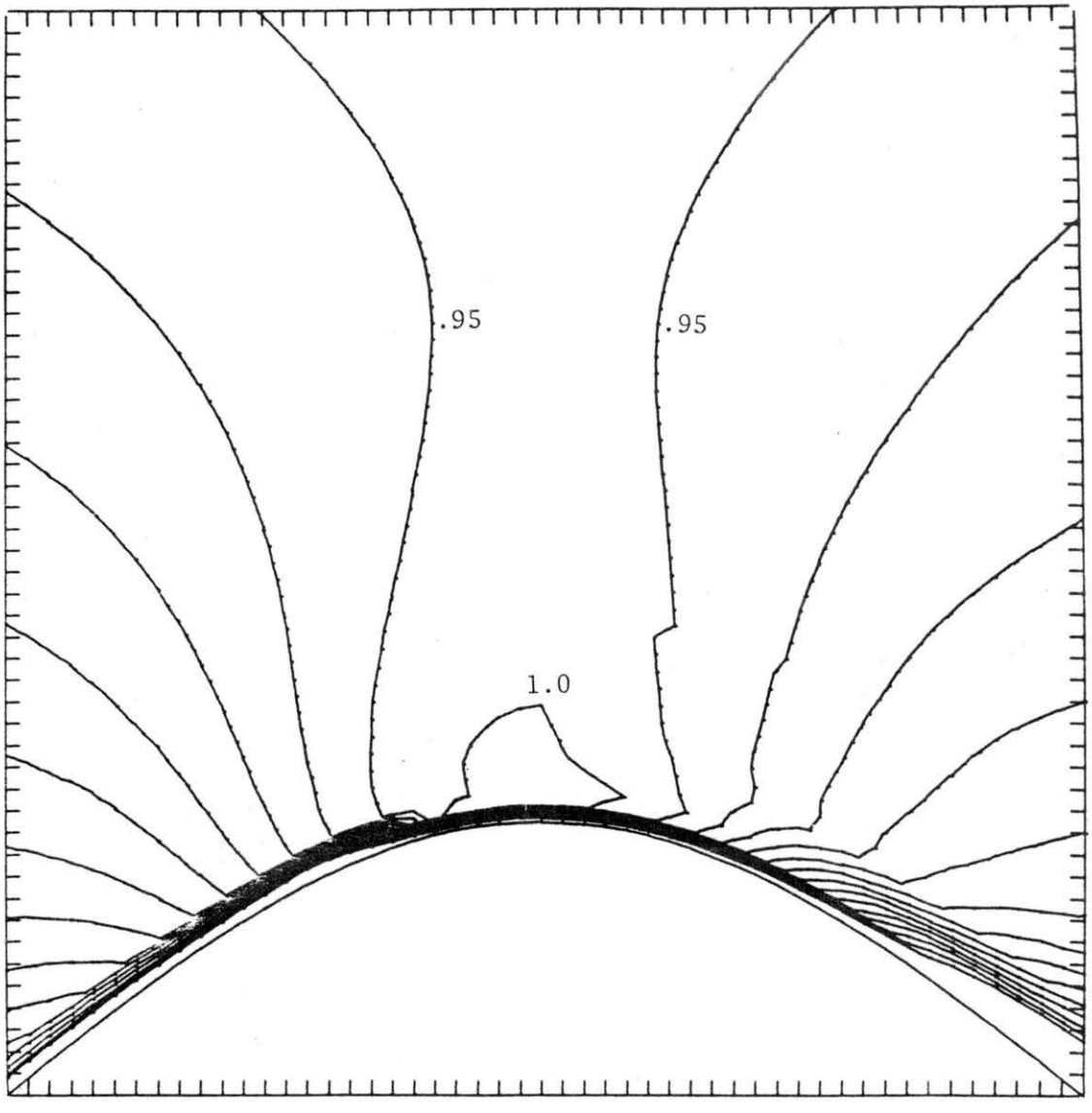

FIGURE D.1k. Contours of Mean Longitudinal Velocities over Sinusoidal Ridge h/L = 1/4. Contour Interval $\Delta u/\bar{u}(10h) = 0.05$

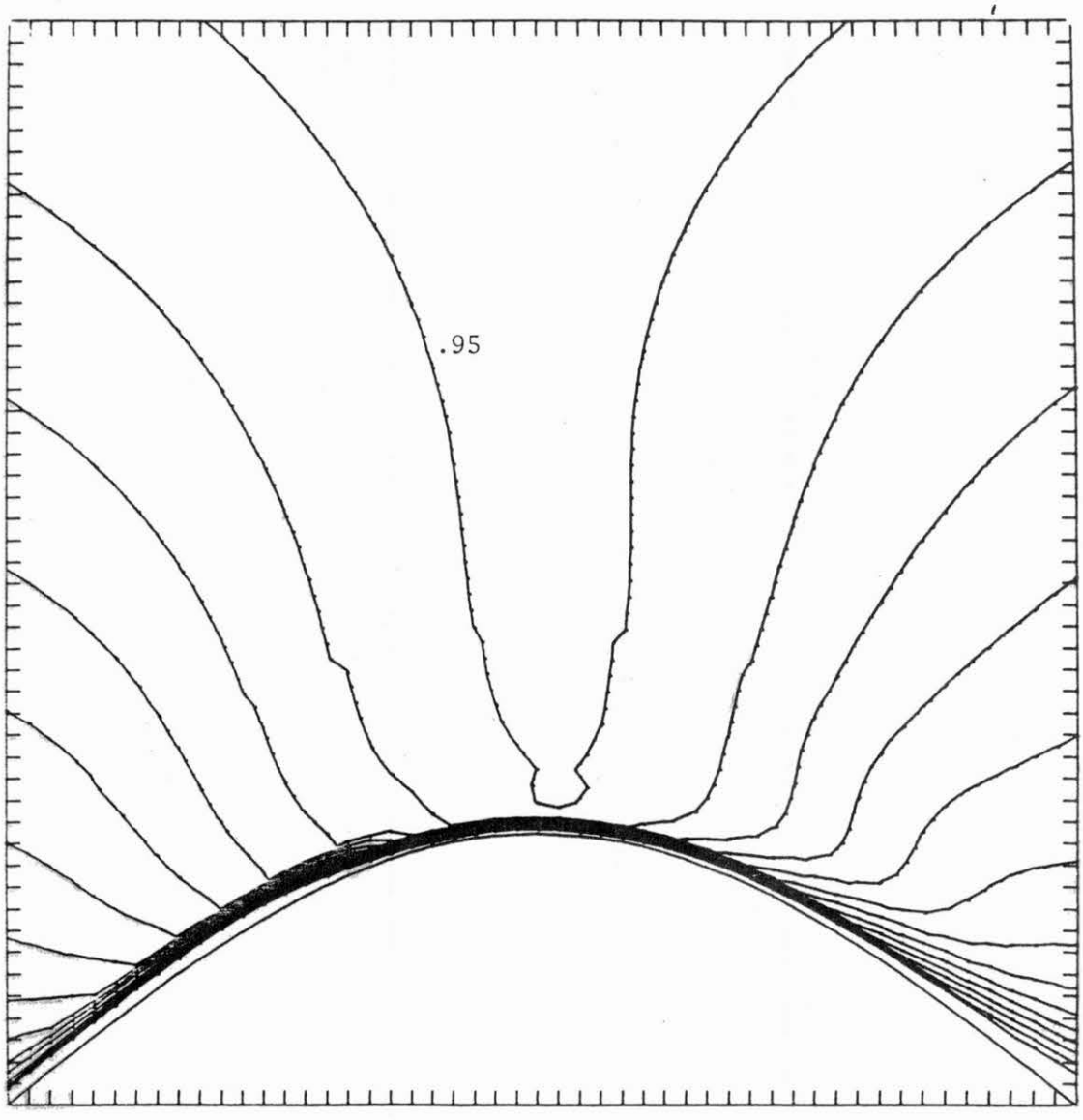

FIGURE D.11. Contours of Mean Longitudinal Velocities over Sinusoidal Ridge h/L = 3/16. Contour Interval $\Delta u/\bar{u}(10h) = 0.05$

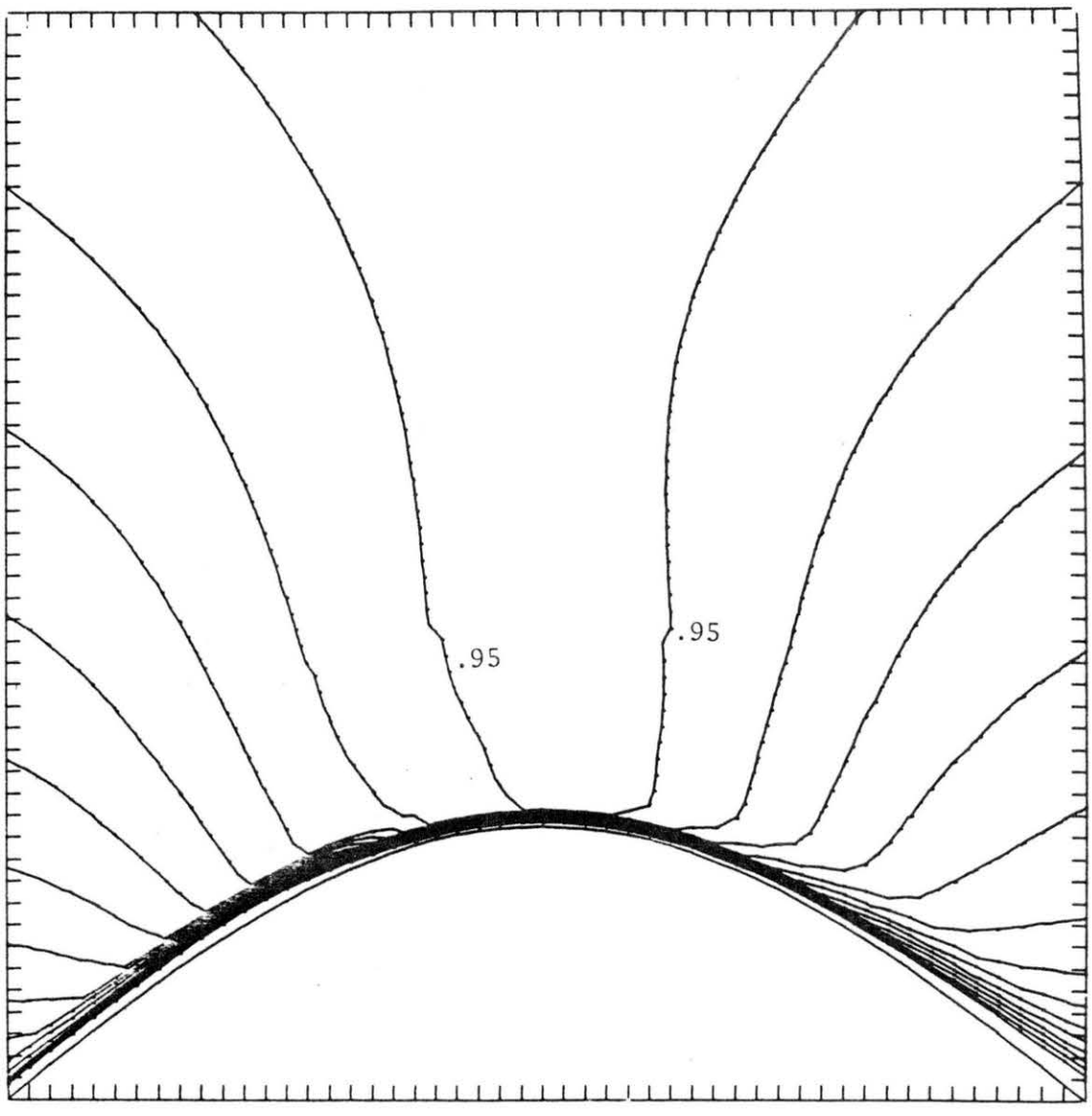

FIGURE D.1m. Contours of Mean Longitudinal Velocities over Sinusoidal Ridge h/L = 3/16. Contour Interval $\Delta u/\bar{u}(10h) = 0.05$

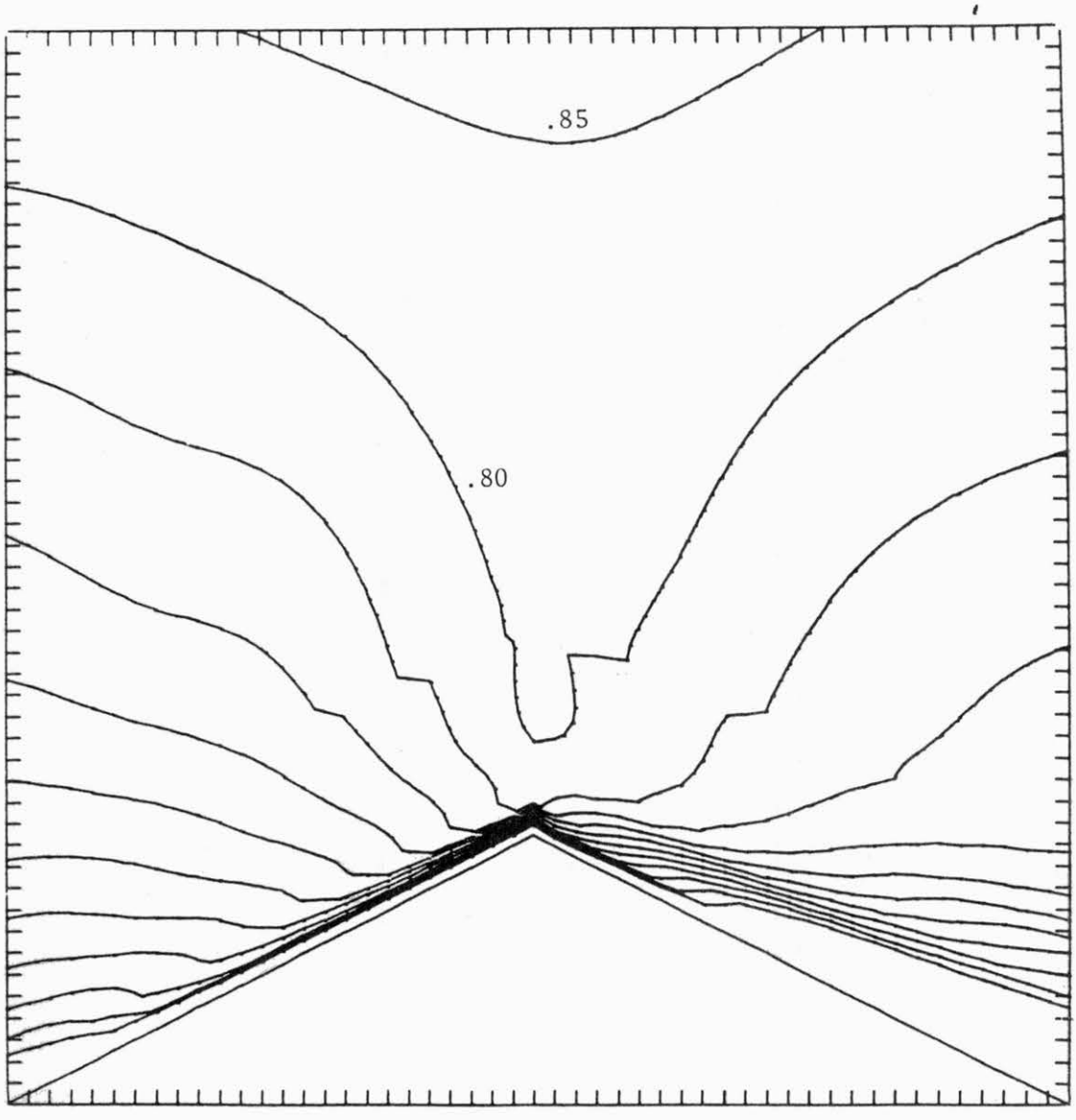

FIGURE D.1n. Contours of Mean Longitudinal Velocities over Sinusoidal Ridge h/L = 1/14. Contour Interval $\Delta u/\bar{u}(10h) = 0.05$

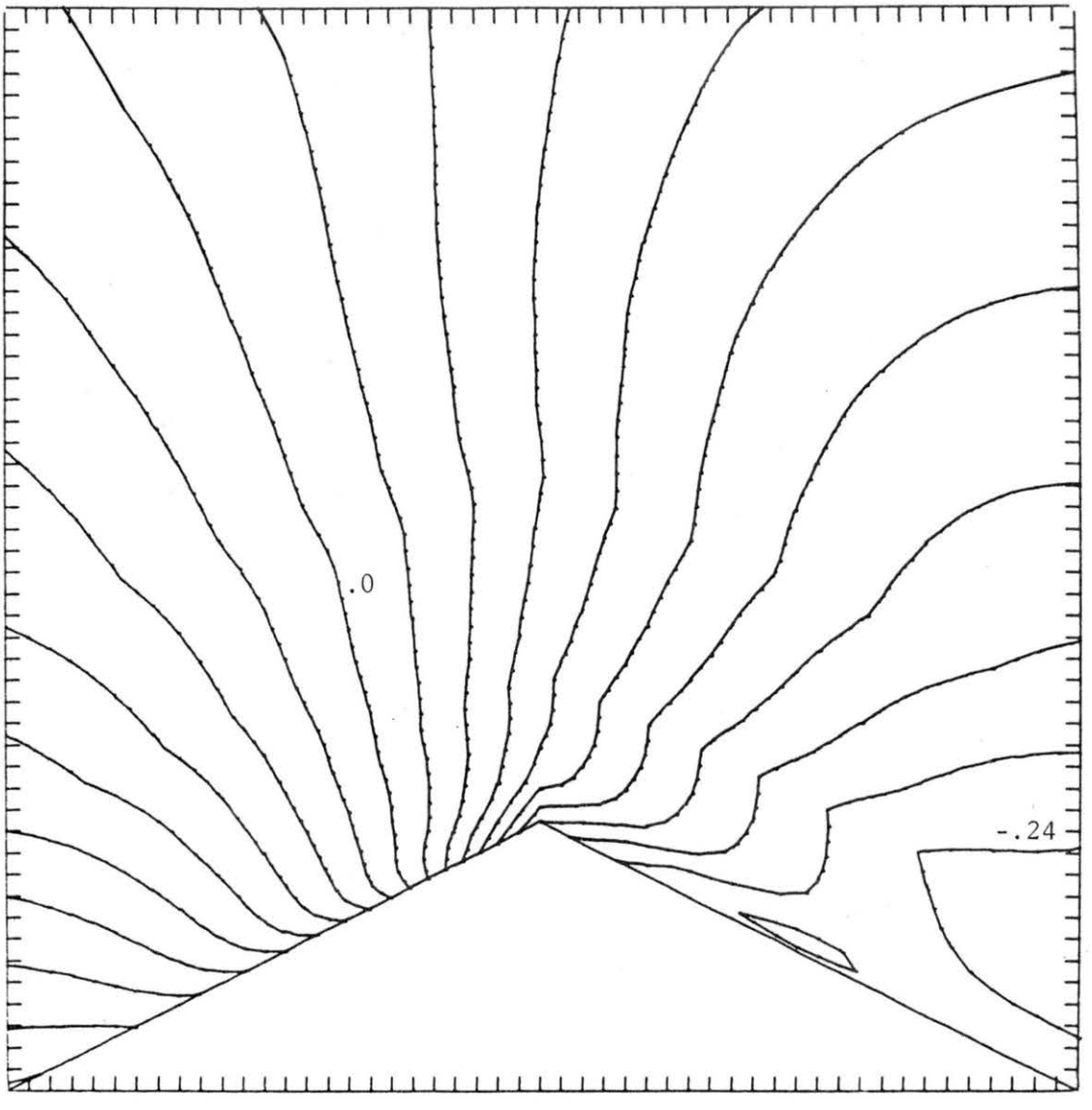

FIGURE D.2a Contours of Static Pressue over Triangular Ridge h/L = 1/2. Contour interval $\Delta C_p = 0.24$

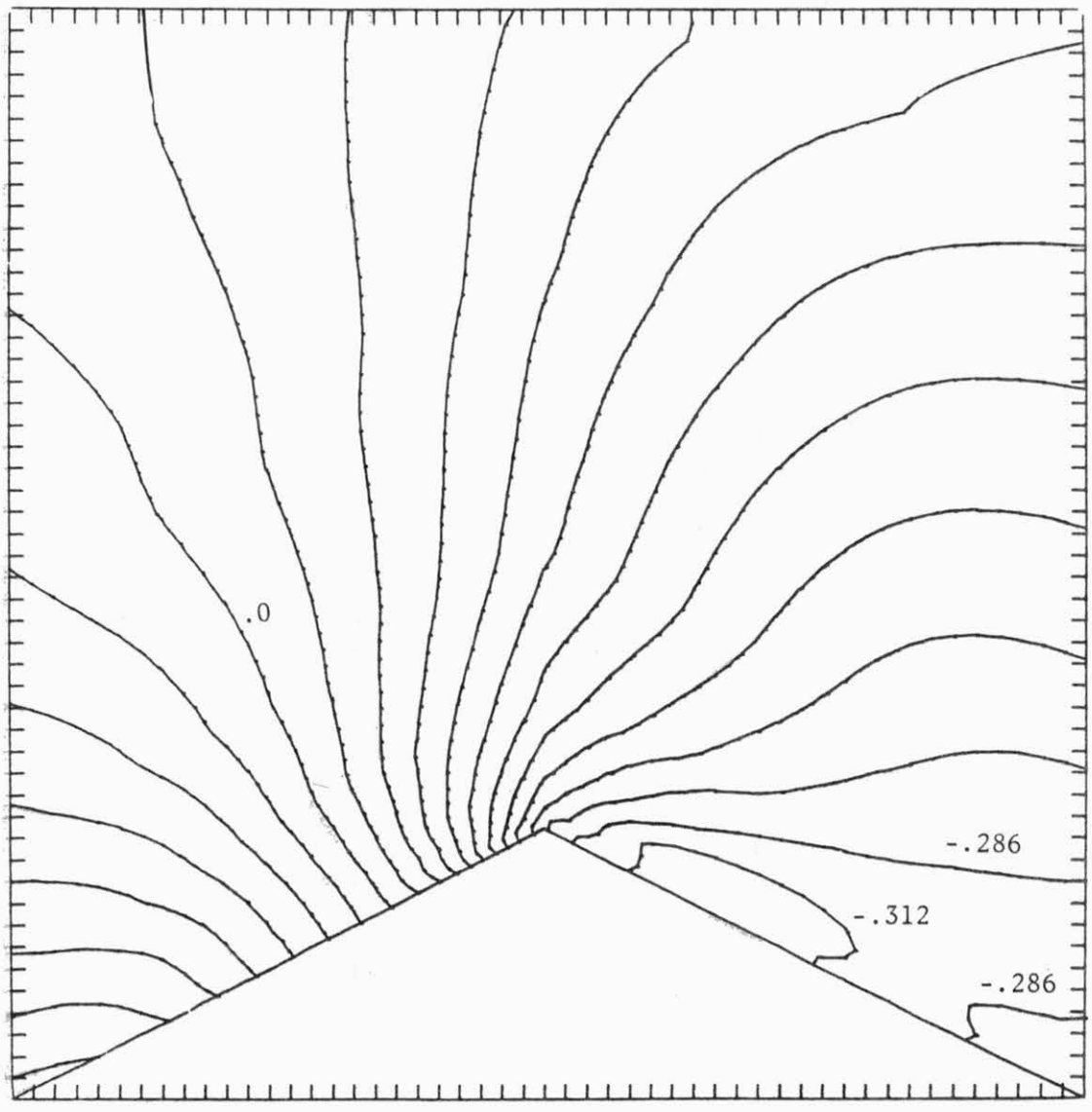

FIGURE D.2b Contours of Static Pressue over Triangular Ridge h/L = 1/2. Contour interval $\Delta C_p = 0.26$

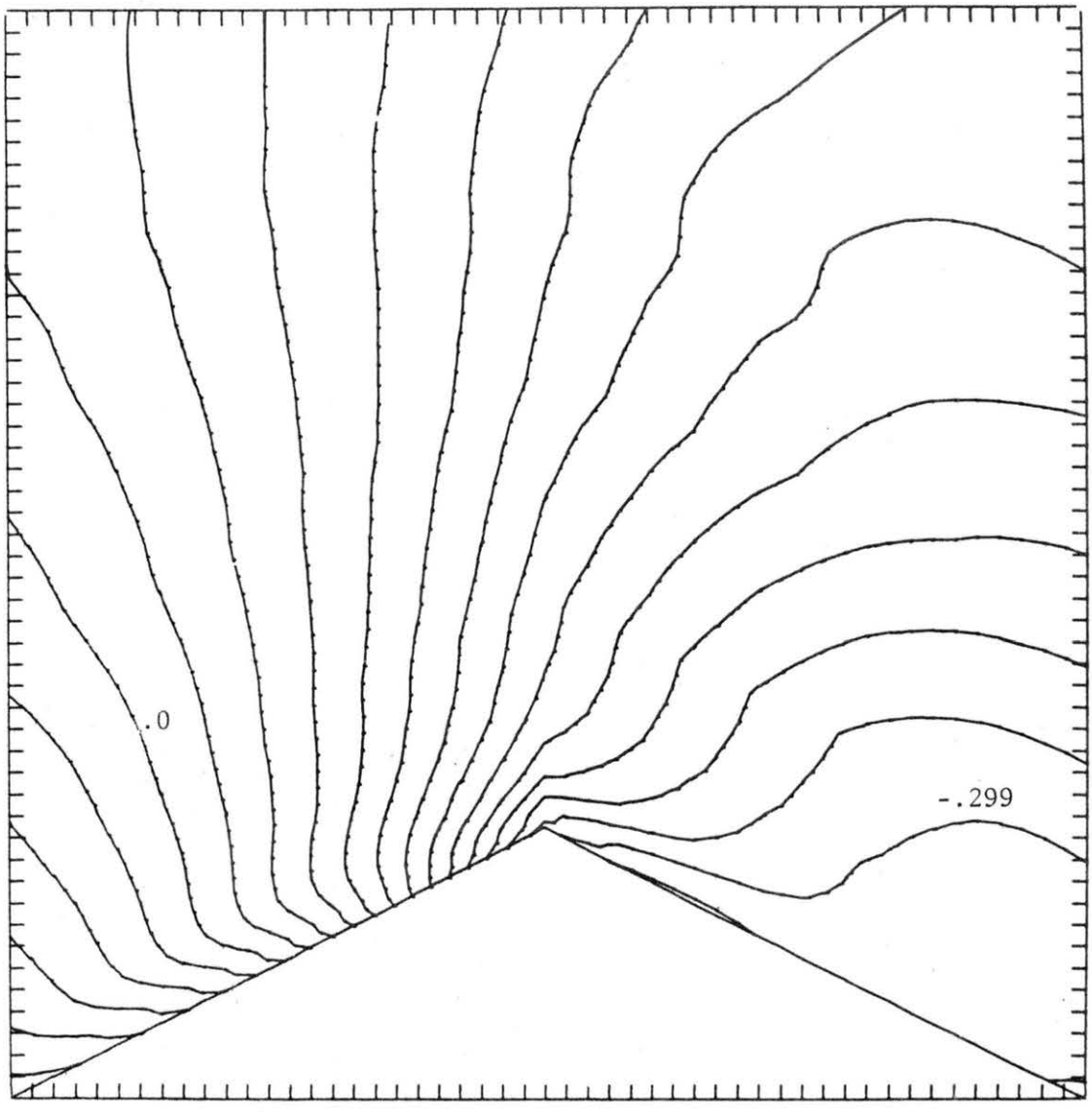

FIGURE D.2c Contours of Static Pressue over Triangular Ridge h/L = 1/3. Contour interval $\Delta C_p = 0.23$

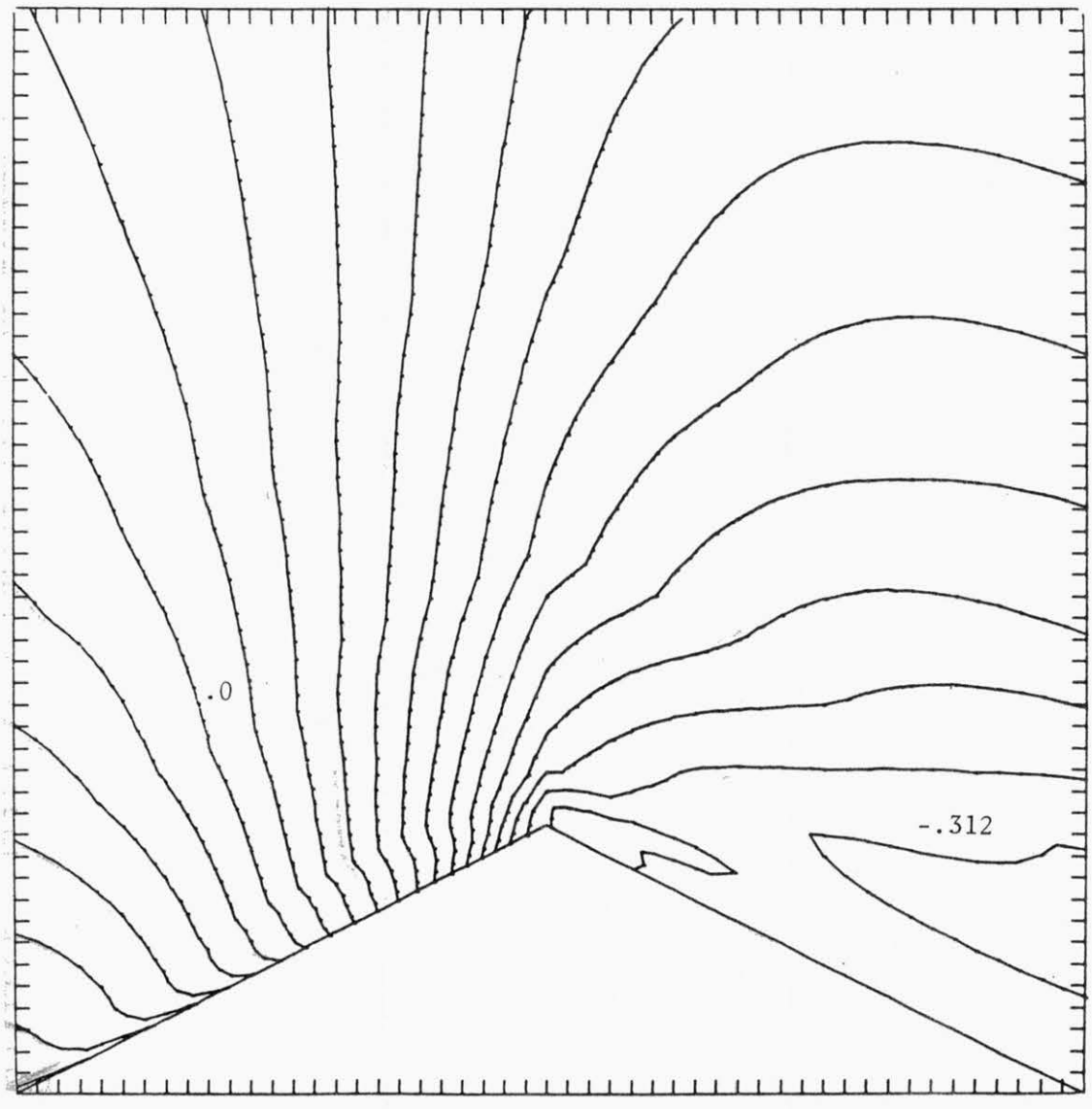

FIGURE D.2d Contours of Static Pressue over Triangular Ridge h/L = 1/3. Contour interval $\Delta C_p = 0.24$

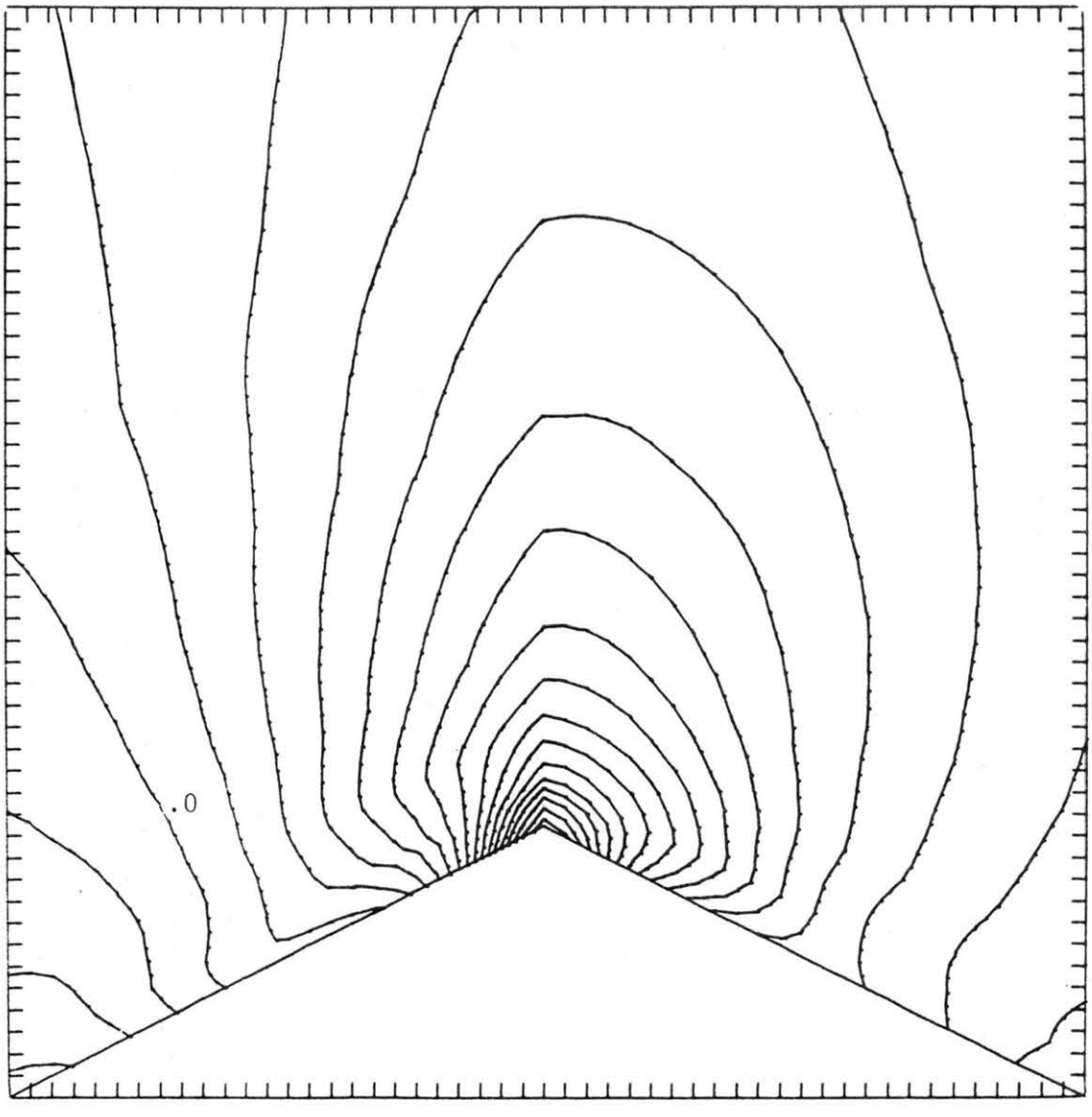

FIGURE D.2e Contours of Static Pressue over Triangular Ridge h/L = 1/4. Contour interval $\Delta C_p = 0.36$

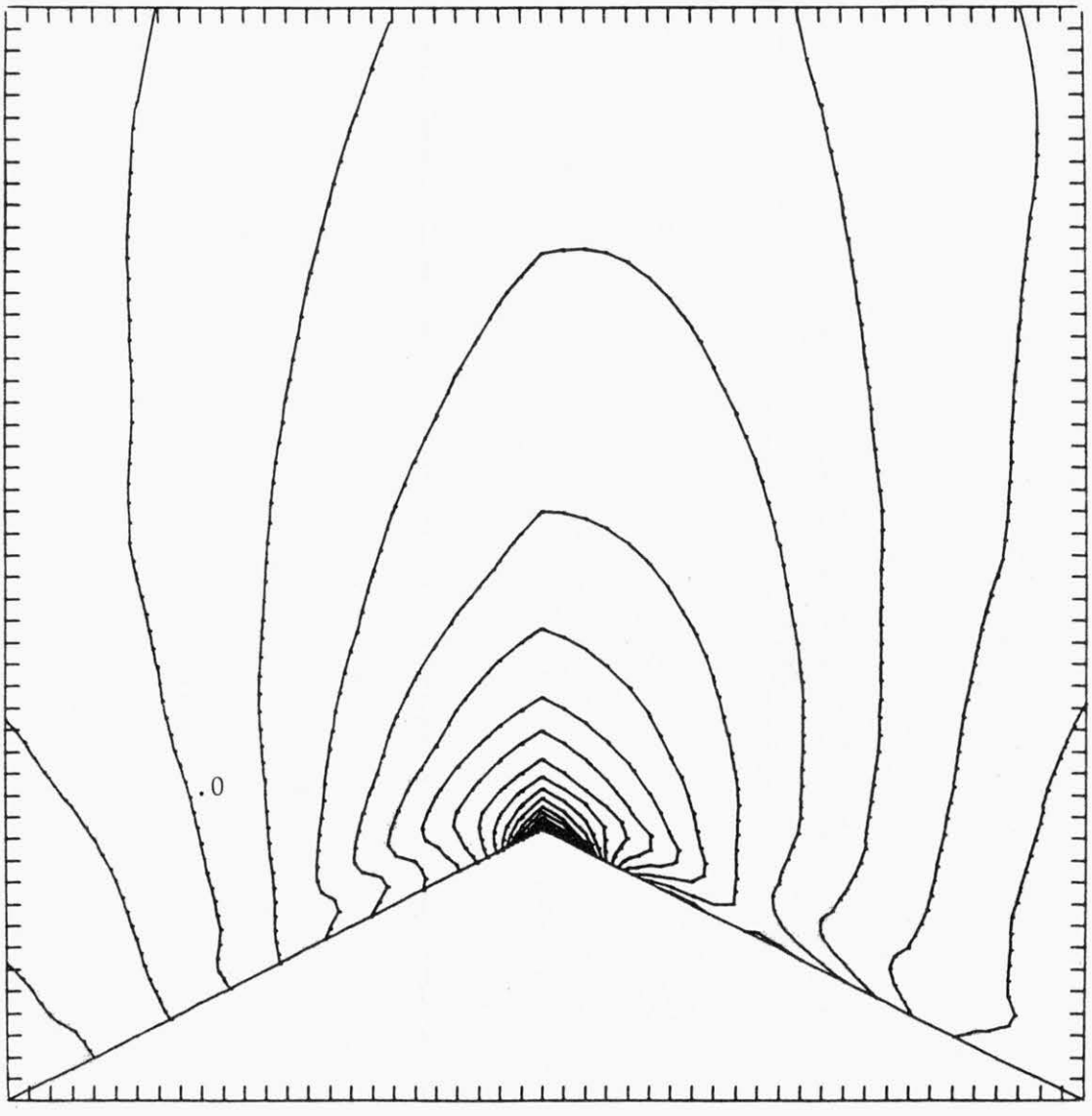

FIGURE D.2f Contours of Static Pressue over Triangular Ridge h/L = 1/4. Contour interval $\Delta C_p = 0.61$

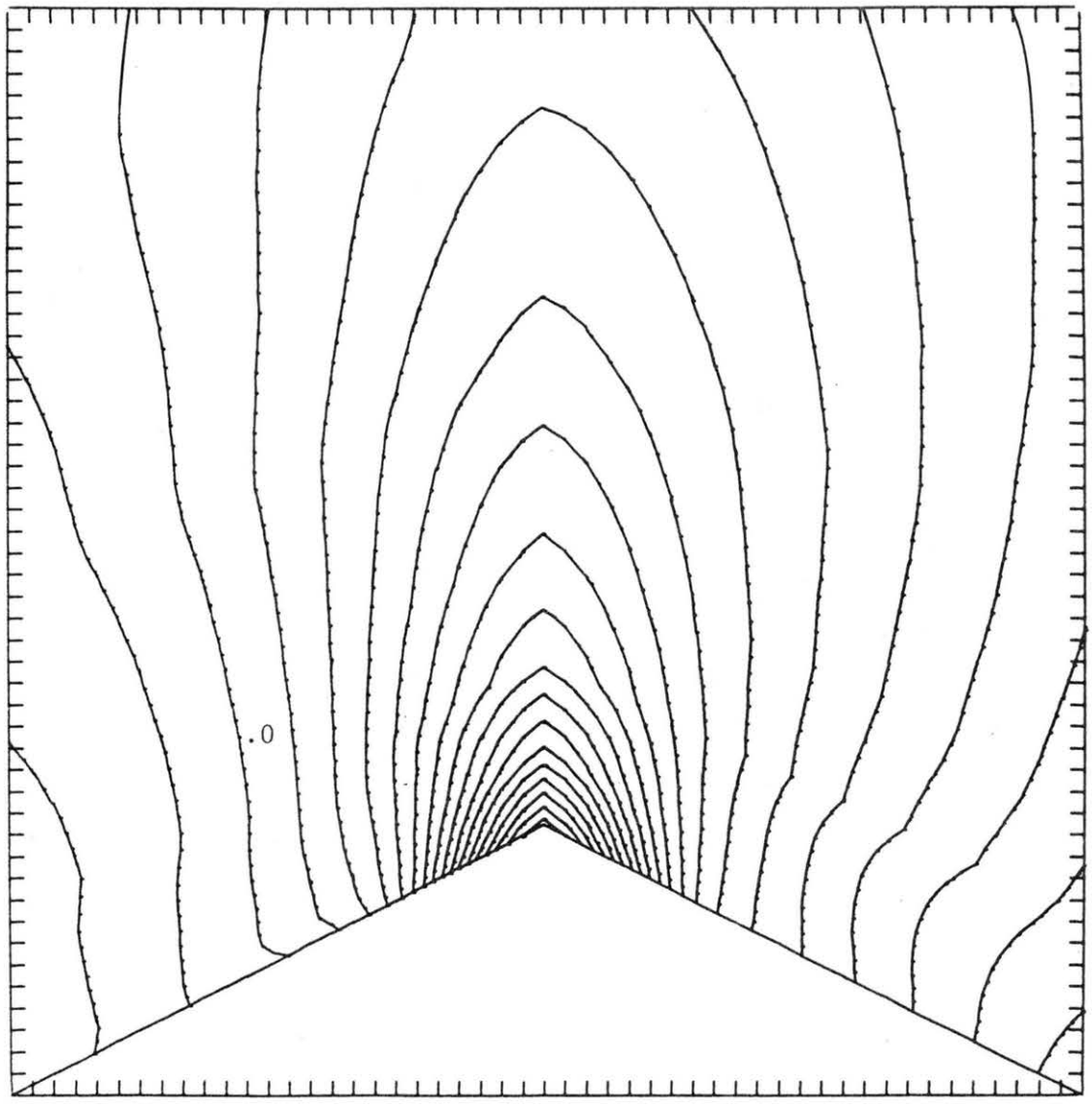

FIGURE D.2g Contours of Static Pressue over Triangular Ridge h/L = 1/6. Contour interval $\Delta C_p = 0.26$

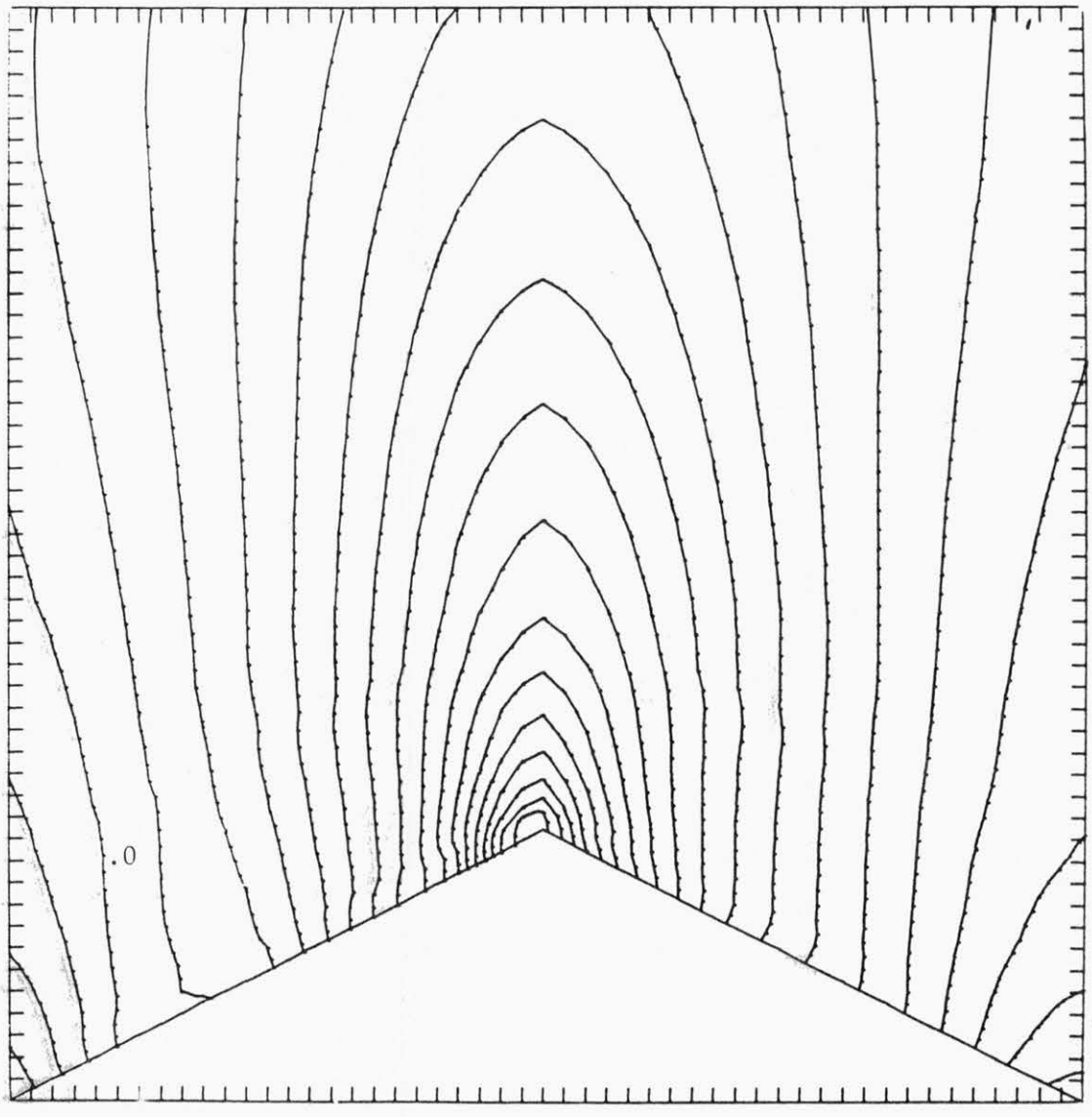

FIGURE D.2h Contours of Static Pressue over Triangular Ridge h/L = 1/6. Contour interval $\Delta C_p = 0.28$

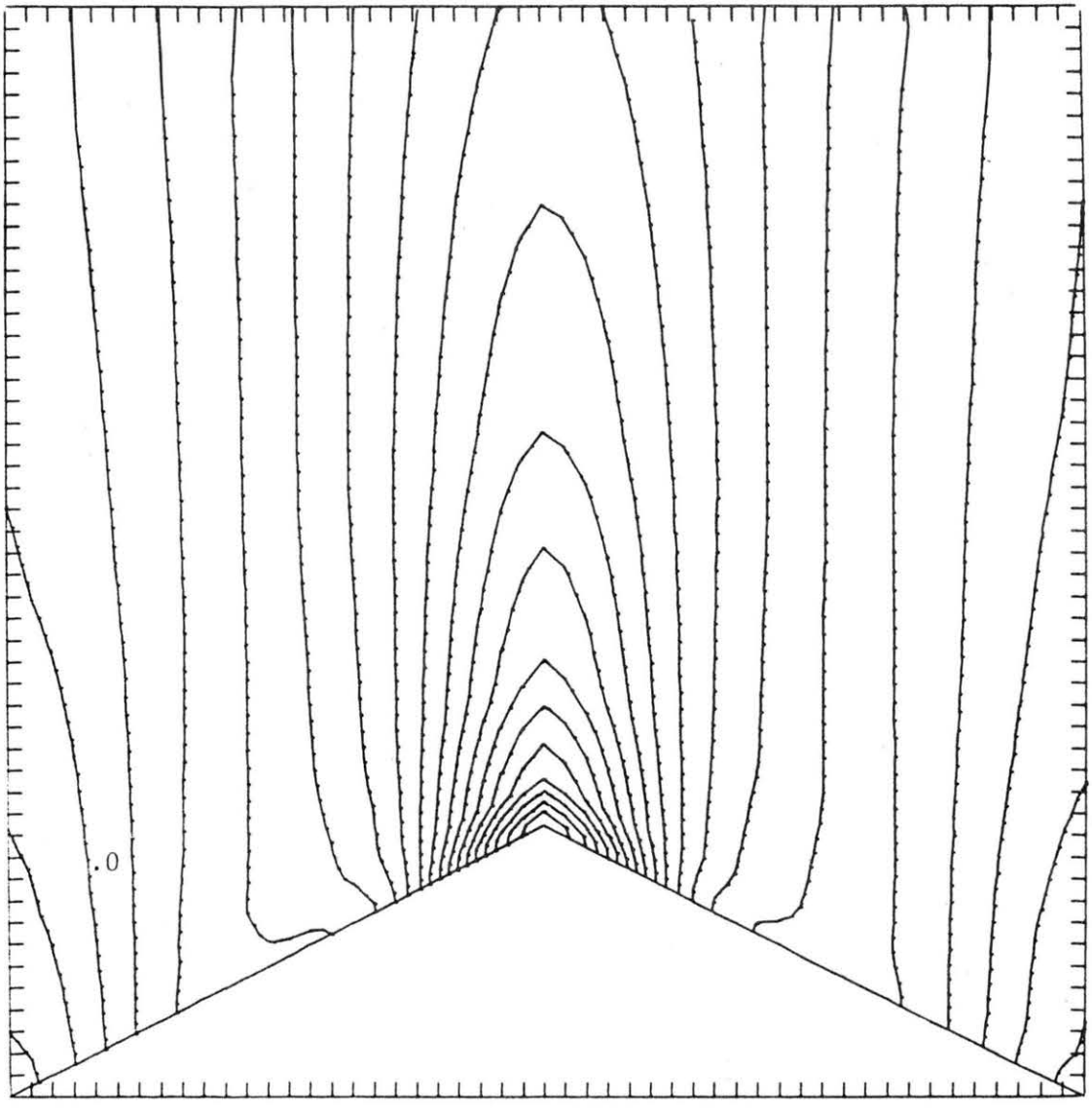

FIGURE D.2i Contours of Static Pressue over Triangular Ridge h/L = 1/20. Contour interval $\Delta C_p = 0.015$

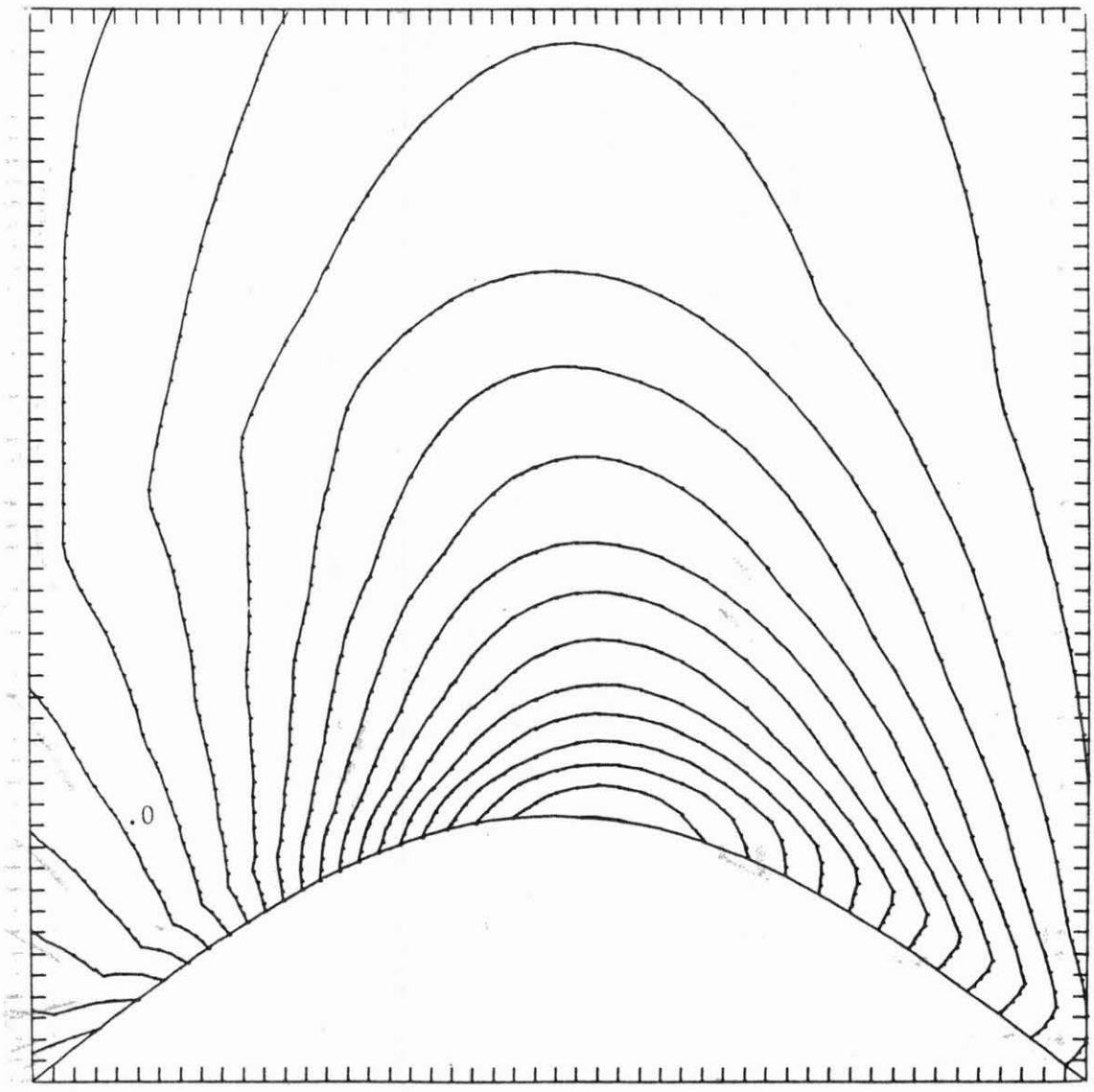

FIGURE D.2j Contours of Static Pressue over Triangular Ridge h/L = 1/4. Contour interval ΔC_p = .041

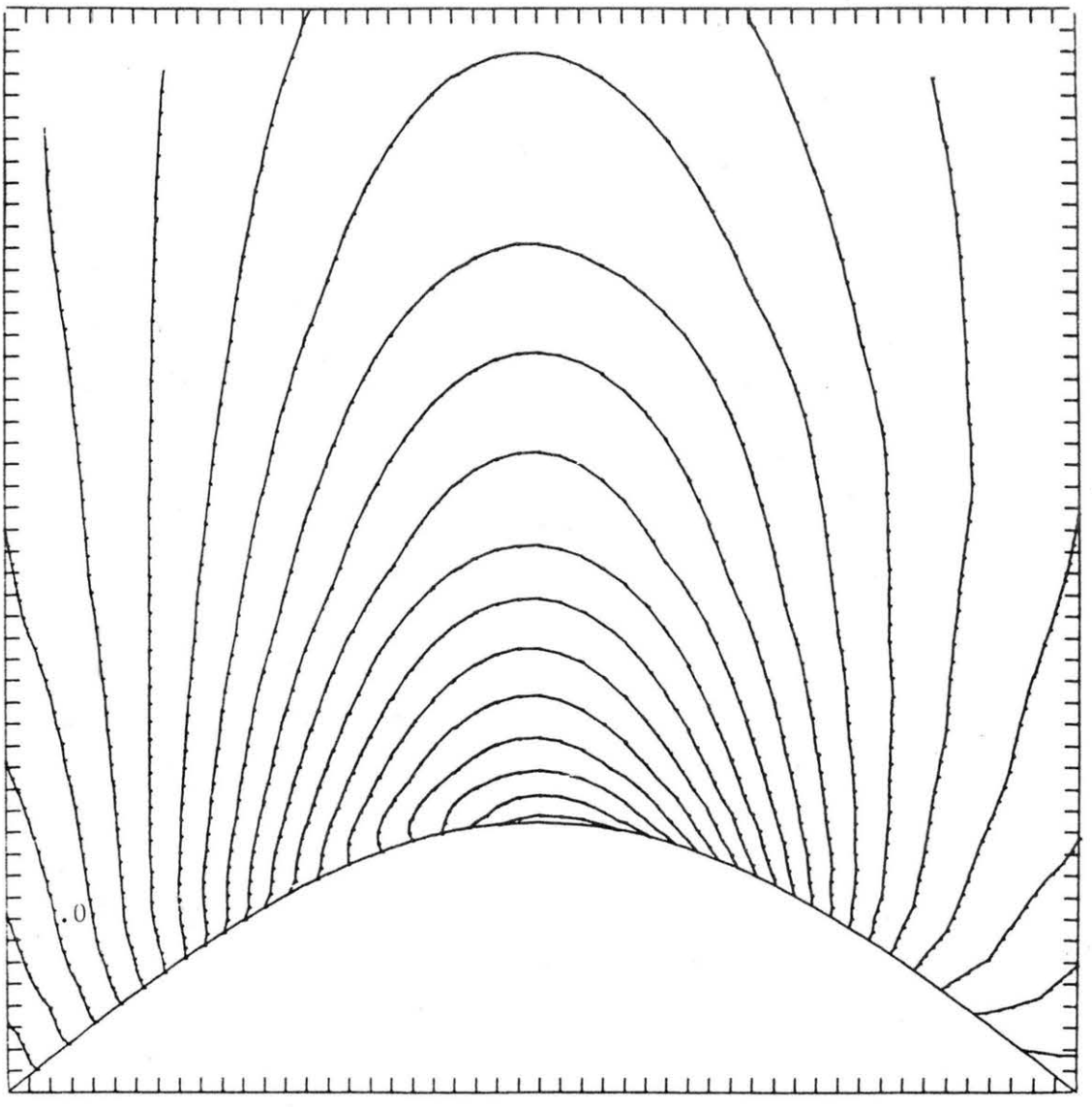

FIGURE D.2k Contours of Static Pressue over Triangular Ridge h/L = 3/16. Contour interval ΔC_p = .031

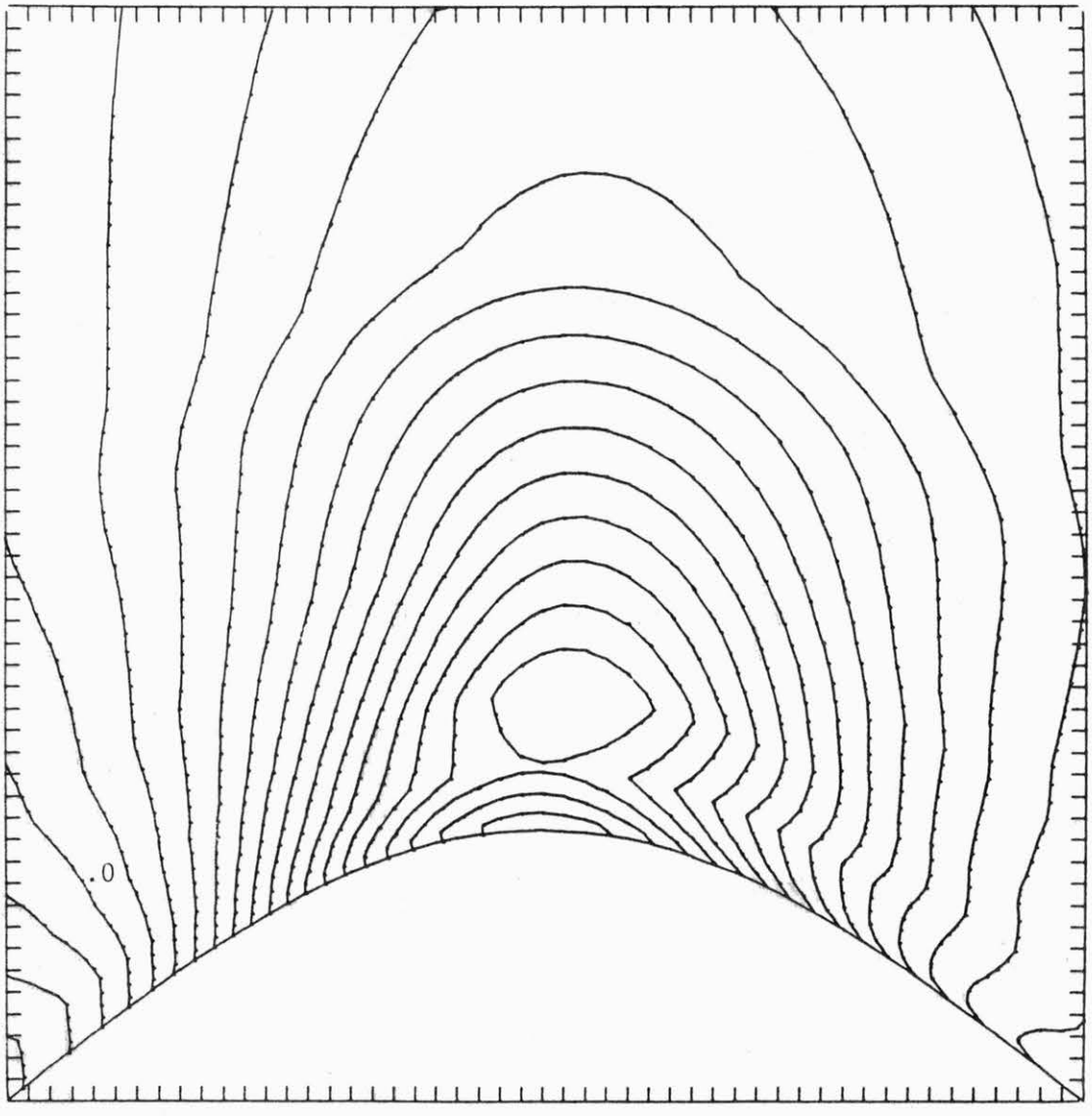

FIGURE D.21 Contours of Static Pressue over Triangular Ridge h/L = 1/4. Contour interval ΔC_p = .037

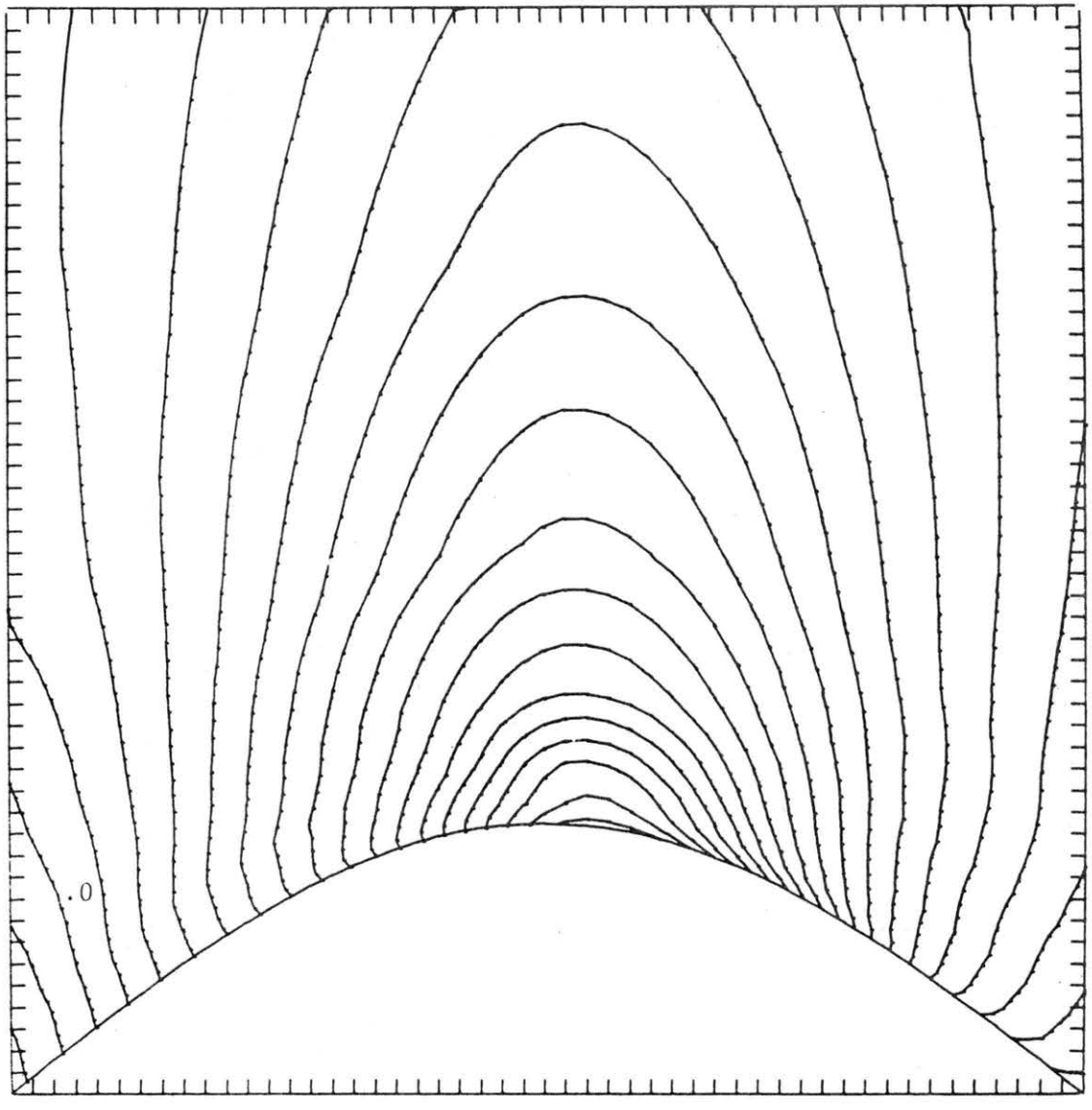

FIGURE D.2m Contours of Static Pressue over Triangular Ridge h/L = 3/16. Contour interval ΔC_p = .033

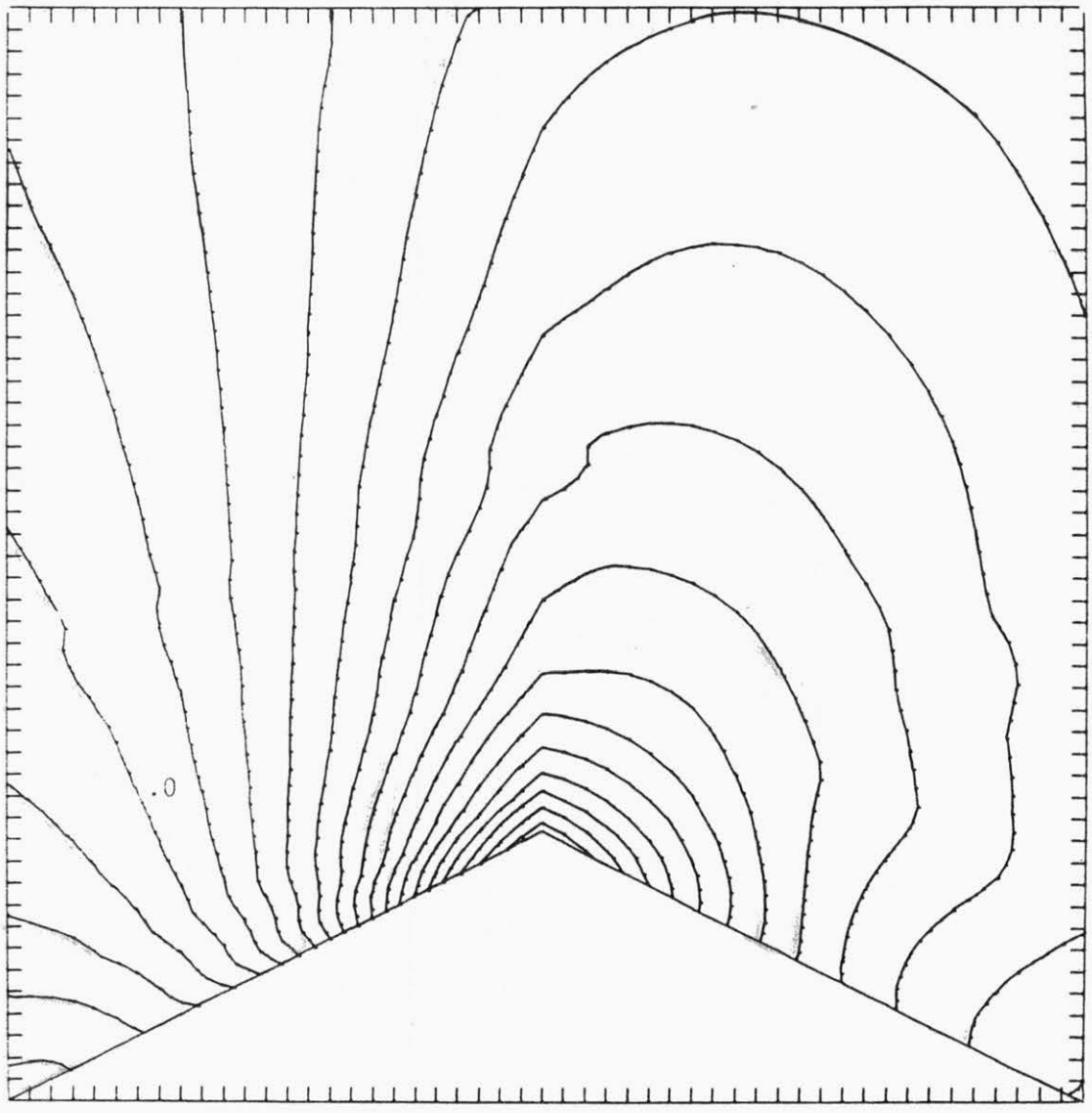

FIGURE D.2n Contours of Static Pressue over Triangular Ridge h/L = 1/4. Contour interval ΔC_p = .021

APPENDIX E

CONSTRAINTS OF WIND CHARACTERISTICS OVER RIDGES ON MATHEMATICAL PREDICTION PROCEDURES

APPENDIX E CONSTRAINTS OF WIND CHARACTERISTICS OVER RIDGES ON MATHEMATICAL PREDICTION PROCEDURES

E.0 INTRODUCTION

The governing equations of fluid motion are given by a set of nonlinear partial differential equations containing unknown Reynolds stress gradient terms. Approximations for the Reynolds stress gradients are required to complete the formulation. Usually numerical techniques are employed to solve for the fluid motion over a ridge. Some analytical solutions have been obtained by applying perturbation techniques which linearize the equations once higher order terms of small quantities are neglected. None of the existing numerical or analytical models accurately predict the flow field resulting from the interaction between main and a separated flow. Nonetheless, semi-analytical models have been developed that include flow separation.

This appendix reviews mathematical models that have been developed specifically to predict the flow over simple-shaped topography. A discussion of the most common closure assumptions is given in Section E.1 and applies to the models reviewed here. The purpose of this chapter is to evaluate the physical implications of analytical and numerical results and to investigate the applicability of the models to WECS site selection.

E.1 IMPLICATIONS OF FLOW PHYSICS IN SELECTION OF NUMERICAL CLOSURE MODELS

The effect of turbulence on the mean velocities over the crest of hills is in many cases not significant because of the large inertia and pressure gradients. Downwind of a hill, however, those gradients may become of the same order as the Reynolds stress gradients. If the effects of turbulence on the mean flow are to be included, or if values of Reynolds stresses are desired, a turbulence closure model must be selected.

E.2 LINEAR MODELS

Most attempts to predict the velocity distributions over surface undulations have used numerical techniques. An exception is the analytical solution of the equations of motion carried out by Jackson and Hunt (1975). Application of their results is limited to cases involving small velocity perturbations.

Only occasionally have the more sophisticated closure models been applied to flow over hills (Yamada, 1978). Usually mixing-length or turbulence kinetic energy models are selected on the basis of their simplicity rather than on the basis of their representation of the turbulence. In this section limitations are proposed for a few of the closure models most frequently used in numerical models for flow over hills. For an extensive discussion on a large variety of closure models the reader is referred to books such as Bradshaw (1976) or Launder and Spalding (1972).

Many closure models are based on the eddy viscosity concept. The most popular version is the "mixing length" formula:

$$-\overline{uw} = l^2 \left|\frac{\partial \bar{u}}{\partial z}\right| \frac{\partial \bar{u}}{\partial z} \qquad \text{(E.1)}$$

where l is the mixing length. The formula is utilized when the boundary layer is considered as a two-layer region, consisting of an inner and outer region. The middle region has to vanish since curvature and history effects are excluded by this model. Typically the model may be applied if

$$\frac{h\delta}{L^2} < 0.01$$

and if

$$\frac{\Delta S \delta}{L} < 0.01$$

(see condition for outer region, Section 2.1).

Bradshaw (1969) extended the mixing-length model by taking into account the streamline-curvature effects on the Reynolds shear stresses. An algebraic analogy was drawn between the meteorological buoyancy parameter, the Richardson number, and the parameters describing the effects of streamline curvature. The analogy proved to be a good first approximation as long as history effects on the turbulence structure were negligible. The effect of curvature on the apparent mixing length was shown to be appreciable if the shear-layer thickness exceeded roughly 1/300 of the radius of curvature. This result can be applied to flow over hills if γ defined in Equation (2.4) is the dominant extra rate of strain ratio. Supposing that the magnitude of the streamline curvature close to the surface extends to a height of $\frac{1}{2}$ L then curvature effects would become significant if

$$\frac{1}{2}L > \frac{1}{300}\frac{L^2}{h} \quad \text{or} \quad \frac{h}{L} > \frac{2}{300} \quad \text{if} \quad \frac{1}{2}L < \delta$$

$$\delta > \frac{1}{300}\frac{L^2}{h} \quad \text{or} \quad \frac{h\delta}{L^2} > \frac{1}{300} \quad \text{if} \quad \frac{1}{2}L > \delta. \tag{E.2}$$

There is some overlap with the closure model discussed previously. The curvature effect only develops after the stress-bearing eddies have adjusted to the extra strain rate; therefore, for hills with $L < \delta$ streamline-curvature effects are exaggerated if Bradshaw's analogy is followed closely.

The eddy viscosity models described above cannot be applied to hill forms if history effects become important; nonetheless, several authors have used these models to make hill flow calculations. The turbulence kinetic energy equation may be used to include history effects (e.g., Townsend, 1972, Taylor and Gent, 1974). The equation is then given by

$$\bar{u}\frac{\partial \frac{1}{2}\overline{q^2}}{\partial x} + \bar{w}\frac{\partial \frac{1}{2}\overline{q^2}}{\partial z} + \overline{uw}\frac{\partial \bar{u}}{\partial z} + \frac{\partial}{\partial z}\left(\frac{1}{2}\overline{q^2 w} + \overline{pw}\right) + \varepsilon = 0, \tag{E.3}$$

where $\frac{1}{2}\overline{q^2}$ is the total kinetic energy of the turbulence. The first two terms represent advection of turbulence kinetic energy, the third and fifth terms represent respectively turbulence production and dissipation, and the fourth term is the lateral transport of turbulent kinetic energy by diffusion.

To use Equation (2.28) as a closure, various unknown terms must be approximated. Townsend (1961) pointed out that turbulent flow attains a condition of structural similarity after prolonged unidirectional shear. If this is true, the local motion is determined by

$$\varepsilon = \frac{2\overline{q^2}^{3/2}}{L_\varepsilon} \tag{E.4}$$

and

$$-\overline{uw} = a_1 \overline{q^2},$$

where a_1 is constant and L_ε is a length scale proportional to the distance from the surface, at least in the region close to the wall. The diffusion may be approximated by

$$\frac{1}{2}\,\overline{q^2 w} + \overline{pw} = a_2(\overline{q^2})^{3/2}\,\mathrm{sgn}\left(\frac{\partial q^2}{\partial z}\right), \tag{E.5}$$

where a_2 is a constant.

This closure model has been applied quite successfully for a variety of flow cases. Most notable is the work of Bradshaw, Ferris, and Atwell (1967), who developed a numerical model to calculate the boundary-layer development. This model is based on the solution of a hyperbolic system of equations by the method of characteristics; boundary-layer approximations are an essential requirement, since this makes the set of equations hyperbolic.

Unfortunately, although history effects and diffusion of turbulent energy are taken into account, important turbulence production terms have been neglected. This is illustrated by considering the turbulence production terms in the full two-dimensional turbulence kinetic energy equation. This equation is

$$\frac{1}{2}\left(\bar{u}\,\frac{\partial q^2}{\partial x} + \bar{w}\,\frac{\partial \overline{q^2}}{\partial z}\right) \overline{uw}\,\frac{\partial \bar{u}}{\partial z} + \overline{uw}\,\frac{\partial \bar{w}}{\partial x} + \overline{u^2}\,\frac{\partial \bar{u}}{\partial x} + \overline{w^2}\,\frac{\partial \bar{w}}{\partial z}$$

$$+ \frac{\partial}{\partial z}\left(\frac{1}{2}\,\overline{q^2 w} + \overline{pw}\right) + \frac{\partial}{\partial x}\left(\frac{1}{2}\overline{q^2 u} + \overline{pu}\right) + \varepsilon = 0 \tag{E.6}$$

The four turbulence production terms are

$$-\overline{u^2}\,\frac{\partial \bar{u}}{\partial x}\,,\quad -\overline{w^2}\,\frac{\partial \bar{w}}{\partial z}\,,\quad -\overline{uw}\,\frac{\partial \bar{u}}{\partial z}\,,\quad -\overline{uw}\,\frac{\partial \bar{w}}{\partial x} \tag{E.7}$$

By continuity the sum of the first two terms may be written

$$(\overline{w^2} - \overline{u^2})\,\frac{\partial \bar{u}}{\partial x}\,. \tag{E.8}$$

If this term is positive, turbulence production increases. Flow approaching the crest accelerates, thus $\frac{\partial \bar{u}}{\partial x} > 0$. The difference in turbulence intensities of the vertical and horizontal component changes due to the distortion of the turbulence structure by the mean flow. A qualitative discussion on the distortion of turbulence over the hill is presented in Section 5.6. For now,

experimental evidence is applied to pursue this discussion. Data presented by Rider and Sandborn (1977a) shows that $\overline{w^2}$ increases towards the crest whereas $\overline{u^2}$ decreases. Since the up-stream values of $\overline{w^2} - \overline{u^2}$ are negative, the turbulence production due to those terms is negative but increases slightly towards the crest. Measurements of intensities over hills with $h/L = 0.25$, 0.33, and 0.5 and $L/\delta = 0.6$, 0.4, and 0.3, respectively, show that $\frac{\overline{w^2} - \overline{u^2}}{\overline{u^2}} < -1$ at the foot, and that this ratio is less than -0.5 at the crest. Thus the effect of the first two terms on the turbulence production is negative, implying that turbulence kinetic energy is transferred to the mean flow.

Apparently the neglect of these terms in the turbulence energy equation cannot be justified if $\frac{\partial \bar{u}}{\partial x} = 0$ $[\frac{\partial \bar{u}}{\partial z}]$. The sum of the two remaining terms is

$$-\overline{uw}\left[\frac{\partial \bar{u}}{\partial z} + \frac{\partial \bar{w}}{\partial x}\right]. \tag{E.9}$$

As was pointed out in Section 2.2, the vorticity remains almost the same along a streamline. (Changes in vorticity of 5-10 percent do not invalidate the following arguments.) Thus

$$[\frac{\partial \bar{u}}{\partial z} + \frac{\partial \bar{w}}{\partial z}]_{\psi=\psi_1} \approx [\frac{\partial u_o}{\partial z}]_{\psi=\psi_1} \tag{E.10}$$

This equation shows that any change in $\frac{\partial \bar{u}}{\partial z}$ along a streamline is accompanied by an almost equal change in $\frac{\partial \bar{w}}{\partial x}$. Data presented by Rider and Sandborn (1977a) shows that the magnitude of $\frac{\partial \bar{u}}{\partial x}$ changes by its own magnitude. Therefore, it may be concluded that in general the omission of the new term $-\overline{uw}\,\frac{\partial \bar{w}}{\partial x}$ in the turbulence kinetic energy equation cannot be justified.

One of the requirements for the approximation of Equations (2.29) and (2.30) is that the flow has to be strained by a unidirectional shear. As explained above, this is not generally the case in flow over hills.

All objectives against the use of this version of the turbulence kinetic energy closure model vanish if the distortion of the mean flow is very small, namely if $\frac{\partial \bar{w}}{\partial x} / \frac{\partial \bar{u}}{\partial z} \ll 1$, thus if $\frac{h}{L} \ll 1$.

The approach of their analysis was briefly mentioned in Section 2.3. The flow field over a hill is divided into two regions: an inner region close to the surface of the hill and an outer region, where a variation in the surface stress has no immediate effect on the flow. Reynolds stress gradients in the outer region are assumed to be negligibly small; hence the perturbed velocity field induces perturbation pressures governed by an inviscid flow model. It is assumed that the inner layer thickness is much less than the characteristic length of the hill. The pressure distribution along streamlines in the inner region are matched to the pressure distribution in the lowest part of the outer region. In the inner region, the Reynolds stress gradient may become as large as the pressure gradients. Indeed, the inner layer thickness is defined to include that zone where the order of magnitude of the Reynolds stress gradient is as large as the pressure gradient.

The solution is obtained by introducing Prandtl's mixing-length hypothesis as a turbulence closure. Velocities are matched asymptotically, in the inner layer as

$$z/\ell \to \infty$$

where z is the vertical coordinate in the inner layer and ℓ is the inner-layer thickness, and the outer layer as

$$z/L \to 0$$

where L is the characteristic length scale of the hill.

The essential limitations to the general applicability of the Jackson and Hunt relations are associated with the linearization of the equations of motion. They argue that their assumptions allow a consistent use of the mixing-length hypothesis and that curvature effects on the turbulence structure are negligible. The basic condition to be satisfied is

$$\frac{h}{L} \ll \frac{k \log \frac{\ell}{z_o}}{\log^2 \frac{L}{z_o}} \qquad \text{(E.11)}$$

where z_o is the equivalent surface roughness length.

The expression for ℓ arises from the condition that Reynolds-stress gradients are of the same order of magnitude as the pressure gradients in the inner region, namely

$$\frac{\ell}{z_o} = \frac{1}{8} \left(\frac{L}{z_o}\right)^{0.9} ; \qquad (E.12)$$

hence a limiting expression for $\frac{h}{L}$ as a function of z_o and L can be written as

$$\frac{h}{L} << \frac{0.9k}{\log \frac{L}{z_o}} - \frac{2.08k}{\log^2 \frac{L}{z_o}} \qquad (E.13)$$

Typical values for $\frac{L}{z_o}$ are in the range of 10^2 to 10^7. Corresponding values for the r.h.s. of Equation (3.3) are then in the range of 0.04 and 0.02. Therefore, according to these theoretical arguments, application of Jackson and Hunt's theory is limited to hills with very gentle slopes. However, Jackson and Hunt found also reasonable agreement between theory and field and wind-tunnel experiments for hills with slopes too steep for the theory to be strictly valid. In the next section a few comparisons are presented between Jackson and Hunt's calculations and inviscid flow calculations.

Sacre (1975) developed an analytical solution for stratified inviscid shear flow over topography. The solution is also based on linearization but in this case of the Euler equations. He cited good agreement with the results of Jackson and Hunt (1975). Larger deviations were found when Sacre's results are compared with nonlinear numerical calculations of Taylor and Gent (1975). Considering the limitations predicted from Jackson and Hunt's theory, results of Sacre's model should be used with caution for hills with slopes larger than 0.01.

Early interest in shear flow over surface perturbations was associated with the generation and damping of water waves. The first theoretical contributions came from Miles (1957). Efforts since have been directed at finding means to assess the role of turbulence and to incorporate an adequate closure model in the equations of motion. Most analytical contributions consider the linearized equations of motion. Notable is the work of Miles (1967) and Davis (1970, 1972) which has been reviewed below.

After several attempts to predict wave growth, Miles (1967) concluded that satisfactory agreement between theory and experiment had not been achieved. According to Miles, this was primarily because the dynamics of the turbulence over the waves was not adequately understood. Davis (1970) subsequently conducted research to investigate the importance of this turbulence. He applied two hypothesized turblence models to flow over a traveling wave of infinitesimal amplitude (this permitted the equations of motion to be linearized). The first model's hypothesis was based on an assumption that the turbulence field is not influenced by the waves. The second model was based on the assumption that the magnitude of the Reynolds stresses depends on the height above the instantaneous water surface. The wave-induced velocity field predicted by these two models differed considerably. Thus within the limitations of the linearized theory Miles's statement was confirmed.

In a later study, Davis (1972) applied more sophisticated closure models but continued to solve linearized equations. One new model was similar to that developed by Bradshaw, Ferris, and Atwell (1967). The second improved model was based on the assumption that the turbulent stresses are determined by the recent history of the strain that a fluid parcel has undergone. The results were compared to measurements by Stewart (1970), who measured the mean flow over waves in laboratory experiments, and Kendahl (1970), who measured mean flow and Reynolds stresses over waves. The agreement between calculated and measured values was not good. Townsend (1972) also used linearized equations of motion and a closure model similar to that used by Bradshaw et. al. (1967). He concluded

> "Although the attention paid to the turbulent motion makes for a more realistic account for the flow, the linearized theory is not able to account for the considerable discrepancy between calculated surface pressures and those measured in recent field studies by Snyder and Cox (1966) and by Dobson (1971)."

Townsend indicated that the linearized theory may be applied only to waves with a height-length ratio less than 0.1.

Two important conclusions may be drawn from these investigations on the velocity field over water waves: 1) the linear theory does not predict the velocities and pressures accurately for larger wave height to wave length ratios, and 2) the turbulence closure model selected for insertion into linearized equations of motion affects the predicted mean velocities significantly.

E.3 NONLINEAR MODELS EXCLUDING FLOW SEPARATION

In the last 15 years nonlinear models have been introdced to study flow over topography. Two classes of models may be distinguished: 1) nonlinear inviscid flow models, and 2) nonlinear flow models that include the Reynolds stress terms in the equations of motion. The latter will be denoted by "turbulence flow" models. As was pointed out in Sections 2.1 and 2.2, the Reynolds stresses affect the mean flow in the inner and middle region. The effect in the middle region only becomes significant when Reynolds stresses have had the time to adjust to the distorted flow field and when their action has resulted in a significant transfer of momentum across streamlines. In the following portion of this section, several numerical models are discussed in the light of the inviscid character of the flow, or more precisely, by considering the effects of the approximations for Reynolds stresses.

Alexander and Coles (1971) developed a numerical model solving the Navier-Stokes equations with a constant eddy viscosity. Deaves (1975) improved their model by including a more realistic eddy viscosity based on a mixing-length model. Taylor and Gent (1974) presented a solution incorporating turbulence length scale and turbulence kinetic energy equations to assist turbulence closure. Deaves as well as Taylor and Gent presented results for the flow over hills with shapes similar to those considered by Jackson and Hunt (1975).

Inviscid flow calculations have been completed herein for almost identical flow conditions as those considered by these authors using a numerical model developed by Derickson and Meroney (1977). An inviscid flow solution is obtained using stream function-vorticity coupled with an equation for potential temperature to handle unstable, neutral, and stable stratification as follows:

$$\nabla^2\psi = \eta \tag{E.14}$$

$$\frac{\partial}{\partial x}\left(\eta \frac{\partial\psi}{\partial z}\right) - \frac{\partial}{\partial z}\left(\eta \frac{\partial\psi}{\partial x}\right) = \frac{-g}{\theta}\frac{\partial\theta'}{\partial x} \tag{E.15}$$

$$\frac{\partial}{\partial x}\left(\theta' \frac{\partial\psi}{\partial z}\right) - \frac{\partial}{\partial z}\left(\theta' \frac{\partial\psi}{\partial x}\right) = 0 \tag{E.16}$$

where $\bar{u} = \frac{\partial\psi}{\partial z}$; $\bar{w} = \frac{\partial\psi}{\partial x}$.

A simple coordinate transformation was applied to solve the equation in a rectangular domain. The transformation is given by

$$\bar{x} = x; \quad \bar{z} = \frac{H}{H-z_s} (z - z_s) \tag{E.17}$$

in which $z_s(x)$ is the topography height, and H is the height of the top of the grid. The transformed spatial operators are thus defined in numerical conservative form as

$$\frac{\partial()}{\partial x} = \frac{1}{\sqrt{G}} \left(\frac{\partial\sqrt{G}\ ()}{\partial\bar{x}} + \frac{\partial\sqrt{G}\ G^{13}\ ()}{\partial\bar{z}}\right) \tag{E.18}$$

and

$$\frac{\partial()}{\partial z} = \frac{1}{\sqrt{G}} \frac{\partial()}{\partial z} \tag{E.19}$$

where $$\sqrt{G} = 1 - \frac{z_s}{H} \text{ and } G^{13} = \frac{1}{\sqrt{G}} \left(\frac{\bar{z}}{H} - 1\right) \frac{\partial z_s}{\partial x}$$

Vertical and horizontal grid expansion were applied to obtain higher spatial resolution at the crest. For a more detailed description the reader is referred to Derickson and Meroney (1977).

This inviscid flow model has been applied to calculate mean velocity field over bell-shaped hills. The surface elevation is defined by

$$\frac{z_s}{L} = \frac{1.04h}{L} \left(\frac{1}{1 + (\frac{2x}{L})^2} - \frac{1}{26}\right) \tag{E.20}$$

and approximates the bell-shaped hills considered by Deaves, Taylor and Gent, and Jackson and Hunt to within three percent of h. The upwind and downwind boundary conditions were varied according to the upwind conditions of the flow cases to which the inviscid flow calculations are compared. In all cases the approach profile is approximated by

$$\frac{\bar{u}_o(z)}{\bar{u}_o(\delta)} = \frac{u_*}{k\bar{u}_o(\delta)} \ln\left(\frac{z+z_o}{z_o}\right) \quad z < \delta \tag{E.21}$$

$$\frac{\bar{u}_o(z)}{\bar{u}_o(\delta)} = 1 \quad z > \delta \tag{E.22}$$

Up and downwind conditions were specified at respectively $x = \pm 2.5$ L. The height of the top of the grid was varied and is indicated in Table E.1. The no-slip condition was applied at the surface boundary.

Of particular interest is the thickness of the inner region where the shear stresses change most substantially and where by definition, a strong interaction between mean flow and turbulence occurs. A sensitive measure of the importance of a closure model may be provided by comparing surface shear stresses computed by the inviscid and turbulence flow models. The surface shear stresses of the inviscid flow model were obtained by assuming that no interaction between mean flow and turbulence occurs and that the mixing-length closure provides an accurate relation between mean flow and shear stress. Thus the nondimensionalized surface shear stresses were calculated by the following expression:

$$\frac{\tau_s}{\tau_{s_o}} = \lim_{z \to 0} \frac{\left(\frac{\partial \bar{u}}{\partial z}\right)^2}{\left(\frac{\partial \bar{u}_o}{\partial x}\right)^2} \qquad \text{(E.23)}$$

where the x-axis is parallel and the z-axis is perpendicular to the surface.

A comparison between the surface shear stress distributions over a bell-shaped hill (Case I of Table E.1) as calculated by Taylor and Gent and as calculated with the inviscid flow model is presented in Figure E.1. The asymmetric surface shear stress distributions of the turbulence flow models are caused by the action of the shear stress on the mean flow. This clearly shows that the mean flow is affected by the surface friction. The overall good agreement between the shear stress distributions of the inviscid and turbulence flow models may indicate, however, that the flow is inviscid at least down to a distance equal to the first grid point above the surface. In the inviscid flow calculations this point was located at $z = 0.04$ h. In terms of hill length, the inner-layer thickness would be less than 0.004 L. Alternatively, the good agreement may be fortuitous since discretization may have introduced inaccuracies, particularly, in the surface region where large velocity gradients occur.

Table E.1 includes 13 flow cases for which maximum surface shear stresses have been calculated by the inviscid flow model. Results are compared with the data given by both the nonlinear model of Taylor and Gent and the linear

TABLE E.1. Comparison of Maximum Surface Shear Stress over Bell-Shaped Hills Calculated with Turbulence and Inviscid Flow Models

Run	Author	$\frac{z_o}{\delta}$	$\frac{u_*}{\bar{u}(\delta)}$	$\frac{h}{\delta}$	$\frac{h}{L}$	$\frac{H}{h}$	Prediction of $\frac{\tau_{s\,crest}}{\tau_o}$	
							Turbulence Model	Inviscid Model[1]
1	JH[2]	4.6×10^{-4}	.052	4	.2	10.	1.81	2.8
2	JH	4.6×10^{-5}	.040	.4	.2	10.	3.10	3.4
3	JH	4.6×10^{-6}	.033	.04	.2	10.	6.32	3.6
4	JH	3.6×10^{-5}	.039	4	.2	10.	1.87	2.4
5	JH	3.6×10^{-6}	.032	.4	.2	10.	3.21	2.8
6	JH	3.6×10^{-7}	.027	.04	.2	10.	4.75	2.9
7	JH	2.8×10^{-6}	.031	4	.2	10.	1.86	2.3
8	JH	2.8×10^{-7}	.026	.4	.2	10.	2.60	2.5
9	JH	2.8×10^{-8}	.026	.04	.2	10.	3.95	2.6
10	TG[3]	6.1×10^{-6}	.033	.003	.05	20.	1 8	2.06
11	TG	6.1×10^{-6}	.033	.030	.05	20.	1.8	1.44
12	TG	6.1×10^{-6}	.033	.006	.1	20.	3.2	2.55
13	TG	6.1×10^{-6}	.033	.006	.1	10.	3.2	4.77
14	TG	6.1×10^{-6}	.033	.012	.2	10.	10.1	3.35

1) Derickson and Meroney (1977)

2) Jackson and Hunt (1975)

3) Taylor and Gent (1974)

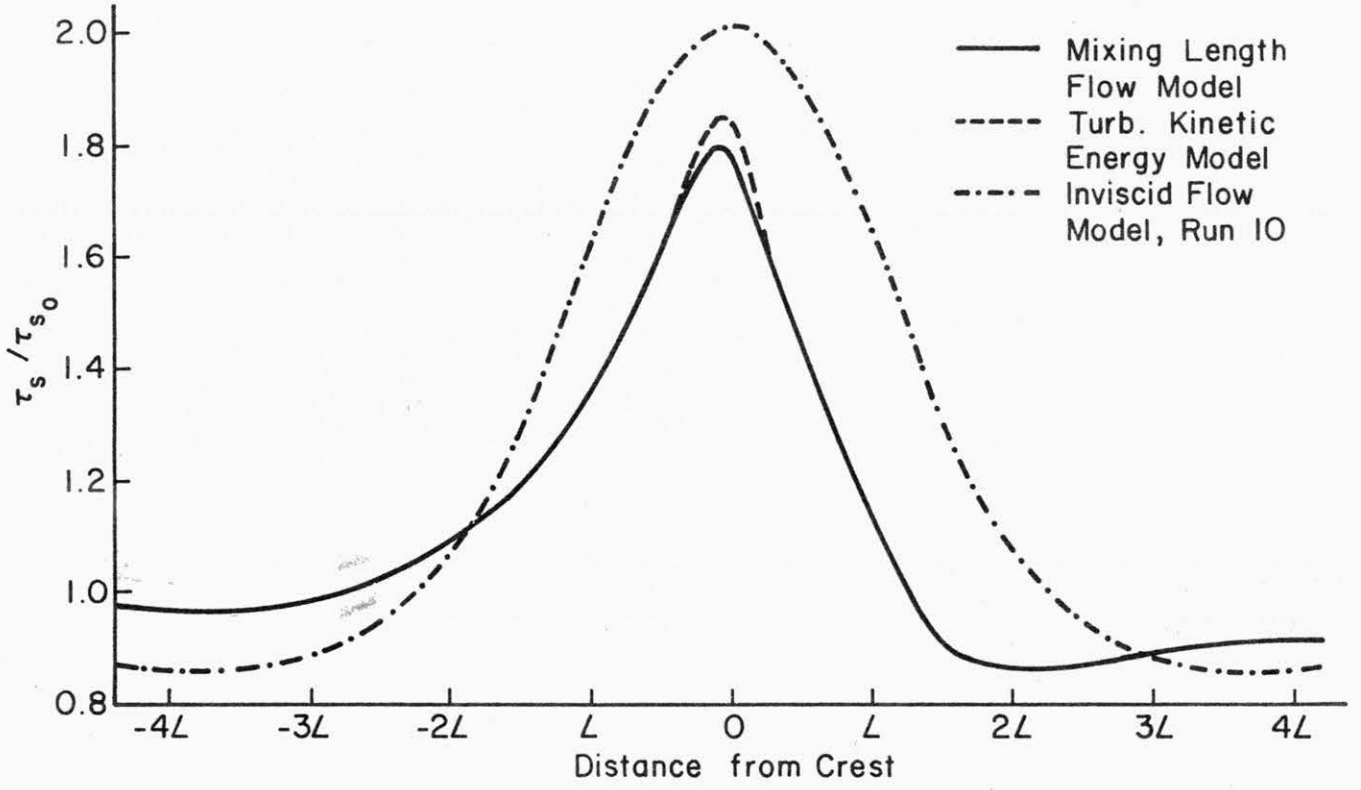

FIGURE E.1. Comparison of Numerically Calculated Surface Shear Stress Distributions over a Bell-shaped Hill

model of Jackson and Hunt. Taylor and Gent's results show a much larger increase in τ_{max} with increasing hill steepness than the increase in τ_{max} from the inviscid flow calculations. Discrepancies between calculations obtained with the turbulence flow models of Taylor and Gent and of Deaves were reported by Deaves (1975). Since there is no clear correspondence between the results of the nonlinear models, evaluation of the effects of the numerical modeling techniques used for each method would be desirable, but is beyond the scope of this research.

Astley et al. (1977) have developed a numerical model applying the finite element method to solve the equation of motion for inviscid flow over hills and escarpments. Velocities were calculated over escarpments with slopes 1:1, 1:2, and 1:4. The results were compared to wind-tunnel measurements of Bowen and Lindley (1977). There is in general good agreement for $z > 0.5$ h. In the surface region, $z < 2$ h downstream of the crest separation of the streamlines and the action of the Reynolds stresses cause the mean velocities to be significantly less than the predicted velocities.

E.4 NONLINEAR MODELS INCLUDING FLOW SEPARATION

Separation of the flow over hills occurs upwind and downwind of the hill if the slopes are sufficiently steep. A purely mathematical treatment of the flow is not yet possible because of the lack of knowledge about the interaction between the wake and the main flow. Present mathematical models that predict a separated flow region have included some empiricism. A number of existing models were developed to study the flow field over bluff surface obstacles such as buildings and may as well be applied to predict flow over hills. Other models were developed particularly for application in the aeronautics industry and include the usual boundary-layer approximations (pressure gradients across the streamlines are neglected) in the surface boundary layer (Kuhn et al., 1974). Application of such models to flow over hills embedded in a boundary layer does not seem to be justified.

An analytical solution of the equations of motion to plane inviscid shear flow over surface obstacles was presented by Fraenkel (1961). The solution includes closed streamlines just upstream and downstream of the obstacle. It is noted that in this model the separated flow regions are not the result or are not affected by mean flow wake interactions (see also Section 2.4). Although theoretically solutions could be obtained for a large variety of

conditions, at present solutions can realistically be obtained only if the vorticity is constant and if the physical plane can be mapped onto a complex plane. Application of this model to flow over hills is therefore limited and only justified if the interaction between the wake and the main flow is insignificant.

Kiya and Arie (1972) extended Fraenkel's model by including the freestreamline theory of Parkinson and Jandali (1970). The freestreamline theory describes the separation phenomenon resulting from the interaction between main flow and wake. The technique is developed for two-dimensional, incompressible flow external to a bluff body and its wake. The desired flow separation points are made the "critical" points. The stagnation streamlines then transform to tangential separation streamlines in the physical plane with separation at the desired pressure. The position and strength of the sources are determined by empirical parameters, namely the separation point and the pressure coefficient at the separation point. The flow inside the separation streamlines is ignored and the base pressure is constant between the separation points. One of the limitations of this freestreamline theory is that the wake width is finite for any downstream distance. Kiya and Arie's model requires two more empirical parameters in order to determine the value of the constant vorticity and slip velocity at the surface. They selected the location and pressure at the stagnation point.

Kiya and Arie (1972) compared experimental results of Good and Joubert (1968) for flow over a fence submerged in the boundary layer with their theoretical predictions. They showed that excellent agreement was obtained for the pressure distribution over the upwind face of the fence and for the location of the freestreamline up to a distance of 4 h from the fence. The upwind separated flow region was also predicted accurately.

Kiya and Arie's theory was extended recently by Bitte and Frost (1976). They added a sink equal in strength to the existing source to include the reattachment of the boundary layers downstream of the obstacle. An additional empirical parameter has to be specified, namely the location of the rear reattachment point.

The theory as developed by Kiya and Arie (1972) and Bitte and Frost (1976) requires a substantial amount of empirical information and is difficult to apply to other than very simple surface obstacle shapes. But the theory is

unique in the general description of flow separation and is adequate for parametric studies such as the effect of upwind velocity gradients on the velocity field over hills.

Bitte and Frost (1976) present a numerical model to analyze atmospheric flow over a bluff surface obstruction by applying concepts of boundary-layer theory. This work is an extension of the model developed by Frost, Maus, and Simpson (1973). Although predicted velocities are qualitatively similar to those calculated with other models, the model is unrealistic because it ignores vertical pressure gradients.

APPENDIX F

LABORATORY SIMULATION OF WIND OVER RIDGES

APPENDIX F LABORATORY SIMULATION OF WIND OVER RIDGES

Since Meroney et al. (1978a) reviewed similitude criteria as they relate to shear flow over irregular terrain this section only summarizes the limitations of wind-tunnel modeling and discusses their implications for this research. A number of nondimensional parameters can be derived from the full Navier-Stokes equations, which have to be equal for model and prototype in order to have exact similarity. Although equality cannot be obtained for some of those parameters, partial simulation seems adequate.

Two dimensionless parameters for which models simulation of atmospheric boundary layer flow over complex terrain are partial or incomplete are the Rossby number and the Reynolds number.

ROSSBY NUMBER

The Rossby number represents the ratio of inertial to Coriolis force and may be estimated from:

$$Ro = \frac{\Delta U_x}{L\Omega_o}$$

where ΔU_x is the speedup over a distance L. Coriolis forces affect primarily the variation of wind direction with height and were of course not simulated in the experiments. They have to be taken into account, however, for say $Ro < 3$. Such small Rossby numbers exist only at large distances from the surface or over low hills. For example, assume that one is interested in correcting for speedup as small as 0.5 m/sec, then at a latitude of 40°, where $\Omega_o = 9 \times 10^{-5}$ sec^{-1}, the hill length has to be larger than 2 km before Coriolis forces affect the mean flow field.

REYNOLDS NUMBER

This parameter is the ratio of inertial to viscous forces. Different Reynolds number effects may be distinguished. For aerodynamically smooth surfaces the Reynolds number effects limit the capabilities of physical modeling in a region close to the surface. In the present study an aerodynamically smooth surface had to be selected in order to scale the equivalent surface-roughness length to realistic proportions. The surface-roughness selection was based on the following approximations: 1) the atmospheric boundary-layer thickness was assumed to be 600 m, 2) the atmospheric surface condition to be simulated varied from grassland to rural wood, [corresponding to a surface

roughness length variation between 0.01 m and 1.0 m (Counihan 1975)], and 3) the boundary-layer thickness in the wind tunnel was approximately 0.60 m. Hence the surface roughness in the wind tunnel should be modeled between 10^{-5} and 10^{-3} m. The smooth floor "roughness lengths" were 6.8×10^{-5} m for $U_\infty = 9.1$ m/sec, and 3.5×10^{-5} m for $U_\infty = 15.2$ m/sec.

Close to a smooth surface under a turbulent shear layer there exists a viscous sublayer in which similitude may be violated. Its thickness may be estimated from

$$\frac{u_* \delta_v}{} = 10$$

where δ_v is the thickness of the viscous sublayer. This height is 0.05 cm in the wind tunnel corresponding to a thickness of 50 cm in atmosphere. This layer is usually irrelevant to wind velocity predictions.

Another Reynolds number effect that may jeopardize similitude between model and prototype is related to the fetch. In the atmosphere the upwind conditions may often be nonuniform causing a nonequilibrium boundary layer. In a wind tunnel, however, it is desired to have equilibrium-flow conditions so that changes in the turbulence structure are solely due to the surface obstacle. Zoric and Sandborn (1972) conducted an extensive study investigating where in the Meteorological Wind Tunnel equilibrium-flow condition would be established. Their analysis demonstrates that the turbulent boundary layer develops to a similarity form by 6 m from the entrance. Downwind of 6 m changes in flow characteristics were insignificant over the section where the measurements were made.

The Reynolds number effect on flow separation is the final aspect that needs consideration. Different velocities or hill dimensions may affect the location of the separation point over a gently curved hill. The separation phenomenon was studied by employing a triangular-shaped ridge which fixed the separation point at the crest. When the Reynolds number based on hill length is sufficiently large for flow over sharp edged geometries separation and reattachment are independent of Reynolds number magnitude.

The remaining similitude parameters which govern flow over terrain relate to geometric similarity and similarity of the approach windfield. These parameters can be identified by consideration of a few additional independent

variables. The features of the flow field and terrain which perform as independent variables are:

- hill height, h,
- hill length upwind of the crest, L_u,
- hill downwind of the crest, L_d,
- detailed hill shape (or distinction is to be made between sharp-crested and round-crested ridges),
- the boundary layer thickness, δ,
- the equivalent surface roughness length, z_o,
- the shear velocity in the upwind surface layer, u_*,
- the velocity at a height δ, $\bar{u}(\delta)$, and
- the thermal stratification characterized by a temperature differential over the height of the hill, $(T(h) - T(o))/h$.

For these 9 variables, plus the kinematic viscosity of air and the gravitational constant, the following nondimensional parameters may be developed by inspection:

$$\frac{h}{L_u}, \frac{h}{L_d}, \frac{h}{\delta}, \frac{z_o}{\delta}, \frac{u_*}{\bar{u}(\delta)}, \text{Re} = \frac{\bar{u}(\delta)h}{\nu}, \text{ and } \text{Ri} = \frac{g}{T}\frac{\Delta T}{\Delta U_z^2}h,$$

where ΔU_z is the characteristic change in velocity over the height of the ridge. The eighth parameter is the detailed hill shape. The limitations discussed above notwithstanding it is generally possible to simulate the parameters noted above.

Physical magnitudes such as the integral length scales and Monin Obukhov length in the equilibrium boundary layer are not included since they are implicitly determined by the other parameters. For detailed information the reader is referred to Zoric and Sandborn (1972) and Arya (1968).